
Functional and Developmental Characterization of Local Motion Sensing Neurons in the Fly Visual System

Tabea Rebecca Schilling



München 2019

Functional and Developmental Characterization of Local Motion Sensing Neurons in the Fly Visual System

Tabea Rebecca Schilling

Dissertation
an der Fakultät für Biologie
der Ludwig–Maximilians–Universität
München

vorgelegt von
Tabea Rebecca Schilling
aus Stühlingen

München, den 25.04.2019

Erstgutachter: Prof. Dr. Alexander Borst

Zweitgutachter: Prof. Dr. John Parsch

Datum der Einreichung: 25.04.2019

Datum der mündlichen Prüfung: 28.08.2019

Eidesstattliche Erklärung

Ich versichere hiermit an Eides statt, dass die vorgelegte Dissertation von mir selbstständig und ohne unerlaubte Hilfe angefertigt ist.

München, den 25.04.2019 Tabea Schilling

(Unterschrift)

Erklärung

Hiermit erkläre ich, *

dass die Dissertation nicht ganz oder in wesentlichen Teilen einer anderen Prüfungskommission vorgelegt worden ist.

dass ich mich anderweitig einer Doktorprüfung ohne Erfolg **nicht** unterzogen habe.

dass ich mich mit Erfolg der Doktorprüfung im Hauptfach
und in den Nebenfächern
bei der Fakultät für der

(Hochschule/Universität)
unterzogen habe.

dass ich ohne Erfolg versucht habe, eine Dissertation einzureichen oder mich der Doktorprüfung zu unterziehen.

München, den 25.04.2019 Tabea Schilling

(Unterschrift)

*) Nichtzutreffendes streichen

Contents

| | |
|--|-------------|
| Table of Contents | vii |
| List of Figures | ix |
| Abbreviations | x |
| Summary | xiii |
| Zusammenfassung | xv |
| 1 Introduction | 1 |
| 1.1 <i>Drosophila</i> as a Model for Circuit Neuroscience | 1 |
| 1.2 How <i>Drosophila</i> Became a Favorite Model Animal | 2 |
| 1.3 <i>Drosophila</i> Tools for Circuit Neuroscience | 4 |
| 1.3.1 Genetic Tools | 4 |
| 1.3.2 Anatomy of Neuronal Circuits | 7 |
| 1.3.3 Manipulating Neuronal Function | 10 |
| 1.3.4 Recording Neuronal Activity | 12 |
| 1.3.5 Transcriptomics | 14 |
| 1.3.6 Manipulating Gene Function | 15 |
| 1.4 Visual Behavior of <i>Drosophila</i> | 22 |
| 1.4.1 The Optomotor Response | 22 |
| 1.4.2 Object Orientation | 25 |
| 1.4.3 Looming Evoked Behavior | 27 |
| 1.5 Visual Pathways | 29 |
| 1.5.1 The Photoreceptors | 29 |
| 1.5.2 Phototransduction | 31 |
| 1.5.3 Lamina, Medulla and Lobula Plate Neurons | 33 |
| 1.5.4 Functional Properties of the Lobula Plate Tangential Cells | 35 |
| 1.5.5 Behavioral Relevance of the Lobula Plate Tangential Cells | 36 |
| 1.5.6 Color Vision Pathway | 38 |
| 1.5.7 Lobula Columnar Cells | 39 |
| 1.5.8 The Central Complex | 39 |
| 1.6 Algorithmic Models of Motion Computation | 40 |
| 1.6.1 The Hassenstein-Reichardt Detector | 40 |
| 1.6.2 Looming Detectors | 42 |
| 1.7 Development of the Optic Lobe | 43 |

| | | |
|-------------------------|---|------------|
| 1.7.1 | Neurogenesis in the OPC | 44 |
| 1.7.2 | Neurogenesis in the IPC | 45 |
| 1.7.3 | The T4 and T5 subtypes | 46 |
| 2 | Publications | 49 |
| 2.1 | A Directional Tuning Map of <i>Drosophila</i> Elementary Motion Detectors | 50 |
| 2.2 | Object Tracking in Motion-Blind Flies | 60 |
| 2.3 | Local Motion Detectors are Required for the Computation of Expansion Flow-Fields | 81 |
| 2.4 | Transcriptional Control of Morphological Properties of Direction-Selective T4/T5 Neurons in <i>Drosophila</i> | 86 |
| 3 | Discussion | 113 |
| 3.1 | Direction Selectivity of T4 and T5 Neurons | 113 |
| 3.1.1 | Motion Detection in the T4 and T5 Dendrites | 115 |
| 3.1.2 | Hassenstein-Reichardt/Barlow-Levick Detector | 117 |
| 3.1.3 | Direction Selective Cells in the Mouse Retina | 119 |
| 3.1.4 | Comparison of DS Cells in the Mouse Retina and the Fly Optic Lobe | 121 |
| 3.2 | Object Orientation | 123 |
| 3.3 | Looming Detection in <i>Drosophila</i> | 124 |
| 3.3.1 | Looming Sensitive Cells in the Lobula | 126 |
| 3.3.2 | Comparison to Looming Sensitive Neurons in other Arthropod Species | 127 |
| 3.4 | Differentiation of T4 and T5 Cells | 127 |
| 3.4.1 | Possible Role of Sox102F in Defining Cell Identity | 129 |
| 3.4.2 | Sox Transcription Factors as Terminal Differentiation Factors in T4 and T5 Cells | 130 |
| 3.4.3 | The T4 and T5 subtypes | 131 |
| 3.5 | Outlook | 133 |
| Danksagung | | 163 |
| Curriculum Vitae | | 165 |

List of Figures

| | | |
|------|--|-----|
| 1.1 | Pioneers of <i>Drosophila</i> Research | 3 |
| 1.2 | Binary Expression Systems | 6 |
| 1.3 | MultiColor FlpOut Method | 8 |
| 1.4 | Blocking Neuronal Function | 11 |
| 1.5 | Mosaic Analysis with a Repressible Cell Marker | 15 |
| 1.6 | <i>Minos</i> -Mediated Integration Cassettes | 17 |
| 1.7 | RNA Interference Pathways | 18 |
| 1.8 | Transcriptional Activation with CRISPRa flySAM2.0 | 21 |
| 1.9 | Different Setups to measure Optomotor Behavior | 23 |
| 1.10 | Optomotor Response Characteristics | 24 |
| 1.11 | Object Orientation Behavior | 25 |
| 1.12 | The Position System | 26 |
| 1.13 | Escape Jumps and Avoidance Turns | 27 |
| 1.14 | The <i>Drosophila</i> Photoreceptors | 30 |
| 1.15 | Comparison of Optic Superposition and Neural Superposition | 31 |
| 1.16 | <i>Drosophila</i> Phototransduction Compared to Vertebrate Phototransduction | 32 |
| 1.17 | Neurons of the Motion Vision Pathway | 34 |
| 1.18 | Anatomy and Response Vector Fields from Lobula Plate Tangential Cells | 36 |
| 1.19 | Patch-clamp Recordings of HS Cells | 37 |
| 1.20 | Neurons Involved in Color Vision | 38 |
| 1.21 | A Comparison of Different Correlation Detectors | 41 |
| 1.22 | Looming Detection Models | 43 |
| 1.23 | The Inner and Outer Anlagen of the Optic Lobe | 44 |
| 1.24 | Neurogenesis in the OPC and IPC | 45 |
| 1.25 | Development of the T4 and T5 Subtypes | 47 |
| 3.1 | Inputs on the T4 Dendrite | 116 |
| 3.2 | The HR/BL Detector | 118 |
| 3.3 | Direction Selectivity in the Mouse Retina | 120 |
| 3.4 | Comparison of the Fly and Mouse Motion Vision Pathway | 121 |
| 3.5 | Looming Sensitive Neurons | 125 |
| 3.6 | Comparison of Sox102F Knockdown T4 Cells with T3 Cells | 129 |

Abbreviations

| | |
|------------------|--|
| 2-MAG | monoglycerol |
| 3'UTR | three prime untranslated region |
| 5'GMP | guanosine monophosphate |
| Ago | argonaute protein |
| ASAP | accelerated sensor of action potentials |
| BAPTA | 1,2-bis(o-aminophenoxy)ethane-N,N,N',N'-tetraacetic acid |
| Brk | brinker |
| Brp | bruchpilot |
| CaLexA | calcium dependent nuclear import of LexA |
| CaMPARI | calcium-modulated photoactivatable ratiometric integrator |
| Cas9 | CRISPR associated endonuclease 9 |
| CD4 | cluster of differentiation 4 |
| CD8 | cluster of differentiation 8 |
| CFP | cyan fluorescent protein |
| cGMP | cyclic guanosine monophosphate |
| CH cell | centrifugal horizontal lobula plate tangential cell |
| Chat | choline acetyltransferase |
| CRISPR | clustered regulatory interspaced short palindromic repeat |
| crRNA | CRISPR RNA |
| CT1 cell | complex tangential cell 1 |
| C/T cells | centrifugal cells C2 and C3 together with T2 and T3 cells |
| D α 7-GFP | GFP tagged nicotinic acetylcholine receptor subunit |
| Dac | dachshound |
| DAG | diacylglycerol |
| Dcr | dicer protein |
| DNA | deoxyribonucleic acid |
| DNHS | descending neuron of the horizontal system |
| DNOVS | descending neurons of the ocellar and vertical system |
| Dpp | decapentaplegic |
| DSGC | direction selective retinal ganglion cells |
| dCas9 | dead CRISPR associated protein 9 |
| dCH cell | dorsal centrifugal horizontal lobula plate tangential cell |
| Dm cells | distal medulla cells |
| dsRNA | double stranded RNA |
| dTripA1 | thermosensitive cation channel |
| EM | electron microscopy |

| | |
|-----------|---|
| EMS | ethyl methan sulphonate |
| FACS | fluorescence activated cell sorting |
| Flp12 | flippase with glycine at position 5 and leucine at position 70 |
| FRET | Förster Resonance Energy Transfer |
| FRT site | flippase recognition target |
| GABA | gamma-aminobutyric acid |
| GCaMP | GFP, calmodulin M13, myosin light chain kinase peptide fusion protein |
| GDP | guanosine diphosphate |
| GFP | green fluorescent protein |
| GRASP | GFP reconstitution across synaptic partners |
| GtACR | <i>Guillardia theta</i> anion channel rhodopsins |
| DCMD | descending contralateral motion detector neuron |
| dIPC | distal inner proliferation center |
| GTP | guanosine triphosphate |
| GTPase | enzyme that hydrolyzes guanosine triphosphate |
| HR/BL | Hassenstein-Reichardt/Barlow-Levick |
| Hsc70 | heat shock cognate 71 kilodalton protein |
| HS cell | horizontal system lobula plate tangential cell |
| HSF1 | human heat shock factor 1 |
| Hsp90 | heat shock protein 90 |
| INTACT | isolation of nuclei tagged in specific cell types |
| InsP3 | inositol 1,4,5 triphosphate |
| IPC | inner proliferation center |
| IVS | intervening sequence within the 5'UTR |
| LC cell | lobula columnar cell |
| Li cell | lobula intrinsic cell |
| LGMD | lobula giant movement detector |
| Lop | lobula plate-less ^{N684} |
| Lpi cells | lobula plate intrinsic cells |
| LPLC | lobula plate/lobula columnar |
| LPTC | lobula plate tangential cell |
| MARCM | mosaic analysis with a repressible cell marker |
| MCP | MS2 bacteriophage coat protein |
| Mi cells | medulla intrinsic cells |
| MiMIC | Minos-mediated integration cassette |
| Omb | optomotor blind |
| OPC | outer proliferation center |
| Pasha | partner of Drosha |
| PD | preferred direction |
| pIPC | proximal inner proliferation center |
| miRNA | microRNA |
| mRNA | messenger RNA |
| ND | null direction |
| NFAT | nuclear factor of activated T cells |
| PEST | peptide sequence rich in proline, glutamic acid and serine, threonine |
| PIP2 | phosphatidylinositol 4,5-bisphosphate |

| | |
|-------------|---|
| PLC | phospholipase-C |
| Rh | rhodopsin |
| RFP | red fluorescent protein |
| RISC | RNA-induced silencer complex |
| RNA | ribonucleic acid |
| RNAi | RNA interference |
| SA | splice acceptor |
| SAM complex | synergistic activation mediator complex |
| Sb | stubble |
| smGdp | spaghetti monster Green darkend Protein |
| spGFP1-10 | GFP fragment consisting of beta barrel 1-10 |
| spGFP11 | GFP fragment consisting of beta barrel 11 |
| scRNA-seq | single cell RNA sequencing |
| sgRNA | single guide RNA |
| shRNA | short hairpin RNA |
| sIPC | surface inner proliferation center |
| Sox | Sry-related high-mobility-group box |
| STaR | synaptic tagging with Recombination |
| Syb | synaptobrevin |
| TAPIN | tandem affinity purification of intact nuclei method |
| tdGFP | tandem GFP |
| tdTomato | tandem Tomato |
| TeTxLC | tetanus toxin light chain |
| Tm cells | transmedulla cells |
| tracrRNA | trans-encoded CRISPR RNA |
| TRIP | transgenic RNAi Project |
| TRIP-KO | TRIP CRISPR Knockout |
| TRP | transient receptor potential |
| TRPL | transient receptor potential-like |
| t-SNARE | target soluble NSF attachment protein receptor |
| Tn-XI | troponin C X-large |
| TM3 | third multiple balancer 3 |
| UAS | upstream activation sequence |
| UV | ultraviolet |
| vCH cell | ventral centrifugal horizontal lobula plate tangential cell |
| VDRC | Vienna Drosophila Research Center |
| VPR | VP64-p65-Rta CRISPR activator |
| VACHT | vesicular acetylcholine transporter |
| VS cell | vertical system lobula plate tangential cell |
| vSNARE | vesicle soluble NSF attachment protein receptor |
| YFP | yellow fluorescent protein |

Summary

Sighted animals use visual motion information to navigate in their environment, to search for food sources or mating partners and to avoid potentials predators. However, directional motion information is not explicitly represented in the photoreceptor signals, but rather needs to be extracted by postsynaptic circuits. For such a motion computation, different algorithmic models were proposed. The most prominent model multiplies the signal of two neighboring photoreceptors after one of them was temporally delayed. Fruit flies are well suited as a model organism to study the neuronal mechanisms underlying motion perception. With a low spatial but high temporal visual resolution, fruit flies are able to detect many different kinds of motion stimuli and perform a wide range of visually evoked behaviors. Thanks to the multitude of genetic tools optimized for *Drosophila melanogaster*, detailed manipulation of neuronal function can be performed on a molecular as well as on a cellular level. These tools allow to dissect the components of a neuronal circuit and investigate their respective function. In the visual system of flies exist neurons sensitive to wide field motion, which are important for the course control of flies. An open question remains the computation of upstream neurons detecting local motion.

During my doctoral work I studied various aspects of the local motion sensing cells in the fly visual system: their functional properties, their importance for different behavioral tasks as well as their differentiation during development. In the first manuscript included in this thesis, we demonstrated that T4 and T5 cells are the elementary local motion sensing neurons of the fly. Calcium activity imaging of T4 and T5 cells revealed that four subtypes exist, each sensitive to motion along one of the four cardinal directions. Moreover, T4 cells responded specifically to light increments and T5 cells to light decrements. Blocking T4 neurons abolished the ON motion responses of postsynaptic lobula plate tangential cells. Accordingly, inactivating T5 cells inhibited the reaction of lobula plate tangential cells to OFF motion. We confirmed this effect by examining the turning behavior of walking flies with either T4 or T5 cells blocked. Flies without T4 output responded only to OFF edge motion, while flies with blocked T5 cells responded exclusively to ON edge motion.

To investigate the functional role of the local motion sensing T4 and T5 cells, we studied the consequences of blocking these neurons and tested visual behavior. In the second manuscript, we described that inactivating T4 and T5 cells abolished the optomotor turning response of the flies. However, the motion blind flies were still able to orient towards a dark, vertical bar. We

demonstrated that flies respond to the position of a bar independent of a motion cue. Therefore, we concluded that flies use positional as well as motion information to orient towards an attractive object.

In the third manuscript, we further investigated the role of T4 and T5 cells in flight behavior and found these cells involved in the detection of expansion motion. Flight avoidance turns as well as landing responses of flies depend on functional T4 and T5 cells. These behaviors are evoked by expansion motion like a looming stimulus, which mimics an approaching predator or object. The importance of T4 and T5 cells for looming evoked behavior suggests, that these cells are not only connected to lobula plate tangential cells, which respond to rotatory wide-field motion, but are also presynaptic to looming sensitive neurons in the lobula plate.

The last manuscript describes transcription factors important for the differentiation of T4 and T5 neurons. The morphology of all T4 and T5 subtypes is comparable; their dendrites are oriented opposite to the preferred direction of the cell and the axon terminals target one of the four lobula plate layers. Both the dendrites and the axon terminals are limited to only one layer of their respective neuropil. We found two postmitotic transcription factors expressed in the young T4 and T5 cells, *SoxN* and *Sox102F*, which regulate the common features of all subtypes. These transcription factors are crucial for the proper morphology of the T4 and T5 cells, as well as the function of the adult neurons.

Zusammenfassung

Sehende Tiere nutzen visuelle Bewegungsinformationen, um sich in ihrer Umgebung zu orientieren, nach Nahrungsquellen oder Paarungspartnern zu suchen, oder auch um potentiellen Fressfeinden zu entgehen. Informationen über die Bewegungsrichtung eines visuellen Reizes werden nicht von den Photorezeptoren selbst bestimmt, sondern den postsynaptischen Schaltkreisen entnommen. Für eine derartige Bewegungsdetektion wurden verschiedene algorithmische Modelle vorgeschlagen. Das bekannteste Modell multipliziert das Signal von zwei nebenliegenden Photorezeptoren, nachdem eines von ihnen zeitlich verzögert wurde. *Drosophila melanogaster* eignet sich exzellent als Modellorganismus, um die neuronalen Mechanismen der Bewegungswahrnehmung zu untersuchen. Mit einer zwar geringen räumlichen, aber hohen zeitlichen visuellen Auflösung können Fruchtfliegen viele verschiedene Arten von Bewegungsreizen erkennen, dabei zeigen sie ein breites Repertoire an visuell induzierten Verhaltensweisen. Dank der Vielzahl an möglichen genetischen Methoden können detaillierte Manipulationen der neuronalen Funktion auf molekularer, aber auch auf zellulärer Ebene durchgeführt werden. Diese Methoden ermöglichen es, die Komponenten eines neuronalen Schaltkreises zu analysieren und ihre jeweilige Funktion zu untersuchen. Im visuellen System der Fliege existieren Neurone, welche Weitfeld-Bewegungen detektieren. Diese Neurone sind wichtig um ungewollte Kursänderungen auszugleichen und eine Richtung beizubehalten. Die neuronale Berechnung der vorgeschalteten Zellen, welche lokale Bewegungen erfassen, bleibt eine offene Frage.

In der vorliegenden Doktorarbeit untersuchte ich verschiedene Aspekte der lokalen Bewegungsdetektoren im visuellen System der Fliege: Ihre funktionalen Eigenschaften, ihre Bedeutung für verschiedene Verhaltensweisen sowie ihre Differenzierung während der Entwicklung. Im ersten Manuskript wird gezeigt, dass Interneurone der optischen Loben, die T4- und T5-Zellen, als elementare, lokale Bewegungsdetektoren der Fliege agieren. Die Kalzium-Aktivitätssignale der T4- und T5-Zellen zeichneten vier Subtypen ab, welche jeweils sensitiv auf Bewegung entlang einer der vier Himmelsrichtungen sind. Darüber hinaus reagierten T4-Zellen spezifisch auf eine positive Helligkeitsänderung und T5-Zellen auf eine negative Helligkeitsänderung. Mit Hilfe einer spezifischen Inhibition der T4-Zellen Aktivität wurde die Bewegungsreaktion der postsynaptischen Lobula Platte Tangentialzellen auf Bewegungsstimulation mit einer positiven Helligkeitsänderung blockiert. Dementsprechend inhibierte die Inaktivierung der T5-Zellen Aktivität die Reaktion der Tangentialzellen auf Bewegungsstimulation mit einer negativen Helligkeitsänderung. Diesen Effekt

konnten wir zusätzlich im Verhalten bestätigen, dabei untersuchten wir die Drehbewegung der laufenden Fliege als Reaktion auf dunkle oder helle bewegende Kanten. Fliegen in denen wir die T4-Zellen inhibierten, reagierten nur auf die Bewegung der dunklen Kanten, während die Fliegen mit inaktiven T5-Zellen nur noch die Bewegung der hellen Kanten wahrnahmen.

Um herauszufinden inwieweit unterschiedliche visuelle Verhaltensweisen von einer lokalen Bewegungsdetektion der T4- und T5-Zellen abhängen, untersuchten wir das Verhalten von Fliegen in denen wir die Aktivität dieser Neurone inhibierten. In dem zweiten Manuskript wird eine Abhängigkeit der optomotorische Drehreaktion von T4- und T5-Zellen dargestellt. Eine Inaktivierung dieser Zellen blockiert daher die Bewegungs-Wahrnehmung der Fliegen. Dennoch waren diese Tiere noch in der Lage, einen dunklen, vertikalen Streifen in einer frontalen Position zu fixieren. Wir konnten demonstrieren, dass solche bewegungs-blinde Fliegen auf die Position eines Streifens reagieren, unabhängig von einer Bewegungsinformation. Daher schlussfolgerten wir, dass Fliegen sowohl Informationen über die Position, als auch über die Bewegung eines attraktiven Objektes verwenden, um sich zu diesem hin zu orientieren.

Im dritten Manuskript untersuchten wir darüber hinaus die Rolle von T4- und T5-Zellen im Flugverhalten und fanden heraus, dass diese Zellen an der Erkennung von Expansionsbewegung beteiligt sind. Sowohl die Vermeidungsreaktion im Flug als auch die Landereaktion waren von der Funktion der T4- und T5-Zellen abhängig. Diese Verhaltensweisen werden durch Expansionsbewegungen, wie ein Kollisionsstimulus mit exponentieller Expansion, ausgelöst. Ein solcher Kollisionsstimulus imitiert einen sich nähernden Fressfeind oder ein näherkommendes Objekt. Die Abhängigkeit von T4- und T5-Zellen für die durch Expansionsbewegung stimulierten Verhaltensweisen lässt vermuten, dass diese Zellen nicht nur mit den Tangentialzellen der Lobula-Platte verbunden sind, sondern auch mit weiteren Zellen spezifisch für die Wahrnehmung von Kollisionsstimuli.

Das letzte Manuskript beschreibt Transkriptionsfaktoren welche speziell für die Differenzierung von T4- und T5-Neuronen wichtig sind. Die Morphologie aller T4- und T5-Subtypen ist in mehreren Punkten vergleichbar. Ihre Dendriten sind entgegen der Vorzugsrichtung der Zelle ausgerichtet und die Axone enden in einer der vier Schichten der Lobula-Platte. Dabei sind sowohl die Dendriten als auch die Axonterminale auf nur eine Schicht ihres jeweiligen Neuropils beschränkt. Wir konnten zeigen, dass die postmitotische Transkriptionsfaktoren SoxN und Sox102F die gemeinsamen Eigenschaften aller T4- und T5-Subtypen regulieren. Diese Transkriptionsfaktoren sind entscheidend für die korrekte Morphologie der T4- und T5-Dendriten und daher auch für die Funktion der adulten Neurone.

Chapter 1

Introduction

1.1 *Drosophila* as a Model for Circuit Neuroscience

Circuit neuroscience aims to link behavioral function to a dissected circuit micro-structure (Yuste, 2008). In order to fulfill this goal, one has to face several critical questions beforehand. How does the brain control a behavior and further adapt the behavioral response to a changing environment? How does an animal integrate multiple sensory streams of different modalities? How does this information affect the animals' internal state and ultimately translate to an altered motor output?

One possible approach to answer such questions is to choose a simple model organism with a low number of neurons and minimal variability of anatomy and behavior. Due to a rapid increase of genetic tools, *Drosophila* emerged as a widely used model organism for circuit neuroscience (reviewed by Olsen and Wilson (2008) and Bellen et al. (2010)). One advantage of *Drosophila* is that, despite the relative simplicity of its nervous system, fruit flies exhibit a wide range of different behaviors. Compared to vertebrate model organisms, like mice or zebra fishes, the morphology and connections of *Drosophila* neurons are hard-wired and comparable between individual animals. In addition, the genetic tools allow targeting of single cell types and manipulation of neuronal or gene function. Another model organism for circuit neuroscience is the nematode *Caenorhabditis elegans*. Its small brain, consisting of only 302 neurons with a fully described connectome (White et al., 1986), also enables the study of single neurons. However, the behavioral repertoire of *C. elegans* is quite limited compared to *Drosophila*.]

For several decades, neuroscience studies with *Drosophila* involved mutagenesis and screening for a behavioral phenotype. In this way, many genes important for behaviors like olfactory learning (Keene and Waddell, 2007) or visual course control (Bausenwein et al., 1986) were described. The development of binary expression systems (Brand and Perrimon, 1993) and the creation of GAL4 line libraries (Pfeiffer et al., 2010; Tirian and Dickson, 2017) allows precise manipulation of single cell types in *Drosophila*. Different effector genes enable imaging of neuronal activity, blocking or activation of neurons and labeling neurons to describe their morphology (Kazama, 2015). Thanks to the small size of the *Drosophila* brain, connectome data from a large proportion of the brain is

available, enabling to reconstruct many neuronal connections (Zheng et al., 2018).

The motion vision pathway of *Drosophila* is ideally suited to decipher a neuronal circuit. The inputs are well defined, motion vision elicits different hard-wired behaviors and most neuronal cell types of the *Drosophila* optic lobes are described. Visual stimuli can be presented with high spatio-temporal precision, enabling the derivation of the systems transfer function with high fidelity. Despite their poor spatial resolution, flies respond to a wide range of visual stimuli with a high temporal resolution and are able to perform fast visually-guided flight maneuvers (Muijres et al., 2014). The motion vision circuits of vertebrates and invertebrates developed by convergent evolution, allowing comparison of the fundamental modules. Understanding the neuronal basis of motion detection in different biological systems can help to gain more insights into neuronal computation.

1.2 How *Drosophila* Became a Favorite Model Animal

The career of the fruit fly *Drosophila melanogaster* as one of the most important model organisms began in the early 1900s. After the entomologist Charles W. Woodworth suggested fruit flies as a useful lab animal, William E. Castle, a geneticist at Harvard University, started to breed *Drosophila*. He published his observations about inbreeding and fertility (Castle et al., 1906), in which he emphasized the advantages of fruit flies, like their short life cycle or the possibility to breed at room temperature throughout the whole year. At the same time Frank Lutz, a young biologist at Cold Spring Harbor was breeding fruit flies and described their advantages of being an easy lab animal for student projects (Lutz, 1907).

Nettie Stevens, an extraordinarily talented cytologist, brought fruit flies into the lab of Thomas Hunt Morgan at Bryn Mawr (Fig. 1.1 a). She discovered the chromosomal basis of sex determination by staining the chromosomes of female and male germ cells of meal worms and different fly species (Stevens, 1905, 1908). She found unequal chromosome pairs in male spermatocytes and concluded that sex is inherited through these heterochromosomes. By breeding *Drosophila melanogaster* on different food sources and counting male versus female offspring she further demonstrated that food has no influence on the sex of fly offspring (Stevens, 1908). N. Stevens suspected that cross breeding of flies will help to understand the Mendelian inheritance of sex and supposed that 'in some cases at least, other characters may be so correlated with sex that their behavior in heredity may throw light on the sex question' (Stevens, 1908).

Indeed, her former supervisor Thomas H. Morgan (Fig. 1.1 b) discovered an X chromosomal gene. He realized the immense potential of fruit flies for genetic studies, though he was critical about Nettie Stevens sex chromosome theory for several years. In order to find a genetic mutant, Thomas Morgan observed the phenotype of fruit flies over many generations. His approach was successful as he discovered a white eyed male fly. Fortunately, the location of the *white* gene is on the X chromosome. Backcrossing this white eyed male fly to wild-type females resulted in only red

eyed first filial generation, but white eyed males in the second filial generation (Morgan and Cattell, 1912). Therefore, he could determine the origin of the *white* gene to be the X chromosome and confirm the Mendelian inheritance of a recessive allele.

Drosophila became a broadly used model organism in short time, because it is simple and very cost effective to breed fruit flies, their generation time is short and many mutations induce a clear phenotype. While Thomas Morgan looked for spontaneously occurring mutants, Hermann J. Muller (Fig. 1.1 c) experimented with X-rays in order to induce mutations in *Drosophila* (Muller, 1927). This was the first proof that radiation induces mutagenesis. For this discovery, he was awarded the Nobel Prize in Physiology or Medicine in 1946. Muller's attempts to find a mutational chemical failed, but were solved by Charlotte Auerbach. First she discovered that sulfur mustard, the chemical warfare known as mustard gas, induces mutations. She experimented with possible mutant chemicals until she found that DNA alkylating agents like ethyl methane sulphonate (EMS), which can be fed to *Drosophila* larvae, are also mutagenic (Auerbach, 1967). EMS enabled large screenings for *Drosophila* mutants, leading to substantial genetic discoveries like the description of genes controlling embryogenesis by Christiane Nüsslein-Volhard and Eric Wieschau (Nüsslein-Volhard and Wieschau, 1980). They received the Nobel Prize in Physiology or Medicine in 1995.

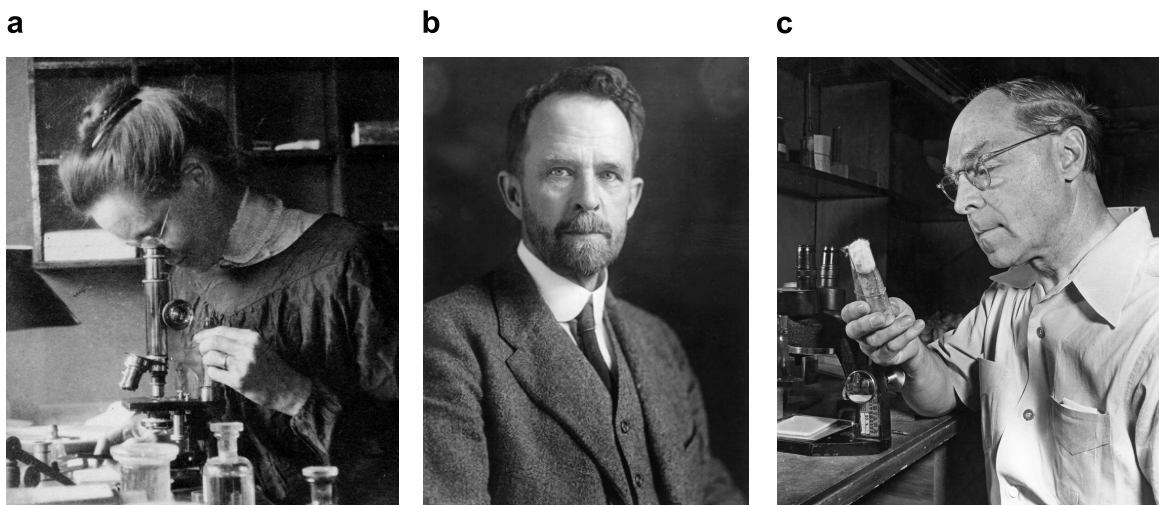


Figure 1.1: Pioneers of *Drosophila* Research.

a Nettie Stevens in 1909, picture from Bryn Mawr College Special Collections. **b** Thomas H. Morgan in 1920, photo taken by A.F. Huettner. **c** Hermann Muller in his laboratory, picture from Encyclopaedia Britannica.

1.3 *Drosophila* Tools for Circuit Neuroscience

Being a model organism for over 100 years, *Drosophila* offers many useful genetic tools. In the following, I will describe methods commonly used to investigate the connectivity and the biophysical properties of neural circuits. These methods allow for anatomical analyses of specific cell types and their synaptic connections, circuit manipulations by knockdown as well as gain-of-function experiments, functional manipulations by targeted activation or silencing of neurons, transcriptomic analyses of neurotransmitter and receptor genes, and the recording of neuronal activity *in vivo*.

1.3.1 Genetic Tools

Balancer Chromosomes

The genome of *Drosophila* is distributed on just four pair of chromosomes: three pair of autosomes and two sex chromosomes, X and Y. They carry the information for at least 15.000 genes (Adams et al., 2000; Hoskins et al., 2015). The fourth chromosome is very short with only 1.4 mega base pairs and contains only a small number of genes. In contrast to the other chromosomes, it does not undergo meiotic recombination. Due to the limited size of the fourth chromosome, it is normally not used for genetic modifications. Therefore, transgenes are mostly inserted into the X chromosome, chromosome II or chromosome III.

In 1935, Hermann Mueller discovered an X chromosome that does not undergo homologous recombination, because multiple chromosomal inversions prevent meiotic crossover with the sister chromosome (Sutton, 1943). Such balancer chromosomes are used to maintain altered chromosomes carrying a recessive lethal mutation or transgene insertion by avoiding recombination. To visualize the balancer chromosomes, they usually carry physical markers. Such markers are mutations that induce easily visible phenotypes, e.g. shorter bristles on the thorax in *Stubble* flies. If the chromosomal inversion are not homozygous lethal, balancer chromosomes carry recessive lethal mutations in addition to keep them heterozygous. Balancer chromosomes are labeled the following way: The first letter describes the chromosome ('F' for X, 'S' for the second and 'T' for the third), the second letter is 'm' for multiple inverted, followed by a number (chronology of the balancer chromosomes) and the marker. For example, *Tm3, Sb* is a balancer for the third chromosome with the marker *Stubble*, whereas *Fm7, Bar* is a balancer for the X chromosome combined with the marker Bar eye. An exception is the *CyO* balancer for the second chromosome, which is named after the marker inducing curly wings.

Generation of Transgenic Lines

The discovery of the *Drosophila* transposon P-element (or P-factor) was a milestone for *Drosophila* research. A P plasmid, containing transposase recognition sites and a marker gene, allows mutagenesis through random insertions (Spradling and Rubin, 1982; Rubin and Spradling, 1983). Expression of the marker gene indicates the successful transposition. Usually, the *white* gene,

which induces red eyes, is used as a marker gene in a *white*⁻ background (Klemenz et al., 1987). Instead of destroying the function of a gene, P plasmid insertions can be used to generate transgenic fly lines expressing a reporter gene (Thummel et al., 1988). In this case, the possibility of disrupting gene expression is a disadvantage, especially since there is a tendency of P-elements to insert near promoters of active genes (Bellen et al., 2004). The second disadvantage is the variability of the reporter gene expression level, it depends strongly on the genomic location of the insertion. Such problems were solved by the use of a bacteriophage phiC31 integrase, which induces a site-specific recombination at attP docking sites (Groth et al., 2004; Bischof et al., 2007). Flies in which attP sites are inserted with a P-element can be tested for the side effects and expression strength at this specific location. The best locations are used for a more effective generation of transgenic lines with comparable expression levels. Most common used insertion sites to generate fly lines are attP18 and attP8 in the X chromosome, attP40, su(Hw)attP5 and attP1 in the second chromosome, attP2 and VK00005 in the third chromosome (Pfeiffer et al., 2010).

Binary Expression Systems

Binary expression systems, like the GAL4-UAS system, allow the cell-type specific expression of a reporter gene. The yeast transactivator GAL4 controlled by a regulatory element (enhancer) binds the activating sequence UAS (= upstream activating sequence) to initiate transcription of a gene downstream of the UAS sequence (Ptashne, 1988). GAL4 expression in *Drosophila* can activate gene translation in combination with a UAS sequence (Fischer et al., 1988). Using enhancer-driven GAL4 expression together with insertion of a UAS-gene of interest allows cell- or tissue-specific gene expression (Fig. 1.2 a) (Brand and Perrimon, 1993).

The GAL4-induced transcription can be repressed by the regulatory protein GAL80 (Lee and Luo, 1999; Suster et al., 2004), a repressor protein binding to GAL4 and inactivating it. This allows refinement of the GAL4-induced translation to a smaller number of cells (Fig. 1.2 b). Moreover, a temperature sensitive version of GAL80, GAL80^{ts}, blocks expression until application of a heat shock by incubation at 37°C for a relatively short time (McGuire et al., 2003). A more restricted UAS expression can be achieved by splitting the transactivator GAL4 into an activation domain and a DNA-binding domain (Luan et al., 2006). Leucine zippers were attached to each protein domain to allow the reconstitution of the GAL4 protein. If the activation domain and the DNA-binding domain are expressed under control of two different enhancers, reporter gene expression is restricted to the overlapping cells containing both proteins (Fig. 1.2 c). The generation of split-GAL4 lines refined the GAL4 line expression pattern and made targeting of one cell type possible. Split-GAL4 lines usually do not reach the same expression strength as conventional GAL4 lines, but their expression can be enhanced by using the p65 activation domain. The GAL80 does not bind to the p65 activation domain, but split-GAL4 expression can be refined with the so-called 'Killer Zipper'. This protein inhibits reconstitution of the activation domain and the DNA-binding domain into GAL4, by binding the leucine zippers (Dolan et al., 2017).

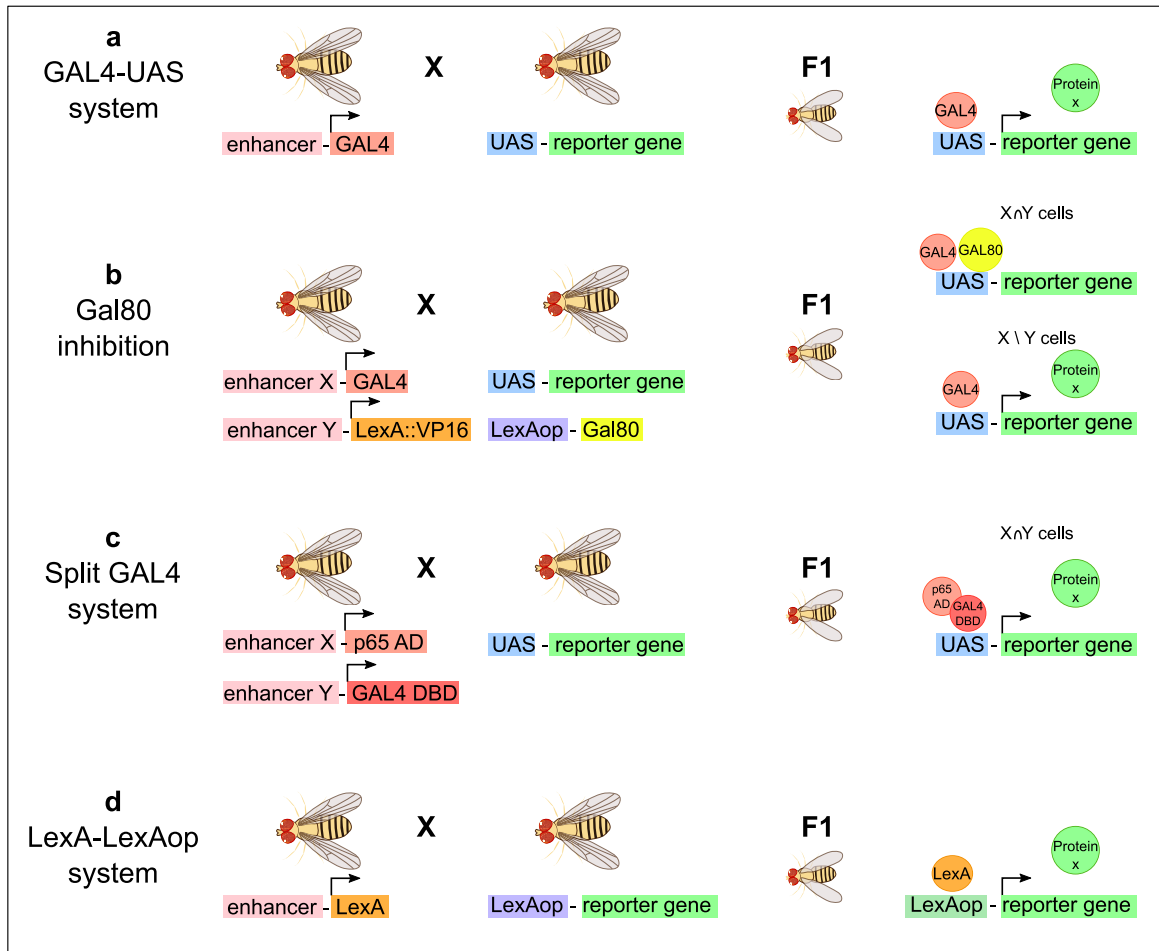


Figure 1.2: Binary Expression Systems.

a The transactivator GAL4 binds to the UAS sequence, which starts expression of the reporter gene. **b** LexA driven expression of GAL80 inhibits GAL4, UAS driven expression occurs only in LexA negative cells. **c** Two different enhancers drive expression of the p65 activation domain and the GAL4 DNA binding domain. Only in cells where both are present, they can form a transactivator and bind to the UAS sequence. **d** The LexA-LexAop binary system works equivalent to the GAL4-UAs system, with the transactivator LexA binding to the LexAop sequence.

The LexA-LexAop binary expression system works in a complementary way (Fig. 1.2 d), here the transcription factor is a chimera of the bacterial DNA-binding LexA protein and the transactivation domain from the yeast GAL4 protein (LexA::GAD) (Szüts and Bienz, 2000). Since the GAL80 protein binds to the GAL4 activation domain, LexAop expression can also be suppressed by expression of GAL80. Other combinations of LexA with the VP16 acidic activation domain (LexA::VP16) or the human p65 activation domain (LexA::p65) result in a GAL80 insensitive protein (Lai and Lee, 2006; Pfeiffer et al., 2010). The LexA protein binds to the LexA operator sequence (LexAop) to drive expression.

The GAL4-UAS as well as the LexA-LexAop system have been improved by increasing the

number of UAS or LexAop repeats. Addition of the post-transcriptional regulatory element intron 16 (IVS) enhances RNA transport to the cytoplasm (Pfeiffer et al., 2010). Whereas early GAL4 lines were created with P element insertions, the development of the phiC31 integrase system and the characterization of useful attP sites enabled the efficient creation of GAL4 and LexA lines with strong expression. Using the best attP sites, thousands of GAL4 and LexA lines with different enhancer fragments were generated to drive expression in most neuronal subpopulations (Pfeiffer et al., 2008; Jenett et al., 2012; Tirian and Dickson, 2017). Thereby, specific lines for most neuronal cell types can be found or combined.

1.3.2 Anatomy of Neuronal Circuits

Labeling Neurons with Fluorescent Proteins

Before specific neurons became genetically accessible, they could be stained randomly. The Golgi staining, a silver staining method in which sparse cells are filled with silver chromate (C. Golgi, 1873), enabled single cell staining. Using this method, Ramón y Cajal described the anatomy of fly visual system neurons (Cajal and Sanchez, 1915). The GAL4-UAS System made it possible to express fluorescent proteins in the neuron of interest. The most prominent example is the green fluorescence protein (GFP) from *Aequorea*, a jellyfish species (Chalfie et al., 1994). By adding several mutations, the brightness of the original GFP variant was optimized to what is named enhanced GFP or eGFP (Zhang et al., 1996). There are also red, yellow and cyan variants of GFP (RFP, YFP, CFP) available (Feng et al., 2000). Another red fluorescence protein is DsRed, a protein responsible for the red color of a *Discosoma* coral species. There are different variants of DsRed with colors from orange to dark red, the most commonly used ones are tdTomato and mCherry (Shaner et al., 2004).

These fluorescent proteins can be membrane bound with a CD4, CD8 or a myristoyl tag, or localized to the nucleus with a nuclear localization signal (nls), for example Stinger-GFP. For single cell labeling, the expression of the fluorescent protein is repressed by a stop codon flanked by flippase recognition target (FRT) sites (Fig. 1.3). To cut out the stop codon in only a few cells, stochastic activity of a flippase is achieved by weak flippase variants. The flippase variant with the lowest activity is the FlpI2 version with a glycine instead of aspartic acid at position 5 and a leucine at position 70. Compared to FlpD5, its activity is tenfold weaker. In addition, adding a PEST tag, which is a peptide sequence enhancing the protein degradation, shortens the half life of the FlpI2 variant (Nern et al., 2015). This flippase FlpI2::PEST allows to label single neurons, thereby the number of neurons labeled is dependent on the GAL4 line. The expression of the weak flippase is controlled by a heat shock promoter or a panneuronal enhancer from the *neuronal Synaptobrevin* gene, which results in panneuronal flippase expression without the need of a heat shock.

To optimize the brightness and allow single cells to be labeled in different colors, a GFP which is tagged with many peptide epitopes (spaghetti monster Green darkend Protein or smGdP) can be used (Fig. 1.3). Antibody staining of the tags results in high brightness and detection of small

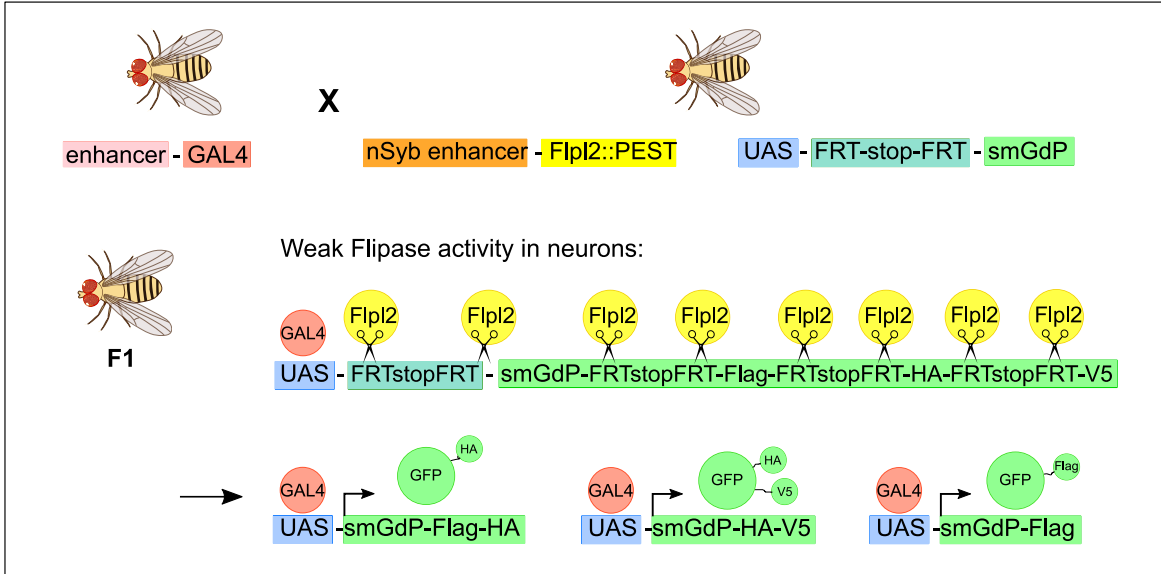


Figure 1.3: MultiColor FlpOut Method.

The weak flippase FlpI2::PEST is expressed under control of a panneuronal enhancer. It cuts out the stop codons of the smGdP construct stochastically, therefore different combinations peptide tags or attached to the sparsely expressed GdP. Antibody staining of the tags results in multicolor staining of single cells.

neuronal branches (Nern et al., 2015). Removal of FRT flanked stop codons can stochastically allows expression of different epitope tags, resulting in differently labeled single cells. The method using a weak flippase and the smGdP construct with different tags is named MultiColor FlpOut. The MultiColor FlpOut methods allows to label many neurons and still see the morphology of individual cells.

Labeling Synapses

Neurons communicate through chemical synapses and gap junctions, both kind of synapses can be detected by electron microscopy. To label chemical synapses with fluorescent proteins and detect them with light microscopy, there are several possibilities. A special modification of two GFP fragments, GFP reconstitution across synaptic partners (GRASP), allows detection of cell-cell contacts (Feinberg et al., 2008). One GFP fragment containing ten of its beta-barrel structures (spGFP1-10) is expressed in one cell type, the second GFP fragment, the eleventh beta-barrel (spGFP11), is expressed in a connected cell type. Both GFP fragments are located extracellular and carry a membrane tag. Close cell-cell contacts like synapses induce whole, detectable GFP formation. If the spGFP1-10 is fused to the neuronal synaptobrevin (nSyb) protein, this nSyb::GRASP will only label active synapses (Macpherson et al., 2015).

Another possibility to visualize synapses is overexpression of pre- or postsynaptic proteins tagged with a fluorescent protein. Brp-Short-mStraw, a fragment of the Bruchpilot protein tagged with

mStrawberry, localizes in the presynaptic active zones (Mosca and Luo, 2014). The Synaptic Tagging with Recombination (STaR) method also labels Bruchpilot, but induces a V5 tag to the endogenous protein in a cell-type specific way, depending on flippase mediated removal of a stop codon (Chen et al., 2014b). Postsynaptic areas can be labeled by overexpression of tagged receptors. For example, the GFP tagged nicotinic acetylcholine receptor subunit $\text{D}\alpha 7$ -GFP can be used to label cholinergic synapses (Mosca and Luo, 2014).

Labeling of Neuronal Activity in Fixed Tissue

Staining of active neurons can help to identify cells involved in a neuronal circuit. In the 1980s, a radioactive staining using tritiated $[3\text{H}]2$ -deoxy-D-glucose allowed detection of activity in the fly brain (Buchner and Buchner, 1980). The active neurons have a higher uptake of $[3\text{H}]2$ -deoxy-D-glucose, which can be detected by autoradiography of the fixed tissue detecting accumulated radioactive deoxyglucose. While this staining method reveals areas in the neuropils with high activity, it does not label single cell types.

More recent methods use activity dependent expression of fluorescent proteins. The calcium-dependent nuclear import of LexA (CaLexA) method uses a transcription factor that is located in the nucleus only in active neurons (nuclear factor of activated T cells or NFAT) linked to a LexA. The expression of the LexA-VP16-NFAT is dependent on GAL4. Inside the nucleus, the LexA can start transcription of a GFP gene under control of LexAop (Masuyama et al., 2012). The calcium-modulated photoactivatable ratiometric integrator (CaMPARI) method uses a fluorescent protein that, provided coincident illumination with violet light and high intracellular calcium levels, changes its emission from green to red (Fosque et al., 2015). Therefore, neurons with high activity can be distinguished from neurons with a lower activity.

These methods can shed light onto an unknown circuit and proof which neurons are involved in stimulus perception. The disadvantages are that they only stain highly active neurons and the cells have to be stimulated over a long period. In addition, they require antibody staining or autoradiography of the fixed tissue.

Connectomics

The little nematode worm *Caenorhabditis elegans* was the first (and so far the only) animal with a complete reconstructed connectome (White et al., 1986). The connectome of *Caenorhabditis elegans* was reconstructed from serial ultrathin sections using transmission electron microscopy, for which the thin slices had to be cut manually. While this small nematode with its 302 neurons is an exceptionally simple model organism, the size of the *Drosophila* brain, containing about 100.000 neurons, poses a bigger challenge. Nevertheless, the technical improvements in electron microscopy techniques enable faster sampling and 3D reconstruction of neurons. Serial block-face scanning electron microscopy allows to obtain data from larger volumes (Denk and Horstmann, 2004). Thereby, an ultramicrotome inside a vacuum chamber removes around 30 nm of the tissue

surface, which is scanned subsequently. The process is automated to achieve fast scanning of large volumes. Another improvement was achieved by using a focused ion beam combined with scanning electron microscopy: a gallium ion beam removes a layer of the tissue surface resulting in serial images (Knott et al., 2008; Bushby et al., 2011). The serial section transmission techniques enable scanning of the whole *Drosophila* brain. However, the biggest challenge became processing the huge amount of data and optimizing computer reconstructions (Boergens et al., 2017).

The connectome of the smaller brain of the *Drosophila* larva is within reach with its mushroom body and eye networks being fully reconstructed (Schneider-Mizell et al., 2016; Larderet et al., 2017). Part of the adult brain like connections in the mushroom body α lobe are already reconstructed (Takemura et al., 2017). A big effort was put into solving the connectomics of the motion vision pathway neurons in the medulla and the lobula (Takemura et al., 2013, 2017; Shinomiya et al., 2019) and their output neurons in the lobula plate (Boergens et al., 2018). In a recent project, the whole adult brain of *Drosophila* was scanned, and so far parts of the olfactory circuit were reconstructed (Zheng et al., 2018).

1.3.3 Manipulating Neuronal Function

Blocking Neurons

Blocking neuronal activity is important to learn more about the role of a neuron within its circuit. An effective way to block neuronal function is expression of pro-apoptosis genes like *hid* or *reaper*. These genes induce programmed cell death in the cell type of interest (Zhou et al., 1997). However, by killing a neuronal cell type, the architecture of the circuit could change due to the absence of this cell type during development of the circuit. Expression of proteins that block neuronal activity instead of ablating the cell can be used to reduce side effects on the connected or surrounding neurons.

Expression of the tetanus toxin light chain (TeTxLC) disturbs neuronal function (Fig. 1.4 a). TeTxLC cleaves the v-SNARE protein synaptobrevin (Ahnert-Hilger et al., 1989), which binds to the t-SNARE protein syntaxin. This process is essential for membrane fusion during exocytosis of neurotransmitters (Broadie et al., 1995; Sweeney et al., 1995). In this way, TeTxLC expression blocks the output of the neuron (Baines et al., 1999). The signaling within the cell remains normal and TeTxLC expression does not affect electrical coupling.

Another method to block neurons is expression of a potassium channel, which can open at resting membrane potential and prevents depolarization of the neuron. The most prominent example is the the inwardly rectifying potassium channel Kir2.1 (Fig. 1.4 b). This channel hyperpolarizes the cell and therefore blocks its normal function (Paradis et al., 2001). A GFP tag enables to detect the Kir2.1 expression. In contrast to TeTxLC expression, Kir2.1 effects are not restricted to chemical synapses because the hyperpolarization can spread to electrically coupled cells.

A less disruptive blocking method is overexpression of the *shibire temperature-sensitive1* (UAS-*shibire*^{ts}), a mutant version of *shibire* (Fig. 1.4 c). The *shibire*^{ts} mutation was found in a screening

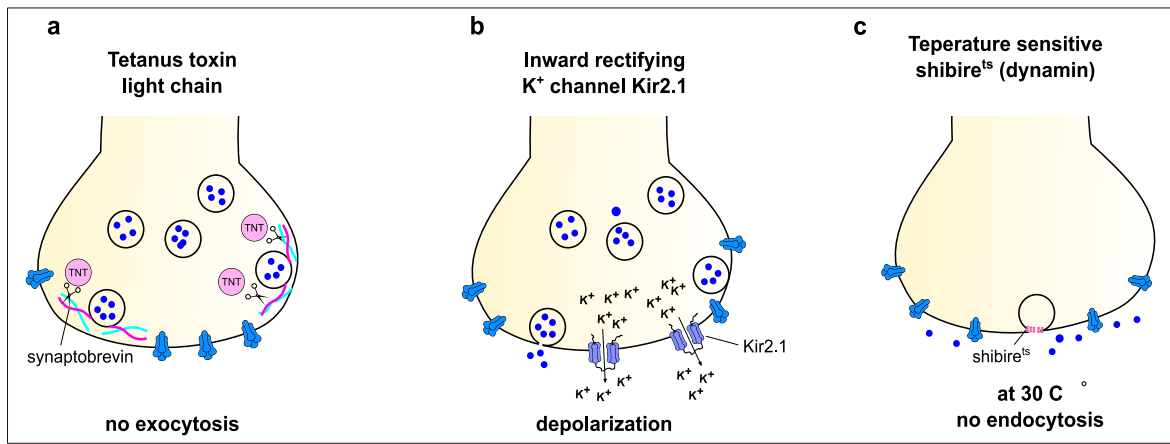


Figure 1.4: Blocking Neuronal Function.

a The tetanus toxin light chain cleaves synaptobrevin, which prevents exocytosis. **b** Overexpression of the inwardly rectifying potassium channel Kir2.1 induces a hyperpolarization of the neuron. **c** A temperature sensitive method to block neurons is overexpression of the dominant negative shibire^{ts}. At high temperatures, the dysfunctional shibire inhibits endocytosis.

for temperature dependent paralysis (Grigliatti et al., 1973). At temperatures above 30°C, the mutant flies quickly became paralyzed but walked in a normal way at lower temperatures. The protein encoded by the *shibire* gene turned out to be the *Drosophila* dynamin, a protein important for vesicle recycling (Chen et al., 1991). Dynamin induces the membrane pinch-off during the membrane fission process of endocytosis by GTPase activity (Poodry and Edgar, 1979; Kosaka and Ikeda, 1983). The *shibire^{ts}* mutation is semidominant, heterozygous flies exhibit the temperature sensitive phenotype. The dominant effect of the mutation is likely due to the function of dynamin in a multimeric complex. If some proteins are dysfunctional in their GTPase activity, this affects the whole complex and inhibits the membrane pinch-off (Antonny et al., 2016). Overexpression of *shibire^{ts}* blocks endocytosis at temperatures above 27°C (Kitamoto, 2001). Since the protein functions normally at lower temperatures, *shibire^{ts}* overexpression provides an internal control. Reducing the temperature again after a period of high temperature results in normal neuronal function after several minutes of recovery. Therefore, expression of *shibire^{ts}* is the least destructive way of blocking neuronal activity. Similar to expression of TeTxLC, *shibire^{ts}* overexpression only blocks chemical synapses.

Optogenetic Effectors

In the last decade, optogenetic activation or inactivation of neurons became more and more utilized in science. Optogenetics uses genetically encoded light-sensitive ion channels and ion pumps. The use of light introduces a new level of spatial and temporal control to manipulate neuronal activity. The first light activation of neurons was achieved by expression of arrestin-2, rhodopsin and a G α subunit (Zemelman et al., 2002). The first manipulating of neuronal activity and fly behavior with

light was achieved by activation of an ATP-gated cation channel. Thereby, caged ATP was injected into flies expressing the ionotropic purinoceptor P2X₂ in all neurons. Light induced uncaging of ATP activated the receptor and subsequently the neurons (Lima and Miesenböck, 2005). Since these experiments, the use of optogenetic methods rapidly increased. Channelrhodopsin, an ion channel from the green algae *Chlamydomonas reinhardtii*, opens after activation with 470 nm light (Nagel et al., 2003). Expression of channelrhodopsin in larval motor neurons resulted in fast depolarization after illumination of the larvae (Schroll et al., 2006). There are several versions of channelrhodopsin available, some are activated by different light wavelengths. For example, Chrimson and Chronos are versions of Channelrhodopsin with the light sensitivity shifted towards red or violet light, respectively (Klapoetke et al., 2014). This allows independent activation of two different neuronal populations. Compared to activating neurons by expression of the thermosensitive cation channel dTrpA1, which opens at 30 dg Celsius (Rosenzweig et al., 2005), optogenetic activation occurs without a temperature shift and at a fast timescale (Pulver et al., 2009).

Optogenetic effectors are also used to block neurons by opening a light sensitive chloride pump. Such a chloride pump from halobacteria, Halorhodopsin, is activated by 593 nm light (Zhang et al., 2007). Another light-gated anion channel discovered in an algae species, GtACR, is more light-sensitive than Halorhodopsin (Govorunova et al., 2015). Expression of GtACR1 enables reversible and effective silencing of neurons (Mauss et al., 2017). Inactivating neurons with chloride pumps while recording behavior or imaging calcium levels of downstream neurons will further increase our understanding of neuronal circuits. The advantage of optogenetic activation or blocking of neurons is the fast timing with changes of the membrane potential in milliseconds. Before light activation, the neurons are not affected and animals can display a normal behavior.

1.3.4 Recording Neuronal Activity

Electrophysiology

Neurons transfer information by releasing neurotransmitters to their downstream partners. This neurotransmitter release is preceded by changes in membrane potential. To access neuronal function, the electrical activity can be measured directly with electrophysiological methods. They allow detection of membrane potential changes with a very high temporal resolution. The first electrophysiological recordings of fly neurons were performed in blowflies and houseflies. Extracellular recordings with sharp electrodes identified motion sensitive areas in the *Calliphora* and *Musca* eyes (Bishop et al., 1968; McCann and Dill, 1969). Due to their small size, intracellular or extracellular recordings with sharp electrodes are technically challenging for most *Drosophila* neurons. Such recordings were restricted to cells with larger somata like motor leg neurons and muscles (Ikeda and Kaplan, 1970; Levine and Tracey, 1973) or the *Drosophila* giant fibers, which are large descending neurons (Tanouye and Wyman, 1980; Thomas and Wyman, 1984).

The development of the whole-cell patch-clamp technique (Sakmann and Neher, 1984) enabled recordings of smaller *Drosophila* neurons. This method uses micropipettes with relatively large

openings, which are moved on the membrane to establish a high resistance seal. Gentle suction or current pulses rupture the membrane, which allows electrical access to the neuron. Whole-cell patch-clamp recordings of *Drosophila* neurons were first performed in developing neurons of the embryo (Baines and Bate, 1998). Different types of adult neurons were recorded in the last decade like neurons in the antennal lobe (Wilson et al., 2004), mushroom body Kenyon cells (Turner et al., 2008; Groschner et al., 2018) and large tangential neurons of the lobula plate (Joesch et al., 2008). Despite the progress with whole cell patch clamp recordings, many *Drosophila* neurons are very challenging to record from due to their small size. Therefore, investigation of their membrane potential remains difficult.

Calcium Imaging

Before the development of genetically encoded calcium indicator proteins, calcium sensitive dyes like Fura-2 (Grynkiewicz et al., 1985) were applied to cell cultures (Barreto-Chang and Dolmetsch, 2009). Such chemical sensors are often based on mild chelators combined with fluorescent domains, whose excitation characteristics change rapidly with the amount of bound calcium. Genetically encoded calcium indicators, on the other hand, fostered *in vivo* calcium imaging in restricted neuronal populations as their expression can be driven by cell-type specific promoters (Reiff et al., 2005). Such indicators are either based on energy transfer between two fluorophores (Förster Resonance Energy Transfer or FRET), like the troponin C variants (Heim and Griesbeck, 2004; Mank et al., 2006), or indicators based on a single fluorescent proteins like GCaMP. GCaMP proteins consist of a GFP, calmodulin and M13, which is a peptide from the myosin light chain binding to calmodulin (Miyawaki et al., 1997; Nakai et al., 2001). There are several different variants of GCaMP available, with improvements in terms of their brightness level and kinetics. Currently, the variants of the CGaMP6 generation are widely used (Helassa et al., 2016a,b).

The advent of two-photon laser scanning microscopy (Denk et al., 1990) revolutionized the possibilities of neuronal activity imaging. Two photon imaging of GCaMP activity signals (Yuste and Denk, 1995; Wang et al., 2003) allows to measure neurons that are inaccessible for electrophysiological methods due to their size or location. The two-photon microscope uses infrared light pulses with a very small pulse duration of about 100 fs and a high laser pulse repetition rate of about 100 MHz (Helmchen and Denk, 2005). Two photons of a long wavelength and therefore low energy can excite a fluorophore if both are absorbed simultaneously. Compared to confocal laser microscopy with pinhole apertures, the resolution is lower, but the infrared light can penetrate the tissue deeper. Other advantages of two photon microscopy are the lower bleaching of the fluorophore and the reduced background signal. Therefore, two photon microscopy enables imaging of calcium activity with a high spatial and temporal resolution.

Using two photon microscopy and cell type specific GCaMP expression enables activity recording of every *Drosophila* neuron. The calcium imaging can be combined with recording behavior like walking (Seelig et al., 2010; Chiappe et al., 2010). A disadvantage of GCaMP calcium imaging is

the low temporal resolution compared to electrophysiological methods, since the neuronal cytosolic calcium transients are slower than the voltage changes. In addition, the calcium sensor acts as a calcium buffer, changing the calcium dynamics in the cell (Borst and Abarbanel, 2007).

Voltage Sensors

A more direct way to image neuronal activity is the use of genetically encoded voltage sensors, which detect the changes in membrane potential. In the last years, several new voltage indicators were developed, but the signal-to-noise ratio is still low. In contrast to calcium indicators, voltage sensors must be transmembrane proteins. Most of the genetically encoded voltage sensors consist of a voltage sensing domain from a phosphatase linked to a fluorescent protein. Two promising voltage sensors developed in the last years and tested *in vivo* are ArcLight and ASAP. The ArcLight sensor consists of a voltage sensing domain from a tunicate phosphatase fused to super ecliptic pHluorin GFP (Jin et al., 2012). ArcLight was successfully tested in *Drosophila* clock neurons and neurons of the olfactory system (Cao et al., 2013). The ASAP1 (short for accelerated sensor of action potentials 1) protein consists of a chicken voltage sensing domain linked to an extracellular GFP variant, which is a circularly permuted superfolder GFP (St-Pierre et al., 2014). Two variants of ASAP1 with slightly higher sensitivity, ASAP2f and ASAP2s were expressed and imaged in lamina neurons of the *Drosophila* optic lobe (Yang et al., 2016; Chamberland et al., 2017). With improving signal to noise ratios and already fast kinetics, voltage sensors might become an important tool in the next years.

1.3.5 Transcriptomics

The transcriptome of neurons, which means the sum of their RNA transcripts, emerges as an important field with new technologies enabling better high-throughput sequencing. To study RNA differentially expressed between cell types is important in many different research fields. In neuroscience, the genes related to neuronal function, like synapse proteins, are of particular interest. The increasing transcriptomic data from *Drosophila* neurons will help to unravel biophysical details of functional properties by revealing the repertoire of ion channels, neurotransmitters and receptors of specific neuronal cell types. Furthermore, it will help to understand how closely related neurons establish their specific properties by differential expression of transcription factor combinations and their effectors. Comparing the transcriptome of developing neurons to adult neurons can demonstrate the upregulation of genes important during development, thereby elucidating what controls neuronal differentiation.

Two different approaches are used to achieve cell-type specific transcriptomics: single cell RNA sequencing (scRNA-seq) and bulk RNA sequencing from a purified cell type. Single cell sequencing allows comparison of many cell types. The technologies for single cell RNA-seq are becoming more efficient with deeper sequencing depths. Recent studies achieving single cell data from the whole *Drosophila* brain, the midbrain or the optic lobes (Davie et al., 2018; Croset et al., 2018;

Konstantinides et al., 2018) used high throughput methods like the nanoliter droplets (Drop-Seq or inDrop) method (Macosko et al., 2015; Klein et al., 2015). While single cell sequencing does not give a full representation of the transcriptome of a cell, it can identify enough genes specifically expressed to compare related cell types. For example, single cell sequencing could reveal differences between olfactory projection neuron subtypes (Li et al., 2017b).

However, RNA sequencing of a purified cell type using a high number of cells from many animals results in a more complete transcriptome. To purify nuclei of one cell type, these cells have to be specifically labeled. With the growing number of split-GAL4 lines, more and more cell types can be purely labeled. The GFP expressing nuclei are either isolated by FACS sorting (Harzer et al., 2013) or with the help of streptavidin-coated magnetic beads binding to an anti-GFP antibody (INTACT or isolation of nuclei tagged in specific cell types method) (Deal and Henikoff, 2011). Adding a second purification step with magnetic beads enhances the specificity of the sample (TAPIN or Tandem affinity purification of intact nuclei) (Davis et al., 2018).

1.3.6 Manipulating Gene Function

Loss-of-Function Mutants

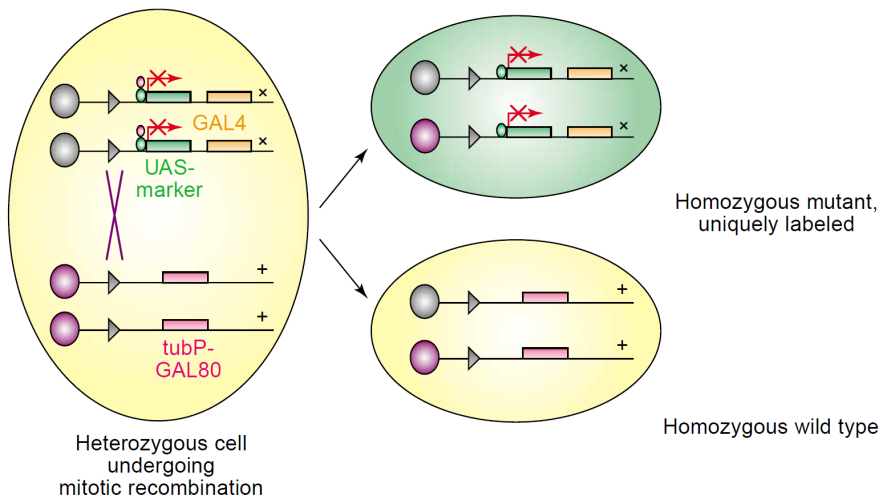


Figure 1.5: Mosaic Analysis with a Repressible Cell Marker (MARCM).

Flippase-FRT mediated mitotic recombination induces homozygous mutant clones with expression of a marker gene in a heterozygous mutant background. Image modified from Lee and Luo (2001).

Since Thomas Morgan's description of the *white* mutant (Morgan and Cattell, 1912) and Hermann Muller's directed mutagenesis (Muller, 1927), *Drosophila* mutants were used to understand the function of the disrupted gene of interest. Many mutations are homozygously lethal and the phenotype can, for example, just be examined in the embryo. A possibility to overcome this problem are single, homozygous mutant cells. The advantage of mutant clones is that the surrounding cells

are unaffected, thus the mutant cells can be directly compared to wild type cells. Furthermore, affecting either a high number of cells or sparse cells can change the effect of a mutation. Such mutant clones are generated by mosaic analysis with a repressible cell marker (MARCM, see Fig. 1.5) (Lee and Luo, 2001). MARCM works in a background heterozygous for the mutation and with a cell-type specific marker suppressed by ubiquitously expression of GAL80. Heat shock induced translation of a flippase induces recombination during mitosis, resulting in sparse cells homozygous for the mutation and cells homozygous for the GAL80 insertion. Therefore, the mutant clones can express the marker gene to label their morphology.

Loss of Function - MiMIC Insertions

The *Minos*-Mediated Integration Casette (MiMIC) lines are a collection of fly lines with MiMIC insertions in most *Drosophila* genes. The MiMIC insertions are useful for gene disruption as well as protein tagging (Venken et al., 2011; Nagarkar-Jaiswal et al., 2015). Compared to P-elements, which are unlikely to insert into introns (Aleksic et al., 2009), *Minos* elements are less biased in their insertion sites. The MiMIC insertions can disrupt gene function, making such MiMIC lines useful as mutant lines. About half of the intragenic MiMIC lines are inserted in coding regions. The cassette contains a stop codon in three reading frames (Fig. 1.6 a), if it is inserted in the same orientation as the gene, it can be used as a gene trap. Since the cassette is flanked by two phiC31 integrase *attP* sites, the sequence can be exchanged with any other cassette. By recombinase-mediated cassette exchange with an artificial exon containing a *eGFP* sequence and a splice donor, the endogenous protein can be tagged with *eGFP* (Fig. 1.6 b) (Nagarkar-Jaiswal et al., 2015). Such an insertion allows, for example, knockdown of the gene by expression of GFP-RNAi.

The MiMIC insertions can also be exchanged with a sequence disturbing the gene function. For instance, the FlpStop method uses MiMIC lines with insertions in the coding intron for cell-type specific gene disruption (Fisher et al., 2017). In the non-disrupting orientation, the FlpStop cassette is removed by RNA splicing. If a flippase is expressed, the orientation becomes inverted and a stop signal blocks transcription. The flip event also enables expression of the marker *tdTomato*. Crossed to a mutant line, the FlpStop method can label homozygous mutant cells.

Loss of Function - RNA Interference

The discovery of the RNA interference (RNAi) mechanism opened completely new possibilities to study gene function. RNA interference is a cellular response to exogenous, double-stranded RNA (dsRNA) or endogenous microRNA (Fig. 1.7). RNA interference is evolutionary conserved throughout eukaryotic species. It was first described in the nematode *C. elegans* (Fire et al., 1998). Exogenous dsRNA is cut by the RNase Dicer-2 together with the dsRNA binding protein R2D2 into small interfering RNA fragments (siRNA) (Liu et al., 2006b). These siRNA fragments build a complex with Argonaute-2, an endonuclease, and heat shock chaperones (Hammond et al., 2001; Nakanishi, 2016). They form the RNA-induced silencer complex (RISC), in which one strand of the

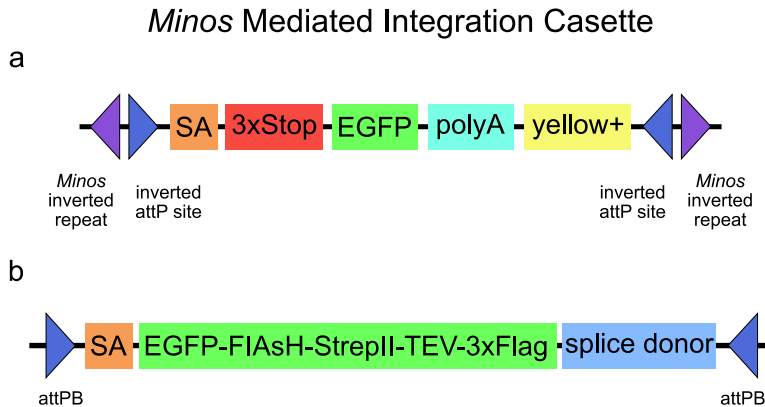


Figure 1.6: *Minos*-Mediated Integration Cassettes.

a MiMIC transposons carry a splice acceptor site (SA), stop codons in three reading frames, a *GFP* sequence, a polyadenylation signal and a *yellow+* marker. Dependent on the insertion site, a MiMIC transposon can disrupt gene expression. In addition, the attP sites allow to replace the sequence within the cassette. **b** MiMIC insertions in introns can be used to tag the endogenous protein, by exchanging the MiMIC with a cassette containing a splice acceptor site, a modified *eGFP* sequence and a splice donor. The GFP is flanked with a linker to enable binding to the protein of interest.

siRNA can target complementary mRNA (Pham et al., 2004). The target mRNA is subsequently cleaved and degraded. This process can be used to knock down a gene of interest.

The first attempt to use RNA interference for gene knockdown was injection of dsRNA into *Drosophila* embryos (Misquitta and Paterson, 1999). Comparison with mutant phenotypes revealed the effective downregulation mediated by the dsRNA. Overexpression of dsRNA is an easy tool for cell type specific gene silencing. Several RNAi-line libraries with UAS-dsRNA constructs are available for *Drosophila*. They cover thousands of target genes, very extensive libraries are the Harvard TRiP lines, the GD, KK and shRNA lines from the Vienna Drosophila Resource Center library and NIG lines from Kyoto (Dietzl et al., 2007; Cook et al., 2010; Hu et al., 2013, 2017).

The most efficient RNA interference constructs are short hairpin RNA (shRNA), which is dsRNA that forms a hairpin turn. Expression of shRNA can achieve a strong knockdown of gene expression, even without the co-expression of transgenic Dicer-2 (Bartolletti et al., 2017). Such shRNA lines are used by the second generation valium vector TRIP lines from the Harvard Medical and the shRNA stocks from the VDRC stock collection. A disadvantage of dsRNA expression are the possible Off-targets. The RISC complex sometimes binds to partly homologous sequences in the 3'UTR region of other mRNAs, which is a major source of off-target effects (Ma et al., 2006).

The endogenous, small non-coding microRNAs are an efficient cell intrinsic way to regulate translation. The first microRNA was described in *C. elegans* (Lee et al., 1993). MicroRNAs are highly conserved, they have a far more extensive role than was anticipated in the first years after their discovery. MicroRNA undergoes preprocessing in the nucleus (Fig. 1.7). There, the pri-

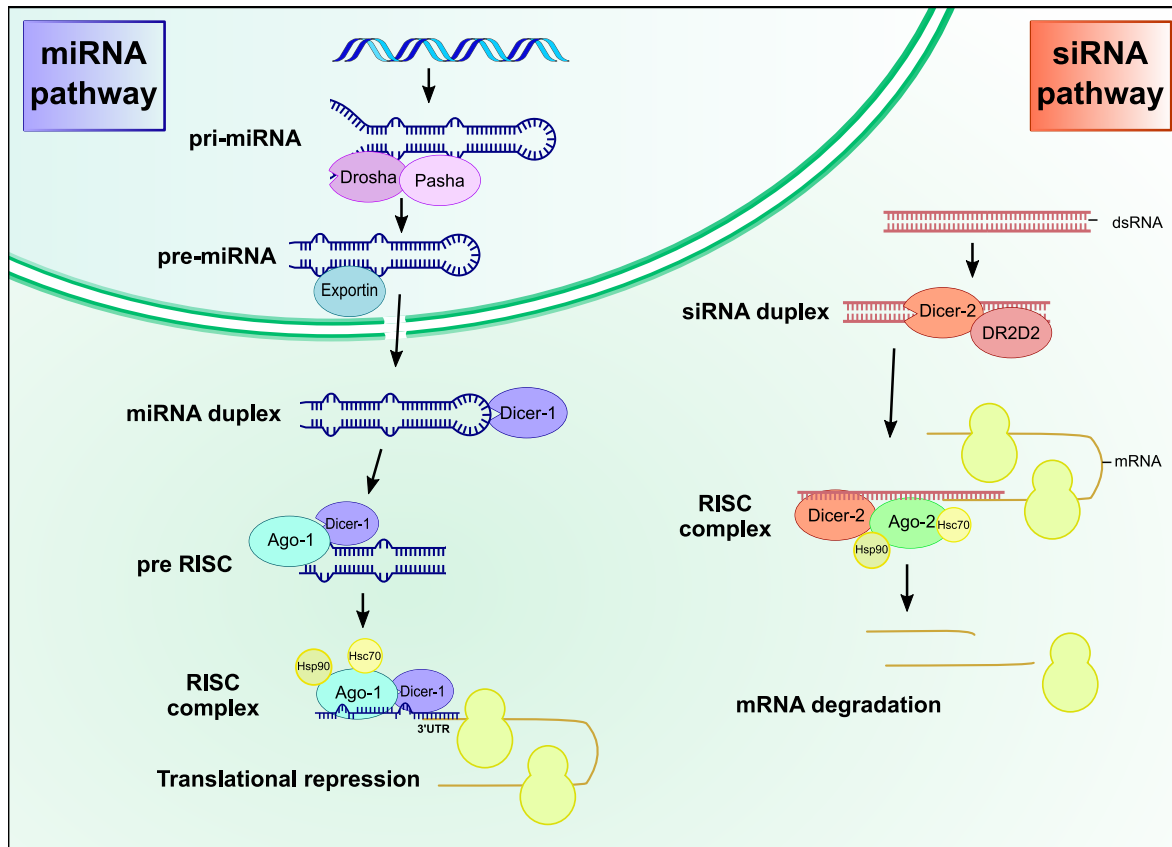


Figure 1.7: RNA Interference Pathways

MiRNA is expressed by the cell itself to control gene expression. The pri-miRNA is modified in the cell nucleus before it is transported into the cytoplasm. Here, miRNA and exogenous dsRNA are processed similarly. Yet, the RISC complexes are built up of slightly different proteins. The miRNA RISC complex contains Ago-1 and Dcr-1, binding to mRNA blocks the translation. In comparison, the dsRNA is processed by a RISC complex containing Dcr-2 and Ago-2. Binding of mRNA by the dsRNA-RISC complex results in mRNA degradation.

miRNA is modified by the dsRNA binding protein Pasha and the RNase Drosha into the pre-miRNA with short hairpin structures (Yeom et al., 2006; Lee et al., 2003). Subsequently, the pre-miRNA is transported to the cytoplasm, where the RNase Dicer-1 recognizes its loop structures (Tsutsumi et al., 2011). It processes the pre-miRNA into smaller fragments, similar to the dsRNA treatment by Dicer-2 (Lee et al., 2004; Jiang et al., 2005). These small RNA fragments are also included into a RISC complex, where they bind to Argonaute-1 (Miyoshi et al., 2005). In comparison to the guide strand of siRNA, the miRNA strand binds only partially to its complementary strand, mediated by Argonaute-1 (Förstemann et al., 2007). The miRNAs target the 3'UTR region of mRNA with an imperfectly complementary site (Lai, 2002). This partial mismatch does not allow Ago-catalyzed cleavage of the mRNA, instead the translation is blocked.

In the recent years, the number of described miRNAs increased rapidly. Developmental and

behavioral consequences of miRNA mutants or miRNA overexpression, as well as their specific gene regulation became an important topic (Kim et al., 2014; Chen et al., 2014a; Busto et al., 2015; Picao-Osorio et al., 2017). There are two possibilities to explore the functional role of miRNAs: to study the phenotype of mutant flies or downregulation of miRNAs with sponge RNA expression (Ebert et al., 2007), which are RNAs with a complementary binding site. Another possibility to regulate microRNA levels are antisense oligonucleotide inhibitors (Meister et al., 2004). MiRNAs could, for example, regulate the development of a neuronal circuit by controlling the levels of transcription factors in related cell types.

Gain of Function

Silencing of genes does not always induce a phenotype for various reasons: the knockdown might be incomplete and the still existing low protein level might be enough to ensure normal. Moreover, protein function can be redundant to other proteins and, in this case, silencing just one has no or only minor effects. Instead of a knockdown, gain-of-function experiments like overexpression can provide information about gene function. In addition, the expression levels of many genes are tightly controlled and even slight changes in either direction can result in a strong phenotype. Gain-of-function experiments can also mean misexpression by expression in other cell types or changing the time-point of expression. The first gain-of-function experiments used a heat shock promoter to drive expression of a gene, with the advantage of a controlled onset by temperature change (Struhl, 1985; Schneuwly et al., 1987; Ish-Horowicz and Pinchin, 1987). Nevertheless, the expression was not cell-type specific but ubiquitous. Using promoters from characterized genes resulted in a more specific expression (Parkhurst and Ish-Horowicz, 1991).

With the establishment of the UAS-GAL4 system in *Drosophila*, the possibilities of gain-of-function experiments were enhanced tremendously. UAS driven overexpression of a gene was used quickly after the establishment of the GAL4-UAS system (Staehling-Hampton and Hoffmann, 1994; Kraus and Lis, 1994; Luo et al., 1994). Compared to transcription controlled by a heat shock promoter, this allowed cell-type specific overexpression and ectopic misexpression.

Instead of the wild type protein, overexpression of mutant versions is often used. Dominant negative mutant proteins block the normal function of the endogenous wild type protein (Herskowitz, 1987). By the use of the GAL4-UAS system, screenings with panneuronal overexpression of wild type or mutant gene variants became possible, searching for the neuronal function of a gene (Luo et al., 1994). Besides dysfunctional mutant genes, also constitutive active version can be used for gain-of-function experiments (Brand and Perrimon, 1994). The GAL4-UAS system also allows screening for misexpression effects by random insertions of P vector carrying UAS sites. The genes near such an insertion will be expressed driven by a GAL4 line (Rørth, 1998).

Gene Editing using CRISPR

A cell specific targeting of genes is possible with the more recent clustered regulatory interspaced short palindromic repeat (CRISPR) method (Ishino et al., 1987; Jansen et al., 2002; Garneau et al., 2010). It is adapted from a bacterial defense system against bacteriophages. The simplest version of CRISPR mediated genome editing, the type II CRISPR-Cas9 system, uses three main components: a CRISPR RNA (crRNA), a *trans-encoded* crRNA (tracrRNA) and the nuclease Cas9 (Jinek et al., 2012; Mali et al., 2013). The pre-crRNA targets a complementary DNA sequence (Brouns et al., 2008; Gasiunas et al., 2012), while the small tracrRNA binds to the pre-crRNA forming an RNA double helix (Deltcheva et al., 2011). Together they recruit the Cas9 protein to the target sequence, where the Cas9 induces DNA double strand breaks. To simplify the application of the CRISPR method, a chimera of both the crRNA and the tracrRNA was created (Jinek et al., 2012). This single guide RNA (or sgRNA) can not only mark the target sequence, but also form a complex with Cas9. This system allows to modify any gene of interest.

Mutagenesis can now be achieved by crossing flies with an ubiquitous expression of sgRNA under control of the Pol-III promoter U6:3 or U6:2 (Huang et al., 2017) to a line with germline specific expression of Cas9 (for example, under control of a *nanos* promoter) (Ren et al., 2013; Bassett et al., 2013; Sebo et al., 2014; Port et al., 2014). The Cas9 induces double strand breaks into the coding sequence of the gene. In this process, DNA modifications are achieved with a higher efficiency by expression of two sgRNAs. GAL4 driven Cas9 expression results in a cell-type specific knockout (Xue et al., 2014).

This approach is already advanced enough to generate a large scale collection of sgRNA lines as well as optimized tissue specific Cas9 lines (Ren et al., 2013; Chavez et al., 2015). The Harvard Medical School and the German Cancer Research Center established a library for CRISPR mediated knockout, the TRIP-KO lines. They provide U6:3-sgRNA fly lines that express the sgRNA ubiquitously. Since the CRISPR method has almost endless possibilities, it will enable more precise regulation of gene expression by, for example, CRISPR knockout of regulating non-coding RNA (Ghosh et al., 2016).

One advantage of CRISPR methods is, that they can not only be used to induce mutations but also for gene overexpression. This can be done by preventing the nuclease activity of Cas9: an inactive version of the protein, the nuclease-null Cas9 or deadCas9/dCas9 (Mali et al., 2013), binds to the target gene without inducing double strand breaks. This inactive nuclease is fused to a transcriptional activator domain like the chimeric VPR activator domain containing a VP64, a p65 and an Rta domain (Gilbert et al., 2013; Chavez et al., 2015). The dCas9-VPR is functioning *in vivo* in *Drosophila* and can induce overexpression phenotypes (Lin et al.). As for CRISPR mediated knockout, the Harvard Medical School is establishing a fly line library for CRISPR based activation (CRISPRa) (Ewen-Campen et al., 2017; Jia et al., 2018).

Since dCas9-VPR is very effective but requires two sgRNAs, the Harvard Medical School established the flySAM approach (Konermann et al., 2015; Jia et al., 2018), which uses the dCas9-VP64

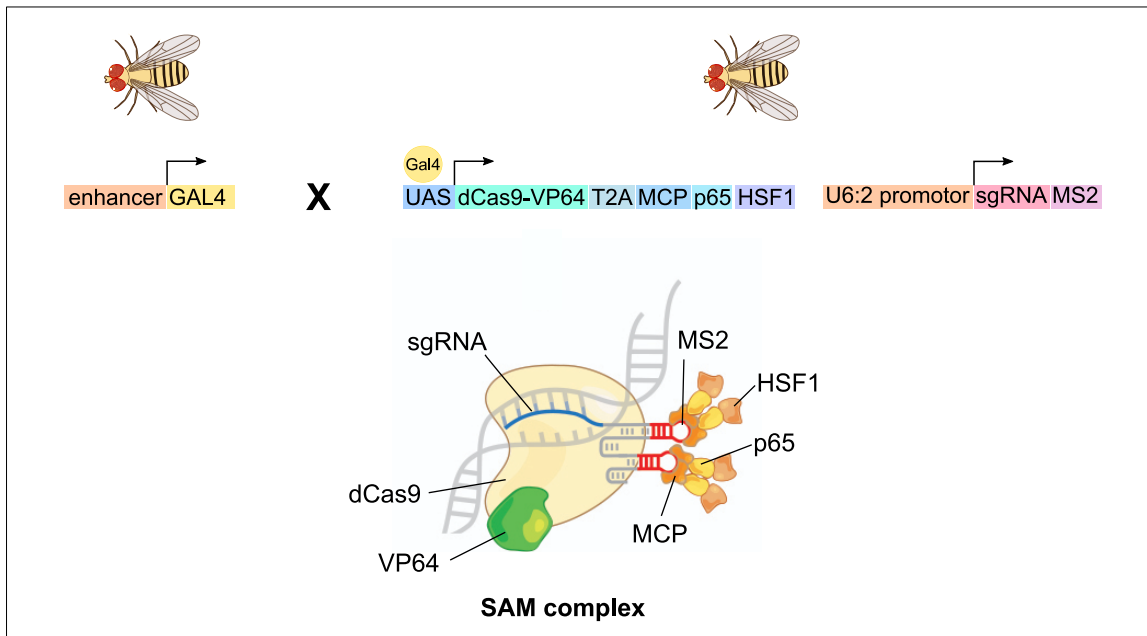


Figure 1.8: Transcriptional Activation with CRISPRa flySAM2.0.

The sgRNA is expressed ubiquitously and targets the gene of interest. Expression of dCas9 and the synergistic activation mediator SAM (MCP, p65 and HSF1) is controlled by GAL4. The SAM mediator binds to the MS2 aptamers of the sgRNA. Together with the dCas9-VP64 it drives expression of the gene of interest. The overexpression is cell-type specific and results in strong activation. SAM complex picture modified from Konermann et al. (2015).

in combination with a low expression of a modified synergistic activation mediator (SAM). The SAM mediator consists of MCP-p65-HSF1 (Fig. 1.8), which is a transactivation chimera together with the MS2 bacteriophage coat protein (MCP). The MCP is recruited to MS2 hairpin structures added to the sgRNA. The SAM genes are combined into a single vector with the sgRNA, reducing the transgenes necessary. Both dCas9-VP64, as well as the (at high levels toxic) SAM proteins, are expressed under control of a 10xUAS. The dCas9-VP64 together with the SAM complex can activate strong gene expression without the requirement of a second sgRNA. The flySAM collection lines contain the UAS-dCas9, the SAM genes and the U6:2-sgRNA-MS2 constructs, therefore the fly can be directly crossed to a GAL4 line.

The advantage of CRISPR activation compared to UAS overexpression is the possibility to overexpress genes with multiple isoforms or large genes, which are difficult to clone. While GAL4-UAS based expression can result in extremely high protein levels, dCas9 mediated gene activation results in more physiological levels (Chavez et al., 2015).

1.4 Visual Behavior of *Drosophila*

At first glance, fruit flies may appear to be very simple animals, but they exhibit a broad repertoire of visually driven behavior. Their motion vision enables fruit flies to keep their path, avoid predators or track an attractive object. The first experiments testing visual responses of fruit flies examined which wave lengths they detect and described simple light driven behavior. The most obvious visual behavior of flies is phototaxis, which means a tendency to walk towards light (McEwen, 1918). Thereby, fruit flies react to a spectrum from UV light to green light, with a preference for shorter wavelengths (Lutz and Richtmyer, 1922; Bertholf, 1932). Flies became a broadly used model organism for visual behavior in short time due to several reasons. Visual behavior of flies is mostly hard-wired and reflexive, with a low variability between individuals. When flying, flies react to motion in all directions and over a wide range of velocities. Visual stimulation can elicit extremely fast turning maneuvers of flying flies (Fry et al., 2003; Muijres et al., 2014). Since the first description of fly phototaxis, a range of visual behaviors was tested, like the response to whole field motion or avoidance behavior. Many visual responses are comparable between different insect species or can even be compared to vertebrate behavior. The behavioral assays are important to test the output of a neuronal circuit. The genetic manipulations possible in *Drosophila* enable to investigate the role of single cell types for different behavioral tasks.

Fly behavior is mainly examined under artificial conditions to control the visual stimulation. Walking or flight behavior of flies can be examined in freely moving animals or by fixing the fly at a certain position. This allows to define the visual stimulus detected by the fly. The visual stimulation used for behavioral assays are often highly simplified compared to a natural environment. Therefore, typical visual stimulation uses patterns like a sinusoidal grating, moving bars or squares.

1.4.1 The Optomotor Response

When presented whole field motion, many animals try to compensate this by moving in the same direction as the stimulus. This turning tendency along with wide-field movement of the environment is described as the 'optomotor response'. This behavior likely helps animals to keep course control and is a part of the stability reflex system. The optomotor behavior serves to maintain a straight course by compensating for involuntary body movements caused, for example, by wind during flight. In 1927, 'optomotoric reactions' of different insect species, a crab and a lizard were described. The animals were fixed and the angle of compensatory eyestalk movement or, in case of the lizard, head rotation were detected while rotating a striped cylinder around them. Moreover, this study described the walking pattern of ladybeetles and bees inside a rotating cylinder; as a response to the rotating cylinder they were walking in small circles (Schlieper, 1927). A similar behavior was observed with ladybeetles walking on a rotating board (Radl, 1903). Compensatory movements along with the environment are performed by most animals, like fishes (Lyon, 1904), lobsters (Hadley, 1906), frogs (King et al., 1993) or pigeons (Fite, 1968). A first attempt to measure the

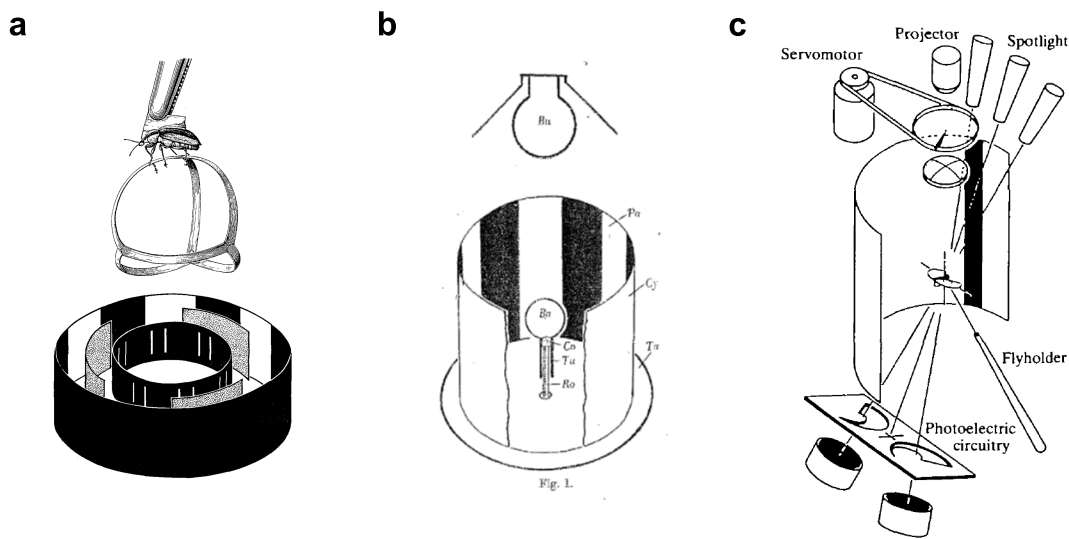


Figure 1.9: Different Setups to measure Optomotor Behavior.

a A *Chlorophanus* beetle holds onto the 'Spangenglobus', a metal Y-maze, which forces the beetle into left-right choices. The beetle is placed in the middle of three cylinders looking through slits in the inner cylinder. Movement of the middle cylinder induces motion reactions of the beetle. Image modified from Hassenstein (1961) b Flies walking in a small glass ball respond to rotation of the surrounding cylinder. Image modified from Kalmus (1943). c Flight simulator measuring the flight turns with a wing-beat analyzer, built up of light sources above the fly and photoelectrodes detecting the wing shadows through crescent shaped masks. Image modified from Götz (1987).

optomotor response quantitatively was carried out with a beetle glued to forceps located in the middle of a rotating cylinder (Fig. 1.9 a). The beetle then held on to a little metal Y-maze named 'Spangenglobus', which forces the beetle into left-right choices (Hassenstein, 1951, 1957). This enabled a quantification of the walking direction chosen by the beetle.

The optomotor response of *Drosophila* was first described in 1943 as a turning reaction of flies walking in a small glass ball (Fig. 1.9 b). Rotating a striped cylinder around the flies induced a compensatory rotational walk (Kalmus, 1943). While this setup allowed to detect the optomotor response of flies, a more quantitative measurement of the behavior was missing. A setup detecting the turning forces of flying *Drosophila* enabled to measure optomotor response turns with a high temporal resolution (Fermi and Richardt, 1963; Götz, 1964). Measuring the flight optomotor behavior of *Drosophila* in response to a cylinder rotation with a periodic pattern of different wavelengths enabled to estimate the inter-ommatidial angle of *Drosophila*. The flies stopped responding when stimulated by a rotating grating with a wavelength of 9.2° , indicating an inter-ommatidial angle of 4.6° . Presenting a grating with a lower wavelength resulted in an inverted response, due to undersampling of the pattern (Götz, 1964, 1970). Another method to measure flight turns uses the change of wing position. The difference and the sum of the wing-beat amplitudes are equivalent to the torque and thrust of the fly, respectively (Götz, 1968). Therefore, a simple setup

using a photoelectric sensor to detect the wing-beat amplitude can measure horizontal flight turns of *Drosophila* (Fig. 1.9 c). However, *Drosophila* optomotor responses are not restricted to flight behavior. To measure the optomotor response of walking flies, they can be fixed on top of a styrofoam sphere rolling over an air stream (Buchner, 1976).

Independent of the way the optomotor response was examined, two characteristics of the behavior stand out: first, the optomotor response increases with a rising stimulus contrast, but saturates for high values (Fig. 1.10 a) (Buchner et al., 1978; Duistermars et al., 2007a). Second, it is tuned to an optimal frequency (Fig. 1.10 b), not velocity (Götz and Wenking, 1973; Blondeau and Heisenberg, 1982; Duistermars et al., 2007a,b; Reiser and Dickinson, 2008). The value of such a maximal response frequency varies between the studies, but is ranging between 5 to 10 Hz.

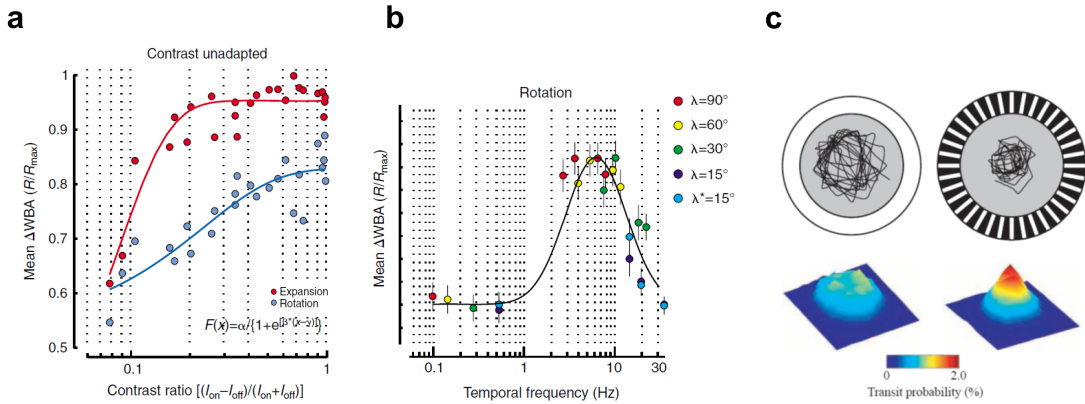


Figure 1.10: Optomotor Response Characteristics.

a The optomotor response of flying flies saturates with increasing stimulus contrast. b The optomotor response is tuned to frequency. a, b Plot modified from Duistermars et al. (2007a). c Free flight behavior with white or textured arena. The stripes induce a more narrow flight path concentrated in the middle of the arena. Plot modified from Tammero and Dickinson (2002b)

Since flight maneuvers are not restricted to horizontal rotations, the optomotor behavior of flies can follow vertical motion. The pitch optomotor responses of flies are comparable to yaw optomotor turns (Buchner et al., 1978; Blondeau and Heisenberg, 1982). In addition, head movements follow whole field motion (Hengstenberg, 1988; Duistermars et al., 2012). If flies can control the movement of their environment during a fixed flight experiment (a closed-loop experiment), they will try to avoid movement, e.g. their optomotor response enables them to stabilize their course (Heisenberg and Wolf, 1979).

Both flight and walking arenas reveal a strong influence of the visual environment on the behavior of freely moving *Drosophila* (Strauss et al., 1997; Mronz and Lehmann, 2008). In a free flight arena with a uniform background, flies moved in circles close to the wall. A textured background changed the flight path to more concentrated circles in the middle of the arena (Fig. 1.10 c) (Tammero and Dickinson, 2002b). If a textured cylinder was turning with different velocities,

the flight path became less concentrated and more distributed with increasing velocity (Mronz and Lehmann, 2008). Therefore, the optomotor response can suppress the normal flight behavior, which alternates between fast saccades and a straight course.

1.4.2 Object Orientation

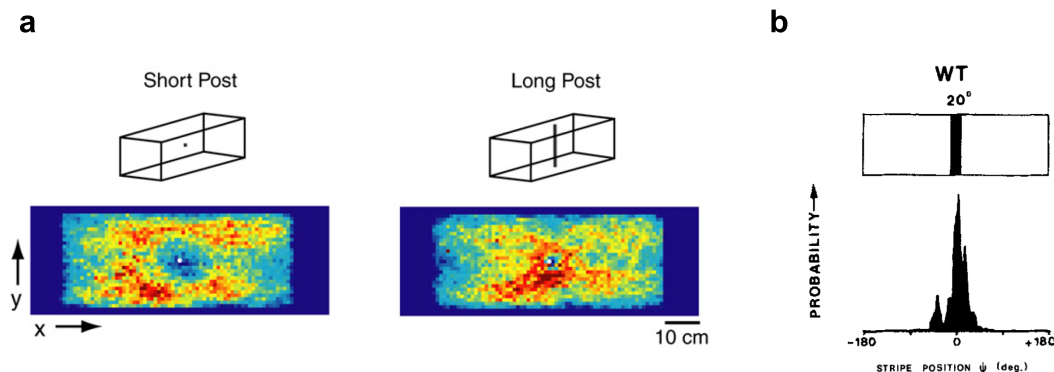


Figure 1.11: Object Orientation Behavior.

a In a free flight arena, fruit flies avoid short objects but are attracted to dark, vertical objects. Picture modified from Maimon et al. (2008). **b** Closed loop experiment with a fixed fly controlling a 20 degree dark bar. The fly keeps the bar in a frontal position. Plot from Coombe and Heisenberg (1986).

If flies are freely walking in an arena with three-dimensional objects, they spend most of the time on the tallest, steepest objects (Robie et al., 2010). Freely flying flies are attracted by long vertical objects, while avoiding short objects (Maimon et al., 2008) (Fig. 1.11 a). This likely reflects the tendency of flies to search for trees in a natural environment. If a dark vertical bar stimulus is presented to a fixed fly in a closed-loop experiment, the fly keeps the bar at a frontal position. Such a response is named a fixation behavior. The first fixation experiments were performed with *Musca domestica*. If able to control the position of a vertical dark stripe, the flies clearly kept the stripe in a frontal position (Reichardt and Wenking, 1969). Similar experiments with *Drosophila* confirmed the observations from blowflies (Fig. 1.11 b). The flies fixate dark, vertical objects in front of them (Heisenberg et al., 1978; Heisenberg and Wolf, 1979; Götz, 1987) or walk towards the position of a vertical stripe in a free walking arena (Horn and Wehner, 1975). Such a fixation behavior is strong enough to suppress the aversive reaction to an expansion stimulus (Reiser and Dickinson, 2010).

Flies have a preference for dark vertical objects, but they also fixate a bright stripe presented on a dark background (Pick, 1974; Heisenberg and Wolf, 1979). If two dark stripes are presented to freely walking *Drosophila* with an angular width of less than 60 degree between the stripes, the flies walk in the middle between the stripes (Horn and Wehner, 1975). Stripes separated with more than 70 degree or just two objects presented at the opposing sides of an arena will induce the fly to

walk back and forth between them (Buridans paradigm) (Horn and Wehner, 1975; Bülthoff, 1982; Strauss and Pichler, 1998).

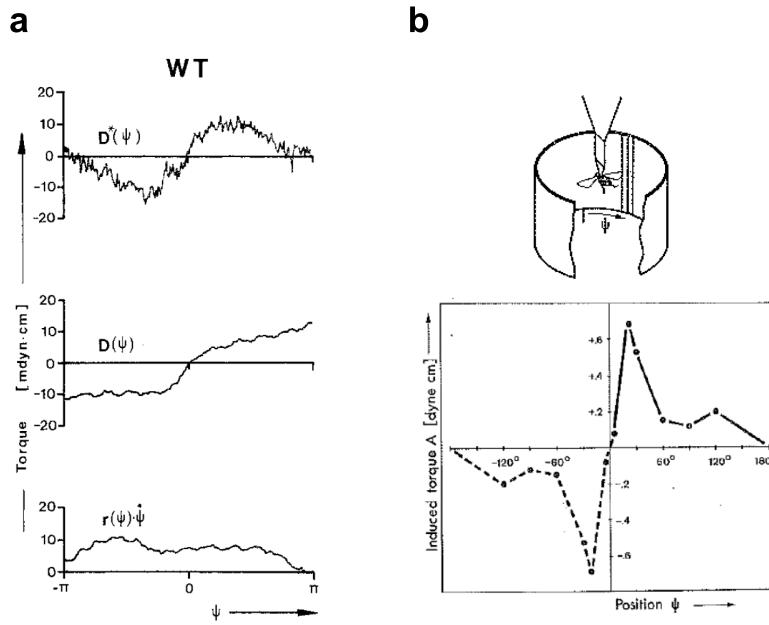


Figure 1.12: The Position System.

a Open-loop responses to a rotating black bar and a theoretical decomposition into a position response $D(\psi)$ and the motion response $r\psi$. Image modified from Heisenberg et al. (1978). **b** Torque responses of a housefly to a flickering lamp at different positions, the fly responded strongest to a flicker stimulus at ± 20 degree. Image modified from Pick (1974).

Under open-loop conditions with a fixed fly, a rotating bar induces a stronger turning response when the bar is moving in a front-to-back direction than when it is moving back-to-front (Heisenberg et al., 1978; Geiger, 1981). Similar reactions were observed with *Musca domestica*; the reaction to progressive (front-to-back) motion is stronger than to regressive (back-to-front) motion (Reichardt, 1973). Such an asymmetric reaction could explain the frontal fixation of a bar in closed-loop experiments. An alternative explanation would be a reaction of the fly towards the position of the bar, as well as to its motion. When presenting a rotating bar in both directions, the theoretical position and motion response can be dissected: the visual response to a rotating bar could be the sum of a motion reaction $r\psi$ and a pure position reaction $D(\psi)$ (Fig. 1.12 a) (Reichardt and Poggio, 1976).

In open-loop experiments with appearing or oscillating stripes, *Musca* flies turned towards the stripe position with the strongest reaction to a lateral position between 30 and 60 degree (Fig. 1.12 b) (Pick, 1974; Heimburger et al., 1976). If this flicker reaction represents a position system, a combination of the position dependent reaction and a symmetrical motion response would also explain the closed-loop fixation. If the fixation behavior of *Drosophila* depends on such a combination or rather asymmetric responses to front-to-back and back-to-front motion remains

unsolved.

1.4.3 Looming Evoked Behavior

Escape Jumps

Avoidance of an approaching object, which could be a predator, is essential for most animals. It is no surprise that avoidance of looming objects and neurons sensing looming have been described throughout the animal kingdom for arthropods like locusts, mantis or crabs (Robertson and Johnson, 1993; Sato and Yamawaki, 2014; Oliva and Tomsic, 2014), in birds (Wu et al., 2005) and also mammals like mice and human infants (Yilmaz and Meister, 2013; Ball and Tronick, 1971).

In a natural environment, flies have to be able to avoid predators or collision by correcting their flight path quickly. If a resting fly is approached by a predator, the fly has to jump off and start flying. Such escape jumps are most reliably elicited by an approaching dark disc, which can be described as a looming stimulus (Holmqvist and Srinivasan, 1991; Fotowat et al., 2009). Flies can escape in two different ways: an instable but fast jump or a longer, directed one (Fig. 1.13 a) (von Reyn et al., 2014). Thus, flies can jump away from the direction of the looming stimulus (Card and Dickinson, 2008).

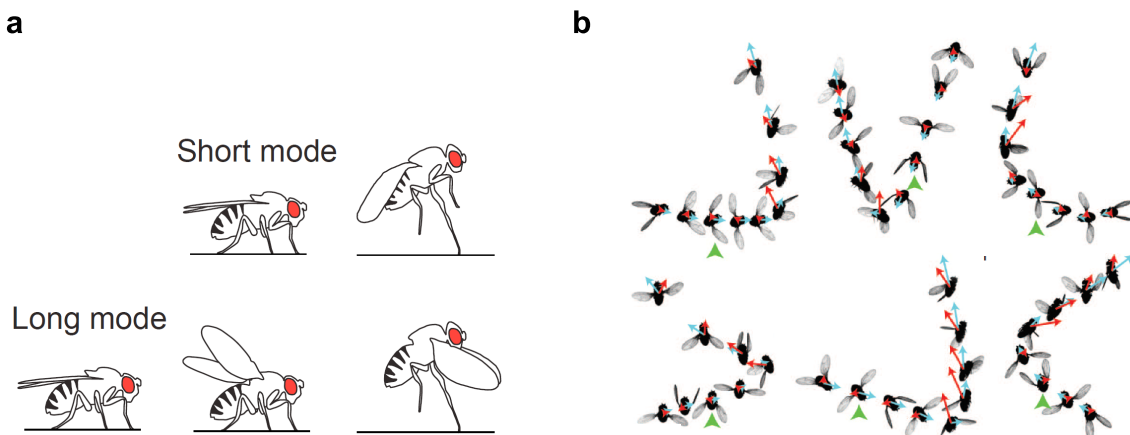


Figure 1.13: Escape Jumps and Avoidance Turns.

a There are two modes of escape jumps in response to a looming stimulus, short-duration jumps or oriented, long-duration escape jumps. The directed escape jumps consist of four steps: freezing, postural adjustment, wing elevation, takeoff. Image modified from von Reyn et al. (2017). **b** High speed tracking of flies avoiding a looming stimulus by directed rapid turns. Image modified from Muijres et al. (2014).

Collision Avoidance Turns

Looming stimuli presented to a flying fly can elicit collision avoidance turns, which are fast, saccadic like turns (Fig. 1.13 b) (Tammero and Dickinson, 2002b; Tammero et al., 2004; Bender and

Dickinson, 2006). These rapid turns are performed within 7 ms (under free flight conditions) with a peak turn rate of 5300 deg/s (Muijres et al., 2014). The speed of the stimulus expansion as well as its more frontal or lateral position determines the response of the fly as an avoidance turn or a landing response (Tammero and Dickinson, 2002b). During a normal flight path, a fly would constantly encounter visual expansion stimuli. How can the fly still keep its course? Fixation of an attractive object can overrule the avoidance to a moderate expansion stimulus (Reiser and Dickinson, 2010). In addition, mechanosensory wind stimuli, which a fly would experience during flight, suppress the reaction to visual expansion to some extent (Budick et al., 2007). The effect of an expansion stimulus is strongly dependent on its velocity. A slow expansion can even appear attractive to the fly (Reiser and Dickinson, 2013).

Landing Response

A dark expanding or looming stimulus presented in front of a flying *Drosophila* will induce leg extension and an increase in the wingbeat frequency, which indicates that the fly is trying to land on the approaching object (Braitenberg and Ferretti, 1966; Tammero and Dickinson, 2002a). The landing response is dependent on the contrast, the position and the expansion velocity of the stimulus (de Talens and Ferretti, 1970; Taddei-Ferretti and de Talens, 1973). Not only looming stimuli, also bilateral front-to-back motion with a high velocity or a light-off stimulus can elicit landing responses of a flying fly (Heisenberg and Buchner, 1977; Borst, 1986). The latency of the landing response elicited by gratings moving front-to-back is dependent on the stimulus frequency, its contrast and its wavelength (Borst and Bahde, 1986). Compared to the optomotor response, the strongest reaction (or shortest latency) is achieved by much higher velocities.

In contrast to other responses, *Drosophila* can habituate to a progressive stimulus and stop reacting with a landing response (Fischbach, 1981). However, if the response is elicited, the behavior can not be modulated. During an optomotor response or collision avoidance turns, the fly can adapt to the stimulus by changing the wing beat amplitude, the wing beat frequency or the walking velocity. In contrast, the landing response is a fixed pattern once elicited (Borst, 1986).

1.5 Visual Pathways

The compound eye of *Drosophila* consists of 700 to 800 ommatidia (Fig. 1.14 a) resulting in a rather poor resolution (Zeleny, 1922). However, flies have a wide angle of view and detect motion with a high temporal resolution. The optic lobes of most insects consist of the retina and three retinotopic neuropils: the lamina, the medulla and the lobula complex (Johannsen, 1924; Richards and Furrow, 1925). In Diptera, as well as in Lepidoptera and Coleoptera, the lobula complex is subdivided into a lobula and a lobula plate. Like the ommatidia organization of the retina, the lamina and medulla are organized in columns (Braitenberg, 1966; Campos-Ortega and Strausfeld, 1972; Strausfeld, 1971). There are two optic chiasms in the optic lobe, the first one between lamina and medulla, the second one between medulla and lobula complex. In the optic lobe, the retinotopic arrangement of the neurons is kept throughout the different neuropils (Braitenberg and Braitenberg, 1979; Bausenwein et al., 1992).

1.5.1 The Photoreceptors

Each retina ommatidium or facet is built up of the cornea, pigment cells and an arrangement of photoreceptor cells (Fig. 1.14 b). In the center of the ommatidia, eight photoreceptor cells build seven rhabdomeres (the 'light trapping area'). Here, the photoreceptors tightly pack microvilli full of rhodopsin, comparable to the outer segments of vertebrate rod cells (Wolken et al., 1957). The photoreceptors R1 to R6 are arranged around R7, which sits on top of R8 (Dietrich, 1909; Wolken et al., 1957; Braitenberg, 1966, 1967).

The photoreceptors R1-R6 all express the photopigment Rhodopsin1 in their microvilli, which has a maximal sensitivity at 478 nm (Fig. 1.14 c) (Salcedo et al., 1999). R1-R6 cells show a second sensitivity peak for UV light due to a sensitizing pigment (Kirschfeld et al., 1977). The photoreceptors R7 and R8 each express two different rhodopsins: About 30 % of the eyes ommatidia are 'pale ommatidia', with R7 expressing Rhodopsin3 and R8 Rhodopsin5 (Papatsenko et al., 1997; Chou et al., 1996). These rhodopsins are sensitive to UV (Rhodopsin3) and blue (Rhodopsin5) light. The other 70 % ommatidia are 'yellow ommatidia' with R7 expressing Rhodopsin4 and R8 expressing Rhodopsin6. This 70:30 ratio is achieved by stochastic expression of a transcription factor in R7 cells, leading to Rhodopsin4 expression (Wernet et al., 2006). Rhodopsin4 has a maximal sensitivity at 375 nm, Rhodopsin6 at 508 nm (Fig. 1.14 c) (Salcedo et al., 1999).

In the dorsal peripheral area of the retina (the dorsal rim), special R7 and R8 photoreceptors with enlarged rhabdomeres both express Rhodopsin3. The microvilli of these dorsal rim R7 and R8 are oriented orthogonally. The dorsal rim photoreceptors enable *Drosophila* to detect polarized light (Wernet et al., 2012). In addition to the dorsal rim area, photoreceptors in the ventral retina can detect polarized light, too: special R4-6 cells with a reduced rhabdomere twist are polarization sensitive and act together with R7 and R8 cells (Wernet et al., 2012). Like many other insects, flies use the e-vector of polarized light to orient during long travels (Weir and Dickinson, 2012).

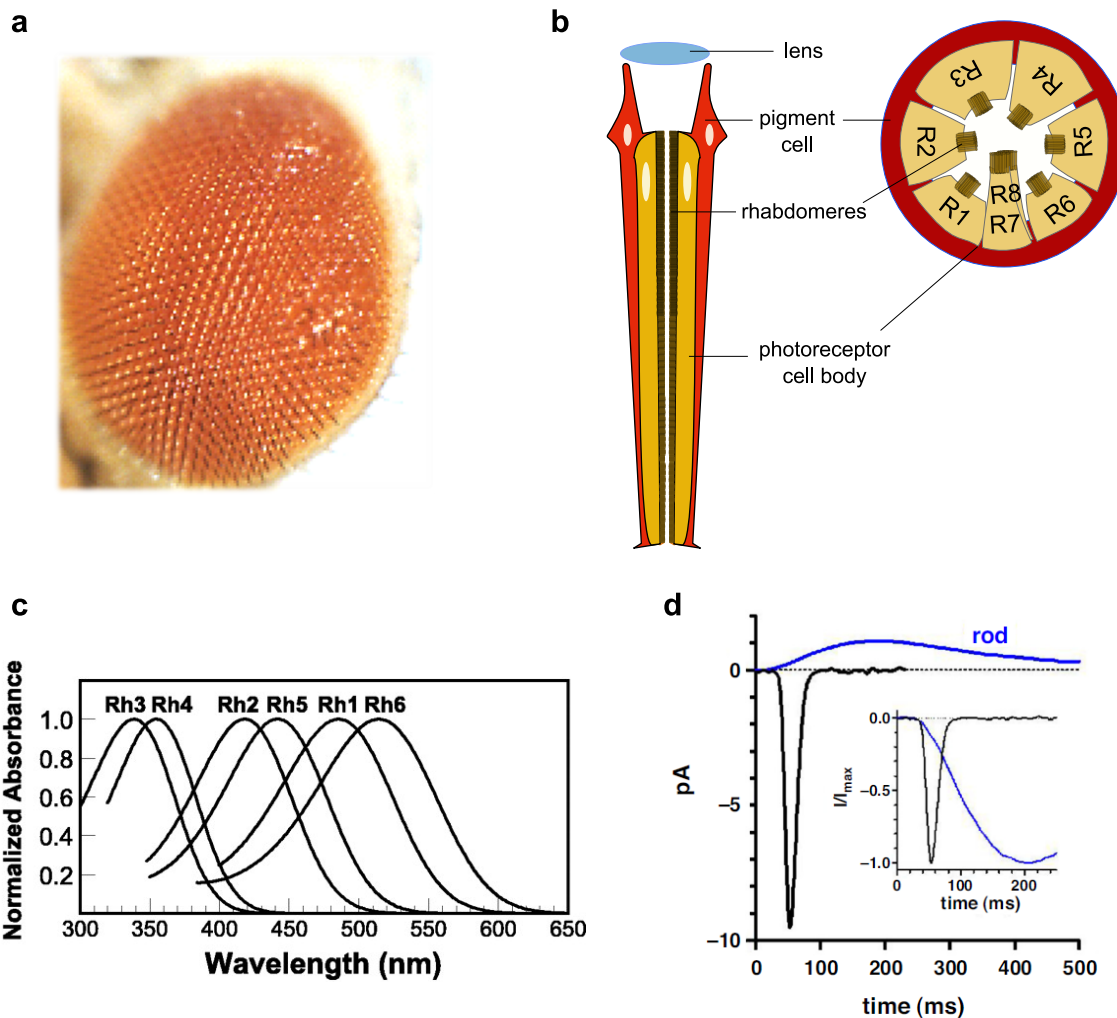


Figure 1.14: The *Drosophila* Photoreceptors.

a The ommatidia structure of a *Drosophila* eye. b Composition of an ommatidium: the red pigment cells surround the eight photoreceptors with their rhabdomeres oriented in the middle. R7 is arranged on top of R8. c Spectral sensitivity of the *Drosophila* Rh1-Rh6 pigments. Image modified from Salcedo et al. (1999). d Single photon responses of a *Drosophila* photoreceptor compared to mouse rod responses. Image modified from Hardie and Juusola (2015).

All photoreceptors are involved in phototaxis, but flies show a preference for the shorter wavelength if they can choose between UV and blue, or blue and green light (Yamaguchi et al., 2010). The main input to the motion vision pathway is provided by the photoreceptors R1-R6. Since flies with a mutant rhodopsin Rh1 (encoded by *ninaE*) were motion blind and could not perform a functional optomotor response (Zhu et al., 2009), it was assumed that R7 and R8 are not contributing to motion vision. Moreover, stimuli with a color but no luminance contrast failed to induce an optomotor response (Schlieper, 1927; Yamaguchi et al., 2008). However, a more recent study

measured a reduced, but still functional flight optomotor response of *ninaE* mutant flies as well as flies with light-insensitive R7/R8 (Wardill et al., 2012). This indicated that R7 and R8 improve motion responses, although they are not necessary for motion vision. A contribution of R7/R8 to the motion vision pathway could be due to the electrical coupling of R7/R8 with R1-R6 photoreceptors via gap junctions (Shaw et al., 1989). In addition, R8 photoreceptors form synapses with medulla neurons of the motion vision pathway (Takemura et al., 2017). Color vision is mediated mainly by R7 and R8 photoreceptors of the yellow ommatidia, but also R1-R6 photoreceptors can contribute (Schnaitmann et al., 2013).

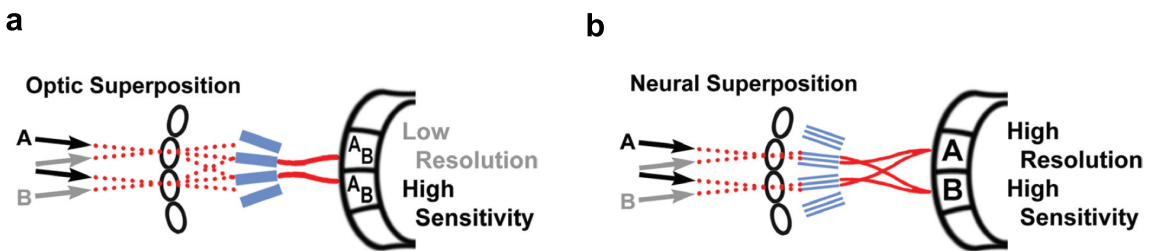


Figure 1.15: Comparison of Optic Superposition and Neural Superposition.

a Optic superposition eyes fuse the input of several ommatidia into one rhabdom. This results in a high sensitivity but low resolution b Neural superposition eyes wire the photoreceptors receiving input from the same light path to the same lamina cartridge. This results in high sensitivity without loosing resolution. a and b modified from Agi et al. (2014).

To achieve a higher sensitivity without loosing resolution, the dipteran eye uses a wiring principle known as neuronal superposition. The axons of photoreceptors activated by the same light path but located in neighboring ommatidia converge on the level of the lamina into one cartridge (Kirschfeld, 1967; Braitenberg, 1967; Strausfeld, 1971). This enhances the sensitivity similar to an optic superposition eye used by many nocturnal insects (Fig. 1.15 a), where input from several ommatidia become superimposed on one rhabdom (Agi et al., 2014). In comparison to an optic superposition, the rhabdomeres of the eight *Drosophila* photoreceptors are not fused, but separated. They detect slightly different optical pathways, insofar allowing the higher resolution of a neuronal superposition eye (Fig. 1.15 b).

1.5.2 Phototransduction

The kinetics of *Drosophila* photoreceptors are very fast with the maximum current after about 50 ms (Fig. 1.14 d) (Hardie, 2001). Invertebrate photoreceptors depolarize in response to light. In comparison, mammalian rods slowly hyperpolarize in response to light (Fig. 1.14 d). The densely packed microvilli membrane of the R1-R6 rhabdomere region are filled with rhodopsins, which are G-protein coupled receptors, and two calcium permeable cation channels, TRP (transient receptor potential) and TRPL (trp-like).

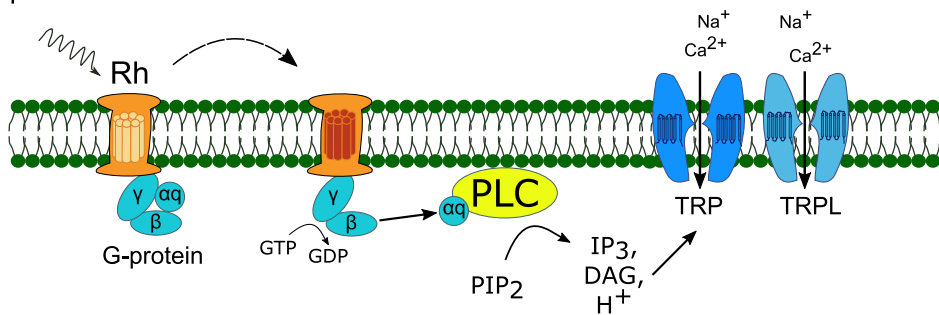
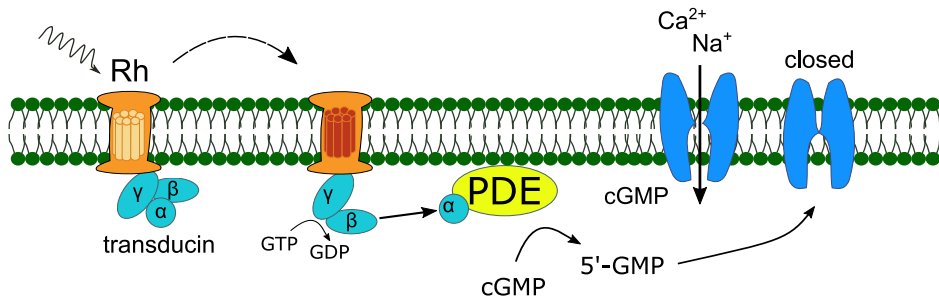
a Drosophila Phototransduction**b Mammalian Phototransduction**

Figure 1.16: *Drosophila* Phototransduction Compared to Vertebrate Phototransduction.

a In invertebrates, photoisomerization of rhodopsin activates a phospholipase-C via a G α q subunit. The PLC signaling results in opening of Ca²⁺ channels. **b** In comparison, vertebrate phototransduction uses phosphodiesterase signaling activated by the G α subunit transducin. The phosphodiesterase increases the levels of 5'-GMP, which closes sodium channels and subsequently voltage-gated calcium channels.

Photon absorption of the rhodopsin results in transformation of 3-OH-11-*cis*-retinal to 3-OH-all-*trans*-retinal. The *Drosophila* rhodopsin is a bistable pigment with the chromophore staying bound to the opsin, until it receives a second photon that isomerizes the retinal back into an 11-*cis*-conformation (Hillman et al., 1983). While it was long assumed that invertebrate pigment cells do not use an enzymatic pathway for chromophore recovery, more recent studies concluded it does exist in addition to the light induced recovery (Wang et al., 2010). Not all 3-OH-*trans*-retinal remain bound to the chromophore, the free opsins become transformed back to 3-OH-11-*cis*-retinal in the retinal pigment cells.

Photoisomerization of rhodopsin to metarhodopsin results in activation of a phospholipase-C (PLC) cascade (Hardie and Juusola, 2015). In detail, the G-protein G α q subunit is released by GTPase activity and activates the phospholipase-C (encoded by *norpA*). PLC hydrolyses phosphatidylinositol 4,5-bisphosphate (PIP₂) into inositol 1,4,5 triphosphate (InsP₃), diacylglycerol (DAG) and a proton (Fig. 1.16 a). The cleavage of PIP₂ induces the opening of the calcium channels TRP (transient receptor potential) and TRPL (transient receptor potential-like), but the

exact mechanism of this interaction is unclear. The protons produced by PIP₂ cleavage probably contribute to it, since acidification can open TRPL channels (Huang et al., 2010). In addition, DAG is necessary to open the TRP channel, either through direct binding or indirect mechanisms (Delgado et al., 2019). One possibility is a physical effect of the PIP₂ cleavage into the lipid-soluble DAG on the membrane properties, such mechanical forces could contribute to the channel opening (Hardie and Franz, 2012). The TRP channels can be phosphorylated to achieve light adaptation, resulting in a different temporal resolution and detection limit of photoreceptors dependent on the light level (Wu and Wong, 1977; Voolstra et al., 2017).

In addition to the canonical phototransduction pathway in photoreceptors, there exists a second one that uses a different Phospholipase-C encoded by *PLC21C* (Ogueta et al., 2018). It resets the circadian rhythm of *Drosophila* together with cryptochrome expressing clock neurons.

Invertebrate phototransduction results in depolarization due to opening of TRP/TRPL channels. In comparison, light activation of mammalian rod and cone photoreceptors results in hyperpolarization due to closure of cGMP gated sodium channels (Fig. 1.16 b). However, the invertebrate phototransduction pathway is similar to signaling in mammalian intrinsically photosensitive retinal ganglion cells, in which light stimulation also starts a PLC signaling cascade (Pickard and Sollars, 2011).

1.5.3 Lamina, Medulla and Lobula Plate Neurons

The *Drosophila* photoreceptors are all histaminergic and connect either to lamina monopolar cells (R1-R6) or transmedulla cells (R7 and R8) (Hardie et al., 1989; Pollack and Hofbauer, 1991). The lamina monopolar cells express the *ort* receptor, a histamine-gated chloride channel, resulting in a hyperpolarization after histamine release from the photoreceptors (Gengs et al., 2002; Pantazis et al., 2008).

Ramón y Cajal first described the anatomy of *Drosophila* optic lobe neurons like lamina monopolar cells, transmedulla cells and T4/T5 cells (Cajal and Sanchez, 1915). In the 1970s and 1980s, Golgi staining of sparse cells was used to describe the morphology of almost all optic lobe cell types (Buschbeck and Strausfeld, 1996; Strausfeld, 1971; Fischbach and Dittrich, 1989). In one lamina cartridge, the five monopolar cells L1-L5 are postsynaptic to R1-R6 axon terminals (Strausfeld, 1970; Strausfeld and Braitenberg, 1970). The lamina also receives feedback information from T1, Lawf and C2 and C3 cells (Strausfeld, 1970) Fischbach and Dittrich (1989) described mainly three types of medulla cells: the medulla intrinsic neurons, the medulla amacrine cells and the transmedulla cells. Medulla intrinsic (Mi) cells are unicolumnar and connect the upper (distal) with the lower (proximal) part of the medulla. The amacrine cells either arborize in the distal medulla (Dm cells) or in the proximal medulla (Pm cells). The third cell type, transmedulla or Tm cells, connect the medulla with the lobula.

The motion vision pathway is split into an ON and an OFF pathway, similar to the ON and OFF retinal ganglion cells of the mammalian retina (Joesch et al., 2010; Clark et al., 2011). Recent

electron microscopy studies defined the neurons involved in the ON and OFF pathway (Takemura et al., 2013, 2017; Shinomiya et al., 2019). The input to the ON pathway is provided by L1, L3 and L5. While L1 and L5 connect to Mi1, Tm3 and Mi4, L3 connects to Mi9. These medulla neurons, together with CT1, are the main input cells to the T4 cells, which are lobula plate cells with dendrites in the medulla layer 10 (Fig. 1.17 a). In the OFF pathway, L2 and L4 connect to Tm1, Tm2 and Tm4. L3 is a common input lamina monopolar cell of the ON and the OFF pathway, it connects to Tm9. The Tm1, Tm2, Tm4 and Tm9 together with CT1 provide input to T5, which have their dendrites in lobula layer 1.

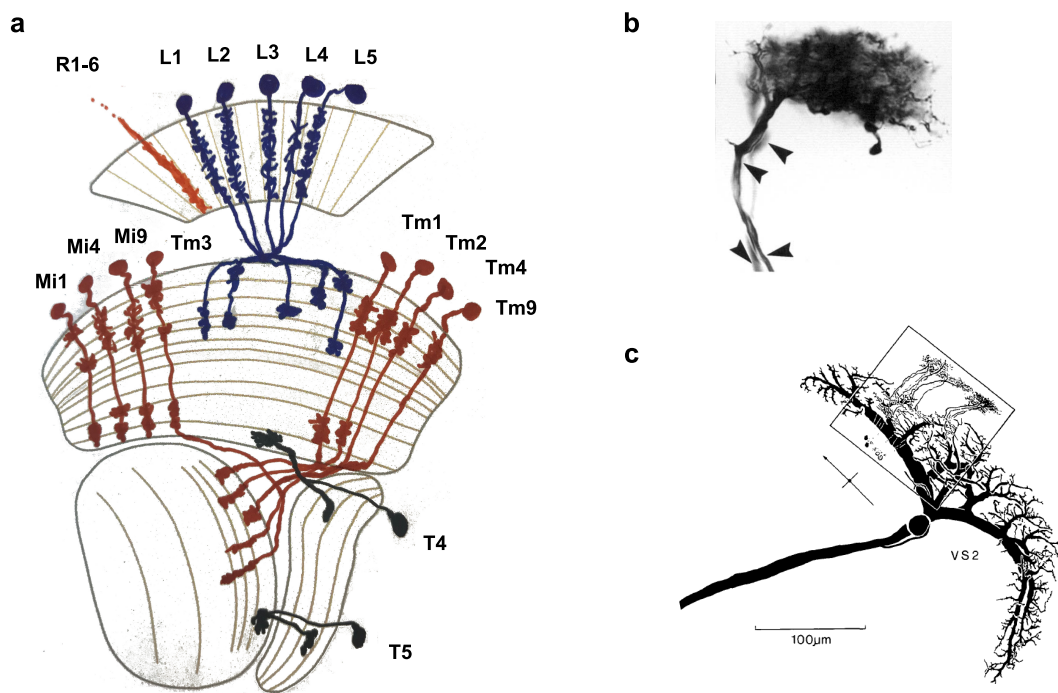


Figure 1.17: Neurons of the Motion Vision Pathway.

a Lamina monopolar cells L1-L5 receive input from R1-R6. Medulla intrinsic neurons and trans-medulla neurons Mi1, Mi4, Mi9 and Tm3 are the main inputs to T4 whereas Tm1, Tm2, Tm4, Tm9 provide input to T5. b Golgi staining of a *Calliphora* T4 dendrite. Arrowheads point towards the two axons deriving from one dendrite. c Drawing of *Calliphora* T4 neurons on a VS2 dendrite. b and c Images modified from Strausfeld and Lee (1991).

The axons of T4 and T5 neurons are divided in the four lobula plate layers with four subtypes (T4 a,b,c,d and T5 a,b,c,d) providing input to one layer (Strausfeld and Lee, 1991). Since the T4 and T5 dendrites are not unicolumnar but span over several medulla or lobula columns, each column is occupied by several overlapping T4 dendrites (Strausfeld and Lee, 1991). The dendrites of the four T4/T5 subtypes are oriented in four directions (example dendrite in Fig. 1.17 b) (Takemura et al., 2013; Shinomiya et al., 2019). In the lobula plate, the T4 and T5 axon terminals form synapses on the dendrites of giant lobula plate tangential cells (Fig. 1.17 c) (Strausfeld and

Lee, 1991). Blocking T4 and T5 cells abolished motion responses of lobula plate tangential cells, proving their critical role in the motion vision pathway (Schnell et al., 2012).

The giant tangential cells (LPTCs) can be subdivided into a vertical and a horizontal system (Pierantoni, 1976; Strausfeld, 1970; Dvorak et al., 1975b; Scott et al., 2002). There are three horizontal system cells, HSN (north), HSE (equatorial) and HSS (south) (Fig. 1.18 a), the same as in the *Calliphora* optic lobe (Hausen, 1982). Vertical system cells differ between *Drosophila* and *Calliphora*, while there are 11 different vertical tangential cells described in *Calliphora* (Hengstenberg et al., 1982) until now only six VS cells are known in *Drosophila*, VS1-6 (Fig. 1.18 a) (Scott et al., 2002; Boergens et al., 2018). Other lobula plate tangential cells next to VS and HS cells are vCH, dCH and VSlike1-3 cells (Chiang et al., 2011; Boergens et al., 2018). Two tangential cells projecting to the other hemisphere are described in *Calliphora*, H1 and H2. There is an H2 like cell in the *Drosophila* optic lobe, but so far no H1 is described (Cruz et al., 2019).

1.5.4 Functional Properties of the Lobula Plate Tangential Cells

The huge dendrites of the lobula plate tangential cells (LPTCs) cover large receptive fields with inputs from often more than 100 columns in *Drosophila*. Electrophysiological characterization of the LPTCs started with extracellular recordings in *Musca* and *Calliphora* flies (Bishop and Keehn, 1966; Mastebroek et al., 1980). Lewis Bishop described directionally selective units next to the lobula region with a response similar to the optomotor behavior. Intracellular recordings and subsequent dye filling confirmed that such directionally selective units are the previously anatomically described vertical system (VS) and horizontal system (HS) tangential cells of the lobula plate (Fig. 1.18 a) (Dvorak et al., 1975a,b). The HS cells respond to progressive horizontal motion (Fig. 1.18 b), with the HSN, HSE and HSS cells covering the upper, middle and lower part of the visual field (Hausen, 1982; Schnell et al., 2010). The VS neurons detect rotatory pitch or roll motion (Fig. 1.18 c) that the fly would encounter during flight (Krapp et al., 1998). The receptive fields of VS cells resemble optic flow fields induced by the fly's own movement, thus the role of VS cells is likely to detect self-motion during flight (Krapp and Hengstenberg, 1996). The receptive fields and the anatomy of LPTC dendrites seem to be hard-wired, since they develop independent of early sensory experiences (Karmeier et al., 2001; Knott et al., 2003).

To achieve their large receptive fields, LPTC dendrites are not always restricted to one lobula plate layer, but can span over several ones (Hengstenberg et al., 1982; Scott et al., 2002; Hopp et al., 2014; Boergens et al., 2018). Whereas HS and VS cells are ipsilateral, some tangential cells like H2 project to the other hemisphere (Haa, 2001). In addition, different VS and HS cells are electrically coupled among each other (Strausfeld and Bassemir, 1983; Haag and Borst, 2004, 2005; Schnell et al., 2010). This broadens their receptive field and allows the tuning to rotational flow fields.

VS and HS cells depolarize in response to their preferred direction of motion and hyperpolarize if presented the null direction motion (Hengstenberg, 1982; Gauck and Borst, 1999; Joesch et al.,

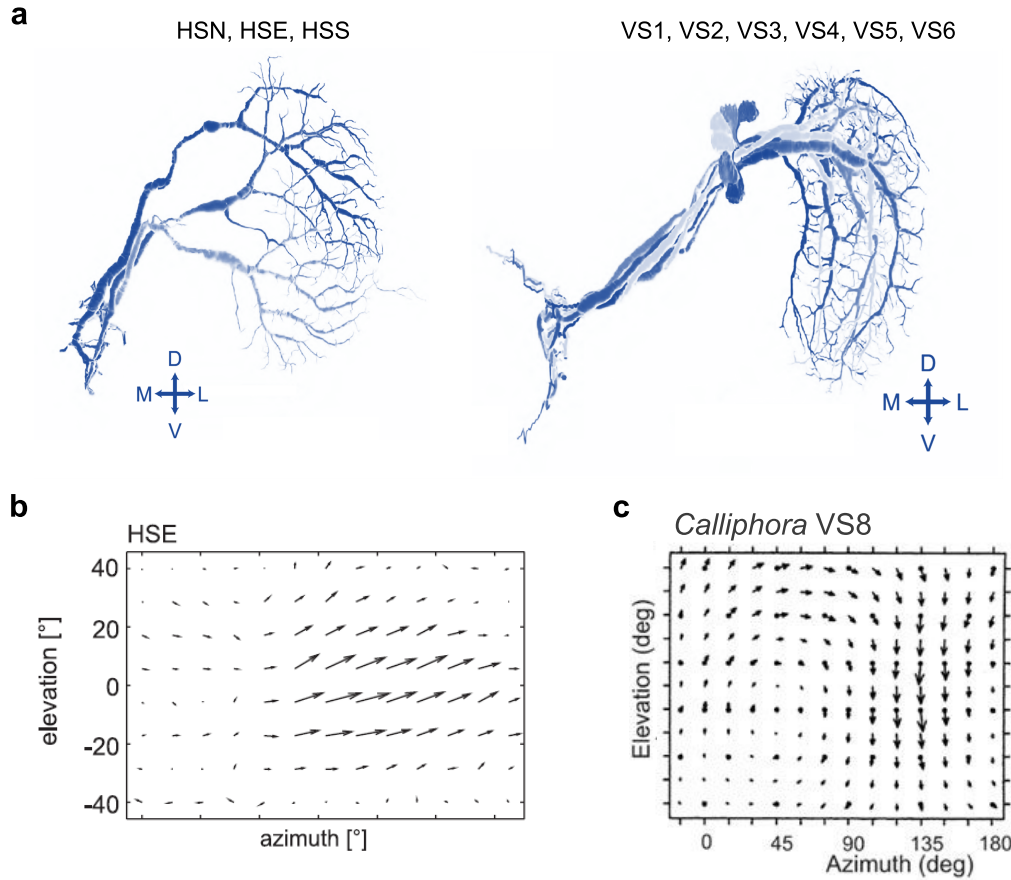


Figure 1.18: Anatomy and Response Vector Fields from Lobula Plate Tangential Cells.

a Reconstruction of the three HS (left panel) and six VS (right panel) cells from *Drosophila*. Images modified from Boergens et al. (2018). **b** Vector field of the *Drosophila* HS-Equatorial cell responding to horizontal motion. Picture modified from Schnell et al. (2010). **c** Vector field of the *Calliphora* VS8 cell. Picture modified from Haag and Borst (2004)

2008). The ipsilateral VS, HS and CH cells transfer information through graded potentials with superimposed action potentials, whereas heterolateral cells like H1-6 and V1-3 are spiking neurons (Hausen, 1982; Haag and Borst, 1997; Wertz et al., 2008; Schnell et al., 2010).

The axons of the VS and HS cells project into the protocerebrum of the central brain (Hausen, 1982; Raghu et al., 2007). They connect to descending neurons like DNHS1, DNOVS2 and DNOVS1 (Pierantoni, 1976; Strausfeld et al., 1984; Strausfeld and Bassemir, 1985; Farrow et al., 2003), which activate motor neurons controlling neck, haltere and wing movement (Suver and Dickinson, 2016).

1.5.5 Behavioral Relevance of the Lobula Plate Tangential Cells

An involvement of the lobula plate tangential cells in course control is likely due to their optic flow fields. Electrophysiological characterization of tangential cells revealed striking similarities to

the properties of the optomotor response, with a dependence on stimulus contrast and a velocity optimum tuned to frequency (Fig. 1.19 a,b) (Mastebroek et al., 1980; Hengstenberg et al., 1982; Joesch et al., 2008; Schnell et al., 2010). Microsurgical removal of *Musca* and *Calliphora* HS cells with a laser beam strongly reduced the optomotor response of the flies (Geiger and Nässel, 1982; Hausen, K. Wehrhahn, C., 1983; Hausen and Wehrhahn, 1990).

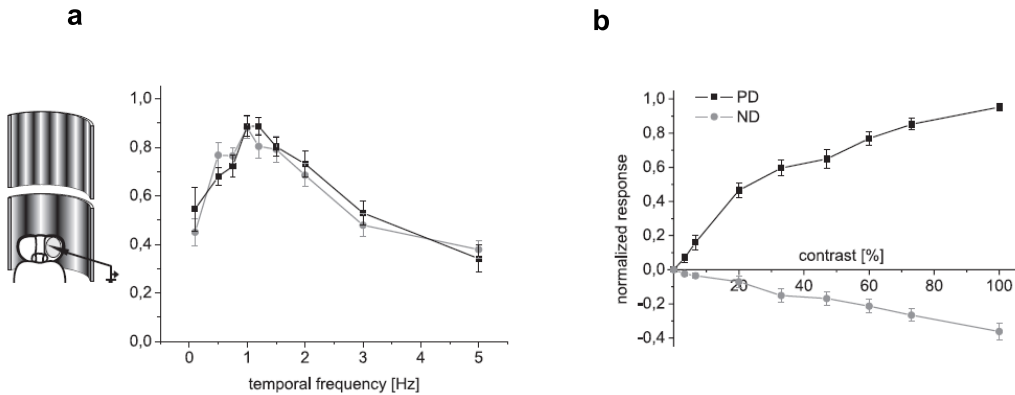


Figure 1.19: Patch-clamp Recordings of HS Cells.

The HS cells were stimulated with horizontal rotation of a grating. a The response is tuned to a frequency optimum, with a maximal response to 1 Hz. b The responses is dependent on the stimulus contrast. Images modification from (Schnell et al., 2010).

The crucial role of VS and HS cells for the optomotor turns was further supported by different motion blind *Drosophila* mutants. The *optomotor blind*^{H31} (*omb*) mutant flies are missing HS and VS cells, whereas the mutant *lobula plate-less*^{N684} (*lop*) lacks a lobula plate and the remaining LPTCs grow into the medulla or lobula (Blondeau and Heisenberg, 1982; Fischbach et al., 1989). The *omb* mutant flies indicated that LPTCs are essential for both optomotor flight responses and optomotor head turns (Pflugfelder and Heisenberg, 1995). LPTCs are not only necessary for the optomotor response but also sufficient to induce a turning behavior. Electrical stimulation of the *Calliphora* lobula plate could indeed evoke flight turns (Blondeau, 1981) similar to optogenetic activation of HS cells in *Drosophila* (Haikala et al., 2013).

The LPTC responses are dependent on the behavioral state of the fly with stronger responses during flight or walking activity (Maimon et al., 2010; Jung et al., 2011; Chiappe et al., 2010). This modulation is due to octopaminergic input into the optic lobe (Suver et al., 2012). While HS cells are more active during flight than in a quiescent state of the animal, their membrane potential failed to predict flight turn responses to whole field motion stimuli. In contrast, the temporal dynamics of presynaptic calcium accumulation fit to the behavioral responses (Schnell et al., 2014).

The role of the LPTCs is likely to detect motion induced by self-movement and compensate for involuntary movement. HS cells also receive information about the velocity and turning movement independent of visual information (Fujiwara et al., 2017). The natural flight behavior of *Drosophila*

alternates between a straight flight course and fast saccade turns. To perform voluntary turns without interference of an optomotor response, the output of LPTCs should be inhibited. Self-motion information suppresses LPTC responses to visual motion during saccade turns (Kim et al., 2015, 2017).

1.5.6 Color Vision Pathway

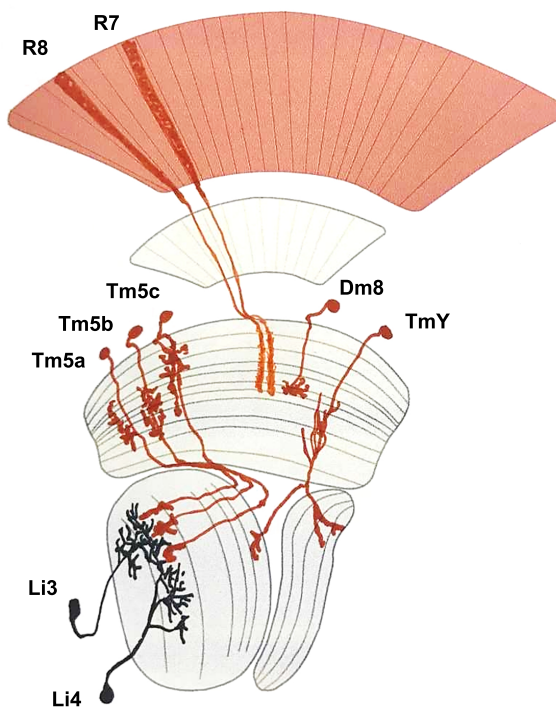


Figure 1.20: Neurons Involved in Color Vision.

The input to the color vision circuit is mainly provided by the photoreceptors R7 and R8. The transmedulla neurons Tm5a, Tm5b, Tm5c, the amacrine cell Dm8 as well as different TmY neurons receive input from R7/R8. In the lobula, the lobula intrinsic neurons Li3 and Li4 are postsynaptic to Tm5a/Tm5b/Tm5c.

Fruit flies can be conditioned to memorize color combined with a stimuli (Menne and Spatz, 1977; Schnaitmann et al., 2010, 2013; Melnattur et al., 2014). Color vision requires the comparison of at least two different photoreceptor outputs with different sensitivities. Indeed R7 and R8 (of both kinds, the pale and yellow ommatidia) inhibit each other via histamine-gated chloride channels at their axon terminals in the medulla (Schnaitmann et al., 2018). Downstream of the R7/R8 photoreceptors are several medulla neurons known to be involved in color vision. UV preference is mediated by the medulla amacrine cell Dm8 and the transmedulla cell Tm5c, which receive input from R7 (Karuppudurai et al., 2014). The medulla neurons Tm5a, Tm5b, Tm5c and Tm20 also receive input from R7 and R8. They are required to distinguish equiluminant blue and green, but

act in a redundant way (Melnattur et al., 2014). These medulla neurons connect to lobula neurons, so far LT11, LC14 and the lobula intrinsic neurons Li3 and Li4 are known to be involved in color vision (Fig. 1.20) (Lin et al., 2016).

1.5.7 Lobula Columnar Cells

Lobula columnar (LC) cells are visual projection neurons that connect the lobula to optic glomeruli in the central brain. They are thought to play a role in many visual behaviors like escape responses or orientation behavior, by detecting specific visual features and providing information about their location. In the last years, several studies addressed the LC neurons. Some are involved in different kind of escape behaviors elicited by looming stimuli. While LC16 activation results in backward walking or 'moonwalk' (Sen et al., 2017), optogenetic activation of LC4, LC6 and LC15 triggers an escape jump (Wu et al., 2016). LC4 connects to the giant fiber, a descending neuron that elicits fast escape jumps, and encodes information about angular velocity of the looming stimulus (von Reyn et al., 2017). Although LC6 and LC16 also respond to looming stimuli (Wu et al., 2016), they are not connected to the giant fiber.

Another avoidance behavior of *Drosophila* is its evasive behavior away from small moving objects (Maimon et al., 2008). LC11 neurons might be involved in this behavior, since they respond specifically to small, moving dark objects. In contrast, they are inhibited by long objects and wide-field motion (Keleş and Frye, 2017; Wu et al., 2016). Similar characteristics were found in optic glomeruli interneurons in the lateral protocerebrum: they respond to small moving objects but not wide-field motion (Kim et al., 2015).

While all so far described behaviors are similar in males and females, there is a sex specific visual behavior: tracking the females during courtship. LC10, another lobula neuron that is responsive to small moving objects, was shown to play a crucial role in courtship behavior (Ribeiro et al., 2018). Optogenetic activation of LC10 results in wing extension, which is part of the male courtship behavior.

1.5.8 The Central Complex

The central complex is involved in higher order processing like navigation over long distances. It receives multisensory information about the internal state of the fly. The main neuropils of the central complex are the protocerebral bridge, the fan-shaped body, the ellipsoid body and the noduli (Franconville et al., 2018; Wolff and Rubin, 2018; Omoto et al., 2018). Flies are able to remember the position of objects and use them as landmarks. The fan-shaped body is involved in detection of visual features used as landmarks and to perceive flight heading (Liu et al., 2006a; Pan et al., 2009; Weir and Dickinson, 2015). The ellipsoid body is also important for navigation, ellipsoid body neurons are essential to remember the position of distinct visual features (Neuser et al., 2008; Ofstad et al., 2011).

Input neurons of the ellipsoid body columnar neurons, the ring neurons, are important to map visual features in the environment of the fly. They respond to visual cues in a retinotopically ordered (Seelig and Jayaraman, 2013). The ring neurons inherit their feature selectivity and their receptive fields from upstream neurons. They receive input from the medulla via the anterior optic tubercle and the bulbs (Sun et al., 2017). Neurons projecting from the anterior optic tubercle to the bulbs as well as bulb neurons have similar tuning properties as the ring neurons (Omoto et al., 2017; Shiozaki and Kazama, 2017). Other neurons of the ellipsoid body, the E-PG neurons (or 'compass neurons'), encode a representation of the fly's orientation relative to visual landmarks (Seelig and Jayaraman, 2015). In the absence of visual cues, the neurons use self-motion cues for orientation. In a behavioral experiment with an artificial sun, the compass neurons were necessary to orient relative to the sun landmark (Giraldo et al., 2018). P-EN neurons, which are connected to the E-PG neurons, exist in two subpopulations. The subpopulations encode the recent rotational velocity of the fly in a mirror symmetric way (Turner-Evans et al., 2017).

While many studies published in recent years addressed the central complex neurons, the computations within its neuropils are still hardly understood. Future studies will reveal how visual information together with other sensory input are processed in the central complex to achieve orientation within a natural environment.

1.6 Algorithmic Models of Motion Computation

1.6.1 The Hassenstein-Reichardt Detector

A single photoreceptor only reacts to light increments or decrements, but not to the direction of an input signal. Direction sensitive cells have to compare the light changes detected from at least two photoreceptors. Two algorithmic models describe such a basic motion detection: correlation and gradient detectors (Borst, 2007). The motion detection of a gradient detector arises from dividing the temporal gradient of local luminance by the spatial gradient. A correlation model compares the luminance change at one location with the delayed change at a neighboring location.

To obtain insights into the underlying algorithm, W. Reichardt and B. Hassenstein measured the optomotor response of the beetle *Chlorophanus* as left-right decisions in response to motion stimuli (described in 1.4.1). They found a temporal frequency optimum of the response, which can not be explained by a gradient detector model. To describe the optomotor response properties of the beetle, Hassenstein and Reichardt proposed a correlation detector model in which inputs of two neighboring photoreceptors are multiplied after one of them has passed a low-pass filter with a time constant τ (Fig. 1.21 a) (Hassenstein, 1951; Hassenstein and Reichardt, 1956; Hassenstein, 1961). Subsequently, two mirror-symmetric subunits with an opposite preferred direction are subtracted from each other, resulting in a positive response to preferred direction and a negative response to null direction stimulation.

To explain the functional properties of direction-selective ganglion cells in the rabbit retina,

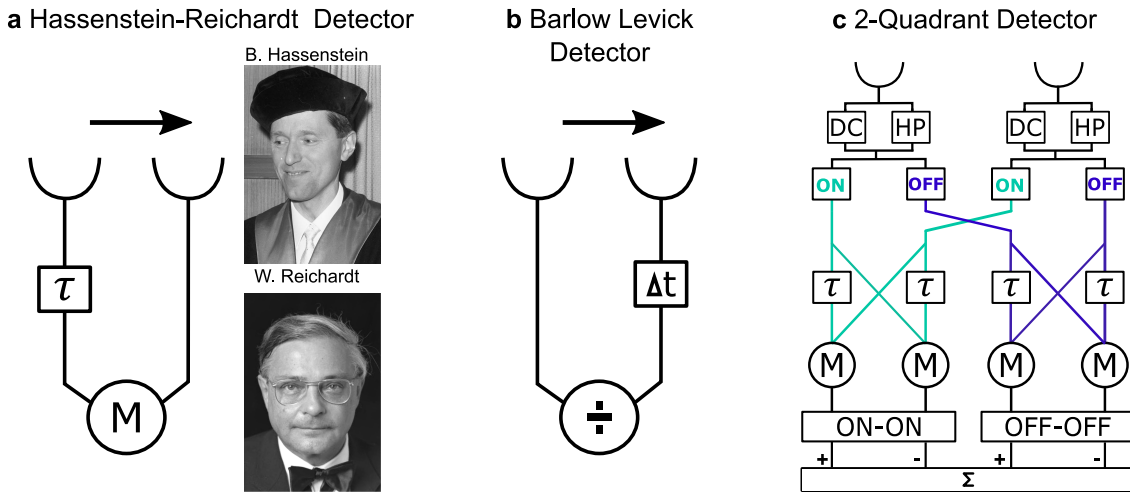


Figure 1.21: A Comparison of Different Correlation Detectors.

a The Hassenstein-Reichardt half achieves direction selectivity by multiplication of a delayed input signal with a fast signal. The arrow points towards the preferred direction of the detector. Photos from Stadtarchiv Kiel and Bundesarchiv, B145. **b** The Barlow Levick inhibits a response to the null direction by dividing a fast signal by a delayed signal. The arrow points towards the preferred direction of the detector. **c** 2-Quadrant Hassenstein-Reichardt detector with ON and OFF inputs. Subtraction of the output from two half detectors induces direction selectivity. ON-ON or OFF-OFF inputs are processed in two independent subunits.

Barlow and Levick (1965) developed another version of a correlation model. The Barlow-Levick model suppresses the response to null direction stimulation using a division of a fast input signal by a delayed signal (Fig. 1.21 b). Therefore, the Barlow-Levick detector results in an inhibition of null direction responses, in contrast to the Hassenstein-Reichardt detector which enhances the preferred direction response. It should be noted that the Barlow-Levick detector explains the direction-selectivity of retinal ganglion cells inadequately, since these cells receive already direction-selective input from starburst amacrine cells (Euler et al., 2002).

The Hassenstein-Reichardt detector takes into account both positive and negative signals at the input stage. However, the fly visual system is subdivided into an ON (sensitive to light increments) and an OFF (sensitive to light decrements) pathway (Joesch et al., 2010; Clark et al., 2011). Blocking the two main input cells to the ON and the OFF pathway, while recording the response of lobula plate tangential cells to apparent motion stimuli with different ON/OFF combinations, revealed that both pathways are separated from each other and feed input to the lobula plate independently (Joesch et al., 2013). This can be simulated by a 2-Quadrant Hassenstein-Reichardt detector with two components multiplying ON-ON and OFF-OFF inputs, thereby the inputs to both subunits are processed by a half-wave rectification resulting in only non-negative signals (Fig. 1.21 c) (Eichner et al., 2011). Since lobula plate tangential cells respond to apparent motion stimuli with several seconds in between stimulation, the model uses a proportion of the input signal

as a tonic (or DC) signal. This also results in an incomplete separation of the ON and OFF pathway, otherwise the two pathways are processed independently. The cellular implementation of the multiplication step was supposed to be the T4/T5 cells, while the dendrites of lobula plate tangential cells represent the summation step (Joesch et al., 2013).

1.6.2 Looming Detectors

Avoidance behavior like escape jumps and avoidance turns, but also the landing response depend on the detection of expansion stimuli. Neurons which are tuned to looming motion should specifically detect nonlinear expansion rather than overall luminance changes or whole-field motion. Such a looming sensing neuron of another insect species, the locust *Schistocerca americana*, is studied in detail. The descending contralateral motion detector neuron (DCMD) is important for gliding (Santer et al., 2008), an escape behavior during flight, and involved in the timing of escape jumps (Simmons et al., 2010). Its input neuron is the lobula giant movement detector (LGMD), which has two dendritic branches in the lobula. DCMD as well as the LGMD are looming sensitive and act as a size threshold detector: after a fixed delay when the looming object reaches an angular threshold size on the retina, the neurons fire maximally (Gabbiani et al., 1999). A model that describes the activity of the LGMD neuron multiplies the logarithm of the angular velocity with an inhibitory input related to the angular size of the looming object (Gabbiani et al., 2002, 2005). On a cellular level, the smaller dendritic branch of the LGMD receives the feed-forward inhibition related to the angular size (Wang et al., 2018), whereas the bigger branch receives excitatory information proportional to the angular velocity (Zhu et al., 2018) (Fig. 1.22 a). The excitatory input is enhanced by lateral excitation in the presynaptic network and receives global, normalizing inhibition. Stimulating single ommatidia of the locust's eye indicated that the input elements of the LGMD do not perform a Reichardt detector like computation, but rather signal the rate of luminance change on individual photoreceptors (Jones and Gabbiani, 2010). The sensitivity of the LGMD inputs to edge acceleration tune this neuron to looming stimuli.

In the *Drosophila* brain, one comparable neuron detecting expansion stimuli is described. The giant fiber, a descending neuron connecting the central brain with motor neurons in the thoracic ganglion, responds to expansion and looming stimuli (Sherman et al., 2004) and is involved in escape behavior (King and Wyman, 1980; Zhang et al., 2007). This neuron was shown to have a peak response at a critical retinal size of the approaching stimulus object (von Reyn et al., 2014). The giant fiber receives two main visual inputs. LC4 neurons provide an excitatory input proportional to the angular velocity of a looming object (Fig. 1.22 b) (von Reyn et al., 2017). The second main input cells to the giant fiber are LPCL2 neurons. These cells provide excitation input to the giant fiber dependent on the angular size of the looming stimulus (Ache et al., 2019). Blocking both LC4 and LPCL2 neurons while recording from the giant fiber revealed an additional input, which inhibits the giant fiber at large disc sizes. A model using a supralinear summation of the LC4 and LPCL2 input, together with the large size inhibition, can predict the giant fiber

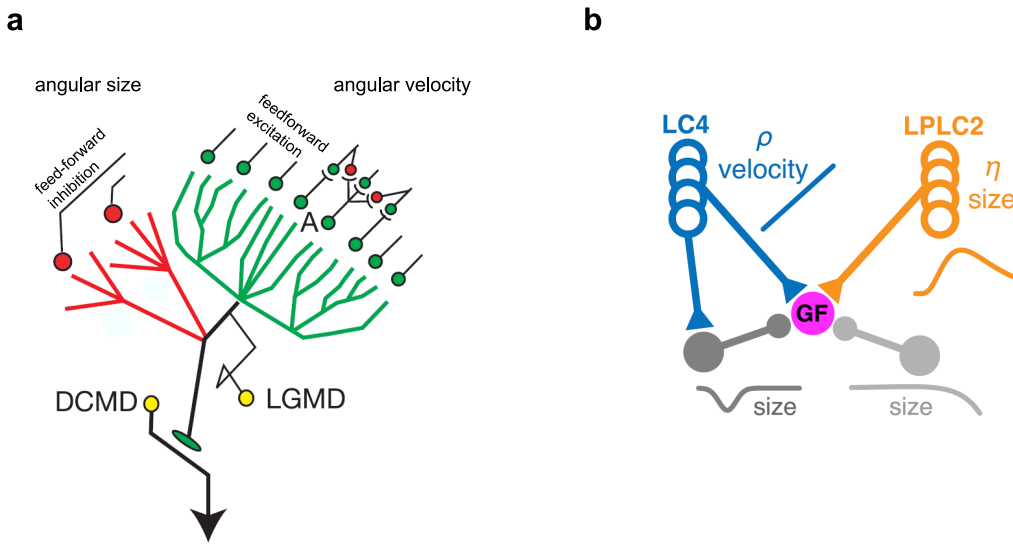


Figure 1.22: Looming Detection Models.

a Model of the looming sensitive LGMD neuron from the locust *Schistocerca americana*. It multiplies an excitatory input proportional to angular velocity of the looming object with a feed-forward inhibition related to angular size. Picture modified from Gabbiani et al. (2002). **b** Model of the *Drosophila* giant fiber sensing looming by a supralinear summation of two excitatory inputs. While LC4 provides input proportional to the angular velocity, LPLC2 encodes the angular size of the looming object. In addition, an unknown input inhibits the giant fiber at a larger stimulus size. Image modified from Ache et al. (2019).

response properties for different looming velocities and also expansion with constant velocity (Ache et al., 2019).

1.7 Development of the Optic Lobe

The neuropils of the optic lobe preserve the retinotopic map from the photoreceptors throughout the lamina, medulla and lobula. During the development of the optic lobe neurons, the retinotopy has to be kept over the different neuropils while at the same time creating a large number of cells, creating many different cell types. For example, the lobula together with the lobula plate consist of about 15.000 cells (Hofbauer and Campos-Ortega, 1990).

The development of most optic lobe neurons starts with two anlagen in the young larva, the outer proliferation center (OPC) and the inner proliferation center (IPC) (Hofbauer and Campos-Ortega, 1990). Both anlagen become crescent shaped during the second larval stage and start producing neurons at the late third larval stage (Fig. 1.23). Whereas the OPC produces the lamina neurons and most medulla neurons, the IPC is the origin of most lobula plate neurons (Meinertzhagen and Hanson, 1993; Apitz and Salecker, 2014; Suzuki et al., 2016). An exception are the optic lobe projection neurons, the lobula plate tangential cells and the lobula columnar cells,

which develop from central brain neuroblasts (Lovick et al., 2013; Wong et al., 2013). During the third larval stage, the OPC becomes separated into two proliferation zones, subdivided by the lamina furrow (White, 1982). The IPC forms three domains: a surface IPC (sIPC), the proximal (pIPC) IPC and the distal IPC (dIPC) (Apitz and Salecker, 2015).

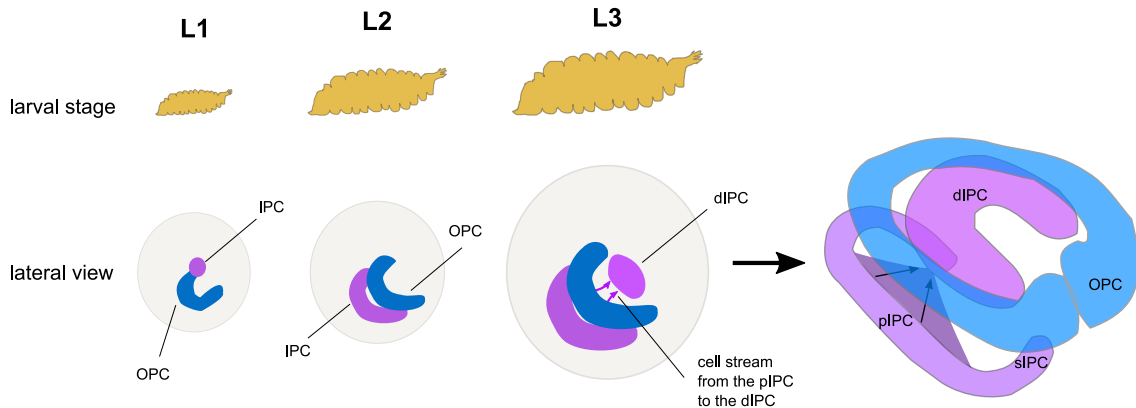


Figure 1.23: The Inner and Outer Anlagen of the Optic Lobe.

During the first larval stage (L1), two proliferation anlagen form: the inner proliferation center (IPC) and the outer proliferation center (OPC). Both anlagen become crescent shaped during the second larval stage. During the third larval stage, progenitor cells migrate from the IPC and form the distal IPC (dIPC). The dIPC separates the IPC and OPC in the late L3 larva.

1.7.1 Neurogenesis in the OPC

The neuroepithelium cells in the OPC start a proneural wave during the second larval stage, in which symmetric division of neuroepithelial cells produce neuroblasts (Yasugi et al., 2008). This proneural wave does not involve delamination or cell migration. The neuroblasts in the medial edge of the OPC divide asymmetrically and produce most medulla neurons (Egger and Boone, 2007). During the third larval stage, the second proliferation zone of the OPC starts to produce the lamina neurons. The division of OPC neuroblasts is a type I division, in which one neuroblast cell divides asymmetrically into a ganglion mother cell (GMC) and a neuroblast (Egger and Boone, 2007; Egger et al., 2010). The GMC divides symmetrically into two postmitotic cells, the progeny cells are either neuron or glia cells. After several divisions, the OPC neuroblasts undergo apoptosis, hereby the survival or death fate is controlled by Notch signaling (Bertet et al., 2014). The neuroblasts are characterized by expression of *Asense* and *Deadpan*, whereas ganglion mother cells express *Prospero*.

The cell fate of the neuroblast progeny in the OPC is determined by temporal patterning (Fig. 1.24 a,b). A sequential expression of different transcription factors (Homothorax, Eyeless, Sloppy paired 1 and 2, Dichaete and Tailless) defines the different identity of the offspring cells (Li et al., 2013; Bertet et al., 2014). The progeny of the ganglion mother cells is further distinguished by a

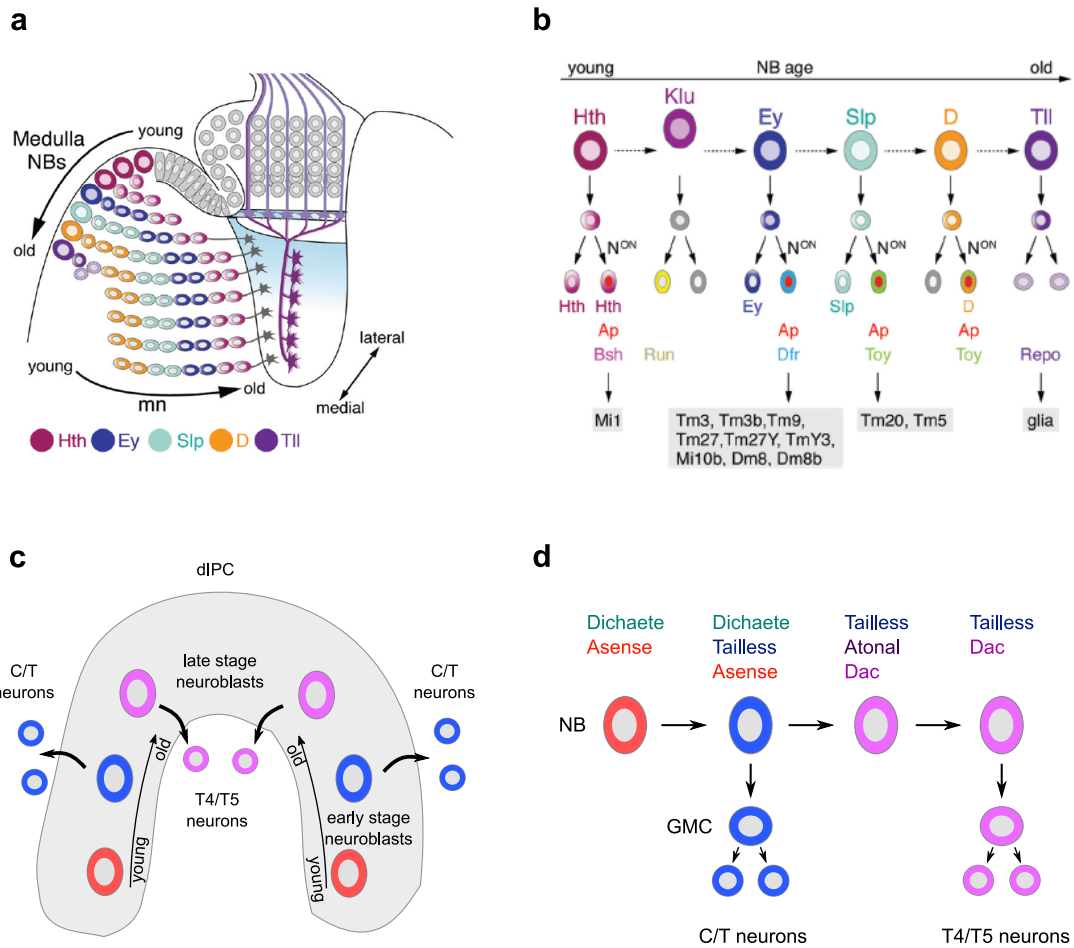


Figure 1.24: Neurogenesis in the OPC and IPC.

a and **b** Sequential expression of temporal transcription factors (Homothorax, Eyeless, Sloppy paired 1 and 2, Dichaete, Tailless) in OPC neuroblasts results in the generation of different medulla neurons. The lateral to medial order of young to old neuroblasts and the ordered growth of young to old neurons ensures that the different neurons target one medulla column. Images modified from Apitz and Salecker (2014). **c** In the dIPC, sequential expression of transcription factors switches the early stage neuroblasts, which generate C/T neurons, to late stage, T4/T5 producing neuroblasts. **d** The early stage neuroblasts express Dichaete, Tailless and Asense. Tailless suppresses Dichaete and Asense, this allows expression of Atonal. The older neuroblasts express Tailless and Dac and divide into T4 and T5 neurons.

Notch mediated binary cell fate choice. That way, every neuroblast produces the medulla neurons of one column Apitz and Salecker (2014).

1.7.2 Neurogenesis in the IPC

The inner and outer proliferation center are connected until the second larval stage. The neuroepithelial cells of the proximal IPC start an epithelial-mesenchymal like transition into neural

progenitors (Apitz and Salecker, 2015). They express the transcription factor Dichaete, which is a neuroblast marker in the OPC. The progenitor cells start migrating between the IPC and the OPC, where they form the distal IPC (Fig. 1.23). In the dIPC, the transition from progenitors to neuroblasts is marked by the proneural factors Lethal of scute and Asense (Apitz and Salecker, 2015). The neuroblasts divide asymmetrically, every neuroblast produces one ganglion mother cell and one neuroblast. These later neuroblasts change their identity by expressing different temporal factors, similar to the OPC neuroblasts (Fig. 1.24 c,d). The transcription factors Dichaete and Tailless control the transition into the second neuroblast identity by inhibiting Asense expression and activating expression of Atonal and Dachshund (Oliva et al., 2014; Apitz and Salecker, 2015).

Unlike the old medulla neuroblasts, the second stage IPC neuroblasts do not undergo apoptosis. Instead, they stop proliferation and divide into two ganglion mother cells (Mora et al., 2018; Pinto-Teixeira et al., 2018). The ganglion mother cells each divide into two neurons with different identity, characterized by a Notch binary choice in the ganglion mother cells (Fig. 1.24 d). The progeny of the first stage, Asense expressing neuroblasts are the C2, C3, T2 and T3 (C/T) neurons, whereas the second stage neuroblasts produce the T4 and T5 neurons.

1.7.3 The T4 and T5 subtypes

There are eight subtypes of T4/T5 cells per cartridge: T4 a-d in every column of medulla layer 10 and T5 a-d in every column of lobula layer 1. Therefore, each optic lobe possesses about 6.400 T4/T5 cells, which have to be produced by the late stage dIPC neuroblasts. T4 and T5 cells of the same subtype and receiving input from the same retina ommatidium, target the same area in the lobula plate.

The identities of T4/T5 a,b and T4/T5 c,d progenitors are specified already in the neuroepithelium (Apitz and Salecker, 2018; Pinto-Teixeira et al., 2018). In this process, the Wingless signaling is necessary to produce the T4 and T5 c,d subtypes. The glial precursor cells, a neuroepithelium domain next to the OPC, releases Wingless in the late second larva stage. The protein diffuses to the sIPC inducing the IPC neuroepithelial cells to start Wingless expression themselves. Subsequently, the Wingless target gene *decapentaplegic* (*dpp*) is expressed in a subregion of the pIPC (Fig. 1.25 a). This wave continues to the progenitor cells, which start expressing the Dpp target *optomotor blind* (*omb* or *bifid*). Expression of the T-box transcription factor Omb is continued until the adult stage, it is important for the identity of T4 c,d and T5 c,d neurons (Apitz and Salecker, 2015, 2018).

The transcriptional repressor *brinker* (*brk*) is specifically expressed in neuroblasts producing T4/T5 a,b (Pinto-Teixeira et al., 2018). It is negatively regulated by Dpp signaling, therefore Omb negative neuroblasts express Brk (Apitz and Salecker, 2015). In the young T4/T5 neurons, Omb represses Dachshund (Dac), a transcriptional cofactor which is expressed at high levels in all T4/T5 neuroblasts. Thus, adult T4/T5 a,b neurons keep expressing Dac, whereas adult T4/T5 c,d neurons still express Omb (Apitz and Salecker, 2018).

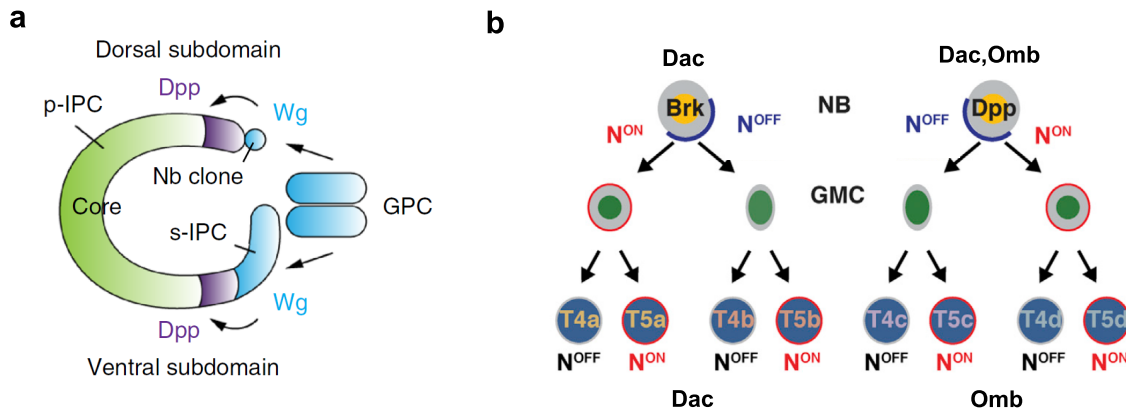


Figure 1.25: Development of the T4 and T5 Subtypes.

a Wingless release in the GPC area induces Dpp expression in a subdomain of the pIPC. This results in a subdivision of the IPC progenitors, the T4/T5 c,d progenitors express Dpp. Image modified from Apitz and Salecker (2018). b The Brk expressing neuroblasts produce T4 a,b and T5 a,b. A Notch on/off binary choice in the neuroblast division and the ganglion mother cell division distinguishes between a or b subtype and T4 or T5 cell. In the same way, Omb⁺ neuroblasts produce T4 c,d and T5 c,d. Image modified from Pinto-Teixeira et al. (2018)

How are the a and b subtypes set up in the Brk⁺ neuroblasts and the c and d subtypes in the Dpp/Omb⁺ neuroblasts? Notch on/off binary choices in the neuroblast define the identity of the GMC progeny as one subtype (Fig. 1.25 b). Another Notch on/off binary choice in the ganglion mother cells results in one T4 and one T5 offspring cell from each ganglion mother cell (Pinto-Teixeira et al., 2018). For example, a Brk⁺ neuroblast divides into one subtype a and one subtype b ganglion mother cell, the ganglion mother cells divide into T4 a/T5 a and T4 b/T5 b.

In contrast to medulla neurons generated by the OPC, the young T4/T5 neurons are not born right next to their target neuropil. To keep the retinotopy, the eight T4/T5 offspring neurons of one neuroblast grow towards the same retinotopic position (Pinto-Teixeira et al., 2018). The developing neuropils establish an anterior to posterior axis of young to older neurons, according to this young T4 or T5 neurons project to the new column of the medulla or lobula, respectively. This keeps a retinotopic order of the optic lobe neurons throughout the different neuropils.

Chapter 2

Publications

2.1 A Directional Tuning Map of *Drosophila* Elementary Motion Detectors

Matthew S. Maisak, Juergen Haag (co-first author), Georg Ammer, Etienne Serbe, Matthias Meier, Aljoscha Leonhardt, **Tabea Schilling**, Armin Bahl, Gerald M. Rubin, Aljoscha Nern, Barry J. Dickson, Dierk F. Reiff, Elisabeth Hopp, and Alexander Borst

Author contributions:

M.S.M. and J.H. jointly performed and, together with A.Bo., evaluated all calcium imaging experiments. G.A., E.S. and M.M. recorded from tangential cells. A.L., **T.S.** and A.Ba. performed the behavioural experiments. G.R., B.D. and A.N. generated the driver lines and characterized their expression pattern. D.F.R. performed preliminary imaging experiments. E.H. helped with programming and developed the PMT shielding for the two-photon microscope. A.Bo. designed the study and wrote the manuscript with the help of all authors.

Tabea Schilling

Alexander Borst

A directional tuning map of *Drosophila* elementary motion detectors

Matthew S. Maisak¹*, Juergen Haag¹*, Georg Ammer¹, Etienne Serbe¹, Matthias Meier¹, Aljoscha Leonhardt¹, Tabea Schilling¹, Armin Bahl¹, Gerald M. Rubin², Aljoscha Nern², Barry J. Dickson³, Dierk F. Reiff¹†, Elisabeth Hopp¹ & Alexander Borst¹

The extraction of directional motion information from changing retinal images is one of the earliest and most important processing steps in any visual system. In the fly optic lobe, two parallel processing streams have been anatomically described, leading from two first-order interneurons, L1 and L2, via T4 and T5 cells onto large, wide-field motion-sensitive interneurons of the lobula plate¹. Therefore, T4 and T5 cells are thought to have a pivotal role in motion processing; however, owing to their small size, it is difficult to obtain electrical recordings of T4 and T5 cells, leaving their visual response properties largely unknown. We circumvent this problem by means of optical recording from these cells in *Drosophila*, using the genetically encoded calcium indicator GCaMP5 (ref. 2). Here we find that specific subpopulations of T4 and T5 cells are directionally tuned to one of the four cardinal directions; that is, front-to-back, back-to-front, upwards and downwards. Depending on their preferred direction, T4 and T5 cells terminate in specific sublayers of the lobula plate. T4 and T5 functionally segregate with respect to contrast polarity: whereas T4 cells selectively respond to moving brightness increments (ON edges), T5 cells only respond to moving brightness decrements (OFF edges). When the output from T4 or T5 cells is blocked, the responses of postsynaptic lobula plate neurons to moving ON (T4 block) or OFF edges (T5 block) are selectively compromised. The same effects are seen in turning responses of tethered walking flies. Thus, starting with L1 and L2, the visual input is split into separate ON and OFF pathways, and motion along all four cardinal directions is computed separately within each pathway. The output of these eight different motion detectors is then sorted such that ON (T4) and OFF (T5) motion detectors with the same directional tuning converge in the same layer of the lobula plate, jointly providing the input to downstream circuits and motion-driven behaviours.

Most of the neurons in the fly brain are dedicated to image processing. The respective part of the head ganglion, called the optic lobe, consists of several layers of neuropile called lamina, medulla, lobula and lobula plate, all built from repetitive columns arranged in a retinotopic way (Fig. 1a). Each column houses a set of identified neurons that, on the basis of Golgi staining, have been described anatomically in great detail^{3–5}. Owing to their small size, however, most of these columnar neurons have never been recorded from electrophysiologically. Therefore, their specific functional role in visual processing is still largely unknown. This fact is contrasted by rather detailed functional models about visual processing inferred from behavioural studies and recordings from the large, electrophysiologically accessible output neurons of the fly lobula plate (tangential cells). As the most prominent example of such models, the Reichardt detector derives directional motion information from primary sensory signals by multiplying the output from adjacent photoreceptors after asymmetric temporal filtering⁶. This model makes a number of rather counter-intuitive predictions all of which have been confirmed experimentally (for review, see ref. 7). Yet, the neurons corresponding to most

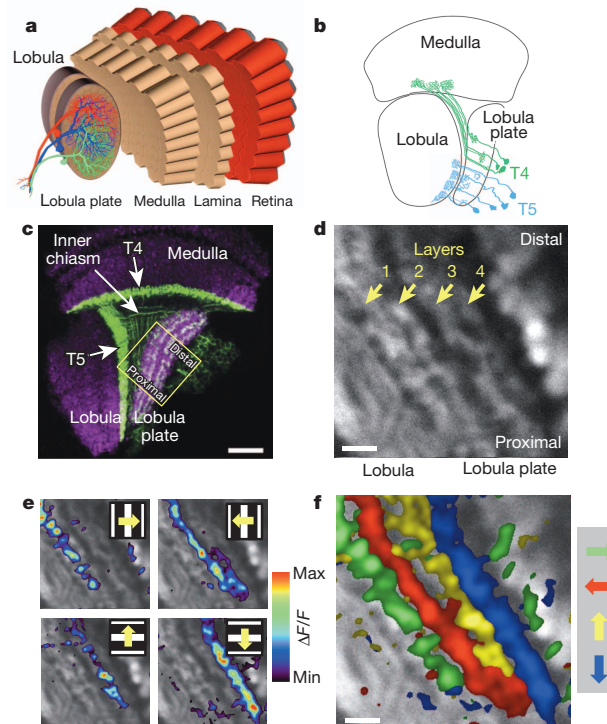


Figure 1 | Directional tuning and layer-specific projection of T4 and T5 cells. **a**, Schematic diagram of the fly optic lobe. In the lobula plate, motion-sensitive tangential cells extend their large dendrites over many hundreds of columns. Shown are the reconstructions of the three cells of the horizontal system²². **b**, Anatomy of T4 and T5 cells, as drawn from Golgi-impregnated material (from ref. 5). **c**, Confocal image of the Gal4-driver line R42F06, shown in a horizontal cross-section (from ref. 10). Neurons are marked in green (Kir2.1-EGFP labelled), whereas the neuropile is stained in purple by an antibody against the postsynaptic protein Dlg. Scale bar, 20 μ m. **d**, Two-photon image of the lobula plate of a fly expressing GCaMP5 under the control of the same driver line R42F06. Scale bar, 5 μ m. The size and orientation of the image approximately corresponds to the yellow square in **c**. **e**, Relative fluorescence changes ($\Delta F/F$) obtained during 4-s grating motion along the four cardinal directions, overlaid on the greyscale image. Each motion direction leads to activity in a different layer. Minimum and maximum $\Delta F/F$ values were 0.3 and 1.0 (horizontal motion), and 0.15 and 0.6 (vertical motion). **f**, Compound representation of the results obtained from the same set of experiments. Scale bar, 5 μ m. Results in **e** and **f** represent the data obtained from a single fly averaged over four stimulus repetitions. Similar results were obtained from six other flies.

¹Max Planck Institute of Neurobiology, 82152 Martinsried, Germany. ²Janelia Farm Research Campus, Ashburn, Virginia 20147, USA. ³Institute of Molecular Pathology, 1030 Vienna, Austria. [†]Present address: Institute Biology 1, Albert-Ludwigs University, 79085 Freiburg, Germany.

*These authors contributed equally to this work.

of the circuit elements of the Reichardt detector have not been identified so far. Here, we focus on a set of neurons called T4 and T5 cells (Fig. 1b) which, on the basis of circumstantial evidence, have long been speculated to be involved in motion detection^{1,8–10}. However, it is unclear to what extent T4 and T5 cells are directionally selective or whether direction selectivity is computed or enhanced within the dendrites of the tangential cells. Another important question concerns the functional separation between T4 and T5 cells; that is, whether they carry equivalent signals, maybe one being excitatory and the other inhibitory on the tangential cells, or whether they segregate into directional- and non-directional pathways¹¹ or into separate ON- and OFF-motion channels^{12,13}.

To answer these questions, we combined Gal4-driver lines specific for T4 and T5 cells¹⁴ with GCaMP5 (ref. 2) and optically recorded the visual response properties using two-photon fluorescence microscopy¹⁵. In a first series of experiments, we used a driver line labelling both T4 and T5 cells. A confocal image (Fig. 1c, modified from ref. 10) revealed clear labelling (in green) in the medulla (T4 cell dendrites), in the lobula (T5 cell dendrites), as well as in four distinct layers of the lobula plate, representing the terminal arborizations of the four subpopulations of both T4 and T5 cells. These four layers of the lobula plate can also be seen in the two-photon microscope when the calcium indicator GCaMP5 is expressed (Fig. 1d). After stimulation of the fly with grating motion along four cardinal directions (front-to-back, back-to-front, upwards and downwards), activity is confined to mostly one of the four layers, depending on the direction in which the grating is moving (Fig. 1e). The outcome of all four stimulus conditions can be combined into a single image by assigning a particular colour to each pixel depending on the stimulus direction to which it responded most strongly (Fig. 1f). From these experiments it is clear that the four subpopulations of T4 and T5 cells produce selective calcium signals depending on the stimulus direction, in agreement with previous deoxyglucose labelling⁸. Sudden changes of the overall luminance evokes no responses in any of the layers (field flicker; $n = 4$ experiments, data not shown). However, gratings flickering in counter-phase lead to layer-specific responses, depending on the orientation of the grating (Supplementary Fig. 1).

The retinotopic arrangement of this input to the lobula plate is demonstrated by experiments where a dark edge was moved within a small area of the visual field only. Depending on the position of this area, activity of T4 and T5 cells is confined to different positions within the lobula plate (Fig. 2a). Consequently, when moving a bright vertical edge horizontally from back to front, activity of T4 and T5 cells is elicited sequentially in layer 2 of the lobula plate (Fig. 2b). These two experiments also demonstrate that T4 and T5 cells indeed signal motion locally. We next investigated the question of where direction selectivity of T4 and T5 cells arises; that is, whether it is already present in the dendrite, or whether it is generated by synaptic interactions within the lobula plate. This question is hard to answer, as the dendrites of both T4 and T5 cells form a dense mesh within the proximal layer of the medulla (T4) and the lobula (T5), respectively. However, signals within the inner chiasm where individual processes of T4 and T5 cells can be resolved in some preparations show a clear selectivity for motion in one over the other directions (Fig. 2c). Such signals are as directionally selective as the ones measured within the lobula plate, demonstrating that the signals delivered from the dendrites of T4 and T5 cells are already directionally selective.

To assess the particular contribution of T4 and T5 cells to the signals observed in the above experiments, we used driver lines specific for T4 and T5 cells, respectively. Applying the same stimulus protocol and data evaluation as in Fig. 1, identical results were obtained as before for both the T4- as well as the T5-specific driver line (Fig. 3a, b). We conclude that T4 and T5 cells each provide directionally selective signals to the lobula plate, in contrast to previous reports¹¹. Thus, both T4 and T5 cells can be grouped, according to their preferred direction, into four subclasses covering all four cardinal directions, reminiscent of ON-OFF ganglion cells of the rabbit retina¹⁶.

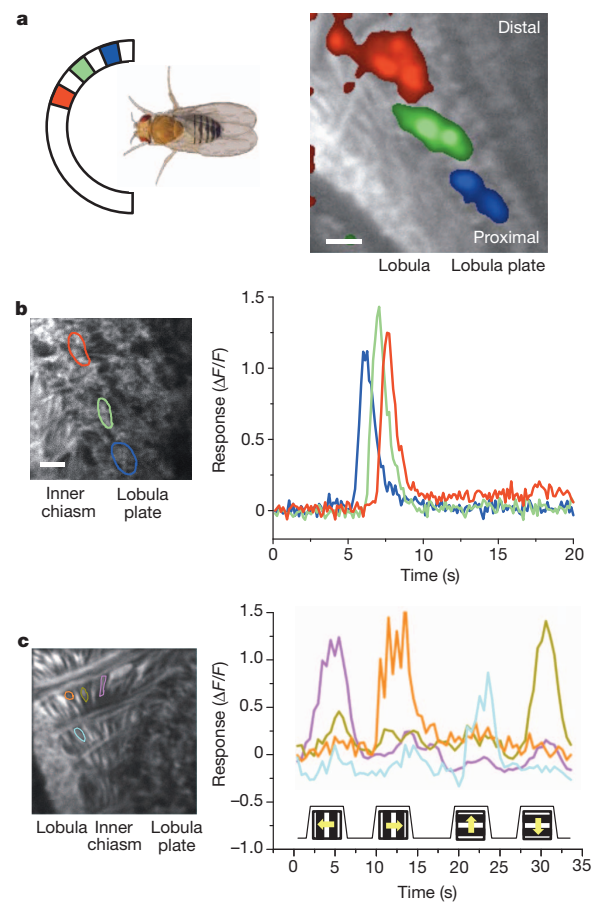


Figure 2 | Local signals of T4 and T5 cells. **a**, Retinotopic arrangement of T4 and T5 cells. A dark edge was moving repeatedly from front-to-back within a 15° wide area at different azimuthal positions (left). This leads to relative fluorescence changes at different positions along the proximal–distal axis within layer 1 of the lobula plate (right). Scale bar, 5 μm . Similar results have been obtained in four other flies. **b**, Sequential activation of T4 and T5 cells. A bright edge was moving from back-to-front at 15° s^{-1} . Scale bar, 5 μm . Similar results have been obtained in six other flies. **c**, Signals recorded from individual fibres within the inner chiasm (left) reveal a high degree of direction selectivity (right). Scale bar, 5 μm . Similar results were obtained from four other flies, including both lines specific for T4 and T5 cells. Response traces in **b** and **c** are derived from the region of interest encircled in the image with the same colour.

We next addressed whether T4 cells respond differently to T5 cells. To answer this question, we used, instead of gratings, moving edges with either positive (ON edge, brightness increment) or negative (OFF edge, brightness decrement) contrast polarity as visual stimuli. We found that T4 cells strongly responded to moving ON edges, but showed little or no response to moving OFF edges (Fig. 3c). This is true for T4 cells terminating in each of the four layers. We found the opposite for T5 cells. T5 cells selectively responded to moving OFF edges and mostly failed to respond to moving ON edges (Fig. 3d). Again, we found this for T5 cells in each of the four layers. We next addressed whether there are any other differences in the response properties between T4 and T5 cells by testing the velocity tuning of both cell populations by means of stimulating flies with grating motion along the horizontal axis from the front to the back at various velocities covering two orders of magnitude. T4 cells revealed a maximum response at a stimulus velocity of 30° s^{-1} , corresponding to a temporal frequency of 1 Hz (Fig. 3e). T5 cell responses showed a similar dependency on stimulus velocity, again with a peak at a temporal frequency of

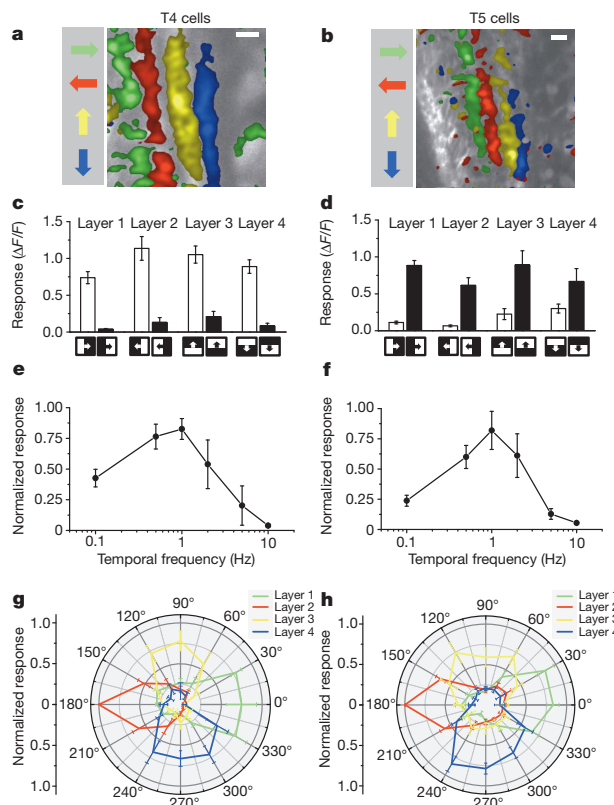


Figure 3 | Comparison of visual response properties between T4 and T5 cells. **a, b**, Relative fluorescence changes ($\Delta F/F$) of the lobula plate terminals of T4 (a) and T5 (b) cells obtained during grating motion along the four cardinal directions. Results represent the data obtained from a single fly each, averaged over two stimulus repetitions. Scale bars, 5 μm . Similar results have been obtained in ten other flies. **c, d**, Responses of T4 (c) and T5 (d) cells to ON and OFF edges moving along all four cardinal directions. ON (white) and OFF (black) responses within each layer are significantly different from each other, with $P < 0.005$ except for layers 3 and 4 in T5 cells, where $P < 0.05$. **e, f**, Responses of T4 (e) and T5 (f) cells to gratings moving horizontally at different temporal frequencies. Relative fluorescence changes were evaluated from layer 1 of the lobula plate and normalized to the maximum response before averaging. **g, h**, Responses of T4 (g) and T5 (h) cells to gratings moving in 12 different directions. Relative fluorescence changes were evaluated from all four layers of the lobula plate normalized to the maximum response before averaging. Data represent the mean \pm s.e.m. of the results obtained in $n = 8$ (c), $n = 7$ (d), $n = 6$ (e), $n = 7$ (f), $n = 6$ (g) and $n = 5$ (h) different flies. Significances indicated are based on two-sample *t*-test.

1 Hz (Fig. 3f). Thus, there is no obvious difference in the velocity tuning between T4 and T5 cells. As another possibility, T4 cells might functionally differ from T5 cells with respect to their directional tuning width. To test this, we stimulated flies with gratings moving into 12 different directions and evaluated the relative change of fluorescence in all four layers of the lobula plate. Using the T4-specific driver line, we found an approximate half width of $60\text{--}90^\circ$ of the tuning curve, with the peak responses in each layer shifted by 90° (Fig. 3g). No decrease of calcium was detectable for grating motion opposite to the preferred direction of the respective layer. When we repeated the experiments using the T5-specific driver line, we found a similar dependence of the relative change of fluorescence on the stimulus direction (Fig. 3h). We conclude that T4 cells have the same velocity and orientation tuning as T5 cells. The only functional difference we were able to detect remains their selectivity for contrast polarity.

Our finding about the different preference of T4 and T5 cells for the polarity of a moving contrast makes the strong prediction that selective

blockade of T4 or T5 cells should selectively compromise the responses of downstream lobula plate tangential cells to either ON or OFF edges. To test this prediction, we blocked the output of either T4 or T5 cells via expression of the light chain of tetanus toxin¹⁷ and recorded the responses of tangential cells via somatic whole-cell patch to moving ON and OFF edges. In response to moving ON edges, strong and reliable directional responses were observed in all control flies (Fig. 4a). However, T4-block flies showed a strongly reduced response to ON edges, whereas the responses of T5-block flies were at the level of control flies (Fig. 4b, c). When we used moving OFF edges, control flies again responded with a large amplitude (Fig. 4d). However, the responses of T4-block flies were at the level of control flies, whereas the responses of T5-block flies were strongly reduced (Fig. 4e, f). These findings are reminiscent on the phenotypes obtained from blocking lamina cells L1 and L2 (ref. 13) and demonstrate that T4 and T5 cells are indeed the motion-coding intermediaries for these contrast polarities on their way to the tangential cells of the lobula plate. Whether the residual responses to ON edges in T4-block flies and to OFF edges in T5-block flies are due to an incomplete signal separation between the two pathways or due to an incomplete genetic block in both fly lines is currently unclear.

To address the question of whether T4 and T5 cells are the only motion detectors of the fly visual system, or whether they represent one cell class, in parallel to other motion-sensitive elements, we used tethered flies walking on an air-suspended sphere¹⁸ and stimulated them by ON and OFF edges moving in opposite directions¹⁹. As in the previous experiments, we blocked T4 and T5 cells specifically by selective expression of the light chain of tetanus toxin. During balanced motion, control flies did not show significant turning responses to either side (Fig. 4g). T4-block flies, however, strongly followed the direction of the moving OFF edges, whereas T5-block flies followed the direction of the moving ON edges (Fig. 4h, i). In summary, the selective preference of T4-block flies for OFF edges and of T5-block flies for ON edges not only corroborates our findings about the selective preference of T4 and T5 cells for different contrast polarities, but also demonstrates that the signals of T4 and T5 cells are indeed the major, if not exclusive, inputs to downstream circuits and motion-driven behaviours.

Almost a hundred years after T4 and T5 cells have been anatomically described³, this study reports their functional properties in a systematic way. Using calcium as a proxy for membrane voltage²⁰, we found that both T4 and T5 cells respond to visual motion in a directionally selective manner and provide these signals to each of the four layers of the lobula plate, depending on their preferred direction. Both cell types show identical velocity and orientation tuning which matches the one of the tangential cells^{21,22}. The strong direction selectivity of both T4 and T5 cells is unexpected, as previous studies had concluded that the high degree of direction selectivity of tangential cells is due to a push-pull configuration of weakly directional input with opposite preferred direction^{23,24}. Furthermore, as the preferred direction of T4 and T5 cells matches the preferred direction of the tangential cells branching within corresponding layers, it is currently unclear which neurons are responsible for the null-direction response of the tangential cells. As for the functional separation between T4 and T5 cells, we found that T4 cells selectively respond to brightness increments, whereas T5 cells exclusively respond to moving brightness decrements. Interestingly, parallel ON and OFF motion pathways had been previously postulated on the basis of selective silencing of lamina neurons L1 and L2 (ref. 13). Studies using apparent motion stimuli to probe the underlying computational structure arrived at controversial conclusions: whereas some studies concluded that there was a separate handling of ON and OFF events by motion detectors^{12,25,26}, others did not favour such a strict separation^{19,27}. The present study directly demonstrates the existence of separate ON and OFF motion detectors, as represented by T4 and T5 cells, respectively. Furthermore, our results anatomically confine the essential processing steps of elementary

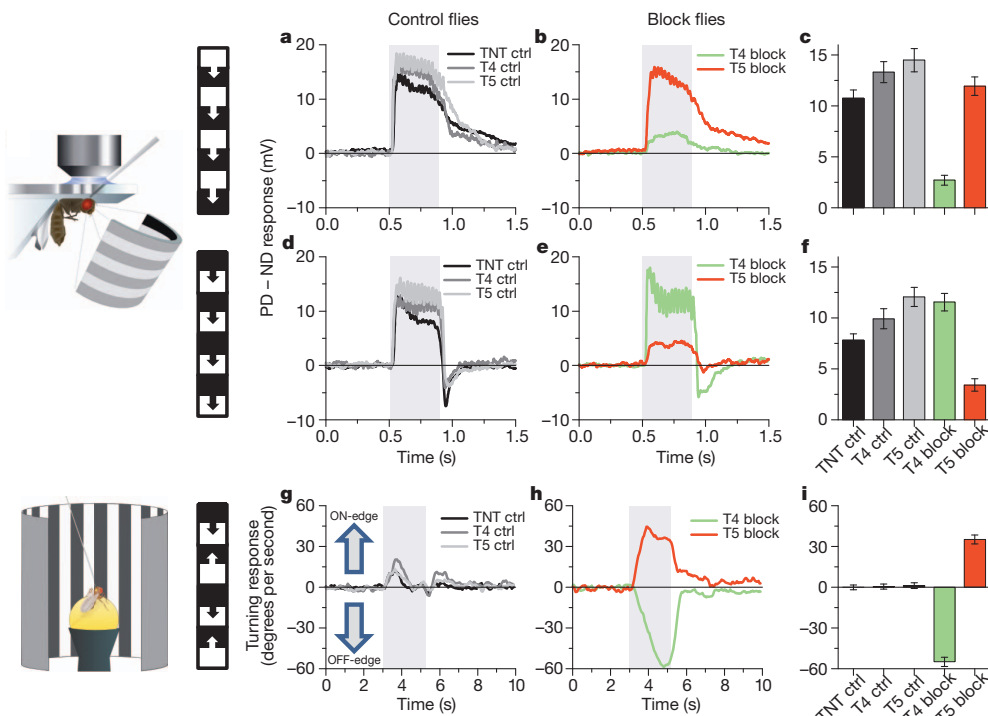


Figure 4 | Voltage responses of lobula plate tangential cells and turning responses of walking flies to moving ON and OFF edges. **a, d**, Average time course of the membrane potential in response to preferred direction motion minus the response to null direction motion (PD – ND response) as recorded in three types of control flies (stimulation period indicated by shaded area). **b, e**, Same as in **a, d**, but recorded in T4-block flies (green) and T5-block flies (red). The stimulus pattern, shown to the left, consisted of multiple ON- (**a**) or OFF-edges (**d**). **c, f**, Mean voltage responses (PD – ND) of tangential cells in the five groups of flies. Recordings were done from cells of the vertical²¹ and the horizontal²² system. Because no difference was detected between them, data were pooled. Data comprise recordings from $n = 20$ (TNT control), $n = 12$ (T4 control), $n = 16$ (T5 control), $n = 17$ (T4 block) and $n = 18$ (T5 block) cells. In both T4 and T5-block flies, ON and OFF responses are significantly different

from each other with $P < 0.001$. In T4-block flies, ON responses are significantly reduced compared to all three types of control flies, whereas in T5-block flies, OFF responses are significantly reduced, both with $P < 0.001$. **g**, Average time course of the turning response of three types of control flies to ON and OFF edges moving simultaneously to opposite directions (stimulation period indicated by shaded area). **h**, Same as in **g**, but recorded from T4-block flies (green) and T5-block flies (red). **i**, Mean turning tendency (\pm s.e.m.) during the last second of the stimulation period averaged across all flies within each group. Data comprise average values obtained in $n = 12$ (TNT controls), $n = 11$ (T4 controls), $n = 11$ (T5 controls), $n = 13$ (T4 block) and $n = 12$ (T5 block) flies. Values of T4 and T5-block flies are highly significantly different from zero with $P < 0.001$. Significances indicated are based on two-sample *t*-test.

motion detection—that is, asymmetric temporal filtering and non-linear interaction—to the neuropile between the axon terminals of lamina neurons L1 and L2 (ref. 28) and the dendrites of directionally selective T4 and T5 cells (Supplementary Fig. 2). The dendrites of T4 and T5 cells might well be the place where signals from neighbouring columns interact in a nonlinear way, similar to the dendrites of starburst amacrine cells of the vertebrate retina²⁹.

METHODS SUMMARY

Flies. Flies used in calcium imaging experiments (Figs 1–3) had the following genotypes: T4/T5 line (w^- ; $+/+$; UAS-GCaMP5, R42F06-GAL4/UAS-GCaMP5, R42F06-GAL4), T4 line (w^- ; $+/+$; UAS-GCaMP5, R54A03-GAL4/UAS-GCaMP5, R54A03-GAL4), T5 line (w^- ; $+/+$; UAS-GCaMP5, R42H07-GAL4/UAS-GCaMP5, R42H07-GAL4). Flies used in electrophysiological and behavioural experiments (Fig. 4) had identical genotypes of the following kind: TNT control flies (w^+/w^+ ; UAS-TNT-E/UAS-TNT-E; $+/+$), T4 control flies (w^+/w^- ; $+/+$; VT37588-GAL4/+), T5 control flies (w^+/w^- ; $+/+$; R42H07-GAL4/+), T4-block flies (w^+/w^- ; UAS-TNT-E/+; VT37588-GAL4/+), T5-block flies (w^+/w^- ; UAS-TNT-E/+; R42H07-GAL4/+).

Two-photon microscopy. We used a custom-built two-photon laser scanning microscope²⁹ equipped with a $\times 40$ water immersion objective and a mode-locked Ti:sapphire laser. To shield the photomultipliers from the stimulus light, two separate barriers were used: the first was placed directly over the LEDs, the second extended from the fly holder over the arena. Images were acquired at a resolution of 256×256 pixels and a frame rate of 1.87 Hz, except where indicated, using ScanImage software³⁰.

Electrophysiology. Recordings were established under visual control using a Zeiss Microscope and a $\times 40$ water immersion objective.

Behavioural analysis. The locomotion recorder was custom-designed according to ref. 18. It consisted of an air-suspended sphere floating in a bowl-shaped sphere holder. Motion of the sphere was recorded by two optical tracking sensors.

Visual stimulation. For calcium imaging and electrophysiological experiments, we used a custom-built LED arena covering 180° and 90° of the visual field along the horizontal and the vertical axis, respectively, at 1.5° resolution. For the behavioural experiments, three 120-Hz LCD screens formed a U-shaped visual arena with the fly in the centre, covering 270° and 114° of the visual field along the horizontal and the vertical axes, respectively, at 0.1° resolution.

Data evaluation. Data were evaluated off-line using custom-written software (Matlab and IDL).

Full Methods and any associated references are available in the online version of the paper.

Received 16 April; accepted 20 May 2013.

1. Bausenwein, B., Dittrich, A. P. M. & Fischbach, K. F. The optic lobe of *Drosophila melanogaster* II. Sorting of retinotopic pathways in the medulla. *Cell Tissue Res.* **267**, 17–28 (1992).
2. Akerboom, J. *et al.* Optimization of a GCaMP calcium indicator for neural activity imaging. *J. Neurosci.* **32**, 13819–13840 (2012).
3. Cajal, S. R. & Sanchez, D. *Contribución al conocimiento de los centros nerviosos de los insectos* (Imprenta de Hijos de Nicholas Moja, 1915).
4. Strausfeld, N. J. *Atlas of an Insect Brain* (Springer, 1976).
5. Fischbach, K. F. & Dittrich, A. P. M. The optic lobe of *Drosophila melanogaster*. I. A Golgi analysis of wild-type structure. *Cell Tissue Res.* **258**, 441–475 (1989).

6. Reichardt, W. Autocorrelation, a principle for the evaluation of sensory information by the central nervous system. In *Sensory Communication* (ed. Rosenblith, W. A.) 303–317 (MIT Press and John Wiley & Sons, 1961).
7. Borst, A., Haag, J. & Reiff, D. F. Fly motion vision. *Annu. Rev. Neurosci.* **33**, 49–70 (2010).
8. Buchner, E., Buchner, S. & Buelthoff, H. Deoxyglucose mapping of nervous activity induced in *Drosophila* brain by visual movement. 1. Wildtype. *J. Comp. Physiol. A* **155**, 471–483 (1984).
9. Strausfeld, N. J. & Lee, J. K. Neuronal basis for parallel visual processing in the fly. *Vis. Neurosci.* **7**, 13–33 (1991).
10. Schnell, B., Raghu, V. S., Nern, A. & Borst, A. Columnar cells necessary for motion responses of wide-field visual interneurons in *Drosophila*. *J. Comp. Physiol. A* **198**, 389–395 (2012).
11. Douglass, J. K. & Strausfeld, N. J. Visual motion-detection circuits in flies: Parallel direction- and non-direction-sensitive pathways between the medulla and lobula plate. *J. Neurosci.* **16**, 4551–4562 (1996).
12. Franceschini, N., Riehle, A. & Le Nestour, A. Directionally selective motion detection by insect neurons. In *Facets of Vision* (ed. Stavenga, H.) 360–390 (Springer, 1989).
13. Joesch, M., Schnell, B., Raghu, S. V., Reiff, D. F. & Borst, A. ON and OFF pathways in *Drosophila* motion vision. *Nature* **468**, 300–304 (2010).
14. Pfeiffer, B. D. *et al.* Tools for neuroanatomy and neurogenetics in *Drosophila*. *Proc. Natl Acad. Sci. USA* **105**, 9715–9720 (2008).
15. Denk, W., Strickler, J. H. & Webb, W. W. Two-photon laser scanning fluorescence microscopy. *Science* **248**, 73–76 (1990).
16. Oyster, C. W. & Barlow, H. B. Direction-selective units in rabbit retina: distribution of preferred directions. *Science* **155**, 841–842 (1967).
17. Sweeney, S. T., Broadie, K., Keane, J., Niemann, H. & O’Kane, C. J. Targeted expression of tetanus toxin light chain in *Drosophila* specifically eliminates synaptic transmission and causes behavioral defects. *Neuron* **14**, 341–351 (1995).
18. Seelig, J. D. *et al.* Two-photon calcium imaging from head-fixed *Drosophila* during optomotor walking behavior. *Nature Methods* **7**, 535–540 (2010).
19. Clark, D. A., Bursztyn, L., Horowitz, M. A., Schnitzer, M. J. & Clandinin, T. R. Defining the computational structure of the motion detector in *Drosophila*. *Neuron* **70**, 1165–1177 (2011).
20. Egelhaaf, M. & Borst, A. Calcium accumulation in visual interneurons of the fly: Stimulus dependence and relationship to membrane potential. *J. Neurophysiol.* **73**, 2540–2552 (1995).
21. Joesch, M., Plett, J., Borst, A. & Reiff, D. F. Response properties of motion-sensitive visual interneurons in the lobula plate of *Drosophila melanogaster*. *Curr. Biol.* **18**, 368–374 (2008).
22. Schnell, B. *et al.* Processing of horizontal optic flow in three visual interneurons of the *Drosophila* brain. *J. Neurophysiol.* **103**, 1646–1657 (2010).
23. Borst, A. & Egelhaaf, M. Direction selectivity of fly motion-sensitive neurons is computed in a two-stage process. *Proc. Natl Acad. Sci. USA* **87**, 9363–9367 (1990).
24. Single, S., Haag, J. & Borst, A. Dendritic computation of direction selectivity and gain control in visual interneurons. *J. Neurosci.* **17**, 6023–6030 (1997).
25. Eichner, H., Joesch, M., Schnell, B., Reiff, D. F. & Borst, A. Internal structure of the fly elementary motion detector. *Neuron* **70**, 1155–1164 (2011).
26. Joesch, M., Weber, F., Eichner, H. & Borst, A. Functional specialization of parallel motion detection circuits in the fly. *J. Neurosci.* **33**, 902–905 (2013).
27. Egelhaaf, M. & Borst, A. Are there separate ON and OFF channels in fly motion vision? *Vis. Neurosci.* **8**, 151–164 (1992).
28. Takemura, S. Y., Lu, Z. & Meinertzhagen, I. A. Synaptic circuits of the *Drosophila* optic lobe: the input terminals to the medulla. *J. Comp. Neurol.* **509**, 493–513 (2008).
29. Euler, T., Detwiler, P. B. & Denk, W. Directionally selective calcium signals in dendrites of starburst amacrine cells. *Nature* **418**, 845–852 (2002).
30. Pologruto, T. A., Sabatini, B. L. & Svoboda, K. ScanImage: Flexible software for operating laser scanning microscopes. *Biomed. Eng. Online* **2**, 13 (2003).

Supplementary Information is available in the online version of the paper.

Acknowledgements We thank L. Looger, J. Simpson, V. Jayaraman and the Janelia GECI team for making and providing us with the GCaMP5 flies before publication; J. Plett for designing and engineering the LED arena; C. Theile, W. Essbauer and M. Sauter for fly work; and A. Mauss, F. Gabbiiani and T. Bonhoeffer for critically reading the manuscript. This work was in part supported by the Deutsche Forschungsgemeinschaft (SFB 870). M.S.M., G.A., E.S., M.M., A.L., A.Ba and A.Bo are members of the Graduate School of Systemic Neurosciences.

Author Contributions M.S.M. and J.H. jointly performed and, together with A.Bo, evaluated all calcium imaging experiments. G.A., E.S. and M.M. recorded from tangential cells. A.L., T.S. and A.Ba. performed the behavioural experiments. G.R., B.D. and A.N. generated the driver lines and characterized their expression pattern. D.F.R. performed preliminary imaging experiments. E.H. helped with programming and developed the PMT shielding for the two-photon microscope. A.Bo. designed the study and wrote the manuscript with the help of all authors.

Author Information Reprints and permissions information is available at www.nature.com/reprints. The authors declare no competing financial interests. Readers are welcome to comment on the online version of the paper. Correspondence and requests for materials should be addressed to A.Bo. (borst@neuro.mpg.de).

METHODS

Flies. Flies were raised on standard cornmeal-agar medium at 25 °C and 60% humidity throughout development on a 12 h light/12 h dark cycle. For calcium imaging, we used the genetically encoded single-wavelength indicator GCaMP5, variant G, with the following mutations: T302L, R303P and D380Y (ref. 2). Expression of GCaMP5 was directed by three different Gal4 lines, all from the Janelia Farm collection¹⁴. Flies used in calcium imaging experiments (Figs 1–3) had the following genotypes: T4/T5 line (*w⁻*; +/++; UAS-GCaMP5, R42F06-GAL4/UAS-GCaMP5, R42F06-GAL4), T4 line (*w⁻*; +/++; UAS-GCaMP5, R54A03-GAL4/UAS-GCaMP5, R54A03-GAL4), T5 line (*w⁻*; +/++; UAS-GCaMP5, R42H07-GAL4/UAS-GCaMP5, R42H07-GAL4). All driver lines were generated by the methods described in ref. 14 and were identified by screening a database of imaged lines, followed by reimaging of selected lines³¹. As homozygous for both the Gal4-driver and the UAS-GCaMP5 genes, T4 flies also showed some residual expression in T5 cells, and T5 flies also in T4 cells. This unspecific expression, however, was in general less than 25% of the expression in the specific cells. Flies used in electrophysiological and behavioural experiments (Fig. 4) had identical genotypes of the following kind: TNT control flies (*w⁺*/*w⁺*; UAS-TNT-E/UAS-TNT-E; +/++), T4 control flies (*w⁺*/*w⁻*; +/++; VT37588-GAL4/+), T5 control flies (*w⁺*/*w⁻*; +/++; R42H07-GAL4/+), T4-block flies (*w⁺*/*w⁻*; UAS-TNT-E/+; VT37588-GAL4/+), T5-block flies (*w⁺*/*w⁻*; UAS-TNT-E/+; R42H07-GAL4/+). UAS-TNT-E flies were derived from the Bloomington Stock Center (stock no. 28837) and VT37588-Gal4 flies were derived from the VDRC (stock no. 205893). Before electrophysiological experiments, flies were anaesthetized on ice and waxed on a Plexiglas holder using bees wax. The dissection of the fly cuticle and exposure of the lobula plate were performed as described previously (for imaging experiments, see ref. 32; for electrophysiology, see ref. 21). Flies used in behavioural experiments were taken from 18 °C just before the experiment and immediately cold-anaesthetized. The head, the thorax and the wings were glued to a needle using near-ultraviolet bonding glue (Sinfony Opaque Dentin) and strong blue LED light (440 nm, dental curing-light, New Woodpecker).

Two-photon microscopy. We used a custom-built two-photon laser scanning microscope³³ equipped with a $\times 40$ water immersion objective (0.80 NA, IR-Achroplan; Zeiss). Fluorescence was excited by a mode locked Ti:sapphire laser (<100 fs, 80 MHz, 700–1,020 nm; pumped by a 10 W CW laser; both Mai Tai; Spectraphysics) with a DeepSee accessory module attached for dispersion compensation control resulting in better pulse compression and fluorescence at the target sample. Laser power was adjusted to 10–20 mW at the sample, and an excitation wavelength of 910 nm was used. The photomultiplier tube (H10770PB-40, Hamamatsu) was equipped with a dichroic band-pass mirror (520/35, Brightline). Images were acquired at a resolution of 256 \times 256 pixels and a frame rate of 1.87 Hz, except in Fig. 2 (7.5 Hz), using the ScanImage software³⁰.

Electrophysiology. Recordings were established under visual control using a $\times 40$ water immersion objective (LumplanF, Olympus), a Zeiss microscope (Axioptik vario 100, Zeiss), and illumination (100 W fluorescence lamp, hot mirror, neutral density filter OD 0.3; all from Zeiss). To enhance tissue contrast, we used two polarization filters, one located as an excitation filter and the other as an emission filter, with slight deviation on their polarization plane. For eye protection, we additionally used a 420-nm LP filter on the light path.

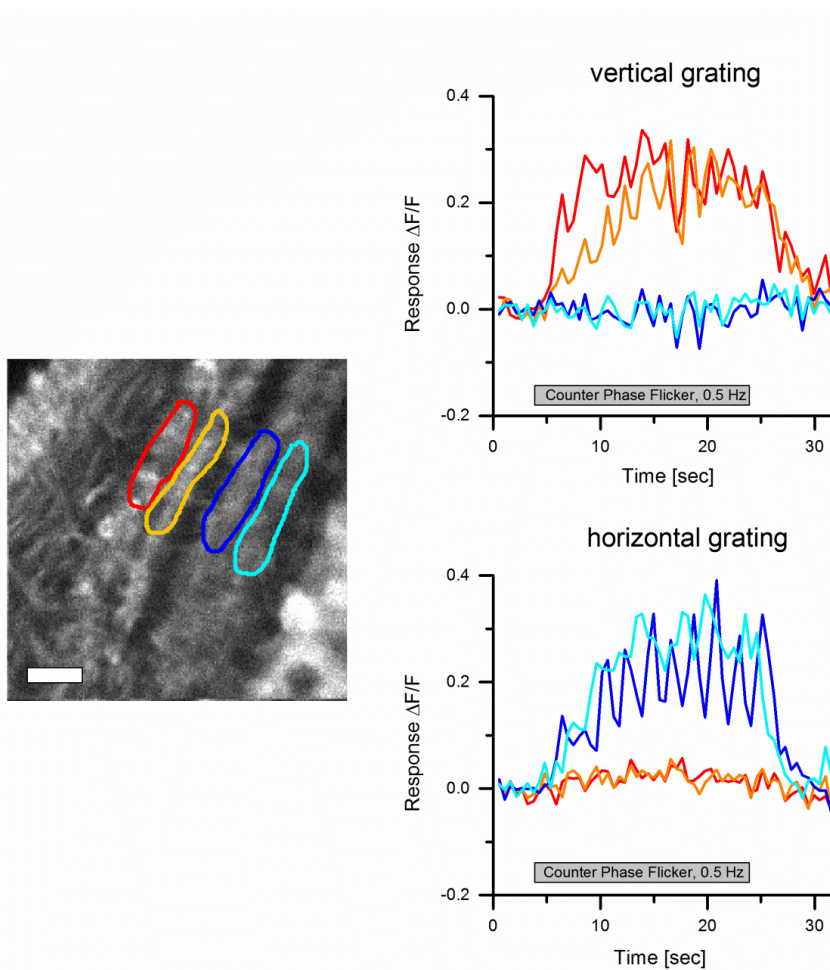
Behavioural analysis. The locomotion recorder was custom-designed according to ref. 18. Briefly, it consists of an air-suspended sphere floating in a bowl-shaped sphere holder. A high-power infrared LED (800 nm, JET series, 90 mW, Roithner Electronics) is located in the back to illuminate the fly and the sphere surface. Two optical tracking sensors are equipped with lens and aperture systems to focus on the sphere behind the fly. The tracking data are processed at 4 kHz internally, read out via a USB interface and processed by a computer at \approx 200 Hz. This allows real-time calculation of the instantaneous rotation axis of the sphere. A third camera (GRAS-20S4M-C, Point Grey Research) is located in the back which is essential for proper positioning of the fly and allows real-time observation and video recording of the fly during experiments.

Visual stimulation. For calcium imaging and electrophysiological experiments, we used a custom-built LED arena that allowed refresh rates of up to 550 Hz and 16 intensity levels. It covered 180° (1.5° resolution) and 90° (1.5° resolution) of the visual field along the horizontal and the vertical axis, respectively. The LED arena was engineered and modified based upon ref. 34. The LED array consists of 7 \times 4 individual TA08-81GWA dot-matrix displays (Kingbright), each harbouring 8 \times 8 individual green (568 nm) LEDs. Each dot-matrix display is controlled by an ATmega168 microcontroller (Atmel) combined with a ULN2804 line driver (Toshiba America) acting as a current sink. All panels are in turn controlled via an I2C interface by an ATmega128 (Atmel)-based main controller board, which reads in pattern information from a compact flash (CF) memory card. Matlab was used for programming and generation of the patterns as well as for sending the serial command sequences via RS-232 to the main controller board. The

luminance range of the stimuli was 0.5–33 cd m⁻². For the calcium imaging experiments, two separate barriers were used to shield the photomultipliers from the stimulus light coming from the LED arena. The first was a spectral filter with transparency to wavelengths >540 nm placed directly over the LEDs (ASF SFG 10, Microchemicals). The second was a layer of black PVC extending from the fly holder over the arena. Square wave gratings had a spatial wavelength of 30° of visual angle and a contrast of 88%. Unless otherwise stated, they were moving at 30° s⁻¹. Edges had the same contrast and were also moving at 30° s⁻¹. For the experiments shown in Figs 1, 2b and 3, each grating or edge motion was shown twice within a single sweep, resulting in a total of eight stimulation periods. Each stimulus period lasted 4 s, and subsequent stimuli were preceded by a 3-s pause. In the experiment shown in Fig. 2a, a dark edge of 88% contrast was moved for 1 s at 15° s⁻¹ from the front to the back at three different positions (22°, 44°, 66° from frontal to lateral). At each position, edge motion was repeated 15 times. For the experiment shown in Fig. 2b, a bright edge of 88% contrast was moving at 15° s⁻¹ from the back to the front, and images were acquired at a frame rate of 7.5 Hz. For the experiments shown in Figs 3e, f, all six stimulus velocities were presented once within one sweep, with the stimulus lasting 4 s, and different stimuli being separated by 2 s. In the experiments shown in Figs 3g, h, a single sweep contained all 12 grating orientations with the same stimulus and pause length as above. For the electrophysiology experiments (Fig. 4a–f), multiple edges were used as stimuli moving simultaneously at 50° s⁻¹. To stimulate cells of horizontal system (HS cells), a vertical, stationary square-wave grating with 45° spatial wavelength was presented. For ON-edge motion, the right (preferred direction, PD) or the left edge (null direction, ND) of each light bar started moving until it merged with the neighbouring bar. For OFF-edge motion, the right or the left edge of each dark bar was moving. To stimulate cells of the vertical system (VS cells), the pattern was rotated by 90° clockwise. For the behavioural experiments (Fig. 4g–i), three 120-Hz LCD screens (Samsung 2233 RZ) were vertically arranged to form a U-shaped visual arena ($w = 31$ cm \times $d = 31$ cm \times $h = 47$ cm) with the fly in the centre. The luminance ranged from 0 to 131 cd m⁻² and covered large parts of the flies' visual field (horizontal, ± 135 °; vertical, ± 57 °; resolution, <0.1 °). The three LCD screens were controlled via NVIDIA 3D Vision Surround Technology on Windows 7 64-bit allowing a synchronized update of the screens at 120 frames per second. Visual stimuli were created using Panda3D, an open-source gaming engine, and Python 2.7, which simultaneously controlled the frame rendering in Panda3D, read out the tracking data and temperature and streamed data to the hard disk. The balanced motion stimulus consisted of a square-wave grating with 45° spatial wavelength and a contrast of 63%. Upon stimulation onset, dark and bright edges moved into opposite directions at 10° s⁻¹ for 2.25 s. This stimulation was performed for both possible edge directions and two initial grating positions shifted by half a wavelength, yielding a total of four stimulus conditions.

Data evaluation. Data were evaluated off-line using custom-written software (Matlab and IDL). For the images shown in Figs 1e, f, 2a and 3a, b, the raw image series was converted into four images representing the relative fluorescence change during each direction of grating motion: $(\Delta F/F)_{\text{stim}} = (F_{\text{stim}} - F_{\text{ref}})/F_{\text{ref}}$. The image representing the stimulus fluorescence (F_{stim}) was obtained by averaging all images during stimulation; the image representing the reference fluorescence (F_{ref}) was obtained by averaging three images before stimulation. Both images were smoothed using a Gaussian filter of 10 pixel half-width. For the images shown in Figs 1f and 3a, b, $\Delta F/F$ images were normalized by their maximum value. Then, a particular colour was assigned to each pixel according to the stimulus direction during which it reached maximum value, provided it passed a threshold of 25%. Otherwise, it was assigned to background. The response strength of each pixel was coded as the saturation of that particular colour. For the data shown in Figs 2b, c and 3c–h, the raw image series was first converted into a $\Delta F/F$ series by using the first three images as reference. Then, a region was defined within a raw image, and average $\Delta F/F$ values were determined within that region for each image, resulting in a $\Delta F/F$ signal over time. Responses were defined as the maximum $\Delta F/F$ value reached during each stimulus presentation minus the average $\Delta F/F$ value during the two images preceding the stimulus. For the bar graphs shown in Fig. 4c, f, the average voltage responses during edge motion (0.45 s) along the cell's preferred (PD) and null direction (ND) were calculated. For each recorded tangential cell, the difference between the PD and the ND response was determined, and these values were averaged across all recorded cells. The data shown in Fig. 4g, h were obtained from the four stimulus conditions by averaging the turning responses for the two starting positions of the grating and calculating the mean difference between the turning responses for the two edge directions. For the bar graph shown in Fig. 4i, the average turning response of each fly during the last second of balanced motion stimulation was calculated. These values were averaged across all recorded flies within each genotype.

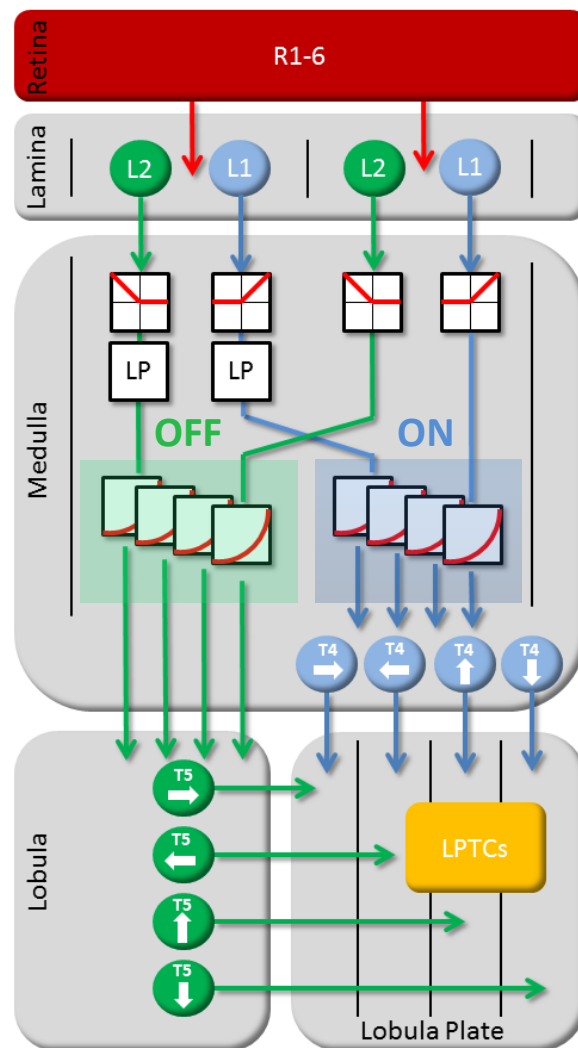
31. Jenett, A. *et al.* A Gal4-driver line resource for *Drosophila* neurobiology. *Cell Rep.* **2**, 991–1001 (2012).
32. Reiff, D. F., Plett, J., Mank, M., Griesbeck, O. & Borst, A. Visualizing retinotopic half-wave rectified input to the motion detection circuitry of *Drosophila*. *Nature Neurosci.* **13**, 973–978 (2010).
33. Euler, T. *et al.* Eyecup scope—optical recording of light stimulus-evoked fluorescence signals in the retina. *Plüger Arch.* **457**, 1393–1414 (2009).
34. Reiser, M. B. & Dickinson, M. H. A modular display system for insect behavioral neuroscience. *J. Neurosci. Methods* **167**, 127–139 (2008).



Supplemental Fig.1 Responses of T4 and T5 cells to counter-phase flicker. Square-wave gratings (15 deg spatial wavelength and 88% contrast) with vertical (top) and horizontal (bottom) orientation were phase-shifted every second by 180 deg for 20 seconds. Response traces are derived from the region of interest encircled in the image to the left with the same color from a single stimulation period. T4 and T5 cells in layers 1 and 2 only respond to the vertical grating, cells in layers 3 and 4 selectively respond to the horizontal grating. Similar results were obtained in $n=4$ flies. Scale bar = 5 μ m. Together with the missing response of T4 and T5 cells to full-field flicker, these findings suggest that T4 and T5 cells receive input signals from neurons with different orientation tuning, depending on whether they respond to motion along the horizontal (layers 1 and 2) or the vertical (layers 3 and 4) axis^{1,2}.

1 Pick, B. & Buchner, E. Visual movement detection under light- and dark-adaptation in the fly, *Musca domestica*. *J. Comp. Physiol.* **134**, 45-54 (1979).

2 Srinivasan, M.V. & Dvorak, D.R. Spatial processing of visual information in the movement-detecting pathway of the fly. *J. Comp. Physiol.* **140**, 1-23 (1980).



Supplemental Fig.2 Circuit diagram of the fly elementary motion detector. Visual input from photoreceptors R1-6 is split into parallel pathways, L1 and L2, at the level of the lamina. Two neighboring columns are shown. The outputs from both L1 and L2 are half-wave rectified, such that downstream elements carry information about ON (L1-pathway) and OFF (L2-pathway) signals separately. After temporal low-pass filtering ('LP') the signals from one column, they interact in a supra-linear way with the instantaneous signals derived from the other column. This interaction takes place, separately in both pathways, along all four cardinal directions. Directionally selective signals are carried via T4 and T5 cells to the four layers of the lobula plate where T4 and T5 cells with the same preferred direction converge again on the dendrites of the tangential cells ('LPTCs').

2.2 Object Tracking in Motion-Blind Flies

Armin Bahl, Georg Ammer, **Tabea Schilling** and Alexander Borst

Author contributions:

A. Bahl set up the locomotion recorder and the stimulus display, and wrote the software for reading the behavioral output and displaying the stimulus. A. Bahl and **T.S.** performed all of the behavioral experiments and evaluated the data. G.A. performed the electrophysiological recordings and analyzed the data. A. Bahl and A. Borst designed the study. A. Borst carried out the modeling work. A. Borst and A. Bahl wrote the manuscript with the help of the other authors.

Tabea Schilling

Alexander Borst

Object tracking in motion-blind flies

Armin Bahl, Georg Ammer, Tabea Schilling & Alexander Borst

Different visual features of an object, such as its position and direction of motion, are important elements for animal orientation, but the neural circuits extracting them are generally not well understood. We analyzed this problem in *Drosophila*, focusing on two well-studied behaviors known as optomotor response and fixation response. In the neural circuit controlling the optomotor response, columnar T4 and T5 cells are thought to be crucial. We found that blocking T4 and T5 cells resulted in a complete loss of the optomotor response. Nevertheless, these flies were still able to fixate a black bar, although at a reduced performance level. Further analysis revealed that flies in which T4 and T5 cells were blocked possess an intact position circuit that is implemented in parallel to the motion circuit; the optomotor response is exclusively controlled by the motion circuit, whereas the fixation response is supported by both the position and the motion circuit.

Optomotor and fixation responses of flies have been studied extensively. Experiments on tethered *Drosophila* walking or flying inside a rotating drum revealed a strong and persistent optomotor response along the direction of the rotating drum^{1–3} (open loop). The effect of large-field stimuli on visual course control can also be seen in free flight, where the structure of the flight path of *Drosophila* depends on the visual pattern of the surrounding environment⁴. When the pattern is rotating, the fly's behavior exhibits distinct, circular flight paths around the center of the arena⁵. Fixation behavior was first observed in tethered flying house flies in which the fly's torque was fed back into a servo motor controlling the position of a black bar^{6,7} (closed loop). Under these conditions, flies keep the bar in front of them most of the time. Moreover, it was shown that bar fixation interacts with the expansion avoidance reaction of *Drosophila* when presented with translatory full-field optic flow⁸. Fixation behavior has also been studied in freely walking and flying *Drosophila*^{9–12}. On the basis of their different dynamics and spatial sensitivity, the optomotor and fixation responses were proposed to represent the output of different visual processing pathways¹³. Similar conclusions were drawn from experiments in which the tangential cells of the lobula plate were either genetically or surgically removed^{14–17}, or in mutants with reduced optic lobes¹⁸; in general, flies seem to be impaired more strongly in their response to large-field rotating patterns than in their reaction to single, moving bars. However, none of the techniques used provided a sufficiently high resolution to make any definitive statements about the involvement of individual cell types of the fly optic lobe in one or the other pathway.

To dissect the neural circuits underlying the optomotor and fixation responses, we built on recent progress in our understanding of the visual processing stream¹⁹ leading from the photoreceptors R1–6 via lamina and medulla to directionally selective motion responses in the lobula plate tangential cells (LPTCs; Fig. 1a). Recording from LPTCs via whole-cell patch^{20,21} combined with selective blockade of individual columnar cells revealed that lamina cells L1 and L2 provide the main input to the motion detection circuit, functionally

segregating into an ON and an OFF pathway, respectively^{22,23}. The L1 and L2 pathways, which have been described anatomically^{24,25}, converge again on the dendrites of the tangential cells in the lobula plate via T4 and T5 cells; blocking the synaptic output from T4 and T5 cells completely abolishes the motion response in tangential cells, but leaves some residual response to full-field flicker²⁶. To test the behavioral performance of these flies, we used a procedure in which a tethered fly walks on a small sphere supported by an air stream^{2,27}. A computer reads the movement of the sphere, controls the visual stimulus presented to the fly and adjusts the ambient temperature. Moreover, we used the *Gal4-UAS* system²⁸ to genetically express a temperature-sensitive allele of *shibire*²⁹ in a small subset of neurons in the fly brain. This permitted a selective shut down of the desired part of the neuronal circuit during the experiment by switching from the permissive temperature for *shibire^{ts}* (25 °C) to its restrictive one (34 °C).

RESULTS

Optomotor and fixation response

We tested the optomotor and fixation response of flies in which *shibire^{ts}* was expressed in T4 and T5 cells (T4/T5 block flies). As the behavior of flies turned out to be highly dependent on temperature (Supplementary Fig. 1), all of our control experiments were carried out with flies of a different genotype using the same temperature protocol. For controls, we used flies with two different genotypes: flies that carried the *shibire^{ts}* effector allele, but no *Gal4* driver gene (*shibire^{ts}* control), and flies that carried the *Gal4* driver gene, but no *shibire^{ts}* effector gene (T4/T5 control). We examined the temperature dependency of the block: T4/T5 block flies behaved similar to control flies at 25 °C, as well as when the temperature was slowly elevated to 34 °C. However, clear differences emerged approximately 5 min after reaching 34 °C (Supplementary Fig. 1). To exclude any motor deficits in T4/T5 block flies, we analyzed their general walking and turning activity, which were not different from those of control flies (Supplementary Fig. 2).

Max Planck Institute of Neurobiology, Martinsried, Germany. Correspondence should be addressed to A. Bahl (bahl@neuro.mpg.de) or A. Borst (borst@neuro.mpg.de).

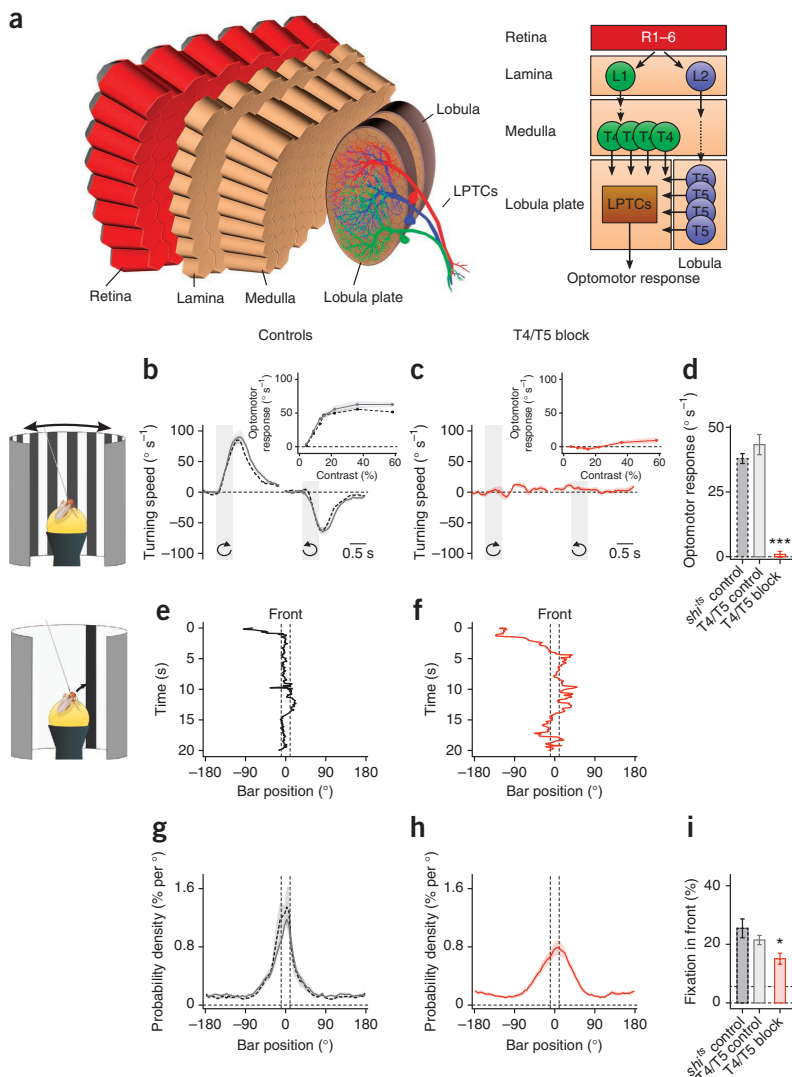
Received 6 February; accepted 28 March; published online 28 April 2013; doi:10.1038/nn.3386

Figure 1 Optomotor response and fixation response of control and T4/T5 block flies. **(a)** Schematic of the fly's optic lobe. In each lamina column, photoreceptors R1–6 synapse onto lamina cells L1 and L2, forming parallel pathways for motion detection. The output signals of both pathways converge via T4 and T5 cells on the dendrites of LPTCs. **(b,c)** Turning speed of control (*sh¹ts* control (dashed black line) and T4/T5 control (solid gray line); **b**) and T4/T5 block (solid red line; **c**) flies in response to clockwise and counterclockwise rotation of a grating pattern (contrast = 22%, gray shaded areas; 20 trials per fly, $n = 10$ flies per group). Inset, optomotor response as function of grating contrast (clockwise minus counterclockwise rotation response divided by 2; averaged in 1 s after stimulus onset). **(d)** Average optomotor response (average over contrasts). *** $P < 0.001$, two-sided t test compared with both control groups. The response of the T4/T5 block group was not significantly different from zero ($P = 0.47$, two-sided t test). **(e,f)** Bar position over time during closed-loop fixation (single trial of one *sh¹ts* control fly **e**), single trial for one T4/T5 block fly **f**). Vertical dashed lines indicate the frontal area ($\pm 10^\circ$). **(g,h)** Average probability density as function of bar position for control (40 trials per fly, $n = 10$ flies per group; **g**) and T4/T5 block (40 trials per fly, $n = 12$ flies; **h**) flies. **(i)** Integration of the probability density curves between $\pm 10^\circ$ gives the percentage of time the bar is held in the frontal visual field (fixation in front). Upper horizontal dashed line represents the chance level (5.6%, no fixation). * $P < 0.05$, two-sided t test compared with both control groups. The value of the T4/T5 block group was significantly different from chance ($P < 0.001$, two-sided t test). All data represent mean \pm s.e.m.

We first confronted the flies with a large-field grating moving clockwise and counterclockwise (Fig. 1b–d). Both types of control flies exhibited a strong and reliable optomotor response over a wide range of pattern contrasts (Fig. 1b,d). Instead, T4/T5 block flies no longer followed the motion of the panorama, no matter how high the pattern contrast (Fig. 1c,d). We next performed closed-loop fixation experiments and coupled the flies' turning tendency to the position of a single black bar such that whenever the fly turned into one direction, the bar moved into the other (Fig. 1e–i). Control flies robustly moved the bar to the front and kept it there (Fig. 1e,g,i). When we tested the flies in which the output from T4 and T5 cells was blocked, we were surprised that they were still clearly able to fixate the bar, although with a somewhat broader position distribution than control flies (Fig. 1f,h,i). Taken together, these results indicate that T4 and T5 cells are a necessary part of the neural circuit controlling the optomotor response to large-field motion, but are not needed for fixation behavior.

Dissection of motion and position system

Does that mean that fixation behavior relies on a separate set of motion-sensitive neurons tuned specifically to small moving objects, or does fixation behavior rely on a purely position-dependent system that is insensitive to motion? To tease apart the response to the



direction and the response to the position of a moving bar, we used a classical approach³⁰ and moved a single bar in open loop around the fly, first in a clockwise and then in a counterclockwise direction, and measured both responses (R_{cw} and R_{ccw} respectively) as a function of bar position (Ψ)³¹.

Assuming that the turning response R of the fly to the rotating bar reflects a superposition of a position system P and a motion system M (with $v = d\Psi/dt$ denoting the angular velocity of the bar), we can write

$$R = P(\Psi, v) + M(\Psi, v)$$

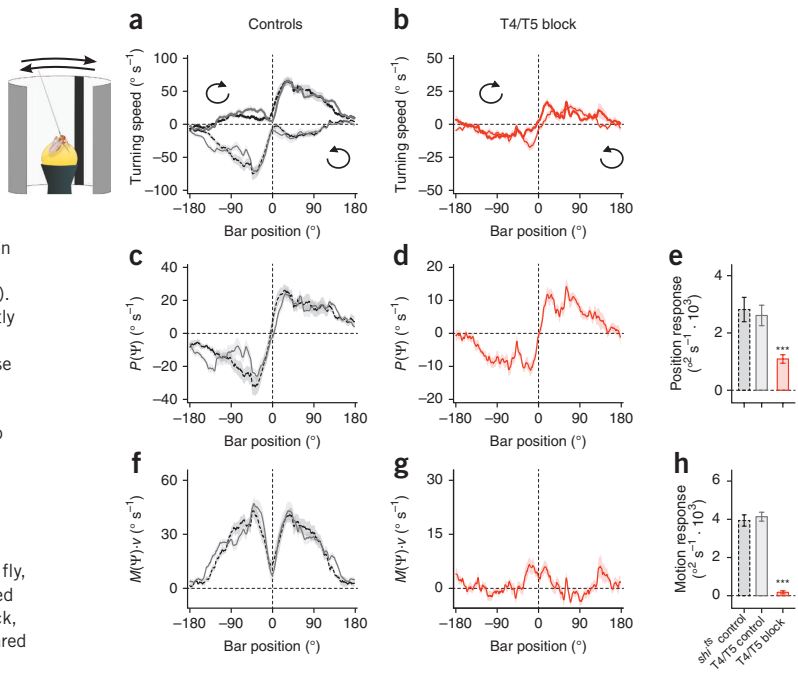
For the two directions of bar rotations, we obtain

$$R_{\text{cw}} = P(\Psi, v) + M(\Psi, v)$$

$$R_{\text{ccw}} = P(\Psi, -v) + M(\Psi, -v)$$

To simplify these equations, two classical assumptions can be made³⁰. First, the position system is velocity independent ($P(\Psi, v) = P(\Psi)$). Second, the motion system is linear in v ($M(\Psi, v) = M(\Psi) \cdot v$). Following

Figure 2 Open-loop analysis of the fixation response. **(a,b)** Responses of control **(a)** and T4/T5 block **(b)** flies to a single black bar moving clockwise (thicker lines) and counterclockwise around the fly. Responses are plotted as a function of the azimuth position of the bar; that is, during counterclockwise rotation, time progresses from right to left. **(c,d)** Summation of the clockwise and counterclockwise responses divided by 2 revealed the position-dependent response component, $P(\Psi)$, of control **(c)** and T4/T5 block **(d)** flies. **(e)** The position response (the integral of the curve $P(0^\circ < \Psi < 180^\circ)$ minus the integral of $P(-180^\circ < \Psi < 0^\circ)$ divided by 2). The response of the T4/T5 block group was significantly greater than zero ($P < 0.001$, two-sided t test). **(f,g)** Subtraction of the clockwise and counterclockwise responses divided by 2 yielded the motion-dependent response component, $M(\Psi) \cdot v$, of control **(f)** and T4/T5 block **(g)** flies (a positive value indicates a tendency to turn with the stimulus). **(h)** The motion response (the integral of the curve $M(0^\circ < \Psi < 180^\circ) \cdot v$ plus the integral of $M(-180^\circ < \Psi < 0^\circ) \cdot v$ divided by 2). The response of the T4/T5 block group was not significantly different than zero ($P = 0.06$, two-sided t test). All data represent mean \pm s.e.m.; 35 trials per fly, $n = 10, 11, 14$ flies per group (sh7s control, dashed black lines; T4/T5 control, solid gray lines; T4/T5 block, solid red lines). *** $P < 0.001$, two-sided t test compared with both control groups.



these assumptions, the position system as well as the motion system can be recovered

$$P(\Psi) = (R_{\text{cw}} + R_{\text{ccw}})/2$$

$$M(\Psi) \cdot v = (R_{\text{cw}} - R_{\text{ccw}})/2$$

We performed such experiments on control and T4/T5 block flies (Fig. 2). With a starting position behind the flies, control flies followed the direction of motion of the bar, turning clockwise (+) during clockwise motion and counterclockwise (-) during counterclockwise motion (Fig. 2a), which is slightly different from what has been measured in flying *Drosophila* under similar conditions⁸. According to the formal decomposition outlined above, we recovered a position-dependent response component, $P(\Psi)$ (Fig. 2c,e), and a motion-dependent response component, $M(\Psi)$ (Fig. 2f,h). The responses of T4/T5 block flies to such stimuli were markedly different from those of control flies; in general, T4/T5 block fly responses had smaller amplitudes and were almost identical for both directions of bar motion (Fig. 2b). Decomposing the reaction into the position- and motion-dependent components revealed that the response of these flies to the position of the bar, $P(\Psi)$, was still present, although reduced in amplitude (Fig. 2d,e). However, the response to the motion of the moving bar, $M(\Psi)$, was completely abolished (Fig. 2g,h). We conclude that T4/T5 block flies are blind to the motion of a single bar, but can still detect its position. Thus, the ability of motion-blind flies to fixate a bar in closed loop (Fig. 1f,h,i) is a result of the remaining position response.

What is the visual cue used by the position system that allows the detection of bar position: is it mere stationary contrast, its temporal change or its local motion? To address these questions, we presented control flies with an appearing black bar (10° width) at +90° azimuth which stayed there for 4 s before disappearing again (Fig. 3). The time during which the bar appeared and disappeared amounted to 0.5 s approximating the local luminance change when a black bar (width = 10° and $v = 20^\circ \text{ s}^{-1}$) moves into a 10°-wide window and, after 4 s, moves

out again. Control flies exhibited a strong, but transient, response toward the position at which the bar was appearing as well as where it was disappearing, but, during the stationary phase of the bar, no response was detectable (Fig. 3a). We then determined the response values as function of bar position. In control flies, the shape of the resulting response functions (Fig. 3c,i) looked similar to $P(\Psi)$ as obtained in the previous experiment (Fig. 2c,d). We next repeated the experiments on T4/T5 block flies. Like control flies, T4/T5 block flies responded transiently to both the appearance as well as to the disappearance of the bar, but not when the bar was stationary (Fig. 3b). Moreover, the shape of the position-dependent response functions was almost identical to the ones of control flies (Fig. 3d,g,j). We conclude that the position system is insensitive to a stationary image but uses the change of luminance over time as its input signal³². Furthermore, the position system is not affected by blocking the output of T4 and T5 cells.

Turning responses to local motion and luminance changes

We observed a clear reduction of the performance of T4/T5 block flies compared to controls when we characterized their position response under closed-loop fixation conditions (Fig. 1e-i) and when we used a rotating bar (Fig. 2). However when we used local luminance changes, we found no difference between T4/T5 block and control flies (Fig. 3). This discrepancy suggests that the detection of motion somehow enhances the fly's response toward the position of the bar. We considered two possible mechanisms. First, the motion and position system may not be fully separable on the neuronal level. In this case, local motion might directly modify the position system to enhance the position response. Second, the motion system may have a stronger response to front-to-back than back-to-front motion. In the behaving fly, this would lead to a stronger compensation of bar motion away from the front, thereby improving fixation³³. In both cases, T4/T5 block flies would no longer be able to detect the motion of the bar and their position response would be reduced. Furthermore, both arguments indicate that our assumptions (Fig. 2), which were adopted from classical experiments³⁰, might not be fully correct.

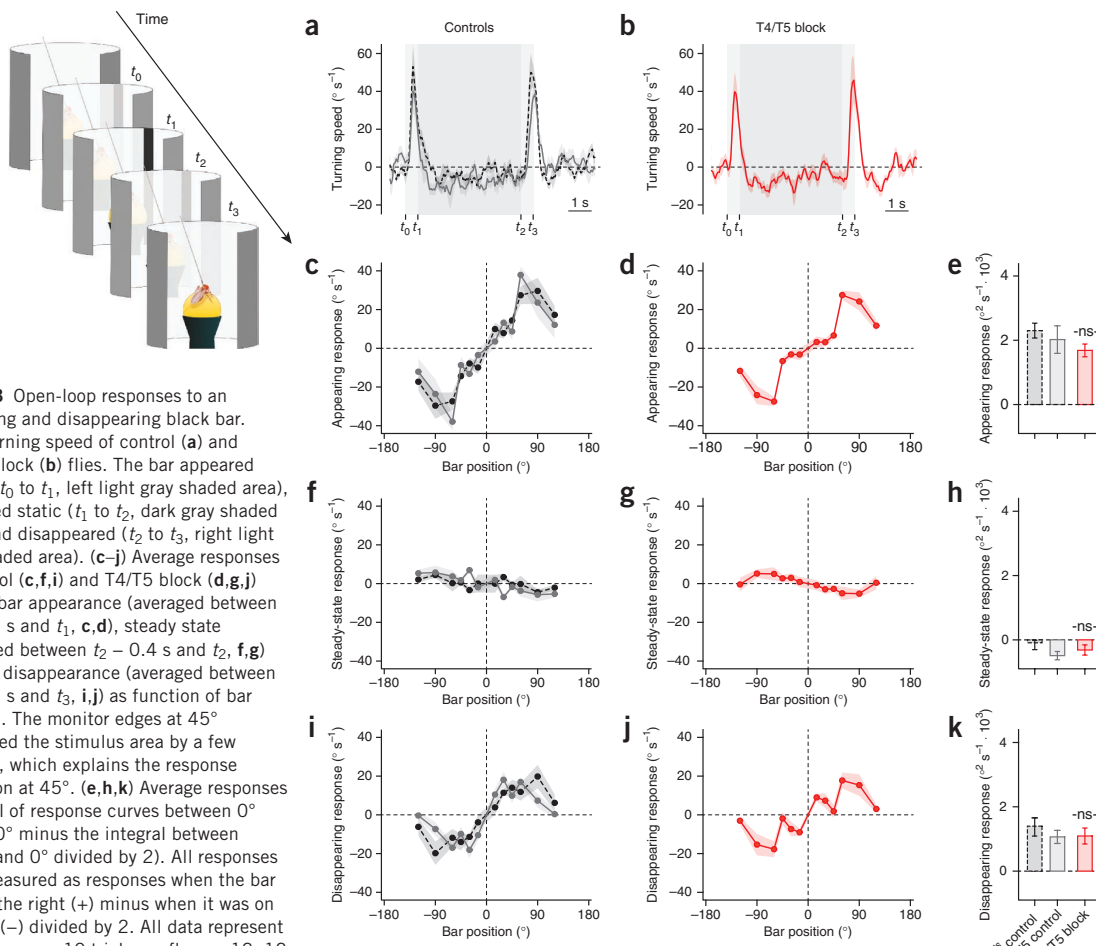


Figure 3 Open-loop responses to an appearing and disappearing black bar. **(a,b)** Turning speed of control **(a)** and T4/T5 block **(b)** flies. The bar appeared at 90° (t_0 to t_1 , left light gray shaded area), remained static (t_1 to t_2 , dark gray shaded area) and disappeared (t_2 to t_3 , right light gray shaded area). **(c-j)** Average responses of control **(c,f,i)** and T4/T5 block **(d,g,j)** flies to bar appearance (averaged between $t_0 + 0.1$ s and t_1 , **c,d**), steady state (averaged between $t_2 - 0.4$ s and t_2 , **f,g**) and bar disappearance (averaged between $t_2 + 0.1$ s and t_3 , **i,j**) as function of bar position. The monitor edges at 45° decreased the stimulus area by a few degrees, which explains the response reduction at 45°. **(e,h,k)** Average responses (integral of response curves between 0° and 120° minus the integral between -120° and 0° divided by 2). All responses were measured as responses when the bar was on the right (+) minus when it was on the left (-) divided by 2. All data represent mean \pm s.e.m.; 10 trials per fly, $n = 12, 12$ and 16 flies per group (*sh^{ts}* control, dashed black lines; T4/T5 control, solid gray lines; T4/T5 block, solid red lines). ns indicates not significant, $P \geq 0.05$, two-sided *t* test compared with both control groups. Responses of T4/T5 block flies at 45° were not significantly different to control responses ($P \geq 0.05$; two-sided *t* test compared with both control groups). Responses of *sh^{ts}* control and T4/T5 block flies during steady state were not significantly different from zero, but the response of T4/T5 control flies was ($P = 0.37, 0.11, 0.02$, respectively; two-sided *t* test).

To test these ideas, we investigated the turning responses to local front-to-back motion, back-to-front motion and luminance changes in isolation (Fig. 4). We created a virtual environment consisting of a gray cylinder with a 10° window at two azimuthal positions (either $\Psi = 30^\circ$ or $\Psi = 60^\circ$). Outside, a 10° black bar rotates at 40 ° s⁻¹ around the cylinder. Whenever the bar passes the window, it briefly allows the fly's motion system to detect the direction of bar motion (either front to back or back to front), inducing a turning tendency (M_{FTB} and M_{BTF}) in the same direction. Moreover, when the bar passes through the window, it produces local luminance changes such that luminance first decreases and then increases again. This change in luminance is detected by the fly's position system, leading to an additional turning tendency toward that position (P_{FTB} and P_{BTF}). Thus, the turning response to local front-to-back and back-to-front motion can be described as the sum of both turning tendencies.

$$R_{FTB} = M_{FTB} + P_{FTB}$$

$$R_{BTF} = M_{BTF} + P_{BTF}$$

To tease apart the different response components, we need the response of the position system alone. We approximated the local

luminance change when the rotating bar passes the window with a non-moving stimulus. The whole window starts at background luminance, darkens and then brightens again. This stimulus should only activate the position system, resulting in a turning tendency toward the position of the local luminance change ($R_L = P_L$).

When measuring the turning response of control flies to the three different stimulus conditions, all turning responses were found to be different. The response to the front-to-back stimulus (R_{FTB}) was positive and large in amplitude (Fig. 4a,c), the response to the back-to-front stimulus (R_{BTF}) was biphasic and weak (Fig. 4d,f), and the response to local luminance changes (R_L) was positive and weak (Fig. 4g,i). In contrast, the responses of T4/T5 block flies to front-to-back motion, back-to-front motion and local luminance changes were all identical (Fig. 4b,e,h,j). We found no differences in the responses to local luminance changes of controls and T4/T5 block flies (Fig. 4i), which is consistent with our earlier observations (Fig. 3). Taken together, these results indicate that the position system only detects changes in local luminance and that local motion does not influence its response properties. Thus,

$$R_L = P_L = P_{FTB} = P_{BTF}$$

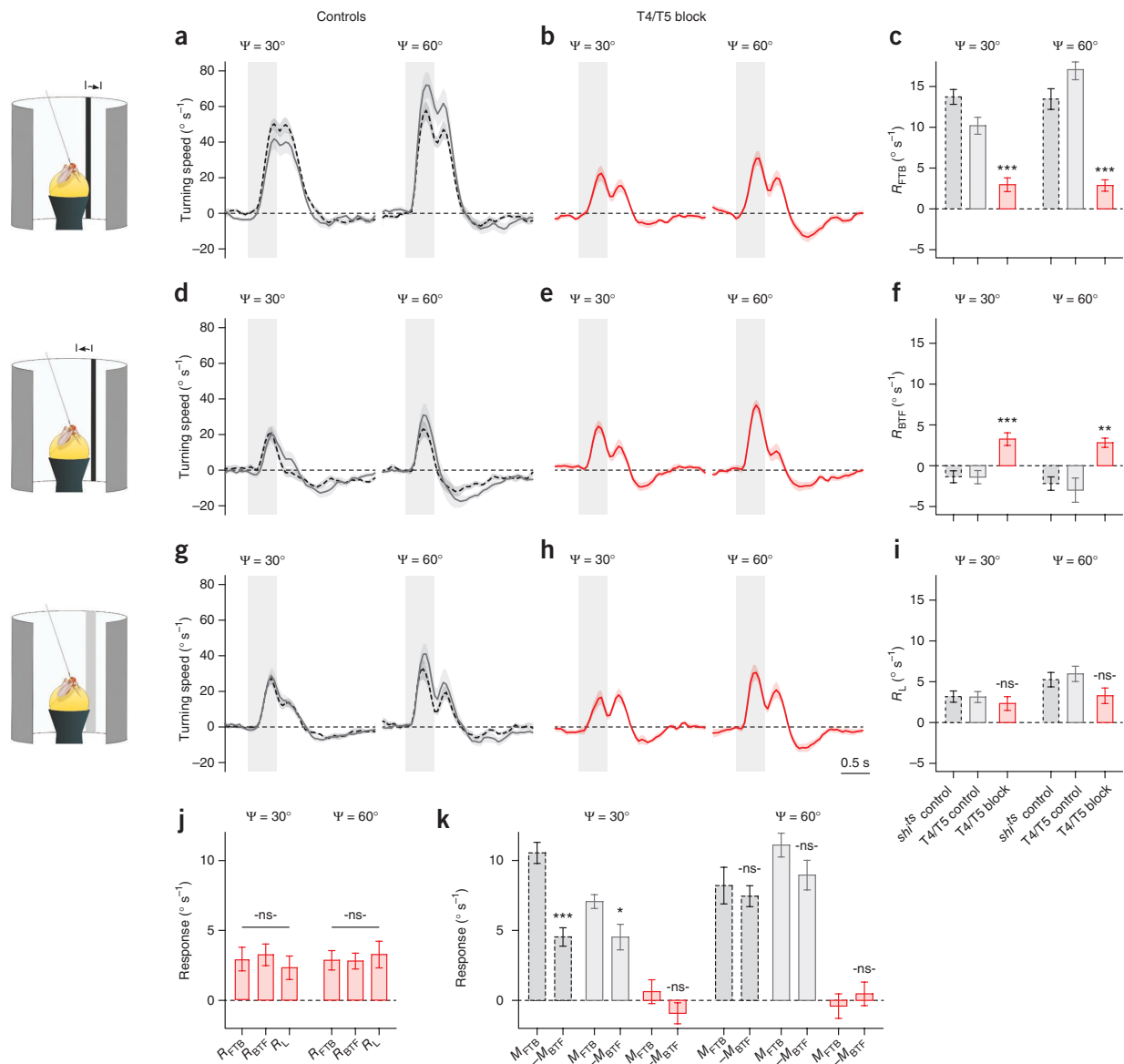


Figure 4 Open-loop responses to local bar motion and to local luminance changes. (a–i) Turning responses of control (a,d,g) and T4/T5 block (b,e,h) flies to local front-to-back motion (a,b), local back-to-front motion (d,e) and local luminance changes (g,h) at $\Psi = 30^{\circ}$ and $\Psi = 60^{\circ}$ (gray shaded areas). The corresponding average turning responses are shown in c, f and i (R_{FTB} , R_{BTF} and R_L , respectively; averaged between $t = 0.1$ s and $t = 2.1$ s after stimulus onset). (j) Comparison of responses to the different stimuli of T4/T5 block flies. (k) Comparison of isolated motion responses ($M_{FTB} = R_{FTB} - R_L$ and $M_{BTF} = R_{BTF} - R_L$). Motion responses of T4/T5 block flies were not significantly different from zero ($P \geq 0.05$, two-sided t test). All responses were measured as the response with the bar at $\Psi = +30^{\circ}$ or $\Psi = +60^{\circ}$ minus the response with the bar at $\Psi = -30^{\circ}$ or $\Psi = -60^{\circ}$, respectively, divided by 2. All data represent mean \pm s.e.m.; 60 trials per fly of $n = 10$, 12 and 11 flies (at $\Psi = 30^{\circ}$) and of $n = 10$, 11 and 11 flies (at $\Psi = 60^{\circ}$) per group (shifts control, dashed black lines; T4/T5 control, solid gray lines; T4/T5 block, solid red lines). ns indicates not significant ($P \geq 0.05$), $*P < 0.05$, $**P < 0.01$ and $***P < 0.001$; two-sided t -test compared with both controls (c,f,i) or comparing M_{FTB} to $-M_{BTF}$ within the groups (k); one-way ANOVA in j.

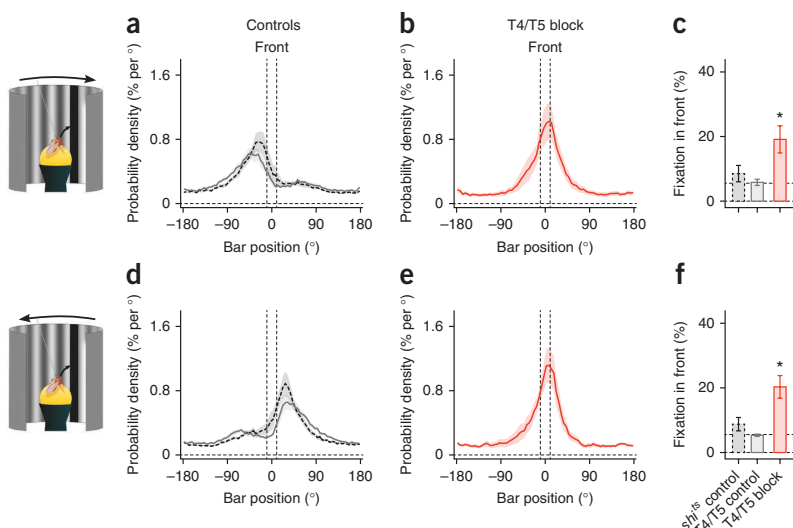
This finding allowed us to isolate the responses of the motion system to front-to-back and back-to-front stimulation.

$$M_{FTB} = R_{FTB} - R_L$$

$$M_{BTF} = R_{BTF} - R_L$$

Analyzing the data of control flies in this way revealed a strong asymmetry in the motion system for the frontal part of the visual field ($\Psi = 30^{\circ}$), where its response to front-to-back was approximately twice as strong as that to back-to-front motion (Fig. 4k). In the lateral part ($\Psi = 60^{\circ}$), we observed a similar tendency (Fig. 4k). This finding implies that $M(\Psi, v) \neq -M(\Psi, -v)$ and suggests that it is

Figure 5 Closed-loop fixation response during open-loop background motion. (a–f) Fixation responses of control (a,d) and T4/T5 block (b,e) flies during clockwise (a,b) and counterclockwise (d,e) rotation of the sine-grating. The ability to keep the bar in front is shown in c and f (same measure as in Fig. 1i). Upper horizontal dashed lines represent the chance level (5.6%, no fixation). All data represent mean \pm s.e.m.; 30 trials of $n = 11$, 9 and 9 flies per group (*sh118* control, dashed black lines; T4/T5 control, solid gray lines; T4/T5 block, solid red lines). * $P < 0.05$, two-sided *t* test compared with both controls.



necessary to omit the classical assumption of velocity linearity of the motion system³⁰. Consequently, we revised the interpretation of $P(\Psi)$ obtained in the previous experiment with the rotating bar (Fig. 2). Thus, $P(\Psi)$ actually overestimates the response of the pure position system (P_L) in control flies.

$$\begin{aligned} P(\Psi)^{\text{controls}} &= (R_{\text{cw}} + R_{\text{ccw}})/2 \\ &= (M(\Psi, \nu) + M(\Psi, -\nu) + 2 \cdot P_L)/2 \\ &> P_L \end{aligned}$$

On the other hand, for T4/T5 block flies, the motion responses were zero (Figs. 2h and 4k). Under these conditions, $P(\Psi)$ corresponds to the response of the position system alone (P_L).

$$\begin{aligned} P(\Psi)^{\text{T4/T5 block}} &= (R_{\text{cw}} + R_{\text{ccw}})/2 \\ &= (M(\Psi, \nu) + M(\Psi, -\nu) + 2 \cdot P_L)/2 \\ &= P_L \end{aligned}$$

Taken together, these results indicate that the visual pathways of the motion and position system are indeed separable at the neuronal level. However, fixation is shaped by an interaction of both systems at the level of behavior.

Object tracking with background motion

Do both control systems also superimpose when the fly encounters a more natural situation where it has to track an object while the whole background is in motion? To answer this question, we fed back the fly's turning tendency on the position of the black bar, as in the usual fixation procedure (closed loop), and displayed a large-field sine-grating rotating in one or the other direction without giving the fly control over it (open loop) (Fig. 5). If both responses superimpose at the level of the fly's turning tendency, the large field stimulus should create a permanent offset, leading to a shift of the position where the fly fixates the bar.

We tested whether the presence of the sine-grating alone would alter the fixation response. To our surprise, the fixation response clearly improved for both control and T4/T5 block flies when the background was a static sine-grating (Supplementary Fig. 3), although the grating had the same average luminance as the uniformly gray background used in previous fixation experiments (Fig. 1e–i). This indicates that the fixation response is modulated by the spatial properties of the background, yet the detailed mechanism of this effect remains unknown.

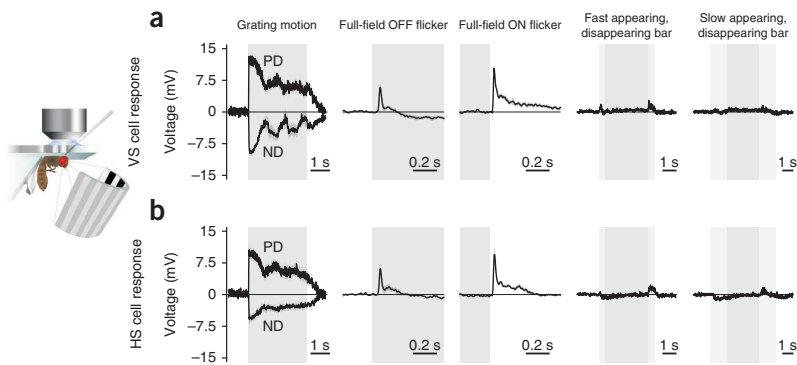
With the sine-grating background moving clockwise or counterclockwise, control flies were still able to fixate the bar, but the peak of the position histogram was shifted in the direction opposite to the direction of the moving large-field stimulus (Fig. 5a,d). The motion system produced a tendency to turn in the direction of the moving background, whereas the position system induced turning toward the position of the bar. When the bar was shifted opposite to the direction of background motion, both responses summed to zero. Under the same conditions, T4/T5 block flies did not shift the fixation peak, but rather kept the bar in front of them, regardless of whether the large-field stimulus was moving clockwise or counterclockwise (Fig. 5b,e). These results suggest a superposition of the large-field motion system and the position system at the level of behavioral output, as has been proposed³⁰.

Electrophysiology in horizontal and vertical system cells

In our behavioral experiments, we found that a turning response could be elicited by local luminance changes and that this response was not changed when blocking T4 and T5 cell output (Figs. 3 and 4). In electrophysiological recordings from LPTCs sensitive to horizontal and vertical motion (horizontal and vertical system cells, respectively), the response to full-field flicker is only moderately reduced when T4 and T5 cell output is blocked²⁶, indicating that horizontal system and vertical system cells receive additional input from an unidentified flicker pathway. To investigate whether horizontal system or vertical system cells use this information to mediate the position response, we performed electrophysiological recordings from horizontal system and vertical system cells in the immobilized fly (Fig. 6). We presented gratings moving in different directions, full-field OFF and ON flicker, as well as appearing and disappearing black bars at different positions along the azimuth. Vertical system cells responded strongly in a direction-selective manner to vertical motion (Fig. 6a), whereas horizontal system cells responded most strongly to horizontal motion (Fig. 6b). Both cell types also responded strongly to full-field OFF and ON flicker. However, cellular responses to appearing and disappearing vertical bars were orders of magnitude weaker. Moreover, horizontal system cells slightly hyperpolarized when the black bar appeared, but depolarized when it disappeared.

These recordings conflict with the behavioral responses that we observed in several ways. First, flies robustly turned toward the

Figure 6 *In vivo* electrophysiological recordings from vertical system (VS) and horizontal system (HS) cells in the immobilized fly. (a,b) Voltage traces obtained from vertical system (a) and horizontal system cells (b) while presenting vertical (a) or horizontal (b) grating motion into the preferred direction (PD) and the null direction (ND) of the cell, full-field OFF and ON flicker, and a vertical dark bar that appeared and disappeared (fast or slow in 0.5 s or 1.5 s, respectively) at $\Psi = 30^\circ$ in the front of the fly (responses at $\Psi = 60^\circ$ and $\Psi = 90^\circ$ were similar in amplitude; data not shown). All data represent mean \pm s.e.m. obtained from $n = 8$ vertical system cells and $n = 6$ horizontal system cells from wild-type Canton S flies.



location of an appearing and a disappearing black bar, and this position response was on the same order of magnitude as the optomotor response to full-field grating motion (Figs. 1b and 3a). Second, assuming that horizontal system and vertical system cells convey position information, we would not expect the fly to remain capable of tracking objects when the background is moving (Fig. 5); the tiny

voltage responses to local luminance changes would vanish in the much stronger voltage response to the background motion. These discrepancies between electrophysiological responses of horizontal system and vertical system cells and behavioral responses render it unlikely that horizontal system and vertical system cells are part of the fly's position circuit.

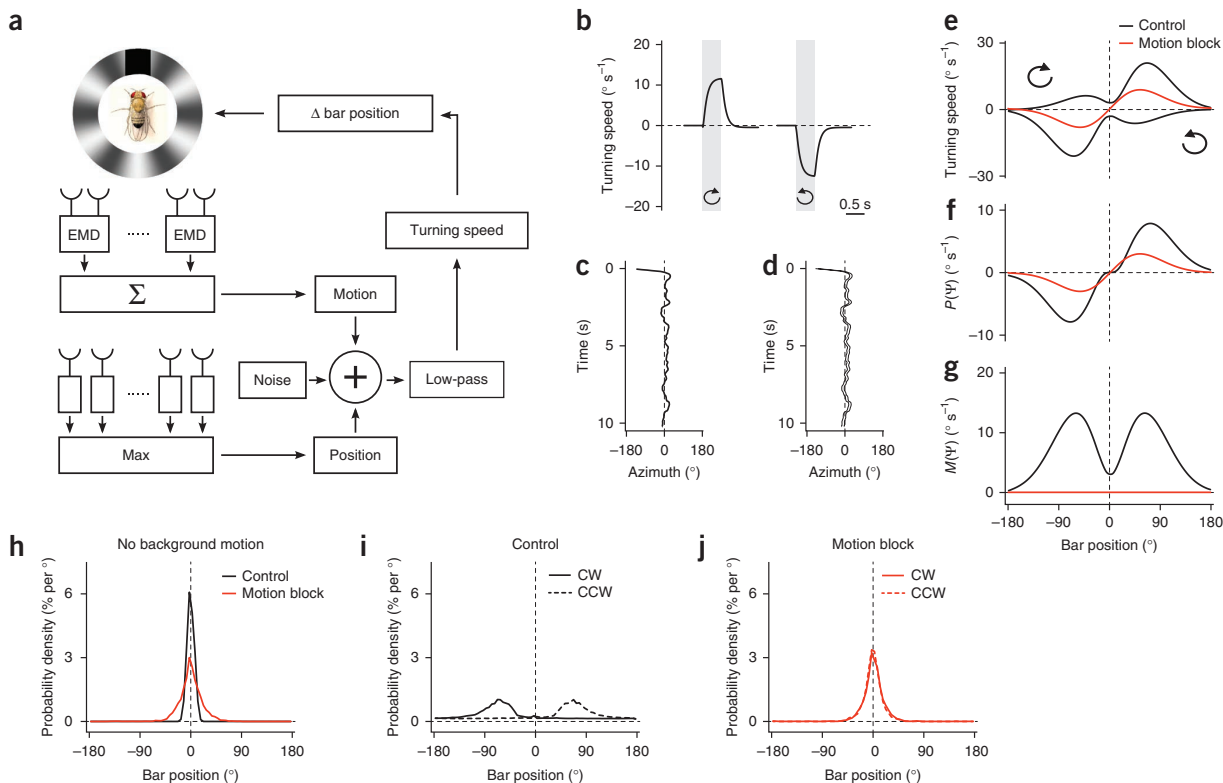


Figure 7 Model simulations of the fly's course control system. (a) Outline of the model. The visual scene was analyzed in parallel by a motion and a position system. Their output signals, plus noise, were summed and low-pass filtered to yield the fly's turning speed. To simulate closed-loop fixation behavior, this signal was used to control the bar position. (b) Turning responses of the model to full-field clockwise and counterclockwise grating rotation. (c,d) Bar position over time (c) and the resulting activity pattern of the array of position detectors (d) during a single run of closed-loop fixation. (e) Model responses to a bar rotating in open-loop clockwise, followed by counterclockwise. (f) Position component, $P(\Psi)$ (calculated by summing the two responses obtained in e and dividing them by 2). (g) Motion component, $M(\Psi)$ (calculated by subtracting the two responses obtained in e and dividing by 2). (h) Probability density as function of bar position obtained from 20 runs of closed-loop bar fixation. (i,j) Closed-loop fixation behavior during superimposed open-loop background sine-grating motion (solid lines, 10° s^{-1} clockwise (CW) rotation of the grating; dashed lines, -10° s^{-1} counterclockwise (CCW) rotation of the grating). Model responses were calculated with an intact motion system (black lines) and with the gain of the motion system set to zero (red lines).

Modeling

Our results suggest the existence of two course control systems operating in parallel. Can such a system track a single object effectively and quantitatively account for the observed behavior of the flies? To address this question, we modeled the two course control systems and tested them under the conditions that were used in the experiments (Fig. 7). We implemented the large-field motion system as an array of elementary motion detectors of the Reichardt type³⁴ weighted by a spatial sensitivity profile similar to $M(\Psi)$, as obtained in the experiments (Fig. 2f), and with a 50% stronger weight on front-to-back than on back-to-front motion, as we observed (Fig. 4k). The output signals of all motion detectors were summed. The position system was modeled as an array of squared high-pass filters. From the array, the location of the maximum response was extracted at each time point. The response amplitude toward this position was determined from a spatial sensitivity profile similar to the experimentally determined one (Fig. 2c,d). Both signals were multiplied by a gain factor, added together with white noise and low-pass filtered to obtain a turning signal. This could either be interpreted as the output signal under open-loop conditions or fed back into the bar position when simulating closed-loop fixation behavior (Fig. 7a).

Stimulating the model with grating motion under open-loop conditions resulted in a syndirectional optomotor response (Fig. 7b). When tested under closed-loop conditions, the model revealed a pronounced fixation behavior, bringing and keeping the bar in a frontal position (Fig. 7c,h). Comparing the bar position (Fig. 7c) with the output of the squared high-pass filters over time (Fig. 7d) revealed the effective detection of bar position. Moving the bar in open loop, first clockwise, then counterclockwise, led to a response profile that was consistent with the respective experimental data (Fig. 7e). We added and subtracted both responses to reveal the position-dependent and motion-dependent components ($P(\Psi)$ and $M(\Psi)$, respectively) and obtained similar profiles as in our experiments (Fig. 7f,g). We then tested the system for closed-loop fixation during open-loop background grating motion. As seen in the experiments, the maximum of the fixation histograms moved opposite to the direction of the drifting grating and the histograms became broader (Fig. 7i).

We then tested the model with the gain of the large-field motion system set to zero, simulating the blockage of T4 and T5 cell output; the model was still able to keep the bar in front, yet with a broader distribution (Fig. 7h). When the model was presented with the clockwise and counterclockwise rotating bar, the responses were identical for both directions of bar motion and only depended on the bar's position (Fig. 7e). Moreover, the resulting position-dependent response function, $P(\Psi)$, was reduced in amplitude compared with the control (Fig. 7f). Finally, in the case of closed-loop fixation with background motion, the model kept the bar in front, no matter the direction in which the background was moving (Fig. 7j). In summary, all of the effects that we observed in the experiments were reproduced by the model with one set of parameters.

DISCUSSION

Behavioral and electrophysiological studies in larger fly species have proposed that fixation behavior is mediated by a special class of lobula plate neurons that are selective for small moving objects^{35–38}. These cells are thought to receive retinotopic input from the same set of columnar, motion-sensitive neurons as the large field-sensitive tangential cells. Their selectivity for small moving objects arises from additional inhibition that they receive from other large-field neurons of the lobula plate^{39–41}. In contrast, we found that transgenic *Drosophila* in which the T4 and T5 cells were blocked were

still able to fixate and track individual objects, even though their lobula plate tangential cells were motion blind and flies consequently did not show an optomotor response²⁶. Our genetic and behavioral experiments revealed a control system that is purely sensitive to the position of the object and not to the direction in which it is moving, with the exact same spatial sensitivity profile as that revealed by the mathematical examination of behavioral results in wild-type houseflies performed many years ago³⁰. Although the reduction in fixation strength observed in T4/T5 block flies might, at first sight, be interpreted as a partial overlap between the motion and the position circuit at the neuronal level, our analysis indicates that this is not the case; as a result of its asymmetry with respect to the direction of motion (front to back as compared to back to front), the motion circuit contributes to the fixation response at the behavioral level, but is separate from the position circuit at the neuronal level. An asymmetry in turning was also observed in the responses to rotating stripes^{8,30} (Fig. 2), but, from these findings, one cannot conclude that the response of the motion circuit is asymmetrical. Even a perfectly symmetrical motion response, combined with the position response, would lead to the very same behavior. Our investigation of the two response components revealed that the asymmetrical turning response has two sources: a turning response to the position of the rotating bar and an asymmetrical motion response to its direction of motion. The powerful genetic tools available in *Drosophila*⁴² will allow the future identification of the specific neural components of the position circuit.

METHODS

Methods and any associated references are available in the [online version of the paper](#).

Note: Supplementary information is available in the [online version of the paper](#).

ACKNOWLEDGMENTS

We wish to thank G. Rubin and A. Nern for providing the T4/T5 cell-specific driver line *R42F06-Gal4* and V. Jayaraman for advice on setting up the locomotion recorder. We are also grateful to J. Haag, A. Mauss, A. Arenz and A. Leonhardt for many helpful discussions and critically reading the manuscript, S. Prech for help with the design of the Peltier temperature control system, C. Theile for fly work, and F. Foerstner for reconstructing the three horizontal system cells shown in Figure 1a. A. Bahl and A. Borst are members of the Bernstein Center for Computational Neuroscience and the Graduate School of Systemic Neurosciences.

AUTHOR CONTRIBUTIONS

A. Bahl set up the locomotion recorder and the stimulus display, and wrote the software for reading the behavioral output and displaying the stimulus. A. Bahl and T.S. performed all of the behavioral experiments and evaluated the data. G.A. performed the electrophysiological recordings and analyzed the data. A. Bahl and A. Borst designed the study. A. Borst carried out the modeling work. A. Borst and A. Bahl wrote the manuscript with the help of the other authors.

COMPETING FINANCIAL INTERESTS

The authors declare no competing financial interests.

Reprints and permissions information is available online at <http://www.nature.com/reprints/index.html>.

1. Götz, K.G. Optomotorische Untersuchung des visuellen Systems einiger Augenmutanten der Fruchtfliege *Drosophila*. *Kybernetik* **2**, 77–92 (1964).
2. Buchner, E. Elementary movement detectors in an insect visual system. *Biol. Cybern.* **24**, 85–101 (1976).
3. Blondeau, J. & Heisenberg, M. The three-dimensional optomotor torque system of *Drosophila melanogaster*. Studies on wild type and the mutant optomotor blind H31. *J. Comp. Physiol. A* **145**, 321–329 (1982).
4. Tammero, L.F. & Dickinson, M.H. The influence of visual landscape on the free flight behavior of the fruit fly *Drosophila melanogaster*. *J. Exp. Biol.* **205**, 327–343 (2002).

5. Mronz, M. & Lehmann, F.-O. The free-flight response of *Drosophila* to motion of the visual environment. *J. Exp. Biol.* **211**, 2026–2045 (2008).
6. Reichardt, W. & Wenking, H. Optical detection and fixation of objects by fixed flying flies. *Naturwissenschaften* **56**, 424–425 (1969).
7. Heisenberg, M. & Wolf, R. *Vision in Drosophila: Genetics of Microbehavior* (Springer-Verlag, Berlin, 1984).
8. Reiser, M.B. & Dickinson, M.H. *Drosophila* fly straight by fixating objects in the face of expanding optic flow. *J. Exp. Biol.* **213**, 1771–1781 (2010).
9. Rister, J. *et al.* Dissection of the peripheral motion channel in the visual system of *Drosophila melanogaster*. *Neuron* **56**, 155–170 (2007).
10. Götz, K.G. Visual guidance in *Drosophila*. in *Development and Neurobiology of Drosophila* (eds. Siddiqi, O., Babu, P., Hall, M.L. & Hall, J.C.) 391–407 (Plenum Press, New York, 1980).
11. Strauss, R. & Pichler, J. Persistence of orientation toward a temporarily invisible landmark in *Drosophila melanogaster*. *J. Comp. Physiol. A* **182**, 411–423 (1998).
12. Maimon, G., Straw, A.D. & Dickinson, M.H. A simple vision-based algorithm for decision making in flying *Drosophila*. *Curr. Biol.* **18**, 464–470 (2008).
13. Aptekar, J.W., Shoemaker, P.A. & Frye, M.A. Figure tracking by flies is supported by parallel visual streams. *Curr. Biol.* **22**, 482–487 (2012).
14. Heisenberg, M., Wonneberger, R. & Wolf, R. Optomotor-blind (H31): a *Drosophila* mutant of the lobula plate giant neurons. *J. Comp. Physiol. A* **124**, 287–296 (1978).
15. Geiger, G. & Nässel, D.R. Visual orientation behavior of flies after selective laser beam ablation of interneurons. *Nature* **293**, 398–399 (1981).
16. Hausen, K. & Wehrhahn, C. Neural circuits mediating visual flight control in flies. II. Separation of two control systems by microsurgical brain lesions. *J. Neurosci.* **10**, 351–360 (1990).
17. Bausenwein, B., Wolf, R. & Heisenberg, M. Genetic dissection of optomotor behavior in *Drosophila melanogaster*. Studies on wild-type and the mutant optomotor-blind (H31). *J. Neurogenet.* **3**, 87–109 (1986).
18. Wolf, R. & Heisenberg, M. Visual orientation in motion-blind flies is an operant behavior. *Nature* **323**, 154–156 (1986).
19. Meinertzhagen, I.A. & O’Neil, S.D. Synaptic organization of columnar elements in the lamina of the wild type in *Drosophila melanogaster*. *J. Comp. Neurol.* **305**, 232–263 (1991).
20. Joesch, M., Plett, J., Borst, A. & Reiff, D.F. Response properties of motion-sensitive visual interneurons in the lobula plate of *Drosophila melanogaster*. *Curr. Biol.* **18**, 368–374 (2008).
21. Schnell, B. *et al.* Processing of horizontal optic flow in three visual interneurons of the *Drosophila* brain. *J. Neurophysiol.* **103**, 1646–1657 (2010).
22. Joesch, M., Schnell, B., Raghu, S.V., Reiff, D.F. & Borst, A. ON and OFF pathways in *Drosophila* motion vision. *Nature* **468**, 300–304 (2010).
23. Eichner, H., Joesch, M., Schnell, B., Reiff, D.F. & Borst, A. Internal structure of the fly elementary motion detector. *Neuron* **70**, 1155–1164 (2011).
24. Bausenwein, B. & Fischbach, K. Activity labeling patterns in the medulla of *Drosophila melanogaster* caused by motion stimuli. *Cell Tissue Res.* **270**, 25–35 (1992).
25. Bausenwein, B., Dittrich, A.P. & Fischbach, K.F. The optic lobe of *Drosophila melanogaster*. II. Sorting of retinotopic pathways in the medulla. *Cell Tissue Res.* **267**, 17–28 (1992).
26. Schnell, B., Raghu, S.V., Nern, A. & Borst, A. Columnar cells necessary for motion responses of wide-field visual interneurons in *Drosophila*. *J. Comp. Physiol. A* **198**, 389–395 (2012).
27. Seelig, J.D. *et al.* Two-photon calcium imaging from head-fixed *Drosophila* during optomotor walking behavior. *Nat. Methods* **7**, 535–540 (2010).
28. Brand, A.H. & Perrimon, N. Targeted gene expression as a means of altering cell fates and generating dominant phenotypes. *Development* **118**, 401–415 (1993).
29. Kitamoto, T. Conditional modification of behavior in *Drosophila* by targeted expression of a temperature-sensitive *shibire* allele in defined neurons. *J. Neurobiol.* **47**, 81–92 (2001).
30. Poggio, T. & Reichardt, W. A theory of the pattern induced flight orientation of the fly *Musca domestica*. *Kybernetik* **12**, 185–203 (1973).
31. Wehrhahn, C. Flight torque and lift responses of the housefly (*Musca domestica*) to a single stripe moving in different parts of the visual field. *Biol. Cybern.* **29**, 237–247 (1978).
32. Pick, B. Visual flicker induces orientation behavior in the fly *Musca*. *Z. Naturforsch. C* **29c**, 310–312 (1974).
33. Wehrhahn, C. Fast and slow flight torque responses in flies and their possible role in visual orientation behavior. *Biol. Cybern.* **40**, 213–221 (1981).
34. Reichardt, W. Evaluation of optical motion information by movement detectors. *J. Comp. Physiol. A* **161**, 533–547 (1987).
35. Reichardt, W. & Poggio, T.A. Figure-ground discrimination by relative movement in the visual system of the fly. Part I: Experimental Results. *Biol. Cybern.* **35**, 81–100 (1979).
36. Egelhaaf, M. On the neuronal basis of figure-ground discrimination by relative motion in the visual system of the fly. I. Behavioral constraints imposed on the neuronal network and the role of the optomotor system. *Biol. Cybern.* **52**, 123–140 (1985).
37. Egelhaaf, M. On the neuronal basis of figure-ground discrimination by relative motion in the visual system of the fly. II. Figure-detection cells, a new class of visual interneurons. *Biol. Cybern.* **52**, 195–209 (1985).
38. Liang, P., Heitwerth, J., Kern, R., Kurtz, R. & Egelhaaf, M. Object representation and distance encoding in three-dimensional environments by a neural circuit in the visual system of the blowfly. *J. Neurophysiol.* **107**, 3446–3457 (2012).
39. Egelhaaf, M. On the neuronal basis of figure-ground discrimination by relative motion in the visual system of the fly. III. Possible input circuitries and behavioral significance of the FD cells. *Biol. Cybern.* **52**, 267–280 (1985).
40. Warzecha, A.K., Borst, A. & Egelhaaf, M. Photo-ablation of single neurons in the fly visual system reveals neural circuit for the detection of small moving objects. *Neurosci. Lett.* **141**, 119–122 (1992).
41. Cuntz, H., Haag, J. & Borst, A. Neural image processing by dendritic networks. *Proc. Natl. Acad. Sci. USA* **100**, 11082–11085 (2003).
42. Borst, A. *Drosophila*’s view on insect vision. *Curr. Biol.* **19**, R36–R47 (2009).

ONLINE METHODS

Behavioral experiments. The locomotion recorder^{2,27} consisted of an air-suspended sphere floating in a bowl-shaped sphere holder. The sphere had a diameter of 6 mm and a weight of 40 mg; it was made from polyurethane foam and coated with polyurethane spray (spheres were kindly provided by V. Jayaraman, Janelia Farm). The airflow is adjusted to ~ 0.7 l min⁻¹ by a rotary vane pump (G6/01-K-EB9L Gardner Denver Thomas GmbH) such that the sphere rotated freely in the holder, but did not jump out. A high-power infrared LED (800 nm, JET series, 90 mW, Roithner Electronics) was located in the back to illuminate the fly and the sphere surface. Two optical tracking sensors were equipped with lens and aperture systems to focus two 1-mm² equatorial spots (at $\pm 30^\circ$) on the sphere at a distance 15 cm behind the fly. The tracking data were processed in a custom-designed circuit²⁷ at 4 kHz internally, read out via a USB interface and processed by a computer at ~ 200 Hz. This allowed real-time calculation of the instantaneous rotation axis of the sphere. A third camera (GRAS-20S4M-C, Point Grey Research) was located in the back, which is essential for proper positioning of the fly and allowed real-time observation and video recording of the fly during experiments. The bottom of the sphere holder was surrounded by an open plastic funnel connected to a metal fan with an aluminum tube. A self-designed Peltier controlling system read out the temperature of a thermometer placed just below the sphere and controlled the fan temperature such that the air temperature around the fly was regulated precisely (± 0.1 °C). In all experiments, the temperature started at the permissive temperature level for *shibire*^{ts} (25 °C) and was raised linearly to the restrictive temperature of 34 °C in 10–20 min. Three 120-Hz LCD screens (Samsung 2233 RZ) were vertically arranged and formed a U-shaped visual arena (31 × 31 × 47 cm) with the fly in the center. We removed the monitor covers to minimize the borders between the screens in the corners of the arena and glued thin sheets of parchment paper onto the screens to scatter and evenly distribute the emitted light. The visual arena had a luminance ranging from 0–131 cd m⁻² and covered almost the whole visual field of the fly (horizontal, $\pm 135^\circ$; vertical, $\pm 57^\circ$; resolution $< 0.1^\circ$). The three LCD screens were controlled via NVIDIA 3D Vision Surround Technology on Windows 7 64 bit, allowing a synchronized update of the screens at 120 frames per s. For visual stimulation, we use Panda3D, an open-source gaming engine, and Python 2.7, which simultaneously controlled the frame rendering in Panda3D, read out the tracking data and temperature, and streamed data to the hard disk.

Time-position plots for the visual stimuli are illustrated in **Supplementary Figure 4** for all experiments. The large-field open-loop optomotor stimulus (**Fig. 1b–d** and **Supplementary Fig. 4a,b**) consisted of a striped grating ($\lambda = 20^\circ$) rotating clockwise (+) or counterclockwise (-) at a velocity of 20° s⁻¹ for 0.5 s. Seven contrasts were tested. The dark stripes always had a luminance value of 27 cd m⁻², whereas the luminance values of the brighter stripes ranged from 30 – 104 cd m⁻², resulting in contrast values between 4 and 58%, measured as $(I_{\max} - I_{\min}) / (I_{\max} + I_{\min})$. In the open- and closed-loop fixation experiments, we showed a single black bar (10° wide, 114° high, 9 cd m⁻²) on a gray background (58 cd m⁻²). In the first set of open-loop fixation experiments (**Fig. 2** and **Supplementary Fig. 4d,e**), the bar started in the back and rotated at velocities of $\pm 18^\circ$ s⁻¹ around the fly. In another set of experiments (**Fig. 3** and **Supplementary Fig. 4f**), the bar did not move, but slowly appeared (in 0.5 s), remained static for 4 s and disappeared (in 0.5 s) at well-defined locations ($\pm 120^\circ, \pm 90^\circ, \pm 60^\circ, \pm 45^\circ, \pm 30^\circ$ and $\pm 15^\circ$). In another experiment (**Fig. 4** and **Supplementary Fig. 4g–i**), we chose two locations ($\Psi = 30^\circ$ and $\Psi = 60^\circ$) to show local motion (front to back and back to front) and local luminance change. Here, the local luminance change dynamics were chosen such that they approximated the luminance change when the local motion was shown. In the case of closed-loop fixation, the bar was placed at a random position (between -180° and $+180^\circ$) around the fly before each trial and the fly was then given 20 s control of the angular position of that bar ($\Delta\text{bar} = -\text{fly turning}$, updated approximately every 9 ms). This was done either in front of a gray background (**Fig. 1e–i** and **Supplementary Figs. 3a–c** and **4c**) or a large-field sine-grating ($\lambda = 30^\circ$, the luminance values of the pattern were between 27 and 104 cd m⁻²). The sine-grating was either static (**Supplementary Figs. 3d–f** and **4j**) or rotated at $\pm 15^\circ$ s⁻¹ (**Fig. 5** and **Supplementary Fig. 4k,l**).

Flies were raised on standard cornmeal-agar medium at 18 °C and 60% humidity throughout development on a 12-h light, 12-h dark cycle. We used *shibire*^{ts} control flies (*w⁺; +; +/UAS-shibire^{ts}*), T4/T5 control flies (*w⁺/w⁻; +; R42F06-Gal4/+*) and T4/T5 block flies (*w⁺/w⁻; +; R42F06-Gal4/UAS-shibire^{ts}*). The T4 and T5 cell-specific driver line R42F06-Gal4 was kindly provided by A. Nern and G. Rubin

(Janelia Farm) and was generated⁴³ using a 4.0-kb DNA fragment of the *bab2* gene amplified from genomic DNA with primers CGGCTGATCCAACAAAGGATG CACC and CTCAGTGTAGCCGCACCTTGTTCCT. The *shibire*^{ts} effector has multiple insertions on the third chromosome. We used wild-type Canton S flies for the control crosses. Only female flies aged 2–10 d were used in experiments. Flies were taken from 18 °C just before the experiment and immediately cold anesthetized. The head, thorax and wings were glued to a needle using near-ultraviolet bonding glue (Sinfony Opaque Dentin) and strong blue LED light (440 nm, dental curing light, New Woodpecker).

For each fly, the experiment lasted approximately 50 min and was split into 50–200 trials depending on the length and the number of visual stimuli. Stimuli in one trial were presented in random order. For data analysis, we chose a range of trials (same for control and T4/T5 block flies per experiment) during which the temperature was constant at 34 °C and during which flies had a constant average turning and walking speed. The experimental raw data were first downsampled (interpolated from 120 to 20 Hz). Turning speed traces were then determined by taking the average over trials and low-pass filtering the resulting trace ($\tau = 0.1$ s in all experiments, except those shown in **Fig. 2**, where $\tau = 0.4$ s). Probability density functions of bar position were calculated separately for each trial with a bin size of 5° and then averaged over trials and flies. The measure 'fixation in front' was determined by integrating the probability density function of one trial between -10° and 10° , which resulted in a percentage value for how probable it was to find the bar in that area during that trial. These values were then averaged over trials and flies. Flies were excluded from data analysis when the average walking speed during the whole experiment was below 0.1 cm s⁻¹, indicating severe walking problems, or (only in closed-loop fixation experiments with static background) when the average turning speed was either larger than $+10^\circ$ s⁻¹ or smaller than -10° s⁻¹, indicating an asymmetry in walking behavior that led to a substantially reduced fixation performance. All data analysis was performed in Python 2.7 using NumPy and SciPy on Mac OSX 10.8.

P values were obtained using different statistical tests. To test the hypothesis that a group had a certain mean, we performed a two-sided *t* test. When two groups were compared (**Fig. 4k**), we performed a two-sided *t* test. When T4/T5 block flies were compared with *shibire*^{ts} control and T4/T5 control flies, we performed a two-sided *t* test comparing each control with the block flies and chose the larger *P* value. When three groups were compared (**Fig. 4j**), we performed a one-way ANOVA. We used approximately the same sample size (smallest $n = 9$ flies, largest $n = 16$ flies) per group and experiment, which permitted a statistical comparison between the different experiments. This sample size was considered as sufficiently large because the optomotor response of T4/T5 block flies shown in **Figure 1b–d** was highly significantly reduced at $n = 10$ flies ($P < 0.001$, two-sided *t* test compared with both controls). See **Supplementary Statistics** for a detailed list of group sizes, statistical tests and *P* values.

Electrophysiology. Patch-clamp recordings were performed as described previously²⁰ with minor modifications. All electrophysiological experiments were performed with female wild-type Canton S flies 6–24 h post-eclosion. Flies were raised on standard cornmeal-agar medium and kept at 25 °C and 60% humidity on a 12-h dark/light cycle.

Flies were anesthetized on ice and immobilized on a plexiglas holder with wax. The head was bent downwards and fixed by waxing the proboscis to the thorax. The fly was then inserted into an opening cut into a piece of aluminum foil mounted in a recording chamber. A part of the posterior side of the head cuticle and the muscle that covers the cell bodies of LPTCs was removed with fine forceps. Extracellular saline (103 mM NaCl, 3 mM KCl, 5 mM TES, 10 mM trehalose, 10 mM glucose, 7 mM sucrose, 26 mM NaHCO₃, 1 mM NaH₂PO₄, 1.5 mM CaCl₂ and 4 mM MgCl₂, pH 7.3, 280 mOsm) was bubbled with 95% O₂ and 5% CO₂ and continuously perfused over the preparation. The brain of the fly was visualized with an upright microscope (Axiotech Vario 100, Zeiss) equipped with a 40 \times water-immersion objective (LumPlanFL, NA 0.8, Olympus) and an Hg-light source (HXP-120, Visitron Systems). For contrast enhancement, we used two polarization filters that were slightly shifted with respect to their polarization plane. The health of the flies was checked regularly by monitoring periodic movements of the brain. A glass electrode filled with collagenase (Collagenase IV, Gibco, 0.5 mg ml⁻¹ in extracellular saline) was used to weaken the perineural sheath and expose the somata of LPTCs.



Somata of vertical system and horizontal system cells were patched with a glass electrode ($6\text{--}9\text{ M}\Omega$) filled with internal solution (140 mM potassium aspartate, 10 mM HEPES, 4 mM Mg-ATP, 0.5 mM Na-GTP, 1 mM EGTA, 1 mM KCl and 0.03 mM Alexa 568-hydrazide sodium, pH 7.26, 265 mOsm). All recordings were performed in current-clamp bridge mode with an NPI BA-1S amplifier (NPI electronics), low-pass filtered at 3 kHz and digitized at 10 kHz. Data acquisition was performed with Matlab (version R2011a, MathWorks). Cells had an average resting membrane potential of -51.6 ± 0.7 mV (corrected for a liquid junction potential of 12 mV) and an average input resistance of 204.5 ± 16.7 M Ω . Cell types were identified on the basis of their typical response profiles to moving gratings. In addition, fluorescence images of each cell were taken after the recording with a CCD camera (Spot Pursuit, Visitron Systems) to verify their identity.

Visual stimuli were presented on a custom-built LED arena that subtended 170° in azimuth and 85° in elevation with a resolution of approximately 1.4° per LED. The arena allowed refresh rates of up to 600 Hz and had a maximum luminance of 80 cd m^{-2} . Motion stimuli consisted of square-wave gratings with a wavelength of 20° moving at 1 Hz. Stimuli lasted for 3 s with an interstimulus interval of 5 s and were repeated three times. For bar flicker stimuli, the arena background was set to full luminance. After 1.5 s, a dark bar that had a width of 10° and was centered at 30° , 60° or 90° along the azimuth appeared. The contrast of that bar was increased linearly to a maximum of 66% over 0.5 s or 1.5 s. After an interval of 3 s, the dark bar disappeared again in the same time period. Bar flicker stimuli were presented five times. For full-field flicker stimuli, the arena was stepped to full luminance for 3 s and then back to zero again for 3 s. Full-field flicker stimuli were presented ten times per cell.

Data analysis was performed with Matlab (version R2011b, MathWorks) using custom-written scripts. For all stimuli, we averaged voltage traces over sweeps and calculated the mean and s.e.m. over cells. The baseline membrane potential was calculated by averaging over a period of 500 ms preceding the stimulus onset and subtracted from the responses. For horizontal system cells, we pooled responses of all three horizontal system cell types. To properly match the receptive field of vertical system cells²⁰, we averaged the responses of vertical system cells with frontal receptive fields (VS1–VS3) to obtain the responses to the appearing and disappearing bar at 30° and 60° . Responses of vertical system cells with lateral receptive fields (VS5–6) were averaged to determine the responses at 90° .

Modeling. Visual patterns were modeled as one-dimensional luminance functions at a spatial resolution of 0.01° and a temporal resolution of 1 ms. They were covered by 360 elementary motion detectors of the Reichardt type³⁴. Briefly, the luminance value at one location was low-pass filtered (first-order, 20-ms time constant) and subsequently multiplied with the instantaneous value derived from the neighboring location, separated by 1° of visual angle. This was done

twice in a mirror-symmetrical fashion, and the output signals of both operations were subtracted. All elementary motion detectors were weighted according to the $M(\Psi)$ sensitivity profile and subsequently summated. In each hemisphere, motion detection subunits tuned to back-to-front motion were given half the response amplitude of those tuned to front-to-back motion. The visual pattern was also viewed by an array of 360 position detectors. These were modeled as high-pass filters (first-order, 10-ms time constant), the outputs of which were squared. From this array, the location of the maximum was determined. If this maximum was below a certain threshold, the location decayed back to zero with a 20-ms time constant. The output of the position system was calculated as the value of the $P(\Psi)$ function at this location. The $M(\Psi)$ and $P(\Psi)$ functions were approximated in the following way, with $Z(\Psi)$ describing the shape of their profiles, g_P being the gain factor of the position system ($= 3$) and g_M being the gain factor of the motion system ($= 5$).

$$Z(\Psi) = -\frac{d}{d\Psi} e^{-(\Psi/75)^2}$$

$$P(\Psi) = g_P \cdot Z(\Psi)$$

$$M(\Psi) = g_M \cdot |Z(\Psi)|$$

$M(\Psi)$ was subsequently smoothed by a box filter of 20° width. As a noise function we used Gaussian white noise that was filtered by a first-order low-pass filter with 100-ms time constant and multiplied with a noise-gain factor ($g_N = 15$). The sum of noise, motion and position system was then fed through a first-order low-pass filter with 100-ms time-constant to result in the turning speed. In closed-loop simulations, the turning speed was used to update the bar position each millisecond.

$$\text{bar position}(t+1) = \text{bar position}(t) - 0.1 \cdot \text{turning speed}(t)$$

Fixation histograms were obtained from 20 simulation runs, each 30 s long. At the beginning of each run, the bar was positioned in front of the fly. As large field pattern, we used a sine-grating with a spatial wavelength of 22.5° , a mean luminance of 0.5 and a contrast of 1. When activated, it moved at 10° s^{-1} , resulting in a temporal frequency of 0.44 Hz. The black bar was simulated as zero luminance from -5° to $+5^\circ$ around the bar location, replacing the luminance value of either the grating or the one of a uniform background of luminance value 1. The model was simulated in IDL (Exelis) on 64-bit Windows 7.

43. Pfeiffer, B.D. *et al.* Tools for neuroanatomy and neurogenetics in *Drosophila*. *Proc. Natl. Acad. Sci. USA* **105**, 9715–9720 (2008).

Object Tracking in Motion-Blind Flies

Armin Bahl, Georg Ammer, Tabea Schilling and Alexander Borst*

Max-Planck-Institute of Neurobiology, Am Klopferspitz 18, 82152 Martinsried, Germany

* Corresponding author: borst@neuro.mpg.de

Supplemental Material

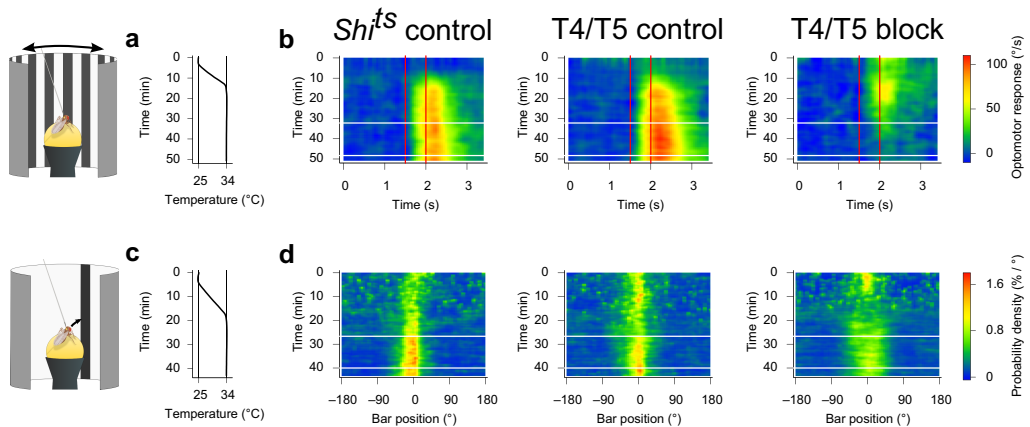
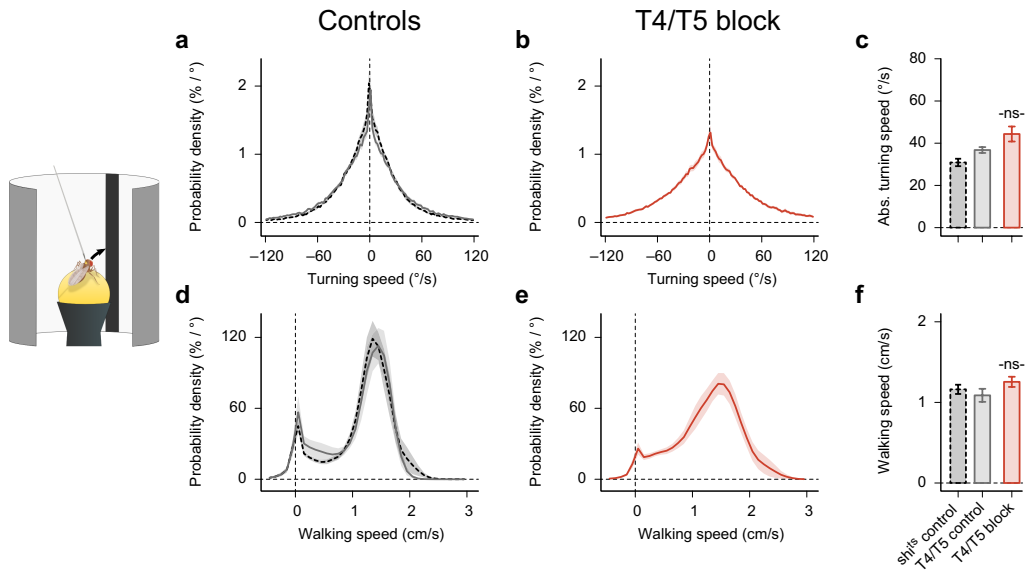


Fig. S1 Temperature control data for the optomotor response and fixation response. **a** Temperature protocol during the full-field grating motion experiment (Fig. 1b-d). The temperature around the fly starts at 25 °C and rises slowly to 34 °C within 10 minutes. **b** The optomotor response – defined as the turning speed in response to clockwise motion minus the turning speed in response to counterclockwise motion divided by two – as a function of stimulus time (x-axis) and overall experimental time (y-axis) for the three groups. Red vertical lines illustrate the time points when grating motion starts and ends. White horizontal lines indicate the time span during which the trials were used for detailed data analysis (Fig. 1). **c** Temperature protocol for closed-loop bar fixation (Fig. 1e-i). **d** Probability density of bar positions (x-axis) as function of overall experimental time (y-axis). All data represent mean of $N = 10, 10, 10$ (b) and $N = 10, 10, 12$ (d) flies per group (left to right). Same flies as in Fig. 1.



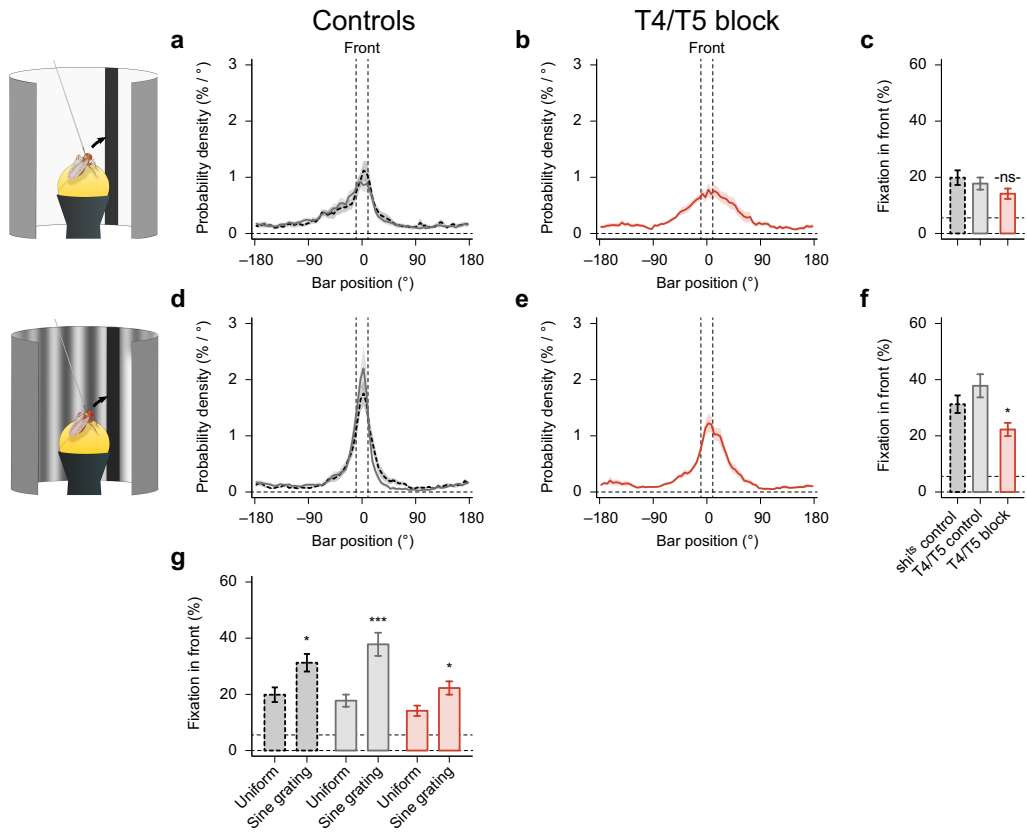


Fig. S3 The fixation response improves with a static background pattern. **a,d** Average probability density as function of bar position for the two controls when the background is gray (a) and when it is a static sine-grating pattern with the same average luminance (d). **b,e** Same as in (a,d) but for flies in which the output of T4/T5 cells was blocked. **c,f** Ability to keep the stripe in the frontal field (same measure as in Fig. 1i) when the background is gray (c) or when it is a static sine-grating background (f). **g** Comparison of the ability to keep the bar in the frontal field between uniform and sine-grating background for all groups. Upper horizontal dashed lines in (c,f,g) indicate the chance level (= 5.6 %; no fixation). All data represent mean \pm SEM; 15 trials per fly of $N = 10,10,9$ flies per group (shi^{ts} control, dashed black lines; T4/T5 control, solid gray lines; T4/T5 block, solid red lines). $^{ns}p \geq 0.05$, $*p < 0.05$, $***p < 0.001$; two-sided t-test comparing to both controls (c,f) or comparing uniform to sine-grating within the groups (g).

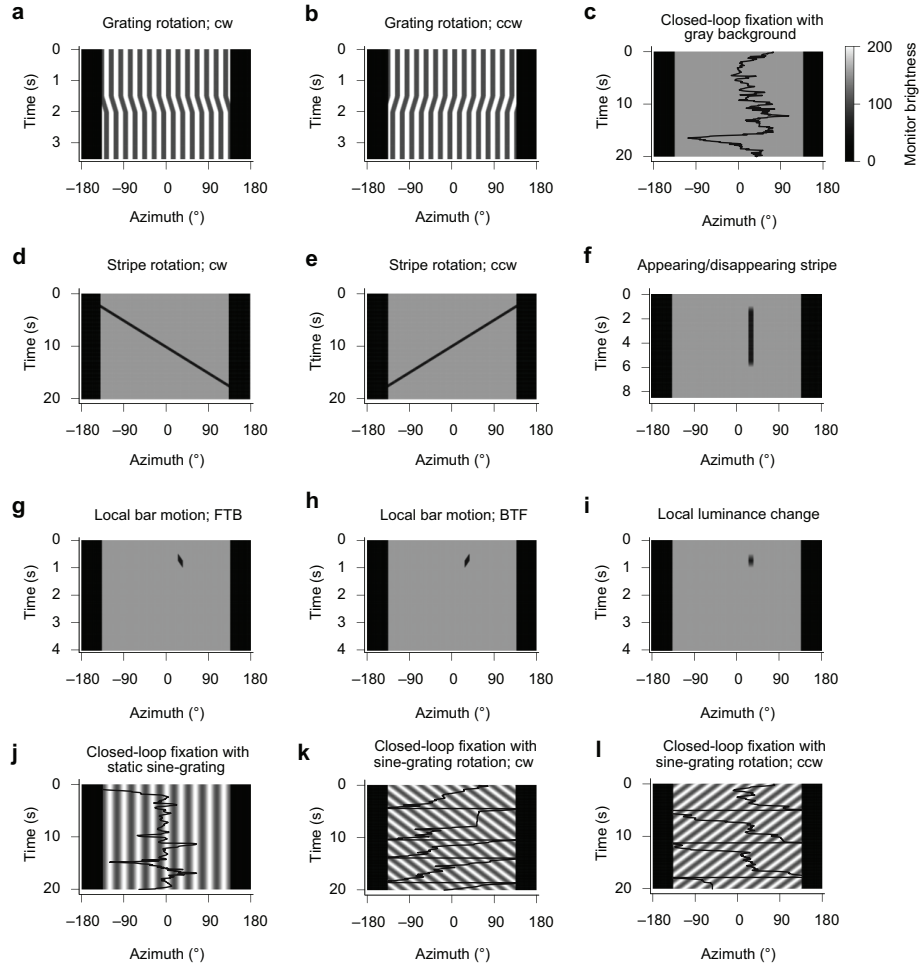


Fig. S4 Position-time plots of all visual stimuli in all experiments. **a,b** Full-field grating moving clockwise (cw) or counterclockwise (ccw). **c** Closed-loop fixation of a black bar on an uniformly gray background. **d,e** Rotating black bar (cw, ccw). **f** Slowly appearing and disappearing black bar at $\Psi = +60^\circ$ (other locations were $\pm 15^\circ$, $\pm 30^\circ$, $\pm 45^\circ$, -60° , $\pm 90^\circ$, $\pm 120^\circ$). **g,h** A localized black bar moves front-to-back (g) and back-to-front (h) at $\Psi = +60^\circ$ (other locations were $\Psi = \pm 30^\circ$, $\Psi = -60^\circ$). **i** Approximation of the local luminance dynamics in (g,h). **j** Closed-loop fixation of a black bar on a static sine-grating with the same average brightness as in (c). **k,l** Closed-loop bar fixation during background motion (cw, ccw, respectively); the black traces in (c,j-l) are experimental example traces of bar position for a single trial of a *shi^{ts}* control fly. Monitor position 0° is directly in front of the fly. The black areas indicate the region of no visual stimulation behind the fly ($-180^\circ < x < -135^\circ$ and $+135^\circ < x < +180^\circ$ in azimuth).

Detailed statistics (list of group sizes, statistical tests and p-values)

The degree of significance was given as follows: not significant (-ns-) when $p \geq 0.05$; * when $p < 0.05$; ** when $p < 0.01$; *** when $p < 0.001$.

Figure 1

Fig. 1d

20 trials per fly; $N^{shi\ control} = 10$ flies, $N^{T4/T5\ control} = 10$ flies, $N^{T4/T5\ block} = 10$ flies.
 Shi^{ts} control \leftrightarrow T4/T5 control: $p = 0.254$, $t = -1.177$ (two-sided t-test)
 Shi^{ts} control \leftrightarrow T4/T5 block: $p < 0.001$, $t = 15.663$ (two-sided t-test)
T4/T5 control \leftrightarrow T4/T5 block: $p < 0.001$, $t = 9.882$ (two-sided t-test)
T4/T5 block \leftrightarrow zero: $p = 0.473$, $t = 0.749$ (two-sided t-test)

Fig. 1i

40 trials per fly; $N^{shi\ control} = 10$ flies, $N^{T4/T5\ control} = 10$ flies, $N^{T4/T5\ block} = 12$ flies.
 Shi^{ts} control \leftrightarrow T4/T5 control: $p = 0.307$, $t = 1.052$ (two-sided t-test)
 Shi^{ts} control \leftrightarrow T4/T5 block: $p = 0.012$, $t = 2.759$ (two-sided t-test)
T4/T5 control \leftrightarrow T4/T5 block: $p = 0.025$, $t = 2.427$ (two-sided t-test)
T4/T5 block \leftrightarrow chance: $p < 0.001$, $t = 5.862$ (two-sided t-test)

Figure 2

35 trials per fly; $N^{shi\ control} = 10$ flies, $N^{T4/T5\ control} = 11$ flies, $N^{T4/T5\ block} = 14$ flies.

Fig. 2e

Shi^{ts} control \leftrightarrow T4/T5 control: $p = 0.725$, $t = 0.356$ (two-sided t-test)
 Shi^{ts} control \leftrightarrow T4/T5 block: $p < 0.001$, $t = 4.136$ (two-sided t-test)
T4/T5 control \leftrightarrow T4/T5 block: $p < 0.001$, $t = 4.068$ (two-sided t-test)
T4/T5 block \leftrightarrow zero: $p < 0.001$, $t = 7.086$ (two-sided t-test)

Fig. 2h

Shi^{ts} control \leftrightarrow T4/T5 control: $p = 0.618$, $t = 0.507$ (two-sided t-test)
 Shi^{ts} control \leftrightarrow T4/T5 block: $p < 0.001$, $t = 13.408$ (two-sided t-test)
T4/T5 control \leftrightarrow T4/T5 block: $p < 0.001$, $t = 16.735$ (two-sided t-test)
T4/T5 block \leftrightarrow zero: $p = 0.056$, $t = 2.098$ (two-sided t-test)

Figure 3

10 trials per fly; $N^{shi\ control} = 12$ flies, $N^{T4/T5\ control} = 12$ flies, $N^{T4/T5\ block} = 16$ flies. Half of each group was used to measure responses at positions $\pm 15^\circ$, $\pm 60^\circ$, $\pm 120^\circ$, the other half at $\pm 30^\circ$, $\pm 45^\circ$, $\pm 90^\circ$.

Fig. 3e

Shi^{ts} control \leftrightarrow T4/T5 control: $p = 0.611$, $t = 0.524$ (two-sided t-test)
 Shi^{ts} control \leftrightarrow T4/T5 block: $p = 0.086$, $t = 1.872$ (two-sided t-test)
T4/T5 control \leftrightarrow T4/T5 block: $p = 0.489$, $t = 0.713$ (two-sided t-test)

Fig. 3h

Shi^{ts} control \leftrightarrow T4/T5 control: $p = 0.151$, $t = 1.553$ (two-sided t-test)

Shi^{ts} control ↔ T4/T5 block: **p = 0.527, t = 0.650** (two-sided t-test)
 T4/T5 control ↔ T4/T5 block: **p = 0.465, t = -0.753** (two-sided t-test)
Shi^{ts} control ↔ zero: **p = 0.368, t = -0.990** (two-sided t-test)
 T4/T5 control ↔ zero: **p = 0.018, t = -3.451** (two-sided t-test)
 T4/T5 block ↔ zero: **p = 0.107, t = -1.851** (two-sided t-test)

Fig. 3i,j

At 45°:

Shi^{ts} control ↔ T4/T5 block: **p = 0.054, t = 2.137** (two-sided t-test)
 T4/T5 control ↔ T4/T5 block: **p = 0.155, t = 1.517** (two-sided t-test)

Fig. 3k

Shi^{ts} control ↔ T4/T5 control: **p = 0.407, t = 0.865** (two-sided t-test)
Shi^{ts} control ↔ T4/T5 block: **p = 0.470, t = 0.745** (two-sided t-test)
 T4/T5 control ↔ T4/T5 block: **p = 0.939, t = -0.077** (two-sided t-test)

Figure 4

60 trials per fly; At $\Psi = 30^\circ$: $N^{shi \text{ control}} = 10$ flies, $N^{T4/T5 \text{ control}} = 12$ flies, $N^{T4/T5 \text{ block}} = 11$ flies. At $\Psi = 60^\circ$: Additional $N^{shi \text{ control}} = 10$ flies, $N^{T4/T5 \text{ control}} = 11$ flies, $N^{T4/T5 \text{ block}} = 11$ flies.

Fig. 4c

At 30°

Shi^{ts} control ↔ T4/T5 control: **p = 0.027, t = 2.390** (two-sided t-test)
Shi^{ts} control ↔ T4/T5 block: **p < 0.001, t = 8.262** (two-sided t-test)
 T4/T5 control ↔ T4/T5 block: **p < 0.001, t = 5.103** (two-sided t-test)

At 60°:

Shi^{ts} control ↔ T4/T5 control: **p = 0.067, t = -1.939** (two-sided t-test)
Shi^{ts} control ↔ T4/T5 block: **p < 0.001, t = 7.148** (two-sided t-test)
 T4/T5 control ↔ T4/T5 block: **p < 0.001, t = 9.596** (two-sided t-test)

Fig. 4f

At 30°

Shi^{ts} control ↔ T4/T5 control: **p = 0.969, t = 0.039** (two-sided t-test)
Shi^{ts} control ↔ T4/T5 block: **p < 0.001, t = -4.101** (two-sided t-test)
 T4/T5 control ↔ T4/T5 block: **p < 0.001, t = -3.962** (two-sided t-test)

At 60°:

Shi^{ts} control ↔ T4/T5 control: **p = 0.666, t = 0.438** (two-sided t-test)
Shi^{ts} control ↔ T4/T5 block: **p < 0.001, t = -4.842** (two-sided t-test)
 T4/T5 control ↔ T4/T5 block: **p = 0.002, t = -3.488** (two-sided t-test)

Fig. 4i

At 30°

Shi^{ts} control ↔ T4/T5 control: **p = 0.955, t = 0.057** (two-sided t-test)
Shi^{ts} control ↔ T4/T5 block: **p = 0.471, t = 0.736** (two-sided t-test)
 T4/T5 control ↔ T4/T5 block: **p = 0.485, t = 0.711** (two-sided t-test)

At 60°:

Shi^{ts} control ↔ T4/T5 control: **p = 0.609, t = -0.518** (two-sided t-test)

Shi^{ts} control \leftrightarrow T4/T5 block: **p = 0.165, t = 1.443** (two-sided t-test)
 T4/T5 control \leftrightarrow T4/T5 block: **p = 0.069, t = 1.916** (two-sided t-test)

Fig. 4j

At 30°

$R_{FTB} \leftrightarrow R_{BTF} \leftrightarrow R_L$ (T4/T5 block): **p = 0.742, F = 0.300** (one-way ANOVA)

At 60°

$R_{FTB} \leftrightarrow R_{BTF} \leftrightarrow R_L$ (T4/T5 block): **p = 0.902, F = 0.103** (one-way ANOVA)

Fig. 4k

At 30°

$M_{FTB} \leftrightarrow -M_{BTF}$ (*shi*^{ts} control): **p < 0.001, t = 5.696** (two-sided t-test)

$M_{FTB} \leftrightarrow -M_{BTF}$ (T4/T5 control): **p = 0.028, t = 2.346** (two-sided t-test)

$M_{FTB} \leftrightarrow -M_{BTF}$ (T4/T5 block): **p = 0.209, t = 1.299** (two-sided t-test)

$M_{FTB} \leftrightarrow$ zero (T4/T5 block): **p = 0.447, t = 0.790** (two-sided t-test)

$M_{BTF} \leftrightarrow$ zero (T4/T5 block): **p = 0.325, t = -1.035** (two-sided t-test)

At 60°

$M_{FTB} \leftrightarrow -M_{BTF}$ (*shi*^{ts} control): **p = 0.639, t = 0.476** (two-sided t-test)

$M_{FTB} \leftrightarrow -M_{BTF}$ (T4/T5 control): **p = 0.147, t = 1.508** (two-sided t-test)

$M_{FTB} \leftrightarrow -M_{BTF}$ (T4/T5 block): **p = 0.499, t = -0.687** (two-sided t-test)

$M_{FTB} \leftrightarrow$ zero (T4/T5 block): **p = 0.653, t = -0.463** (two-sided t-test)

$M_{BTF} \leftrightarrow$ zero (T4/T5 block): **p = 0.622, t = 0.508** (two-sided t-test)

Figure 5

30 trials per fly; $N^{shi \text{ control}} = 11$ flies, $N^{T4/T5 \text{ control}} = 9$ flies, $N^{T4/T5 \text{ block}} = 9$ flies.

Fig. 5c

Shi^{ts} control \leftrightarrow T4/T5 control: **p = 0.394, t = 0.874** (two-sided t-test)

Shi^{ts} control \leftrightarrow T4/T5 block: **p = 0.047, t = -2.127** (two-sided t-test)

T4/T5 control \leftrightarrow T4/T5 block: **p = 0.010, t = -2.908** (two-sided t-test)

Fig. 5f

Shi^{ts} control \leftrightarrow T4/T5 control: **p = 0.176, t = 1.410** (two-sided t-test)

Shi^{ts} control \leftrightarrow T4/T5 block: **p = 0.012, t = -2.797** (two-sided t-test)

T4/T5 control \leftrightarrow T4/T5 block: **p = 0.001, t = -3.999** (two-sided t-test)

Figure S1

Fig. S1b

$N^{shi \text{ control}} = 10$ flies, $N^{T4/T5 \text{ control}} = 10$ flies, $N^{T4/T5 \text{ block}} = 10$ flies. Same flies as in Fig. 1b-d.

Fig. S1d

$N^{shi \text{ control}} = 10$ flies, $N^{T4/T5 \text{ control}} = 10$ flies, $N^{T4/T5 \text{ block}} = 12$ flies. Same flies as in Fig. 1e-i.

Figure S2

40 trials per fly; $N^{shi \text{ control}} = 10$ flies, $N^{T4/T5 \text{ control}} = 10$ flies, $N^{T4/T5 \text{ block}} = 12$ flies. Same flies as in Fig. 1e-i.

Fig. S2c

Shi^{ts} control \leftrightarrow T4/T5 control: **p = 0.023, t = -2.490** (two-sided t-test)
Shi^{ts} control \leftrightarrow T4/T5 block: **p = 0.006, t = -3.049** (two-sided t-test)
 T4/T5 control \leftrightarrow T4/T5 block: **p = 0.095, t = -1.767** (two-sided t-test)

Fig. S2f

Shi^{ts} control \leftrightarrow T4/T5 control: **p = 0.486, t = 0.710** (two-sided t-test)
Shi^{ts} control \leftrightarrow T4/T5 block: **p = 0.319, t = -1.021** (two-sided t-test)
 T4/T5 control \leftrightarrow T4/T5 block: **p = 0.131, t = -1.575** (two-sided t-test)

Figure S3

15 trials per fly; $N^{shi \text{ control}} = 10$ flies $N^{T4/T5 \text{ control}} = 10$ flies, $N^{T4/T5 \text{ block}} = 9$ flies.

Fig. S3c

Shi^{ts} control \leftrightarrow T4/T5 control: **p = 0.561, t = 0.591** (two-sided t-test)
Shi^{ts} control \leftrightarrow T4/T5 block: **p = 0.115, t = 1.659** (two-sided t-test)
 T4/T5 control \leftrightarrow T4/T5 block: **p = 0.252, t = 1.186** (two-sided t-test)

Fig. S3f

Shi^{ts} control \leftrightarrow T4/T5 control: **p = 0.246, t = -1.200** (two-sided t-test)
Shi^{ts} control \leftrightarrow T4/T5 block: **p = 0.047, t = 2.136** (two-sided t-test)
 T4/T5 control \leftrightarrow T4/T5 block: **p = 0.008, t = 3.004** (two-sided t-test)

Fig. S3g

Uniform \leftrightarrow Sine grating (*shi*^{ts} control): **p = 0.016, t = -2.651** (two-sided t-test)
 Uniform \leftrightarrow Sine grating (T4/T5 control): **p < 0.001, t = -4.079** (two-sided t-test)
 Uniform \leftrightarrow Sine grating (T4/T5 block): **p = 0.021, t = -2.553** (two-sided t-test)

2.3 Local Motion Detectors are Required for the Computation of Expansion Flow-Fields

Tabea Schilling and Alexander Borst

Author contributions:

T.S. performed all of the behavioral experiments and evaluated the data. **T.S.** and A. B. designed the study and wrote the manuscript.

Tabea Schilling

Alexander Borst

RESEARCH ARTICLE

Local motion detectors are required for the computation of expansion flow-fields

Tabea Schilling and Alexander Borst*

ABSTRACT

Avoidance of predators or impending collisions is important for survival. Approaching objects can be mimicked by expanding flow-fields. Tethered flying fruit flies, when confronted with an expansion flow-field, reliably turn away from the pole of expansion when presented laterally, or perform a landing response when presented frontally. Here, we show that the response to an expansion flow-field is independent of the overall luminance change and edge acceleration. As we demonstrate by blocking local motion-sensing neurons T4 and T5, the response depends crucially on the neural computation of appropriately aligned local motion vectors, using the same hardware that also controls the optomotor response to rotational flow-fields.s

KEY WORDS: Collision avoidance, Looming, Local motion detectors

INTRODUCTION

Whenever an animal moves or something else is moving in the environment relative to it, visual motion occurs on the retina. Such visual motion cues are of importance particularly for fast flying animals, enabling them to perform various flight maneuvers such as maintaining a straight course, flying towards an object or avoiding it. A well-studied example is the optomotor response, which represents compensatory movements of the body and head syndirectional with rotational large-field motion that may signal deviation from a straight course (Blondeau and Heisenberg, 1982). This behavior is controlled by lobula plate tangential cells as demonstrated by genetic or surgical ablation (Geiger and Nässel, 1981; Hausen and Wehrhahn, 1983; Heisenberg et al., 1978) and activation studies (Haikala et al., 2013). Lobula plate tangential cells receive their input from a 2-dimensional, retinotopically arranged array of columnar T4 and T5 cells (Schnell et al., 2012) with T4 cells responding preferentially to moving bright and T5 to moving dark edges (Maisak et al., 2013).

Other visually controlled behaviors are evoked by expanding optic flow, which is generated on the retina by objects moving towards the fly or by impending collision with stationary objects. Looming stimuli can induce two different behaviors in flying flies dependent on the position of the stimulus. A frontal position of the pole of expansion elicits a landing response (Borst and Bahde, 1988; Braatenberg and Ferretti, 1966), whereas laterally expanding stimuli evoke an avoidance behavior (Tammero and Dickinson, 2002).

Department of Circuits-Computation-Models, Max-Planck-Institute of Neurobiology, Martinsried D-82152, Germany.

*Author for correspondence (borst@neuro.mpg.de)

This is an Open Access article distributed under the terms of the Creative Commons Attribution License (<http://creativecommons.org/licenses/by/3.0/>), which permits unrestricted use, distribution and reproduction in any medium provided that the original work is properly attributed.

Received 13 May 2015; Accepted 1 July 2015

The avoidance behavior has been studied in freely (Muijres et al., 2014, 2015) as well as in tethered flying flies (Tammero and Dickinson, 2002; Tammero et al., 2004). However, the neuronal basis of both these behaviors is not well understood. We asked whether the T4/T5 cells, which act as local motion detectors known to underlie optomotor responses, are also necessary for avoidance and landing behavior. We first characterized the avoidance and landing response of tethered flying flies using different expanding stimuli. Silencing T4 and T5 neurons genetically, we found that information from local motion circuits is essential for both the avoidance and the landing response. We thus conclude that computation of an expansion flow-field depends on the activity of the same set of elementary motion detecting neurons that control the optomotor response.

RESULTS AND DISCUSSION

In order to characterize visual features which elicit avoidance responses, we confronted tethered flying flies (Fig. 1A) with various visual stimuli presented laterally at an angle of $\pm 50^\circ$ to the flight course. The first stimulus consisted of a vertical dark bar expanding with different angular velocities to 180° width. A typical collision avoidance response to a bar expanding at a constant velocity of 180 deg/s is shown in Fig. 1B: After a brief latency the animals attempted to turn away as long as the stimulus was presented. The strength of the avoidance response was strongly dependent on the angular expansion velocity of the stimulus with a maximal response at a velocity of 340 deg/s (Fig. 1C). Objects moving towards a fly with a constant velocity induce not a constantly but exponentially increasing expansion pattern on the retina. To mimic a physically realistic approach dynamic, we used looming squares and presented them with different patterns inducing either a decrease, an increase or no overall luminance change. A looming dark square (Fig. 1D), a bright square on a dark background (Fig. 1E) and a square with a checkerboard pattern (Fig. 1F) elicited similar avoidance responses independent of the global luminance change. In addition, dimming of a laterally presented square with 120° width induced even a slight turning towards the square (Fig. 1G). A looming horizontal bar expanding only vertically elicited an avoidance yaw turn (Fig. 1H) comparable in amplitude and time-course to the reaction away from a horizontally expanding bar. Finally, we replaced the expanding bar by two vertical bars moving away from each other for 0.25 s at a velocity of 360 deg/s . This elicited an avoidance behavior away from the stimulus (Fig. 1I). In summary, we found no or little influence of the overall luminance change on the reaction of the fly.

Avoidance turns could result from a different tuning of the optomotor response to front to back (FtB) and back to front (BtF) motion. To test this possibility we separated the looming bar stimulus, expanding in both directions, into single edge motion. When presenting a bar looming either FtB or BtF direction, a strong turning along with the respective edge direction was observed (Fig. 1J,K). However, when the bar was expanding in both directions, flies only turned along with the edge moving BtF,

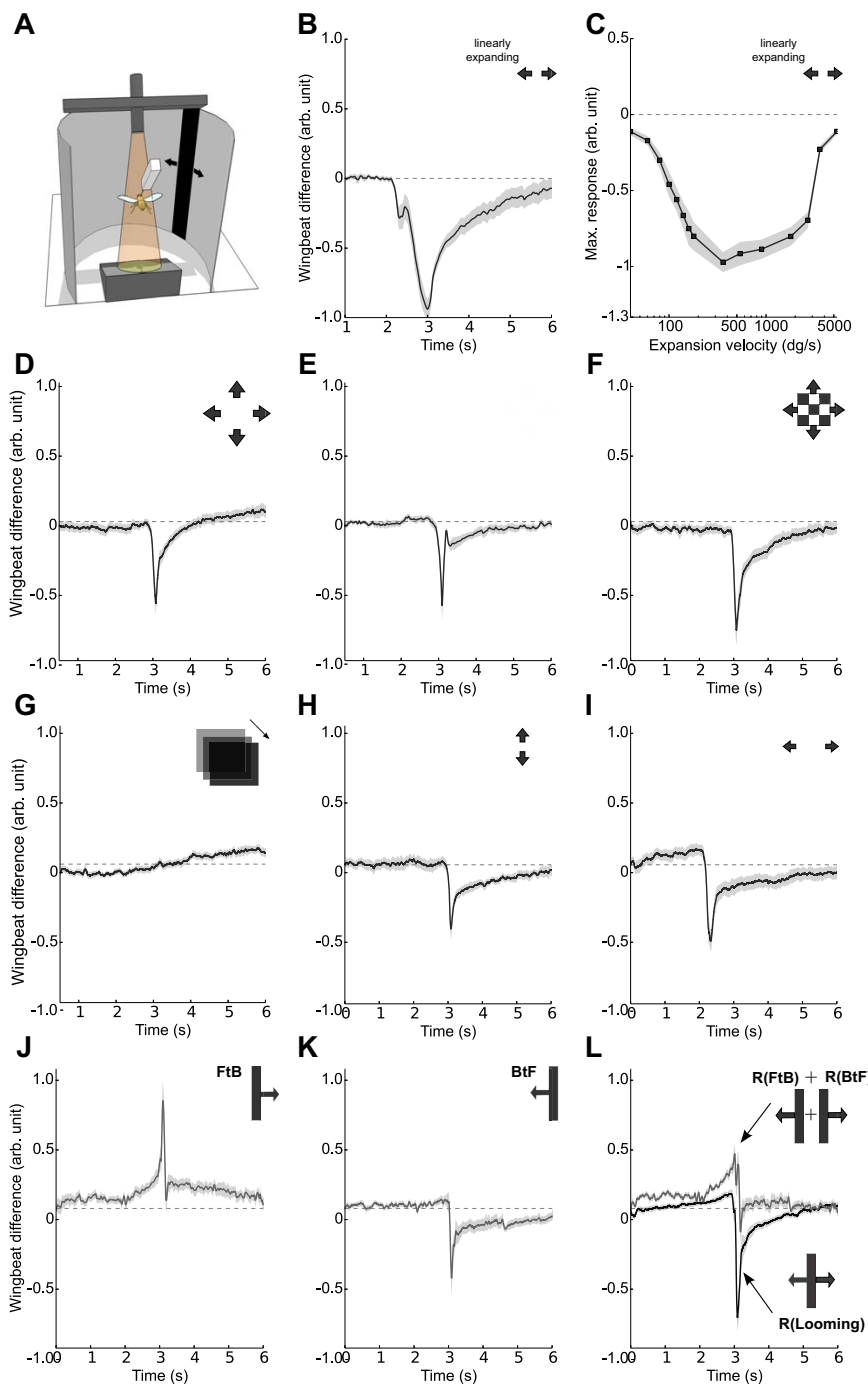


Fig. 1. Characterization of the avoidance behavior elicited by different stimuli. Average turning responses of Canton-S wild-type flies, elicited by expanding stimuli. (A) Illustration of the flight setup. (B) Avoidance response to a vertical bar expanding horizontally presented at $\pm 50^\circ$. The bar expands from 0° to 180° in 1 s, $n=13$. (C) Velocity tuning of the avoidance response to an expanding bar with expansion velocities from 40 to 5400 deg/s. The flies reacted with comparable strong turning to a broad range of expansion velocities from 180° to 2700° with a maximum at 360 deg/s, $n=10$. (D–I) Turning responses to different expansion/looming stimuli, $n=10$. (D–F) Avoidance responses to a dark looming square (D), a bright looming square (E) and a looming square with a checkerboard pattern (F). (G) Response to a dimming $120^\circ \times 120^\circ$ square. (H) Avoidance response to a horizontal bar expanding vertically at a velocity of 360 deg/s, width=60°, presented at $\pm 60^\circ$. (I) Avoidance of two 10° broad vertical stripes moving away from each other for 0.25 s at a velocity of 360 deg/s. (J,K) Reactions to a looming bar where either the anterior or the posterior edge is moving, $n=10$. (L) The sum of the single edge responses (upper line) and the response to the sum of both edges moving (lower line), $n=10$. FtB, front to back; BtF, back to front. All data represent mean \pm s.e.m.

i.e. away from the stimulus. The sum of the responses to individual edges was clearly distinct from the response to the sum of both edges, i.e. the whole bar expansion (Fig. 1L).

Our data so far indicate that the avoidance behavior is distinct from the optomotor response, but depends on the evaluation of local motion signals rather than on overall luminance changes. Since T4 and T5 neurons are known to represent the elementary motion detectors in the fly brain (Maisak et al., 2013), we measured the

avoidance behavior of flies with blocked T4/T5 cells. We silenced T4 and T5 cells by expressing the tetanus-toxin light chain (Sweeney et al., 1995) and measured the response of T4/T5 blocked flies to different looming stimuli. The response to an expanding bar was completely abolished in T4/T5 blocked flies (Fig. 2B) compared to both groups of parental control flies (Fig. 2A). To confirm this with another stimulus, we presented a looming circle, a stimulus eliciting very strong avoidance reactions

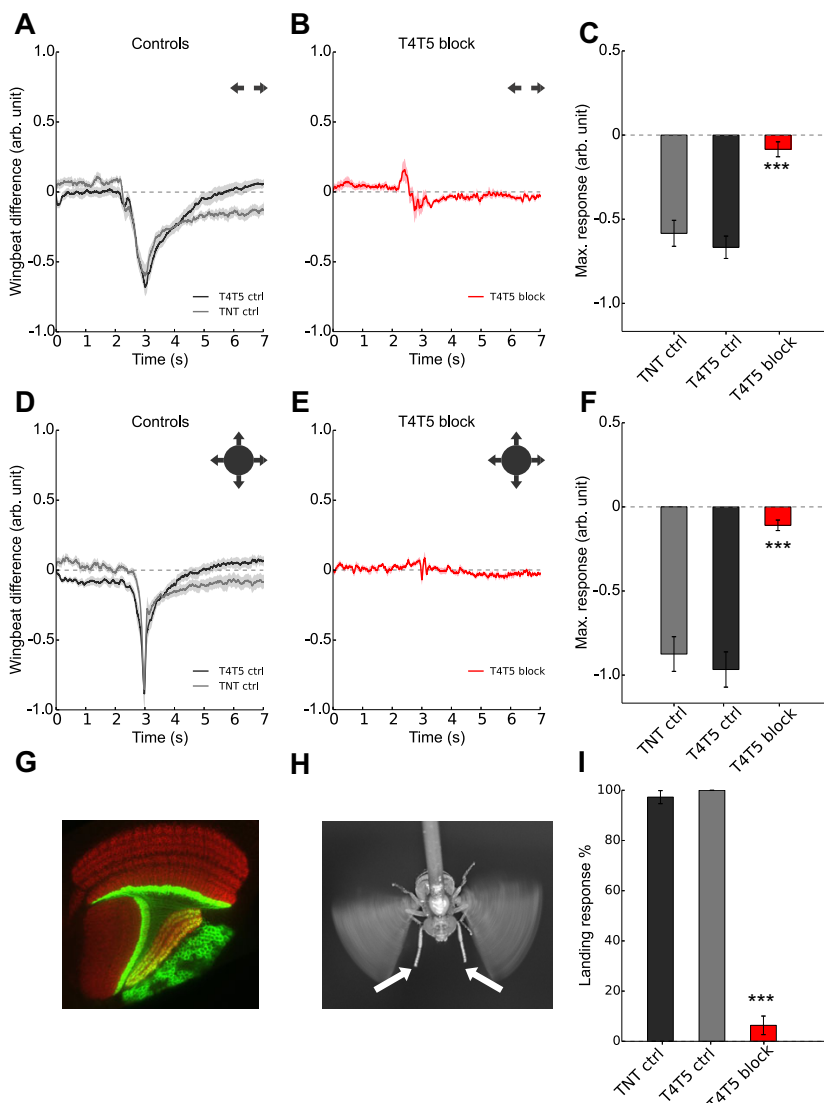


Fig. 2. T4 and T5 block abolished both landing and avoidance responses. Flight behavior and landing responses of flies with TNT-E expression in T4 and T5 cells. (A) Turning responses of TNT and T4/T5 control flies to an expanding bar with an expansion velocity of 180 deg/s, $n=12$. (B) Turning responses of T4/T5 blocked flies to an expanding bar, $n=12$. (C) Maximal turning responses are significantly reduced in T4/T5 block flies (**P<0.001, two-sided t-test compared with both control groups). (D) Flight turning behavior of TNT and T4/T5 control flies in response to a looming circle, $n=12$. (E) Turning responses of T4/T5 blocked flies to a looming circle, $n=14$. (F) Maximal turning responses are significantly reduced in T4/T5 blocked flies (**P<0.001, two-sided t-test compared with both control groups). (G) GFP expression in T4 and T5 cells. (H) Example of a landing response. (I) Percentage of flies showing extension of their front legs in response to a looming square presented in front of them. TNT and T4/T5 controls showed a positive response in 97% and 100% of all trials, respectively, whereas T4/T5 blocked flies performed only 6.3% positive leg extension. This reduction was significant (**P<0.001, two-sided t-test compared with both control groups), $n=11$. All data represent mean \pm s.e.m.

in control flies (Fig. 2D). T4/T5 blocked flies did not react at all to this stimulus (Fig. 2E).

If presented in front of the fly, looming or expanding stimuli do not elicit avoidance turns, but rather a leg extension typical for the landing response (Tammero and Dickinson, 2002). We presented a looming square (expanding to 180° in 1 s) and captured images of the fly from above. We quantified the landing response as the percentage of positive front leg extension at the time point of expected collision with the square stimulus. Control flies almost always reacted with an extension of their front legs (TNT controls 97%, T4/T5 controls 100%), whereas T4/T5 blocked flies showed only 6.3% positive reactions (Fig. 2I). These data strongly indicate that the avoidance as well as the landing response are dependent on the activity of T4 and T5 cells.

Neurons reacting to looming stimuli and induce various kinds of avoidance or escape behaviors have been described in many animal models like locusts, crabs, pigeons and mice (Gabbiani et al., 1999; Oliva and Tomsic, 2014; Wang and Frost, 1992; Zhao et al., 2014). The detection of a looming stimulus can be realized in different

ways. The giant fiber of *Drosophila*, a large neuron receiving part of its input from the lobula, elicits fast escape jumps (von Reyn et al., 2014) and reacts to approaching stimuli, sudden light-ON or light-OFF stimuli and mechanical stimulation (Mu et al., 2014). A giant lobula neuron in the locust, called LGMD neuron, is selectively sensitive to looming stimuli (Gabbiani et al., 1999). The angular size of a looming stimulus increases exponentially, which decreases the latency of the photoreceptor inputs. The LGMD synchronizes these excitatory inputs derived from progressing edges due to the successive latency decrease (Jones and Gabbiani, 2010). A different computation is used by PV-5, an approach-sensitive retinal ganglion cell of the mouse. PV-5 integrates excitatory OFF and inhibitory ON inputs which tunes the neurons to dark approaching or dimming objects (Münch et al., 2009).

In contrast, the landing and avoidance responses of flies were proposed to rely on summation of elementary motion detectors (Borst and Bahde, 1988; Tammero and Dickinson, 2002). We found that both behaviors are indeed dependent on the activity of T4 and T5 neurons, which become directionally selective by performing a

spatiotemporal correlation of their input (Maisak et al., 2013), a computation described by the Hassenstein-Reichardt detector model (Hassenstein and Reichardt, 1956). Accordingly, in our experiments the avoidance response was elicited by the diverging edge motion of expanding or looming stimuli, independent of an overall luminance change or edge acceleration. T4/T5 neurons are grouped in four subtypes each tuned to motion in one out of the four cardinal directions. These T4/T5 subtypes project their axonal terminals into four adjacent layers of the lobula plate, where they form excitatory synapses onto the dendrites of lobula plate tangential cells (Maisak et al., 2013; Mauss et al., 2014). Our data suggest that an approach-sensitive neuron should receive excitatory input from T4/T5 cells in at least two lobula plate layers. Such a neuron would be activated by simultaneous activation of the two vertical or the two horizontal layers. There are cells in the flies optic lobe reported to be looming sensitive and influence escape behavior, the foma-1 neurons (De Vries and Clandinin, 2012). One of them has a dendrite located in the lobula plate and could be a candidate neuron for the avoidance and landing response.

Different visual behaviors use neural modules in the visual lobe which partially overlap with each other. In case of behaviors driven by expansion flow-fields, our results indicate that they share the circuits for elementary motion detection, i.e. T4 and T5 cells and their presynaptic circuitry, with the optomotor response and bifurcate at the level of large-field tangential cells of the lobula plate (Borst, 2014).

MATERIALS AND METHODS

Fly strains

Flies were raised on standard cornmeal-agar medium at 25°C and 60% humidity on a 12 h light/12 h dark cycle. The genotypes used are the following: Wildtype Canton-S flies, T4T5 block flies (w^+/w^- ; UAS-TNT-E/R59E08-AD; R42F06-DBD/+), T4T5 control flies (w^+/w^- ; R59E08-AD/+; R42F06-DBD/+) and TNT-E control flies (w^+/w^- ; UAS-TNT-E/+; +/+). The T4T5 split Gal-4 line was kindly provided by Aljoscha Nern, HHMI Janelia Research Campus (GMRSS00324), the UAS-TNT-E flies derived from the Bloomington Stock Center (stock no. 28837).

Behavioral experiments

We used female flies two days after eclosion. They were anesthetized by cooling to 3°C, glued to a needle with blue-light-activated cement with their heads fixed and, after recovery, placed into the arena. Visual stimulation was provided by three LCD screens arranged around the fly, controlled by a NVIDIA 3D Vision Surround Technology (Bahl et al., 2013). The fly turning behavior was measured with a 'wingbeat analyzer' (Gotz, 1987). Above the fly a camera (Grasshopper 03K2M+Infinity InfiniStix 94 nm/1.00×) helped to position it and allowed video tracking. Landing responses were measured as front leg extension.

Data analysis and presented stimuli

Wing beat data were converted with an analog-digital converter from National Instruments (USB-6009). The left-right wingbeat signal difference was used as a value proportional to the yaw torque of the fly. The stimuli were presented at $\pm 50^\circ$ lateral to the flies with a contrast of 50% for wild type flies and 33% for T4/T5 blocked experiments. Each fly performed eight trials; trials and both sides were averaged to a mean turning response.

Acknowledgements

We wish to thank G. Rubin and A. Nern for providing the T4/T5 cell-specific split Gal-4 driver line GMRSS00324. We also want to thank A. Bahl for programming the software reading the behavioral output, S. Prech for building the amplifiers, W. Essbauer for fly work, A. Maus and J. Pujol-Marti for critically reading the manuscript.

Competing interests

The authors declare no competing or financial interests.

Author contributions

T.S. performed all of the behavioral experiments and evaluated the data. T.S. and A. B. designed the study and wrote the manuscript.

Funding

This work was funded by the Max-Planck-Gesellschaft.

References

Bahl, A., Ammer, G., Schilling, T. and Borst, A. (2013). Object tracking in motion-blind flies. *Nat. Neurosci.* **16**, 730-738.

Blondeau, J. and Heisenberg, M. (1982). The three-dimensional optomotor torque system of *Drosophila melanogaster* - studies on wildtype and the mutant *optomotor-blind* H31. *J. Comp. Physiol.* **145**, 321-329.

Borst, A. (2014). Fly visual course control: behaviour, algorithms and circuits. *Nat. Rev. Neurosci.* **15**, 590-599.

Borst, A. and Bahde, S. (1988). Spatio-temporal integration of motion. *Naturwissenschaften* **75**, 265-267.

Braitenberg, V. and Ferretti, C. T. (1966). Landing reaction of *Musca domestica* induced by visual stimuli. *Naturwissenschaften* **53**, 155-155.

De Vries, S. E. J. and Clandinin, T. R. (2012). Loom-sensitive neurons link computation to action in the *Drosophila* visual system. *Curr. Biol.* **22**, 353-362.

Gabbiani, F., Krapp, H. G. and Laurent, G. (1999). Computation of object approach by a wide-field, motion-sensitive neuron. *J. Neurosci.* **19**, 1122-1141.

Geiger, G. and Nässel, D. (1981). Visual orientation behaviour of flies after selective laser beam ablation of interneurons. *Nature* **293**, 398-399.

Gotz, K. G. (1987). Course-control, metabolism and wing interference during ultralong tethered flight in *Drosophila melanogaster*. *J. Exp. Biol.* **128**, 35-46.

Haikal, V., Joesch, M., Borst, A. and Mauss, A. S. (2013). Optogenetic control of fly optomotor responses. *J. Neurosci.* **33**, 13927-13934.

Hassenstein, B. and Reichardt, W. (1956). Systemtheoretische Analyse der Zeit-, Reihenfolge und Vorzeichenauswertung bei der Bewegungsperzeption des Ruesselkäfers *Chlorophanus*. *Z. Naturforsch.* **11b**, 513-524.

Hausen, K. and Wehrhahn, C. (1983). Microsurgical lesion of horizontal cells changes optomotor yaw responses in the blowfly *Calliphora erythrocephala*. *Proc. R. Soc. Lond. B Biol. Sci.* **219**, 211-216.

Heisenberg, M., Wonneberger, R. and Wolf, R. (1978). Optomotor-blind H31-a *Drosophila* mutant of the lobula plate giant neurons. *J. Comp. Physiol.* **124**, 287-296.

Jones, P. W. and Gabbiani, F. (2010). Synchronized neural input shapes stimulus selectivity in a collision-detecting neuron. *Curr. Biol.* **20**, 2052-2057.

Maisak, M. S., Haag, J., Ammer, G., Serbe, E., Meier, M., Leonhardt, A., Schilling, T., Bahl, A., Rubin, G. M., Nern, A. et al. (2013). A directional tuning map of *Drosophila* elementary motion detectors. *Nature* **500**, 212-216.

Mauss, A. S., Meier, M., Serbe, E. and Borst, A. (2014). Optogenetic and pharmacologic dissection of feedforward inhibition in *Drosophila* motion vision. *J. Neurosci.* **34**, 2254-2263.

Mu, L., Bacon, J. P., Ito, K. and Strausfeld, N. J. (2014). Responses of *Drosophila* giant descending neurons to visual and mechanical stimuli. *J. Exp. Biol.* **217**, 2121-2129.

Muijres, F. T., Elzinga, M. J., Melis, J. M. and Dickinson, M. H. (2014). Flies evade looming targets by executing rapid visually directed banked turns. *Science* **344**, 172-177.

Muijres, F. T., Elzinga, M. J., Iwasaki, N. A. and Dickinson, M. H. (2015). Body saccades of *Drosophila* consist of stereotyped banked turns. *J. Exp. Biol.* **218**, 864-875.

Münch, T. A., da Silveira, R. A., Siegert, S., Viney, T. J., Awatramani, G. B. and Roska, B. (2009). Approach sensitivity in the retina processed by a multifunctional neural circuit. *Nat. Neurosci.* **12**, 1308-1316.

Oliva, D. and Tomsic, D. (2014). Computation of object approach by a system of visual motion-sensitive neurons in the crab *Neohelice*. *J. Neurophysiol.* **112**, 1477-1490.

Schnell, B., Raghu, S. V., Nern, A. and Borst, A. (2012). Columnar cells necessary for motion responses of wide-field visual interneurons in *Drosophila*. *J. Comp. Physiol. A* **198**, 389-395.

Sweeney, S. T., Broadie, K., Keane, J., Niemann, H. and O'Kane, C. J. (1995). Targeted expression of tetanus toxin light chain in *Drosophila* specifically eliminates synaptic transmission and causes behavioral defects. *Neuron* **14**, 341-351.

Tammero, L. F. and Dickinson, M. H. (2002). Collision-avoidance and landing responses are mediated by separate pathways in the fruit fly, *Drosophila melanogaster*. *J. Exp. Biol.* **205**, 2785-2798.

Tammero, L. F., Frye, M. A. and Dickinson, M. H. (2004). Spatial organization of visuomotor reflexes in *Drosophila*. *J. Exp. Biol.* **207**, 113-122.

von Reyn, C. R., Breads, P., Peek, M. Y., Zheng, G. Z., Williamson, W. R., Yee, A. L., Leonardo, A. and Card, G. M. (2014). A spike-timing mechanism for action selection. *Nat. Neurosci.* **17**, 962-970.

Wang, Y. and Frost, B. J. (1992). Time to collision is signalled by neurons in the nucleus rotundus of pigeons. *Nature* **356**, 236-238.

Zhao, X., Liu, M. and Cang, J. (2014). Visual cortex modulates the magnitude but not the selectivity of looming-evoked responses in the superior colliculus of awake mice. *Neuron* **84**, 202-213.

2.4 Transcriptional Control of Morphological Properties of Direction-Selective T4/T5 Neurons in *Drosophila*

Tabea Schilling, Aicha H. Ali, Aljoscha Leonhardt, Alexander Borst and Jesús Pujol-Martí

Author contributions:

Conceptualization: **T.S.**, J.P.-M.; Methodology: **T.S.**, A.L., J.P.-M.; Software: A.L.; Investigation: **T.S.**, A.H.A., J.P.-M.; Writing - original draft: J.P.-M.; Writing - review and editing: **T.S.**, A.H.A., A.L., A.B., J.P.-M.; Visualization: **T.S.**; Supervision: A.B., J.P.-M.; Project administration: A.B.; Funding acquisition: A.B.

Tabea Schilling

Alexander Borst

RESEARCH ARTICLE

Transcriptional control of morphological properties of direction-selective T4/T5 neurons in *Drosophila*

Tabea Schilling, Aicha H. Ali, Aljoscha Leonhardt, Alexander Borst and Jesús Pujol-Martí*

ABSTRACT

In the *Drosophila* visual system, T4/T5 neurons represent the first stage of computation of the direction of visual motion. T4 and T5 neurons exist in four subtypes, each responding to motion in one of the four cardinal directions and projecting axons into one of the four lobula plate layers. However, all T4/T5 neurons share properties essential for sensing motion. How T4/T5 neurons acquire their properties during development is poorly understood. We reveal that the transcription factors SoxN and Sox102F control the acquisition of properties common to all T4/T5 neuron subtypes, i.e. the layer specificity of dendrites and axons. Accordingly, adult flies are motion blind after disruption of SoxN or Sox102F in maturing T4/T5 neurons. We further find that the transcription factors Ato and Dac are redundantly required in T4/T5 neuron progenitors for SoxN and Sox102F expression in T4/T5 neurons, linking the transcriptional programmes specifying progenitor identity to those regulating the acquisition of morphological properties in neurons. Our work will help to link structure, function and development in a neuronal type performing a computation that is conserved across vertebrate and invertebrate visual systems.

KEY WORDS: Neural development, Layer specificity, Optic lobe, *Drosophila*, SoxN, Sox102F

INTRODUCTION

The formation of neural circuits comprising neurons with specific morphological and physiological properties is key for the proper function of the brain. The *Drosophila* optic lobe has emerged as a powerful model in which to study this process. It consists of four neuropils downstream of the retina: lamina, medulla, lobula and lobula plate, all made of repeating columns that process signals from specific points in space and are arranged in a retinotopic fashion. In addition, the medulla, lobula and lobula plate are subdivided into layers that process distinct visual features in parallel (Maisak et al., 2013; Strother et al., 2014). The four neuropils of the optic lobe contain more than 100 different neuronal types (Fischbach and Dittrich, 1989), some of which have been studied in great anatomical and functional detail. Prominent examples are T4 and T5 neurons, the local motion detectors in *Drosophila* (Maisak et al., 2013). Whereas T4 neurons have their dendrites in the medulla and receive input from neurons encoding brightness increments, T5

dendrites arborise in the lobula and receive input from neurons encoding brightness decrements (Joesch et al., 2010; Maisak et al., 2013; Shinomiya et al., 2014; Takemura et al., 2017). Apart from this difference, T4 and T5 neurons share many morphological and functional properties (Shinomiya et al., 2015). Remarkably, their dendrites extend across a similar number of columns, are confined to a specific layer of their target neuropil (Fig. 1A) (Fischbach and Dittrich, 1989), and use a common mechanism to compute local motion from the signals of columnar, non-direction-selective neurons (Haag et al., 2016, 2017). Interestingly, T4 and T5 neurons exist in four subtypes (a, b, c and d), each responding exclusively to motion in one of the four cardinal directions (front-to-back, back-to-front, upwards and downwards) (Maisak et al., 2013). Axons from T4 and T5 neurons of the same subtype terminate specifically in one of four lobula plate layers (Fig. 1A) (Fischbach and Dittrich, 1989; Maisak et al., 2013). There, they establish synapses with the dendrites of wide-field, direction-selective lobula plate tangential cells (Joesch et al., 2008; Mauss et al., 2014; Schnell et al., 2010), some of which are also restricted to a single lobula plate layer (Boergens et al., 2018; Scott et al., 2002). How T4/T5 neurons acquire these properties during development to establish a map of directional tuning is poorly understood.

T4/T5 neurons originate from a progenitor domain in the developing fly brain known as the inner proliferation centre (IPC) (Hofbauer and Campos-Ortega, 1990; Oliva et al., 2014). In a process that extends from late second instar larval stage to early pupal stage, neuroepithelial cells from the proximal IPC (pIPC) progressively become progenitors that migrate to a second zone, the distal IPC (dIPC), where they assume a neuroprogenitor (neuroblast in *Drosophila*) fate (Apitz and Salecker, 2015; Hofbauer and Campos-Ortega, 1990; Nassif et al., 2003; Ngo et al., 2017). Neuroblasts in the dIPC transit through two temporal stages. Early-stage dIPC neuroblasts express Dichaete (D) and Asense (Ase), and generate ganglion mother cells that eventually produce postmitotic C2, C3, T2, T2a and T3 neurons (also known as C/T neurons) (Apitz and Salecker, 2015). Late-stage dIPC neuroblasts express Tailless (Tll), Atonal (Ato) and Dachshund (Dac), and produce ganglion mother cells that are the precursors of postmitotic T4/T5 neurons (Fig. 1B,C) (Apitz and Salecker, 2015; Mora et al., 2018; Oliva et al., 2014; Pinto-Teixeira et al., 2018). Therefore, temporal patterning of dIPC neuroblasts contributes to the specification of C/T versus T4/T5 neuron fate. Two recent studies have uncovered the mechanisms specifying T4 versus T5 identity and the identity of the four T4/T5 neuron subtypes (Apitz and Salecker, 2018; Pinto-Teixeira et al., 2018). These mechanisms involve spatial patterning in the pIPC neuroepithelium and Notch-dependent binary fate choices during the divisions of the neuroblast and ganglion mother cell precursors of T4/T5 neurons. In contrast to our current understanding regarding the specification of T4/T5 neuron progenitor identity, very little is known about how this translates into the acquisition of structural and functional properties in postmitotic T4/T5 neurons.

Department of 'Circuits – Computation – Models', Max Planck Institute of Neurobiology, 82152 Martinsried, Germany.

*Author for correspondence (pujolmarti@neuro.mpg.de)

 J.P.-M., 0000-0001-9500-7106

This is an Open Access article distributed under the terms of the Creative Commons Attribution License (<http://creativecommons.org/licenses/by/4.0/>), which permits unrestricted use, distribution and reproduction in any medium provided that the original work is properly attributed.

Received 9 July 2018; Accepted 7 January 2019

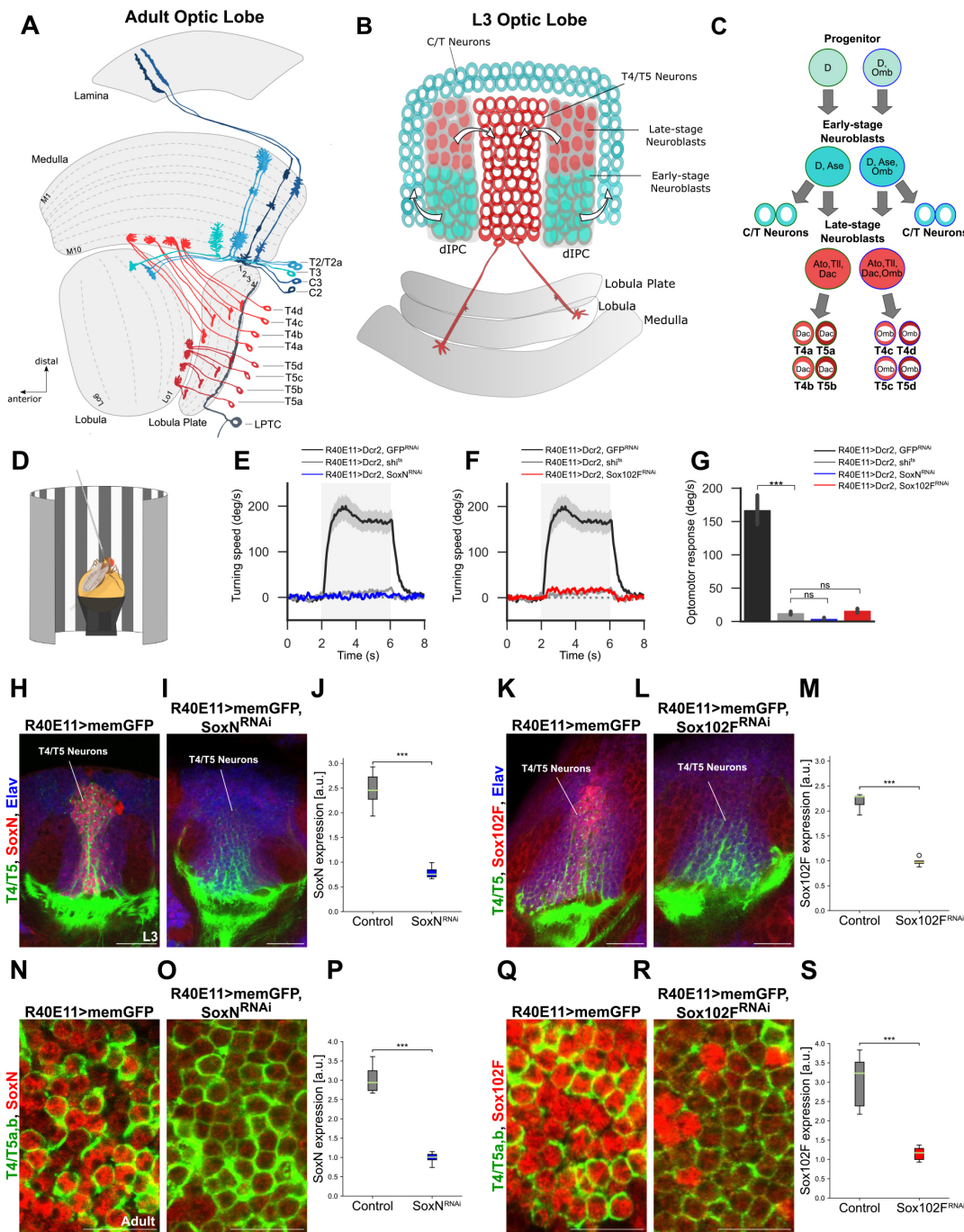


Fig. 1. SoxN or Sox102F knockdown in T4/T5 neurons impairs the optomotor response. (A) Schematic of adult optic lobe (dorsal view) highlighting T4/T5 neuron subtypes (a,b,c,d). C/T neurons (T2, T2a, T3, C2 and C3) and a lobula plate tangential cell (LPTC) with dendrites in lobula plate layer 4 receiving input from T4/T5_d axons are also shown. (B) Schematic of L3 larval optic lobe highlighting early- and late-stage dI^{PC} neuroblasts, and their offspring C/T and T4/T5 neurons. (C) Summary of transcription factors expressed in early- and late-stage dI^{PC} neuroblasts. (D) Set-up used for measuring the optomotor response of adult flies. (E,F) Average turning speeds in response to rotation of a grating pattern (grey shaded areas) of flies expressing GFP-RNAi (negative control), sh^{hs} (positive control, T4/T5 block), SoxN-RNAi or Sox102F-RNAi in T4/T5 neurons (n=10 flies per group). (G) Average optomotor responses of flies expressing GFP-RNAi, sh^{hs}, SoxN-RNAi or Sox102F-RNAi in T4/T5 neurons (n=10 flies per group). (H-S) SoxN and Sox102F expression in late L3 larval and adult optic lobes with wild-type T4/T5 neurons, and with T4/T5 neurons expressing SoxN-RNAi or Sox102F-RNAi. T4/T5 neurons were labelled with membrane-targeted GFP (memGFP). Neuronal somata in H-L were marked with anti-Elav. Quantifications of SoxN and Sox102F levels in T4/T5 somata are shown in J,M,P,S (n=4-11 optic lobes per group; a.u., arbitrary units). ns, not significant (P>0.05); ***P<0.001. Scale bars: 20 μ m (H,I,K,L); 10 μ m (N,O,Q,R).

Each newborn T4 and T5 neuron must initiate gene expression programmes to terminally differentiate, i.e. to express a unique combination of effector genes defining its identity and function (Hobert, 2011). How are these effector genes selected during development? One possibility is that transcription factors expressed in T4/T5 neuron progenitors are inherited through successive cell divisions to regulate the acquisition of terminal characters in postmitotic T4/T5 neurons. This is the case for Optomotor-blind (Omb; also known as Bifid), which is expressed in dIIPC neuroblasts and ganglion mother cells producing T4/T5_{c,d} neurons as a result of dIIPC neuroepithelium spatial patterning. Omb is further maintained in maturing T4/T5_{c,d} neurons to endow them with subtype-specific terminal characters (Fig. 1C) (Apitz and Salecker, 2018). As a complementary mechanism, transcription factors transiently expressed in T4/T5 neuron progenitors might start a transcriptional cascade to control the acquisition of terminal properties in postmitotic T4/T5 neurons. Ato is transiently expressed in late-stage dIIPC neuroblasts (Apitz and Salecker, 2015; Mora et al., 2018; Oliva et al., 2014), where it is required together with Dac for the generation of offspring neurons with T4/T5 neuron identity (Apitz and Salecker, 2018). The transcriptional programmes downstream of Ato/Dac conferring T4/T5 neurons with their properties have remained elusive so far.

Here, we perform an RNA interference (RNAi) screen to identify novel transcription factors affecting the acquisition of terminal characters in postmitotic T4/T5 neurons. We use the optomotor response of adult flies as a readout of T4/T5 neuron function and, thus, of proper terminal differentiation. T4/T5 neuron-specific silencing of *SoxN* or *Sox102F*, two members of the Sox family of transcription factors, abolishes the optomotor response in flies, indicative of aberrant T4/T5 neuron maturation. Notably, both transcription factors regulate the acquisition of dendritic and axonal innervation patterns common to all T4/T5 neuron subtypes. We further show that *SoxN* and *Sox102F* regulate the expression of the cell-surface molecule Connectin in all T4/T5 neuron subtypes, although only T4/T5_{c,d} neurons express high Connectin levels in wild-type flies. Finally, we demonstrate that *ato* and *dac* are redundantly required in late-stage dIIPC neuroblasts to control *SoxN* and *Sox102F* expression in offspring T4/T5 neurons, providing a link between transcription factors previously shown to specify T4/T5 neuron progenitor identity and novel, downstream transcription factors regulating postmitotically morphological properties common to all T4/T5 neurons.

RESULTS

Silencing *SoxN* or *Sox102F* in T4/T5 neurons impairs the optomotor response

To find molecular players involved in the terminal differentiation of T4/T5 neurons, we pursued a candidate gene approach focusing on transcription factors revealed to be highly expressed in T4/T5 neurons by a transcriptome analysis (Pankova and Borst, 2016). We performed specific knockdown of these transcription factors in T4/T5 neurons by combining UAS-RNAi effector lines (Dietzl et al., 2007; Perkins et al., 2015) with the *R40E11-Gal4* driver line. *R40E11-Gal4* drives expression in maturing T4/T5 neurons of all subtypes at late third instar (L3) larval stage, and in mature T4/T5_{a,b} neurons at adult stage (Fig. S1A). The optomotor response consists of turning in the direction of a rotating full-field grating and relies on T4/T5 neuron function (Bahl et al., 2013; Maisak et al., 2013). We reasoned that the optomotor response would be affected upon depletion of transcription factors controlling neuronal properties essential for T4/T5 neuron function.

We found that flies expressing either *SoxN-RNAi* or *Sox102F-RNAi* in T4/T5 neurons lacked an optomotor response, similar to flies with blocked synaptic transmission in T4/T5 neurons (Fig. 1D-G) (Bahl et al., 2013; Maisak et al., 2013). Because RNAi might cause off-target effects (Kaya-Copur and Schnorrer, 2016), we confirmed these results by using additional UAS-RNAi transgenes targeting other regions of *SoxN* and *Sox102F* (Fig. S2A-C). Next, we expressed membrane-targeted GFP in T4/T5 neurons using the *R40E11-Gal4* line and performed immunohistochemistry with antibodies recognising *SoxN* and *Sox102F* to confirm that both transcription factors were expressed in T4/T5 neurons (Fig. 1H,K). We found strongly reduced levels of *SoxN* and *Sox102F* in T4/T5 neurons upon expression of UAS-RNAi transgenes against them, both at late L3 larval and adult stages (Fig. 1H-S, Fig. S2D-G). Together, these results show that sustained knockdown of *SoxN* or *Sox102F* in postmitotic T4/T5 neurons severely impairs the optomotor response.

SoxN and Sox102F are expressed in all T4/T5 neuron subtypes, but not in their progenitors or in C/T neurons

To assess further the role of *SoxN* and *Sox102F* during T4/T5 neuron development, we examined their spatial and temporal patterns of expression in more detail. The *SS00324-splitGal4* line labels specifically mature T4/T5 neurons of the four subtypes in the adult (Schilling and Borst, 2015) and all these neurons expressed *SoxN* and *Sox102F* (Fig. 2A,B). *SoxN* and *Sox102F* were not detected in the region occupied by C/T somata, which were identified with the *SS00779-splitGal4* line (Fig. 2C,D) (Tuthill et al., 2013). Next, we examined the dIIPC in late L3 larvae, when it still contains *Dac⁺* neuroblasts and *Dac⁺* ganglion mother cells producing T4/T5 neurons (Apitz and Salecker, 2015), and found that T4/T5 neuron progenitors lacked *SoxN* and *Sox102F* (Fig. 2E, F). In late L3 larvae, all younger, maturing T4/T5 neurons express *Dac* whereas only older, maturing T4/T5_{a,b} neurons express *Dac* (Apitz and Salecker, 2018). Both *Dac⁺* T4/T5_{a,b} and *Dac⁻* T4/T5_{c,d} neurons expressed *SoxN* and *Sox102F* (Fig. 2E,F). *SoxN* and *Sox102F* were not detected at late L3 larval stage in C/T neurons, which were identified by both the location of their somata and the expression of Abnormal chemosensory jump 6 (Acj6) (Fig. 2G,H) (Apitz and Salecker, 2015). Therefore, *SoxN* and *Sox102F* are expressed in immature and mature T4/T5 neurons of all subtypes, yet they are absent in T4/T5 neuron progenitors and developmentally related C/T neurons.

SoxN-mediated transcriptional activation is required for Sox102F expression in T4/T5 neurons

In late L3 larvae, younger T4/T5 somata form columns closest to the dIIPC whereas older T4/T5 somata are displaced centrally (Apitz and Salecker, 2015). We observed *Sox102F* and *SoxN* expression in the most central columns of T4/T5 somata, whereas the T4/T5 somata closer to the dIIPC showed only *SoxN* expression (Fig. 2E-H). This indicates that *SoxN* is expressed at an earlier time point of T4/T5 neuron maturation than *Sox102F*, and that *SoxN* might regulate *Sox102F* expression. Indeed, *Sox102F* expression was severely reduced in T4/T5 neurons upon *SoxN* knockdown with the *R40E11-Gal4* line (Fig. 3A-C, Fig. S3A-C), and in *SoxN* mutant T4/T5 neurons generated by mosaic analysis with a repressible cell marker (MARCM) (Fig. 3G-J). However, overexpression of a wild-type version, an obligatory activator version, or an obligatory repressor version of *SoxN* (Bahrampour et al., 2017) did not increase *Sox102F* levels in T4/T5 somata (Fig. 3K-N). In fact, T4/T5 somata lacked *Sox102F* when expressing the obligatory repressor version

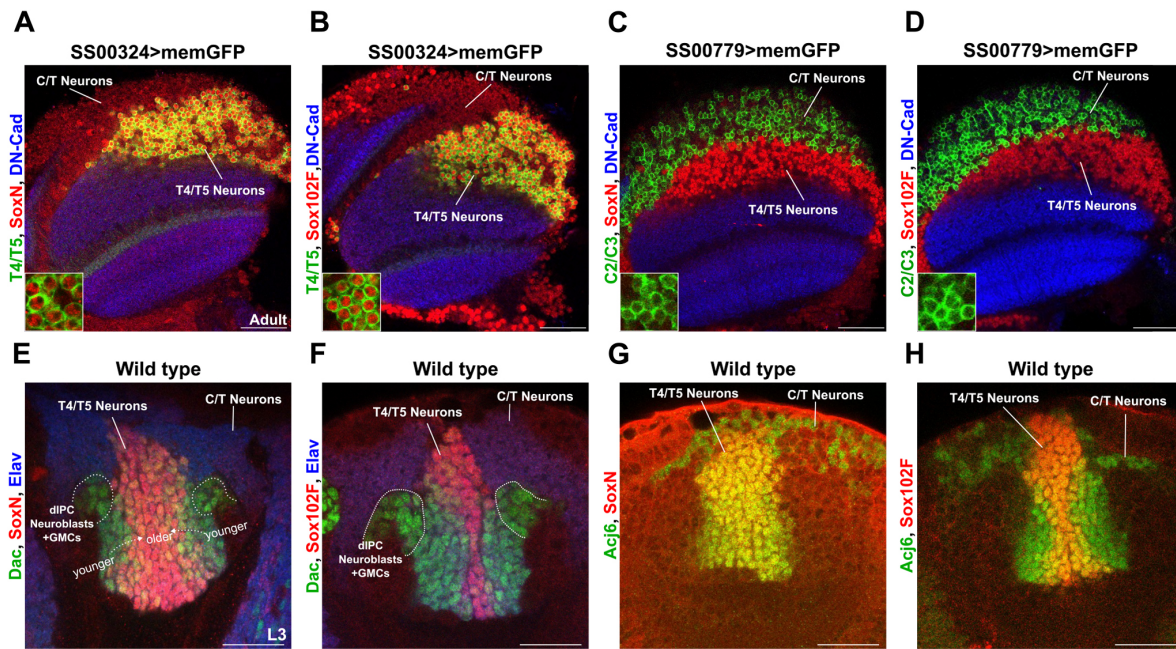


Fig. 2. SoxN and Sox102F are expressed in all T4/T5 neuron subtypes, but not in their progenitors or in C/T neurons. (A-D) SoxN and Sox102F expression in adult optic lobes with T4/T5 or C2/C3 neurons labelled with memGFP. Neuropils were labelled with anti-DN-Cadherin (DN-Cad). Insets show zoomed views of T4/T5 (A,B) or C2/C3 (C,D) somata. (E,F) SoxN and Sox102F expression in late L3 larval optic lobes after immunostaining against Elav and Dac. Late-stage diPc neuroblasts and ganglion mother cells (GMCs) are Dac⁺/Elav⁻. All young T4/T5 neurons (closest to diPc) are Dac⁺/Elav⁺. Older T4/T5_{a,b} neurons are Dac⁺/Elav⁺ whereas older T4/T5_{c,d} neurons are Dac⁻/Elav⁺. (G,H) SoxN and Sox102F expression in late L3 larval optic lobes after immunostaining against Acj6, which labelled somata located in the region occupied by C/T neurons, and T4/T5 somata. Scale bars: 40 µm (A-D); 20 µm (E-H).

of SoxN (Fig. 3N). Altogether, these results indicate that SoxN-mediated transcriptional activation is required for Sox102F expression in T4/T5 neurons. In contrast, *Sox102F* is dispensable for SoxN expression in T4/T5 neurons, as SoxN levels were unchanged after silencing *Sox102F* in T4/T5 neurons with either RNAi transgenes or the microRNA *mir-263a* (also known as *b7*) (Fig. 3D-F, Fig. S3D-J), which is predicted to target *Sox102F* (according to TargetScanFly, Release 7.2, October 2018) and reduces Sox102F levels (Fig. S3H). In agreement with this, SoxN levels were normal in *Sox102F* mutant flies (Fig. 3O-T), generated by combining the *Sox102F^{M01054}* hypomorphic allele with the *Df(4)O2* deficiency chromosome lacking the *Sox102F* locus (Contreras et al., 2018).

SoxN and Sox102F regulate dendritic and axonal development autonomously in T4/T5 neurons, and dendritic development non-autonomously in lobula plate tangential cells

Our previous results suggest that *SoxN* and *Sox102F* are part of the terminal differentiation programmes responsible for defining T4/T5 neuron function. One possibility is that *SoxN* and *Sox102F* control morphological properties of T4/T5 neurons. We examined the shape of membrane-targeted GFP-labelled T4/T5 neurons in adult flies in which *SoxN* or *Sox102F* were silenced from late L3 larval stage onwards with either the *R39H12-Gal4* or the *T4/T5-splitGal4* driver line (Fig. S1B,C). Wild-type T4 and T5 dendrites arborised only in medulla layer M10 and in lobula layer L01, respectively, and wild-type T4/T5 axons formed four layers in the lobula plate (Fig. 4A,A', Fig. S4A). In flies expressing *SoxN-RNAi* in all T4/T5 neurons, T4 and T5 dendrites extended into extra medulla and

lobula layers, and T4/T5 axons did not form four layers but accumulated predominantly in the most anterior half of the lobula plate (Fig. 4B,B', Fig. S4B). Very similar defects were observed in *SoxN* mutant T4/T5 neurons (Fig. 4D,E), confirming that these phenotypes are caused by a specific disruption of *SoxN* function. Moreover, T4/T5 neurons expressing an obligatory repressor version of *SoxN* showed dendritic overgrowth and axons failing to form layers in the lobula plate (Fig. S4G). Upon *Sox102F-RNAi* expression in all T4/T5 neurons, we also observed overgrowth of T4/T5 dendrites and a loss of the layered structure in the lobula plate with T4/T5 axons forming clusters (Fig. 4C,C', Fig. S4C). The specificity of this phenotype was confirmed by examining T4/T5 neurons in *Sox102F* mutants (Fig. 4F,G) and upon expression of *mir-263a* (Fig. S4D). T4/T5 neurons overexpressing *Sox102F* also showed dendritic and axonal defects (Fig. S4H-J).

Moreover, lobula plate volume was reduced when *SoxN* or *Sox102F* were silenced in all T4/T5 neurons (Fig. S5A-D), further supporting the conclusion that T4/T5 axons were defective and suggesting that other neurons innervating the lobula plate might be affected. To test this, we labelled lobula plate tangential cells innervating lobula plate layers 1 and 4 with the *VT23749-LexA* line (Mauss et al., 2015) in control flies and in flies expressing *SoxN-RNAi* or *Sox102F-RNAi* in all T4/T5 neurons. When RNAi⁺ T4/T5 axons failed to form layers, dendrites from RNAi⁻ lobula plate tangential cells did not form layers in the lobula plate either (Fig. S5E-G). These results show that *SoxN* and *Sox102F* regulate dendritic and axonal morphology autonomously in T4/T5 neurons, and dendritic morphology non-autonomously in lobula plate tangential cells.

To determine whether the observed phenotypes were caused by developmental defects, we examined wild-type T4/T5 neurons and

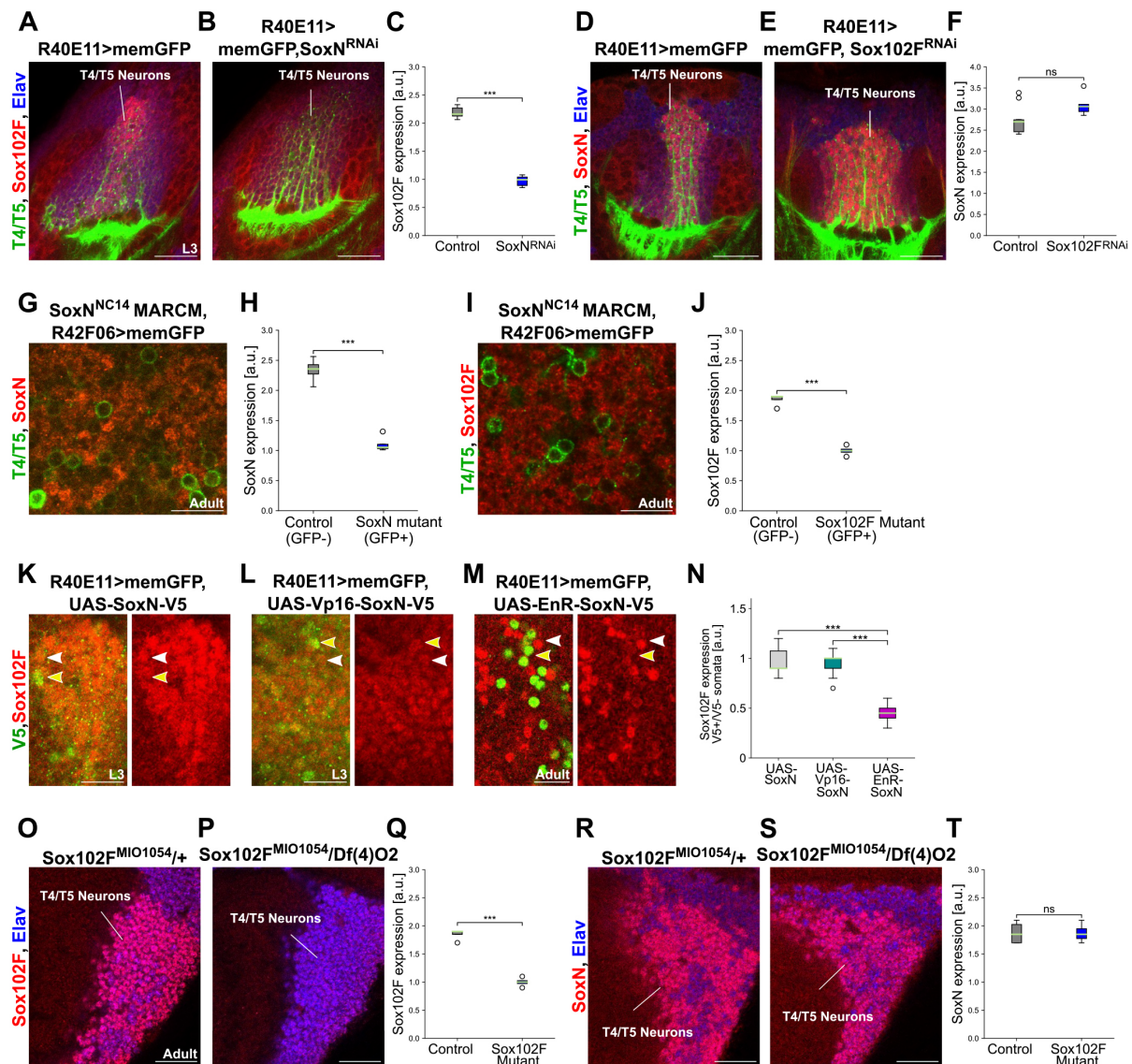


Fig. 3. SoxN-mediated transcriptional activation is required for Sox102F expression in T4/T5 neurons. (A-C) Sox102F expression in late L3 larval optic lobes with wild-type T4/T5 neurons, and with T4/T5 neurons expressing SoxN-RNAi. Quantification is shown in C (control: n=6; SoxN-RNAi: n=7 optic lobes). (D-F) SoxN expression in late L3 larval optic lobes with wild-type T4/T5 neurons, and with T4/T5 neurons expressing Sox102F-RNAi. Quantification is shown in F (control: n=11; Sox102F-RNAi: n=5 optic lobes). (G-J) SoxN and Sox102F expression in adult *SoxN^{NC14}* heterozygous (GFP⁻) and homozygous (GFP⁺) mutant T4/T5 somata after MARCM. Quantifications are shown in H and J [control (GFP⁻): n=6; SoxN mutant (GFP⁺): n=7 optic lobes]. (K-N) Sox102F expression in T4/T5 neurons upon overexpression of SoxN (wild type), Vp16-SoxN (obligatory activator) or EnR-SoxN (obligatory repressor). The three SoxN versions were epitope-tagged with V5. In each panel, the yellow arrowhead marks a T4 or T5 soma with high V5 levels, and the white arrowhead marks a neighbouring T4 or T5 soma without V5 expression. Quantification is shown in N (n=10 pairs of somata per group). (O-T) Sox102F and SoxN expression in adult T4/T5 neurons from controls (*Sox102F^{MIO1054/+}*) and *Sox102F* mutants (*Sox102F^{MIO1054/Df(4)O2}*). Quantifications are shown in Q and T (n=4 optic lobes per group). ns, not significant (P>0.05); ***P<0.001. Scale bars: 20 μ m (A,B,D,E,O,P,R,S); 10 μ m (G,I,K-M).

T4/T5 neurons expressing *SoxN-RNAi* or *Sox102F-RNAi* at late L3 larval stage, and at pupal stages 24 h and 48 h after puparium formation (APF). At late L3 larval stage and at 24 h APF, RNAi⁺ T4/T5 dendrites were indistinguishable from wild-type T4/T5 dendrites (Fig. S6A-F). At 48 h APF, however, we found dendritic overgrowth in RNAi⁺ T4/T5 neurons compared with wild-type T4/T5 neurons. Wild-type T4/T5 axons formed layers in the lobula plate at 48 h APF but not at the earlier stages examined. In contrast,

RNAi⁺ T4/T5 axons failed to form distinct layers in the lobula plate at 48 h APF (Fig. S6G-I). Finally, we excluded a transformation of T4/T5 neurons into developmentally related neurons upon *SoxN* and *Sox102F* disruption by examining markers of T4/T5 and C/T neurons. LIM homeobox 1 (Lim1) expression in T4/T5 neurons (Suzuki et al., 2016) was unchanged after *SoxN* and *Sox102F* knockdown, and C/T neuron markers Twin of Eyeless (Toy) (Apitz and Salecker, 2015) and Apterous (Ap) were absent in T4/T5

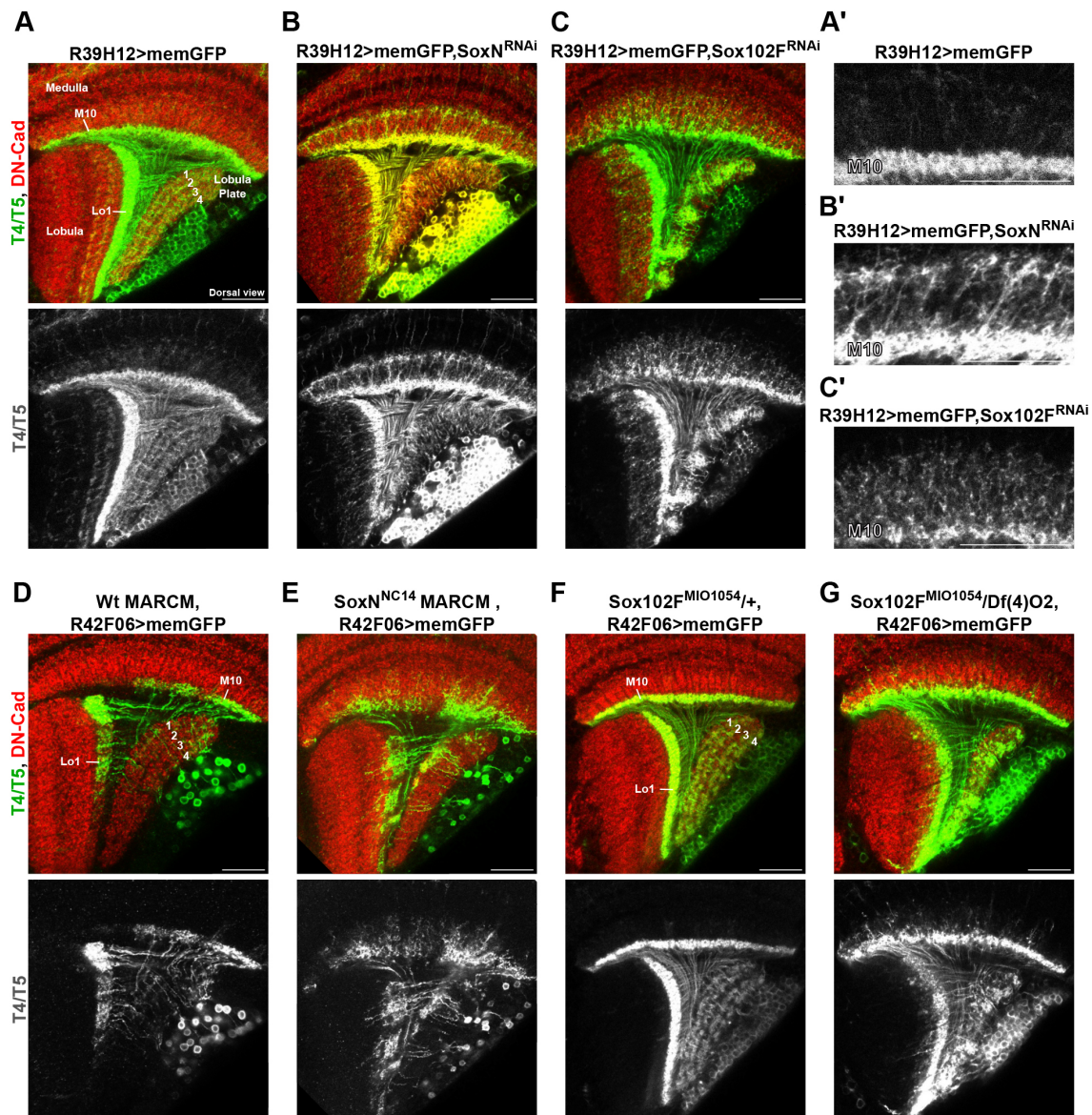


Fig. 4. *SoxN* and *Sox102F* control dendritic and axonal morphology in T4/T5 neurons. (A-C') Dorsal views of adult optic lobes with wild-type T4/T5 neurons, and with T4/T5 neurons expressing *SoxN-RNAi* or *Sox102F-RNAi*. A'-C' show detailed views of T4 dendrites from the conditions in A-C. Anterior is to the left. (D,E) Adult optic lobes with wild-type T4/T5 neurons, and *SoxN^{NC14}* homozygous mutant T4/T5 neurons generated by MARCM and labelled with the *R42F06-Gal4* line. (F,G) Adult optic lobes with T4/T5 neurons labelled with the *R42F06-Gal4* line in controls (*Sox102F^{MI054/+}*) and in *Sox102F* mutants [*Sox102F^{MI054/Df(4)O2}*]. Scale bars: 20 μ m.

neurons upon *SoxN-RNAi* and *Sox102F-RNAi* expression (Fig. S7A-L). From these results, we conclude that *SoxN* and *Sox102F* are required in maturing T4/T5 neurons for dendritic and axonal patterning between 24 and 48 h APF stages.

***SoxN* and *Sox102F* mediate layer-specific innervation of T4/T5 dendrites and axons, and neuropil-specific innervation of T4/T5 axons**

To determine unambiguously which aspects of dendritic and axonal patterning are regulated by *SoxN* and *Sox102F*, we analysed individual neurons labelled stochastically by using the Flp-out technique (Nern et al., 2011) after silencing *SoxN* or *Sox102F* in all

T4/T5 neurons with the *R39H12-Gal4* line. We defined the neuropil layers innervated by single-labelled T4 and T5 dendrites by staining optic lobes with DN-cadherin (Cadherin-N) and Connectin (Gao et al., 2008; Ngo et al., 2017). In control flies, none of the single-labelled T4 and T5 neurons had dendrites in layers other than medulla layer M10 (Fig. 5A,G) and lobula layer Lo1 (Fig. 5D,H), respectively. After *SoxN* or *Sox102F* silencing in all T4/T5 neurons, in contrast, T4 and T5 dendrites spanned over extra layers of neuropil. T4 dendrites often reached medulla layer M7 in the case of *SoxN* silencing and medulla layer M8 in the case of *Sox102F* silencing, and T5 dendrites often reached lobula layer Lo4 when *SoxN* or *Sox102F* were silenced (Fig. 5A-H). We also found that, in contrast to wild-

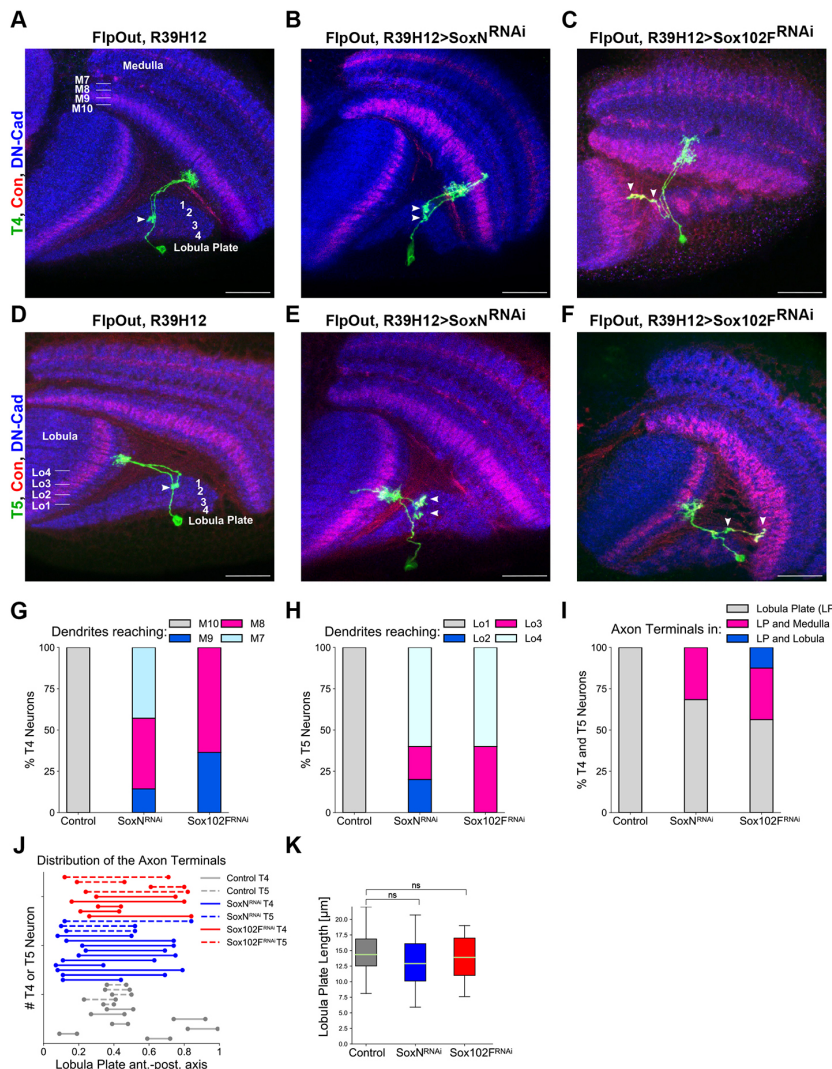


Fig. 5. SoxN and Sox102F mediate layer-specific innervation of T4/T5 dendrites and axons, and neuropil-specific innervation of T4/T5 axons. (A-F) Adult optic lobes with single-labelled T4 and T5 neurons in control flies, and in flies expressing *SoxN-RNAi* or *Sox102F-RNAi* in all T4/T5 neurons. Neuropil layers were identified after immunostaining against DN-Cad and Connectin. Arrowheads mark the presence of axonal boutons. (G) Percentages of T4 dendrites reaching the medulla layers M10, M9, M8 or M7 in control flies, and in flies expressing *SoxN-RNAi* or *Sox102F-RNAi* in all T4/T5 neurons (control: $n=9$; *SoxN-RNAi*: $n=14$; *Sox102F-RNAi*: $n=11$ neurons). (H) Percentages of T5 dendrites reaching the lobula layers Lo1, Lo2, Lo3 or Lo4 in control flies, and in flies expressing *SoxN-RNAi* or *Sox102F-RNAi* in all T4/T5 neurons (control: $n=7$; *SoxN-RNAi*: $n=5$; *Sox102F-RNAi*: $n=5$ neurons). (I) Percentages of T4 and T5 axons innervating only the lobula plate, co-innervating the lobula plate and the medulla, or co-innervating the lobula plate and the lobula, in control flies and in flies expressing *SoxN-RNAi* or *Sox102F-RNAi* in all T4/T5 neurons (control: $n=12$; *SoxN-RNAi*: $n=19$; *Sox102F-RNAi*: $n=16$ neurons). (J) Extension of lobula plate (normalised) along the anteroposterior axis occupied by T4 and T5 axons in control flies, and in flies expressing *SoxN-RNAi* or *Sox102F-RNAi* in all T4/T5 neurons. 0 and 1 represent the most anterior and the most posterior edges of the lobula plate, respectively. (K) Average lobula plate lengths (absolute values) along the anteroposterior axis at the positions occupied by the analysed axons in J (control: $n=12$, *SoxN-RNAi*: $n=13$, *Sox102F-RNAi*: $n=9$ positions). ns, not significant ($P>0.05$). Scale bars: 20 μ m.

type T4 and T5 axons, which always innervated exclusively the lobula plate, one-third of T4 and T5 axons co-innervated the lobula plate and the medulla upon *SoxN* or *Sox102F* silencing in all T4/T5 neurons (Fig. 5F,I). On rare occasions, T4 axons co-innervated the lobula plate and the lobula upon *Sox102F* silencing (Fig. 5C,I). Finally, we analysed in more detail those T4 and T5 axons that specifically innervated the lobula plate upon knockdown of *SoxN* or *Sox102F* and compared them with wild-type T4 and T5 axons. Wild-type T4 and T5 axons occupied $13\pm4\%$ ($n=12$ axons) of the lobula plate along the anteroposterior axis, reflecting layer-specific innervation. Upon *SoxN* or *Sox102F* silencing, T4 and T5 axons occupied $50\pm13\%$ ($n=13$ axons) or $41\pm19\%$ ($n=9$ axons) of the lobula plate along the anteroposterior axis, respectively (Fig. 5J). As the length of the lobula plate along the anteroposterior axis was unchanged at the positions occupied by the analysed wild-type and RNAi⁺ T4/T5 axons (Fig. 5K), we concluded that the axons of T4/T5 neurons expressing *SoxN-RNAi* or *Sox102F-RNAi* lack the layer-specific innervation characteristic of wild-type T4/T5 neurons. These results demonstrate a requirement of *SoxN* and *Sox102F* for the development of the layer-specific innervation of

T4/T5 dendrites and axons, and the neuropil-specific innervation of T4/T5 axons.

SoxN and Sox102F control the layer specificity of dendrites and axons autonomously in different T4/T5 neuron subtypes

Next, we investigated whether *SoxN* and *Sox102F* control neuronal morphology in every T4/T5 neuron subtype in a similar and autonomous manner. To this end, we first silenced *SoxN* or *Sox102F* in specific T4/T5 neuron subsets with the *VT37588-Gal4* (Maisak et al., 2013), *R11F07-Gal4* and *R42H07-Gal4* (Maisak et al., 2013) lines. These lines labelled, respectively, T4_{a-d}, T4/T5_{a,b} and T5_{c,d} neurons in the adult, and drive gene expression in T4/T5 neuron subsets already at late L3 larval or early pupal stages (Fig. S1D-F). Knockdown of *SoxN* or *Sox102F* in T4_{a-d} and T5_{c,d} neurons caused severe dendritic and axonal defects (Fig. 6A-C,G-I), which resembled the defects observed upon their knockdown using lines driving expression in all T4/T5 neurons (Fig. 4A-C). Defects in layer specificity of dendrites and axons were also observed upon *SoxN* or *Sox102F* silencing in T4/T5_{a,b} neurons (Fig. 6D-F), although these defects were less pronounced than those observed upon silencing them in T4_{a-d} and T5_{c,d} neurons.

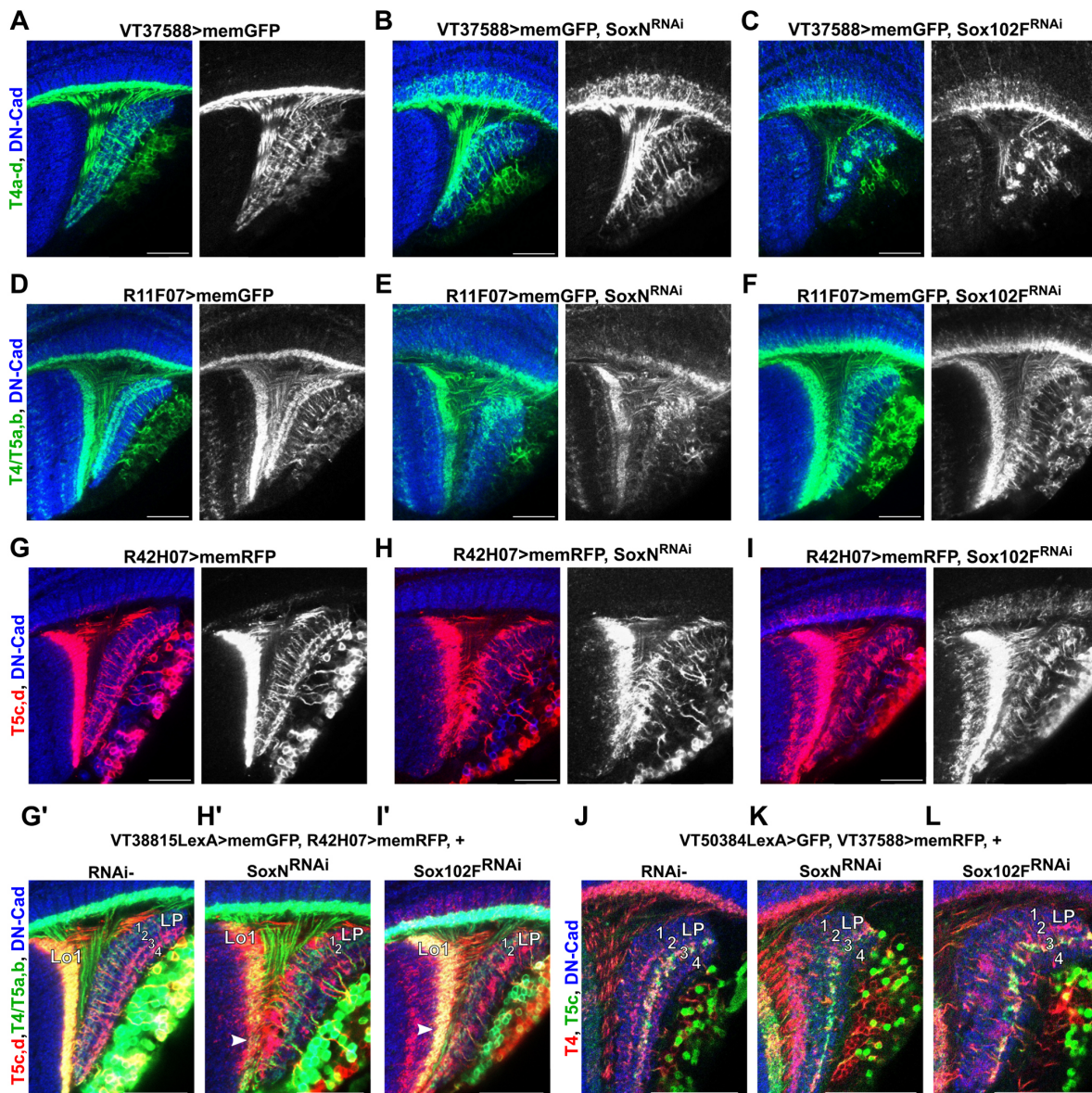


Fig. 6. SoxN and Sox102F regulate the layer specificity of dendrites and axons autonomously in different T4/T5 neuron subtypes. (A-C) Adult optic lobes with wild-type T4_{a-d} neurons, and with T4_{a-d} neurons expressing *SoxN-RNAi* or *Sox102F-RNAi*. (D-F) Adult optic lobes with wild-type T4/T5_{a,b} neurons, and with T4/T5_{a,b} neurons expressing *SoxN-RNAi* or *Sox102F-RNAi*. (G-I) Adult optic lobes with wild-type T5_{c,d} neurons, and with T5_{c,d} neurons expressing *SoxN-RNAi* or *Sox102F-RNAi*. RNAi⁻ T4/T5_{a,b} neurons are shown in G'-H'. Arrowheads indicate T5_{a,b} dendrites restricted to lobula layer Lo1 in the presence of defective, RNAi⁺ T5_{c,d} dendrites. LP, lobula plate. (J-L) Detailed views of the lobula plate showing T5_c axons in the presence of wild-type T4 axons, and in the presence of T4 axons expressing *SoxN-RNAi* or *Sox102F-RNAi*. Scale bars: 20 μ m.

Next, we examined the morphology of RNAi- T4/T5 neurons in the presence of RNAi⁺, defective T4/T5 neurons from other subtypes. The dendrites of RNAi- T5_{a,b} neurons, labelled with the *VT38815-LexA* line, did not reach other layers than lobula layer L01 in the presence of RNAi⁺ T5_{c,d} dendrites with overgrowth. Moreover, the axons of RNAi- T5_{a,b} neurons were undistinguishable from control T5_{a,b} axons when RNAi⁺, defective T5_{c,d} axons were present (Fig. 6G-I'). In line with this, RNAi- T5_c axons, marked with the *VT50384-LexA* line (Haag et al., 2016), terminated in lobula plate layer 3 in spite of the presence of RNAi⁺, defective T4 axons

(Fig. 6J-L). Altogether, these results indicate that *SoxN* and *Sox102F* control the layer specificity of dendrites and axons autonomously in each T4/T5 neuron subtype.

SoxN and Sox102F are required for the regulation of Connectin levels in T4/T5 neurons

We noticed an increase in Connectin levels in the neuropil layers occupied by T4/T5 dendrites upon *Sox102F* silencing in all T4/T5 neurons, and in *Sox102F* mutants (Fig. 7A-C,G,J-L). To determine whether this is caused by a non-cell-autonomous mechanism, such

as ectopic innervation of these layers by adjacent Connectin-expressing neurons, we co-expressed *Sox102F-RNAi* with a validated *Connectin-RNAi* (Fig. 7D,G) in all T4/T5 neurons. In this condition, Connectin levels in medulla layer M10 were comparable to those in controls (Fig. 7E,G), demonstrating that *Sox102F* is required cell-autonomously in T4/T5 neurons for repressing Connectin expression.

In wild-type flies, Connectin signal is higher in layers 3 and 4 than in layers 1 and 2 of the lobula plate (Fig. 7A) (Gao et al., 2008), suggesting a higher Connectin expression in T4/T5_{c,d} than in T4/T5_{a,b} neurons. A recent transcriptome study has indeed revealed that T5_{c,d} neurons express higher Connectin than T5_{a,b} neurons (Davis et al., 2018 preprint). T4/T5 neuron subtype-specific expression of other transcription factors controlling Connectin expression might influence the capacity of distinct T4/T5 neuron subtypes to upregulate Connectin upon *Sox102F* knockdown. This is not the case, however, as *Sox102F-RNAi* expression in T4/T5_{a,b}, T5_{c,d} or T4_{c,d} neurons also resulted in Connectin upregulation (Fig. S8A-I).

Because *Sox102F* expression in T4/T5 neurons requires *SoxN*, we expected *SoxN* and *Sox102F* loss of function to upregulate Connectin levels similarly. However, Connectin levels did not increase in T4/T5 neurons expressing *SoxN-RNAi* or in *SoxN* mutant T4/T5 neurons (Fig. 7F,G,M-O). We excluded that this is caused by a transformation of T4/T5_{c,d} (high Connectin) into T4/T5_{a,b} (low Connectin) neurons because the proportion of Dac^{+/Omb⁻ (T4/T5_{a,b}) and Dac^{-/Omb⁺ (T4/T5_{c,d}) neurons upon *SoxN* silencing was the same as in controls (Fig. S7M-O). Collectively, these observations are consistent with *SoxN* regulating Connectin expression in all T4/T5 neuron subtypes through two pathways with opposing effects. Firstly, *SoxN* is required for *Sox102F* expression, which in turn is necessary for repressing Connectin expression. Secondly, *SoxN* is required for Connectin expression in a *Sox102F*-independent manner. Finally, we attempted to support this model by performing overexpression experiments. However, *Sox102F* or *SoxN* overexpression was not sufficient to downregulate or upregulate, respectively, Connectin expression in T4/T5 neurons (Fig. S8J-O). This might be due to wild-type expression levels of proteins required for *SoxN* and *Sox102F* transcriptional activity in T4/T5 neurons (She and Yang, 2015).}}

ato and dac are redundantly required in late-stage dIPC neuroblasts for SoxN and Sox102F expression in offspring neurons

Loss of the transcription factor Ato in late-stage dIPC neuroblasts, which normally produce T4/T5 neurons, results in offspring neurons with fasciculation problems, dendritic overgrowth (Oliva et al., 2014) and a global downregulation of genes involved in neuronal differentiation (Mora et al., 2018). Loss of the transcription factor Dac in T4/T5 neuron progenitors results in offspring neurons with dendrites that overgrow into medulla layer M9 and more distal layers, and axons that lack neuropil-specific innervation (Apitz and Salecker, 2018). These defects resemble the anatomical phenotypes we reported upon silencing *SoxN* or *Sox102F* in T4/T5 neurons. Ato and/or Dac might start transcriptional programmes in late-stage dIPC neuroblasts that eventually control *SoxN* and *Sox102F* expression in postmitotic T4/T5 neurons. To test this, we analysed *SoxN* and *Sox102F* expression in T4/T5 neurons in *ato* mutants (Fig. 8A-D) (Jarman et al., 1994) and in flies expressing a validated *dac-RNAi* in the dIPC with the *R12G08-Gal4* line (Fig. 8E,F,H,I) (Apitz and Salecker, 2018). In both experiments, *SoxN* and *Sox102F* were detected in the region occupied by T4/T5 somata at prepupal stages, demonstrating that disrupting *ato* or *dac*

individually in late-stage dIPC neuroblasts does not abolish *SoxN* and *Sox102F* expression in offspring T4/T5 neurons.

ato and *dac* in late-stage dIPC neuroblasts might redundantly control *SoxN* and *Sox102F* expression in T4/T5 neurons, leading to one transcription factor compensating for the silencing of the other. In fact, only after simultaneous silencing of *ato* and *dac* in late-stage dIPC neuroblasts, do offspring neurons fail to acquire T4/T5 neuron morphologies, indicating a redundant role of *ato* and *dac* in the control of T4/T5 neuron identity (Apitz and Salecker, 2018). This model predicts that removing simultaneously *ato* and *dac* in late-stage dIPC neuroblasts should remove factors controlling the maturation of T4/T5 neurons, such as *SoxN* and *Sox102F*. We co-expressed validated *ato-RNAi* and *dac-RNAi* in the dIPC with the *R12G08-Gal4* line (Apitz and Salecker, 2018) and found that most of the neurons in the region normally occupied by T4/T5 somata at prepupal stages lacked *SoxN* and *Sox102F* expression (Fig. 8G,J). The remaining *SoxN⁺* and *Sox102F⁺* neurons might be due to incomplete RNAi knockdown. These results demonstrate that *ato* and *dac* are redundantly required in late-stage dIPC neuroblasts for *SoxN* and *Sox102F* expression in offspring neurons.

DISCUSSION

As neurons are generated during development, they acquire a rich and diverse repertoire of morphological and physiological properties in order to form functional neural circuits. T4/T5 neurons represent a very interesting model for understanding this process. All T4/T5 neurons share a set of terminal characteristics, such as dendrites with a stereotyped size and arborisation in single layers of neuropil, and axons terminating in one of the four layers of the lobula plate. These properties are essential for their function as local motion sensors and to communicate with downstream neurons. At the same time, four subtypes of T4/T5 neurons exist with differences in directional tuning and the layer of the lobula plate innervated by their axons, the latter defining the specific postsynaptic partners of each subtype. Here, we show that the acquisition of morphological properties common to all T4/T5 neuron subtypes is controlled by the postmitotic transcription factors *SoxN* and *Sox102F*. Moreover, the two transcription factors appear to play a permissive role in the emergence of subtype-specific properties in T4/T5 neurons. Therefore, *SoxN* and *Sox102F* represent two core components of the programmes controlling the maturation of postmitotic T4/T5 neurons and that act downstream of the identity programmes initiated by Ato and Dac in T4/T5 neuron progenitors (Apitz and Salecker, 2018). In conjunction with other recent studies (Apitz and Salecker, 2015, 2018; Mora et al., 2018; Pinto-Teixeira et al., 2018), our work provides a basis for understanding precisely how T4/T5 neurons acquire their properties during development.

Temporal and spatial transcription factors specify neuroblast identity in the developing *Drosophila* optic lobe (Apitz and Salecker, 2015, 2018; Erlik et al., 2017; Li et al., 2013; Suzuki et al., 2013). How do these transcription factors regulate the acquisition of properties defining identity and function in offspring neurons? Homothorax (Hth) is one of the temporal transcription factors expressed in medulla neuroblasts. Hth expression is maintained in the progeny of Hth⁺ neuroblasts, including Mi1 neurons, where it controls neuronal morphology in part by regulating Brain-specific homeobox (Bsh) and DN-cadherin expression (Hasegawa et al., 2013, 2011; Li et al., 2013; Suzuki et al., 2013). Other temporal transcription factors expressed in medulla neuroblasts, such as Klumpfuss (Klu), are not maintained in offspring neurons and are thought to control neuronal terminal

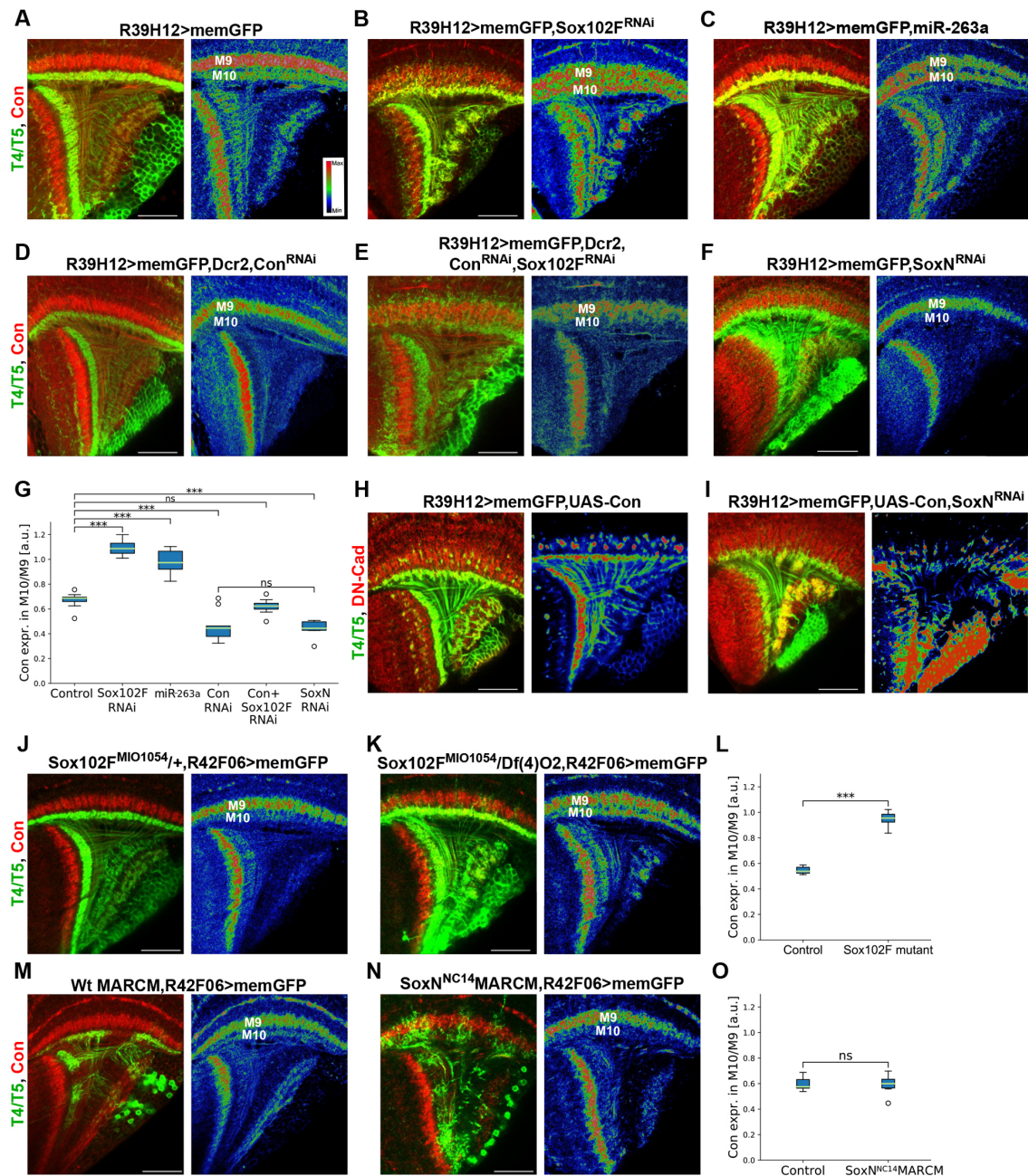


Fig. 7. SoxN and Sox102F are required for the regulation of Connectin levels in T4/T5 neurons. (A-G) Connectin expression in adult optic lobes with wild-type T4/T5 neurons, and with T4/T5 neurons expressing Sox102F-RNAi, miR-263a, Connectin-RNAi, Sox102F-RNAi and Connectin-RNAi, or SoxN-RNAi. The right panels show Connectin signals colour-coded for intensity. Ratios of Connectin signal in medulla layer M10 to Connectin signal in medulla layer M9 are shown in G ($n=8-11$ optic lobes per group). (H,I) Adult optic lobes with T4/T5 neurons overexpressing UAS-Connectin alone or with SoxN-RNAi. Overexpression of Connectin induces the formation of axon clusters. (J-L) Connectin expression in adult optic lobes with T4/T5 neurons labelled with the R42F06-Gal4 line in controls [Sox102F^{M1054/+}] and in Sox102F mutants [Sox102F^{M1054/Df(4)O2}]. Quantification is shown in L (control: $n=7$; Sox102F mutant: $n=9$ optic lobes). (M-O) Connectin expression in adult optic lobes with wild-type T4/T5 neurons, and SoxN^{NC14} homozygous mutant T4/T5 neurons generated by MARCM and labelled with the R42F06-Gal4 line. Quantification is shown in O (control: $n=7$; SoxN^{NC14} MARCM: $n=14$ optic lobes). In H-N, right-hand panels show Connectin signals colour-coded for intensity. ns, not significant ($P>0.05$); *** $P<0.001$. Scale bars: 20 μ m.

differentiation through an intermediate tier of transcription factors (Li et al., 2013; Suzuki et al., 2013). These two complementary mechanisms for conveying identity information from neuroblasts to

neurons also occur during T4/T5 neuron development. Omb is initially expressed in a subset of spatially patterned T4/T5 neuron progenitors and is maintained in their offspring T4/T5_{c,d} neurons,

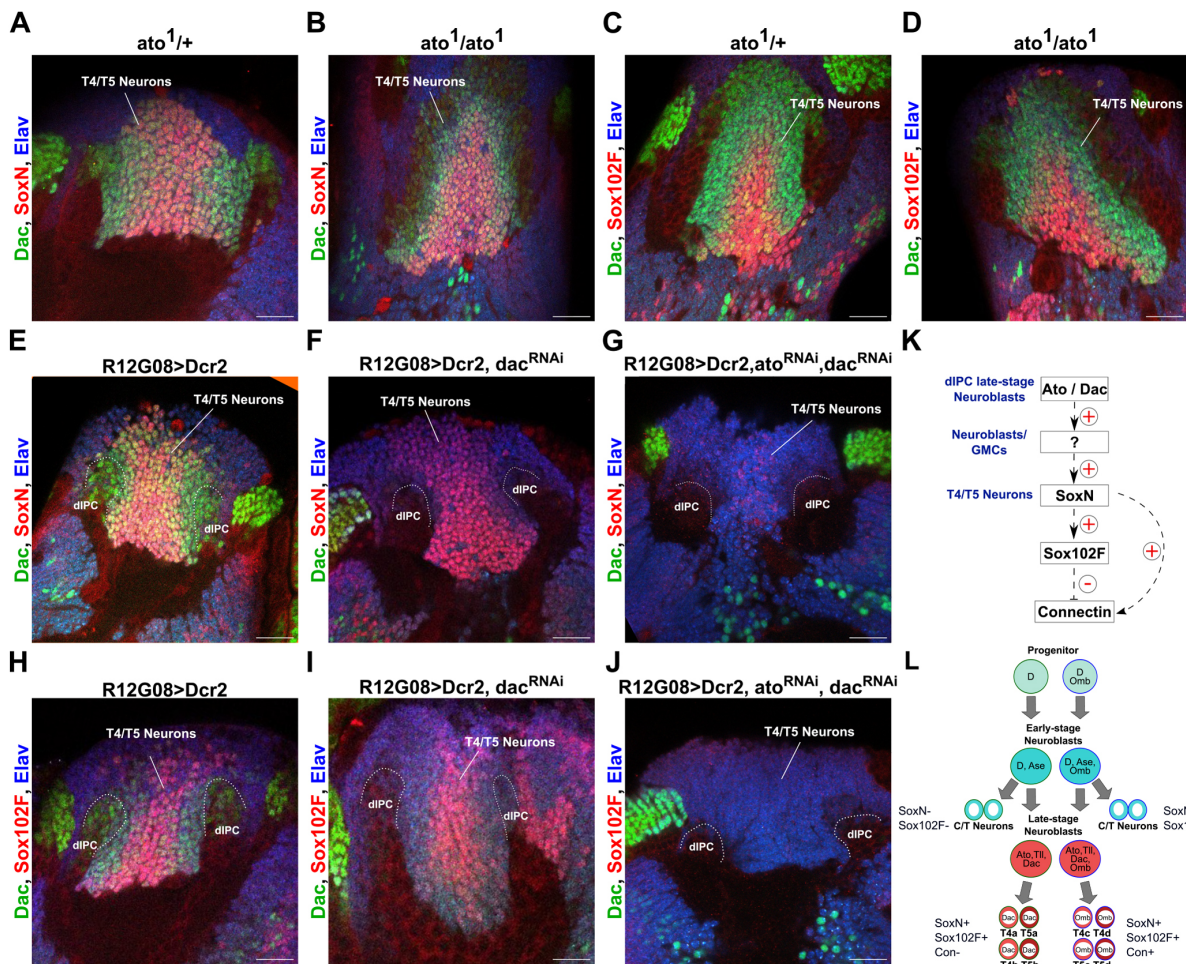


Fig. 8. *ato* and *dac* are redundantly required in late-stage dlIPC neuroblasts to control *SoxN* and *Sox102F* expression in offspring neurons. (A-D) *SoxN* and *Sox102F* expression in prepupal optic lobes from *ato*¹ heterozygous and homozygous mutants. Neuronal somata were marked with anti-*Elav*. T4/T5 somata were labelled with anti-*Dac*. (E-J) *SoxN* and *Sox102F* expression in prepupal optic lobes with wild-type, late-stage dlIPC neuroblasts, and with late-stage dlIPC neuroblasts expressing *Dac-RNAi* alone or together with *Ato-RNAi*. *Dac* signal was absent in the dlIPC upon *Dac-RNAi* expression with the *R12G08-Ga4*. (K) Summary of genetic interactions between *ato/dac*, *SoxN*, *Sox102F* and *Connectin* revealed in this study. (L) Summary of transcription factors expressed in early- and late-stage dlIPC neuroblasts, and in postmitotic T4/T5 neurons revealed by this and a previous study (Apitz and Salecker, 2018). Differential expression of *Connectin* between T4/T5 neuron subtypes is also depicted. Scale bars: 20 μ m.

where it controls subtype-specific properties (Apitz and Salecker, 2018). In contrast, *Ato* is transiently expressed in T4/T5 neuron progenitors. There, together with *Dac*, it initiates transcriptional programmes important for T4/T5 neuron specification (Apitz and Salecker, 2018). The output of these programmes comprises, at least, *SoxN* and *Sox102F* expression in postmitotic T4/T5 neurons. Future studies will be required to identify the transcriptional cascade linking *Ato/Dac* with *SoxN/Sox102F*, and other transcription factors controlling the terminal differentiation of postmitotic T4/T5 neurons. Neuron type-specific expression of transcription factors restricted to postmitotic stages also generates neuronal diversity in nematodes and in mammals (Hobert, 2016; Lodato and Arlotta, 2015). Therefore, we expect that our findings will help to understand how the expression of this type of transcription factors is selected during development in invertebrates and vertebrates.

T4/T5 neurons require *SoxN* and *Sox102F* function in order to establish their specific innervation patterns. In particular, our results

indicate that *SoxN* and *Sox102F* are required for maintaining T4/T5 dendrites and axons within single neuropil layers during neuronal maturation, rather than for guiding them towards the correct target layers (Fig. 5, Fig. S6). In order to understand the cellular and molecular mechanisms preventing the overgrowth of T4/T5 dendrites and axons into extra neuropil layers, future studies will be needed to characterise in detail the development of both wild-type T4/T5 neurons and T4/T5 neurons with *SoxN* or *Sox102F* loss of function, and to identify the direct targets of *SoxN* and *Sox102F* in T4/T5 neurons. These studies will also shed light on the redundant and distinct functions of *SoxN* and *Sox102F* during T4/T5 neuron development.

SoxN and *Sox102F* control dendritic and axonal patterning in every T4/T5 neuron subtype. However, we found that silencing *SoxN* or *Sox102F* in T4/T5_{a,b} caused milder phenotypes than in T4/T5_{c,d} neurons. This might result from different activities of these transcription factors in distinct T4/T5 neuron subtypes upon

subtype-specific post-translational modifications or subtype-specific expression of transcriptional co-regulators (Savare et al., 2005; She and Yang, 2015). Alternatively, *SoxN* and *Sox102F* transcriptional activities might be equivalent in all T4/T5 neuron subtypes. In this scenario, the differences observed between T4/T5 neuron subtypes upon *SoxN* or *Sox102F* knockdown could result from disparate expression levels of target genes that are dysregulated in an equivalent manner but have different basal expression levels between subtypes. In line with this, T4/T5_{a,b} and T4/T5_{c,d} neurons with knockdown of *Sox102F* seem to express moderate and high levels of Connectin, respectively (Fig. S8B,E). This is likely the result of combining a similar upregulation of Connectin in T4/T5_{a,b} and T4/T5_{c,d} neurons with T4/T5_{c,d} expressing higher basal levels of Connectin than T4/T5_{a,b} neurons. As Connectin functions as a homophilic cell-adhesion molecule (Nose et al., 1997; Raghavan and White, 1997), high Connectin levels might be the cause of T4/T5 axons forming clusters upon *Sox102F* silencing. In agreement with this, Connectin overexpression in wild-type T4/T5 neurons or in T4/T5 neurons with *SoxN* silenced induced the formation of axon clusters (Fig. 7H,I). However, knockdown of *Connectin* in T4/T5 neurons with *Sox102F* silenced did not rescue the formation of axon clusters (Fig. 7E). Therefore, one possibility is that other cell-surface molecules dysregulated upon *Sox102F* silencing play redundant roles with Connectin in the generation of this phenotype. Furthermore, *Connectin* knockdown in wild-type T4/T5 neurons did not prevent their axons from forming layers in the lobula plate (Fig. 7D). The role of the differential expression of Connectin between T4/T5 neuron subtypes needs further investigation. Finally, the disparity in the basal levels of Connectin between T4/T5 neuron subtypes appears to emerge from its tight regulation by transcription factors present in all T4/T5 neuron subtypes, such as *SoxN* and *Sox102F*, and transcription factors expressed in a subtype-specific manner, such as *Omb* (Fig. 8K,L) (Apitz and Salecker, 2018). Future studies should explore whether the same holds true for other molecular players controlling subtype-specific morphological properties in T4/T5 neurons. We envision T4/T5 neurons as a powerful system for improving our understanding of how the acquisition of properties common to a neuronal population and the acquisition of subtype-specific characters within this population are coordinated at the transcriptional level.

In addition, some of our findings bring insight into the development of motion vision circuits in *Drosophila* and of layered neural circuits in general. When we disrupted the dendrites and axons of specific T4/T5 neuron subtypes by silencing *SoxN* or *Sox102F*, the dendrites and axons from other T4/T5 neuron subtypes were unaffected. Therefore, *SoxN* and *Sox102F* act autonomously in distinct T4/T5 neuron subtypes to ensure the layer specificity of their dendrites and axons. In contrast, when T4/T5 axons failed to form distinct layers in the lobula plate, the dendrites of their postsynaptic partners also failed to form layers, suggesting that T4/T5 neurons play an instructive role in lobula plate patterning. The finding that *SoxN* and *Sox102F* function in T4/T5 neurons is non-autonomously required for the layer specificity of lobula plate tangential cells supports a recently proposed model describing layer formation as a stepwise process relying on transcription factors that restrict neurons to specific layers in a cell-intrinsic manner, and recruit other circuit components in a cell-extrinsic manner (Peng et al., 2018).

Finally, our finding that *SoxN* plays a role in the terminal differentiation of T4/T5 neurons is in agreement with previous studies that implicated *SoxN* both in the regulation of terminal differentiation genes (Ferrero et al., 2014; Girard et al., 2006) and in

the control of axonal patterning in *Drosophila* embryonic neurons (Girard et al., 2006; Overton et al., 2002). *SoxN* and its mammalian orthologues, the *SoxB1* family genes, have conserved roles in neural stem cell development (Nericic and Desplan, 2014; She and Yang, 2015). Whether mammalian *SoxB1* transcription factors regulate the terminal differentiation of neurons is unclear. In mammals, members of the *SoxD* family are well known for controlling neuronal terminal differentiation (She and Yang, 2015). A previous study showed that neuronal silencing of *Sox102F*, the only *Drosophila* orthologue of the *SoxD* family (Phochamukul and Russell, 2010), leads to abnormal neuronal development and behavioural impairment (Li et al., 2017). However, this study did not identify the specific developmental processes affected. Our work, in agreement with a recent study (Contreras et al., 2018), demonstrates a conserved role of *Sox102F* in controlling the terminal differentiation of neurons. Moreover, our observations suggest that one of the roles of *Sox102F* in T4/T5 neurons is to prevent the acquisition of morphological traits characteristic of developmentally related T2/T3 neurons, such as dendritic arborisation in medulla layer M9 and axons in the lobula. In agreement with this, *Sox102F* negatively regulates Connectin expression in T4/T5 neurons, which is highly expressed in T3 neurons (Konstantinides et al., 2018). *Sox5*, a member of the mammalian *SoxD* family, regulates postmitotically the molecular identity and connectivity of early-born corticofugal neurons by repressing the expression of genes characteristic of late-born corticofugal neurons (Kwan et al., 2008; Lai et al., 2008). Therefore, *SoxD*-mediated transcriptional repression in postmitotic neurons might represent a conserved mechanism for controlling neuronal identities in vertebrates and invertebrates.

MATERIALS AND METHODS

Fly strains

Flies were raised at 25°C and 60% humidity on standard cornmeal agar medium at 12 h light/dark cycle, except for RNAi experiments, in which offspring were shifted from 25°C to 29°C at first larval instar stage. At larval and pupal stages, female and male brains were analysed. At adult stages, only female brains were analysed. The following fly strains were used as driver lines (BL# strains are from Bloomington *Drosophila* Stock Center): *R40E11-Gal4* (BL#48140), *SS00324-splitGal4* (*R59E0-AD attP40; R42F06-DBD attP2*) (Schilling and Borst, 2015), *SS00779-splitGal4* (*R20C11-AD attP40; R48D11-DBD attP2*) (Tuthill et al., 2013), *R39H12-Gal4* (BL#50071), *VT37588-Gal4* (Maisal et al., 2013), *R11F07-Gal4* (BL#39414), *R42H07-Gal4* (BL#50172), *R12G08-Gal4* (BL#47855), *VT23749-LexA* (Mauss et al., 2015), *VT38815-LexA* and *VT50384-LexA* (Haag et al., 2016). The *T4/T5-splitGal4* driver line was generated by combining the *R41G11-AD* (BL#71050) and *R39H12-DBD* (BL#69444) hemidriver lines (Dionne et al., 2018). The *T4c,d-splitGal4* driver line was generated by combining the *VT16255-AD* (BL#75205) and *VT37588-DBD* (BL#75793) hemidriver lines (Tirian and Dickson, 2017 preprint). The following fly strains were used as reporter lines: *UAS-myrl-GFP* (BL#32198), *UAS-mCD8::GFP* (BL#32188), *UAS-CD4-tdGFP* (BL#35836), *UAS-myrl::tdTomato* (BL#32222), *UAS-mCD8::RFP*, *LexAop-mCD8::GFP* (BL#32229) and *LexAop-GCaMP6m* (BL#44275). To label individual neurons stochastically, we combined Gal4 driver lines with the following lines: *R57C10-Flp2::PEST* (Nern et al., 2015) and *UAS-(FRT.stop)myrl::GFP* (Nern et al., 2011). For knockdown experiments, we used the following lines: *UAS-Dcr2* (BL#24646, BL#24650 and BL#24651), *UAS-GFP-RNAi* (BL#41553), *UAS-SoxN-RNAi* (Vienna *Drosophila* Stock Center, shRNA-330056), *UAS-SoxN-RNAi2* (BL#25996), *UAS-Sox102F-RNAi* (Vienna *Drosophila* Stock Center, shRNA-330016), *UAS-Sox102F-RNAi2* (BL#26220), *UAS-mir-263a* (BL#59894), *UAS-Connectin-RNAi* (BL#28967), *UAS-dac-RNAi* (Vienna *Drosophila* Stock Center, KK106040) and *UAS-ato-RNAi* (BL#26316). For overexpression experiments, we used the following lines: *UAS-SoxN-V5* (wild-type version of *SoxN*), *UAS-Vp16-SoxN-V5* (obligatory activator version of

SoxN), *UAS-EnR-SoxN-V5* (obligatory repressor version of SoxN) (provided by S. Thor, Linköping University, Sweden), *UAS-Sox102F* and *UAS-Connectin* (this study). The *UAS-sh^{ts}* line (BL#66600) was used to block synaptic transmission at elevated temperatures (Kitamoto, 2001). We also used *Canton-S* (BL#64349) as a wild-type strain, *Sox102F^{M01054}* flies (BL#32729), *Df(4)O2* flies (BL#7084), and the *ato¹* mutant strain (a gift from B. A. Hassan, ICM – Hôpital Pitié Salpêtrière, Paris). MARCM experiments were performed by crossing *hs-Flp UAS-mCD8::GFP; tub-Gal80 FRT40A; R42F06-Gal4/TM6* flies (a gift from F. Pinto-Teixeira, New York University, USA) with *FRT40A* flies (a gift from I. Salecker, Francis Crick Institute, UK) or *SoxN^{NC14}* *FRT40A/CyO* flies [generated by us after recombining *FRT40A* with the *SoxN^{NC14}* mutant allele (BL#9937)]. Second and third instar larvae resulting from these crosses were heat shocked for 120 min in a 37°C water bath.

The *UAS-Sox102F* and *UAS-Connectin* strains were generated as follows: *Sox102F* and *Connectin* DNAs were produced by gene synthesis (GeneWiz) based on the FlyBase CDS sequences FBpp0100057 and FBpp073231, respectively, and subsequently cloned into *Xba*I-*Xba*I sites of *pJFRC7-20XUAS-IVS-mCD8::GFP* (Pfeiffer et al., 2010; Addgene plasmid #26220, deposited by Gerald Rubin), after removal of the *mCD8::GFP* cassette. The resulting *UAS-Sox102F* and *UAS-Connectin* plasmids were injected into the *su(Hw)attP1* landing site strain BL#34760 and the *VK05* landing site strain BL#9725, respectively, for PhiC31 integrase-mediated transgenesis (BestGene).

Behavioural assay and analysis

We cold-anaesthetised adult flies before the experiment and glued head, thorax and wings to a needle with bonding glue (Sinfony Opaque Dentin) under blue LED light (440 nm). Afterwards, we positioned animals on an air-suspended polyurethane ball. A virtual environment was projected onto three high-definition screens that collectively spanned 270° (along the vertical axis) and 114° (along the horizontal) of the fly eye's visual field. This gave an approximate spatial resolution of below 0.1°. We used six such set-ups for recording fly locomotion as described previously (Bahl et al., 2013). Two set-ups displayed stimuli at a refresh frequency of 120 Hz; on four set-ups, the frequency was 144 Hz. All monitors were equilibrated in brightness and contrast. Within the immediate area surrounding the fly, we controlled temperature using a custom-built closed-loop thermoregulation system. For the first 5 min, temperature was kept at 25°C and then raised to 34°C within 10 min. We used an optomotor stimulus similar to previous studies (Bahl et al., 2013). Flies were presented with a stationary square wave grating that had a spatial wavelength of 45° in visual angle and a Michelson contrast of 50%. Each individual trial lasted 8 s. Between 2 s and 6 s, the pattern travelled at a fixed velocity of 50% (corresponding to a temporal contrast frequency of 2 Hz) in either clockwise or counterclockwise direction. We repeated the stimulus 55 times per fly. The pattern was rendered in real-time using Panda3D, an open source game engine, and Python 2.7.

Data were processed as described previously (Ammer et al., 2015). Tracking data from optical sensors were processed at 4 kHz, read out via a USB interface, and recorded by a computer at 100 Hz. This allowed real-time calculation of the instantaneous rotation axis of the sphere. Rotation traces were re-sampled to 20 Hz for further processing and fed through a first-order low-pass filter with a time constant of 100 ms. We manually selected 30 consecutive trials that fulfilled the following criteria. First, the average turning tendency of the fly was roughly zero. Second, the mean forward velocity of the fly was at least 5 mm/s, indicating visual responsiveness. For further processing, we subtracted responses for the two symmetrical pattern directions to reduce the magnitude of residual walking asymmetries. We then took the mean across trials. For statistical purposes, we calculated the optomotor response of each fly as the average of the turning response between 4 s and 6 s. All data analysis was performed using Python 2.7 and the NumPy library.

Antibodies and immunolabelling

Primary antibodies used in this study were: rabbit anti-GFP (1:600, Biolabs, TP401), mouse anti-GFP (1:600, Sigma-Aldrich, G6539), chicken anti-GFP (1:600, ThermoFisher, A10262), rat anti-DN-Cadherin (1:50, Developmental Studies Hybridoma Bank, AB528121), mouse anti-

Connectin (1:50, Developmental Studies Hybridoma Bank, AB10660830), rabbit anti-DsRed (1:1000, Clontech, 632496), mouse anti-Dachshund (1:20, Developmental Studies Hybridoma Bank, AB528190), rat anti-Elav (1:50, Developmental Studies Hybridoma Bank, Rat-Elav-7E8A10), mouse anti-Acj6 (1:50, Developmental Studies Hybridoma Bank, AB528067), rabbit anti-SoxN (1:300, a gift from S. Russell; Ferrero et al., 2014), rabbit anti-Sox102F (1:300), rabbit anti-Lim1 (1:500), rabbit anti-Toy (1:1000), rabbit anti-Ap (1:200) (gifts from C. Desplan, New York University, USA) and rabbit anti-Omb (1:400, a gift from G. Pflugfelder, Johannes Gutenberg-University, Mainz, Germany). Secondary antibodies used in this study were: Alexa Fluor 488-conjugated goat anti-rabbit (Invitrogen, A11034), Alexa Fluor 488-conjugated goat anti-mouse (Thermo Fisher, A28175), Alexa Fluor 488-conjugated goat anti-rat (Invitrogen, A11006), Alexa Fluor 488-conjugated donkey anti-chicken (Jackson ImmunoResearch, 703-545-155), Alexa Fluor 568-conjugated goat anti-rabbit (Life Technologies, A11011), Alexa Fluor 568-conjugated goat anti-mouse (Invitrogen, A11004), ATTO 647N-conjugated goat anti-mouse (Rockland, 610-156-040) and Alexa Fluor 647-conjugated goat anti-rat (Life Technologies, A21247) (all used at 1:500).

For immunolabelling, brains were dissected in cold PBS and fixed in 4% formaldehyde (containing 0.3% Triton X-100) at room temperature for 24 (adult) or 15 (larval and pupal) min. Afterwards, they were washed three times with PBT (PBS containing 0.3% Triton X-100) and blocked with 10% normal goat serum in PBT at room temperature for 2 h. Brains were incubated with primary antibodies diluted in PBT containing 5% normal goat serum for 24–48 h at 4°C. After washing five times with PBT, brains were incubated with secondary antibodies diluted in PBT containing 5% normal goat serum for 24–48 h at 4°C. After washing five times with PBT and one time with PBS, brains were mounted in Gold Antifade Mountant (Thermo Fisher).

Imaging and quantification

Imaging was performed with a Leica SP8 laser scanning confocal microscope equipped with 488-, 561- and 633-nm lasers, and using a 63× objective. Image processing and quantitative analyses were performed with the Fiji software package (Schindelin et al., 2012).

Relative expression levels of SoxN or Sox102F in T4/T5 neurons were quantified as follows: for each optic lobe, we measured the mean grey values (anti-SoxN or anti-Sox102F channel) of either at least 15 manually segmented T4/T5 somata (in Fig. 1N-S and Fig. 3G-J) or the region occupied by T4/T5 somata (Fig. 1H-M and Fig. 3A-F,O-T) across several optical sections. Afterwards, we obtained the average of these values and divided it by the average of mean grey values (anti-SoxN or anti-Sox102F channel) measured in the region occupied by C/T somata across several optical sections. To assess changes in Sox102F expression in T4/T5 neurons upon overexpression of different V5-tagged versions of SoxN (Fig. 3K-N), we measured the mean grey value (anti-Sox102F channel) of a manually segmented T4/T5 soma overexpressing SoxN (high anti-V5 signal), and divided it by the mean grey value (anti-Sox102F channel) of a neighbouring T4/T5 soma without SoxN overexpression (negative for anti-V5 signal). This was carried out in late L3 larval optic lobes for SoxN-V5 and Vp16-SoxN-V5, and in adult optic lobes for EnR-SoxN-V5 overexpression experiments, because only at these stages could we clearly find T4/T5 somata with very high anti-V5 signal and neighbouring T4/T5 somata without anti-V5 signal.

Lobula plate volume was quantified as follows: for each optic lobe mounted in a posterior orientation, a z-stack of the entire lobula plate (labelled with anti-DN-Cadherin) was acquired with a z-step of 2 μm. In each optical section, the area of the manually segmented lobula plate was measured. The areas obtained from all optical sections were summed to estimate the 3D volume of the lobula plate.

The extension of lobula plate along the anteroposterior axis occupied by individual T4 and T5 axons was quantified as follows: for each lobula plate mounted in a dorsal orientation, individual axons were identified. For each axon, we measured the distance between each of its axonal boutons and the most anterior edge of the lobula plate in single optical sections. These values were normalised by the length of the lobula plate along the anteroposterior axis at the proximodistal position occupied by the axon. Finally, the normalised values of the most anterior and the most posterior axonal boutons were subtracted.

Connectin expression levels were measured as follows: for each optic lobe imaged in a dorsal orientation, we first averaged the mean grey values (anti-Connectin channel) measured in a manually defined neuropil layer across several optical sections. Next, to detect changes between experimental conditions in Connectin expression in a specific neuropil layer, for instance medulla M10, we divided Connectin levels in M10 by Connectin levels in M9, which was unchanged between conditions. For Fig. 7M-O, Connectin levels in M10 were only measured in the regions occupied by memGFP T4 dendrites.

Calculations were performed and plots were generated using Microsoft Excel Software and Python 2.7 using the NumPy and Scipy libraries. In box-and-whisker plots, the end of the whiskers represent the minimum and maximum values, and outliers were plotted as individual points. Statistical significance was assessed by calculating the *P*-value for unpaired two-tailed Student's *t*-test (**P*<0.05; ***P*<0.01; ****P*<0.001). Figures were prepared using Inkscape software.

Acknowledgements

We are grateful to S. Russell, C. Desplan, S. Thor, I. Salecker, F. Pinto-Teixeira, G. Pflugfelder, B. A. Hassan, the Janelia Research Campus, the Bloomington *Drosophila* Stock Center, the Vienna *Drosophila* Stock Center and the Developmental Studies Hybridoma Bank for flies and antibodies. We also thank R. Kutlesa and C. Theile for technical assistance with behavioural experiments; R. Kasper of the Imaging Facility for technical assistance with confocal imaging; I. Ribeiro, A. Mauss and S. Fendt for carefully reading the manuscript; and F. Pinto-Teixeira and N. Hoermann for discussions.

Competing interests

The authors declare no competing or financial interests.

Author contributions

Conceptualization: T.S., J.P.-M.; Methodology: T.S., A.L., J.P.-M.; Software: A.L.; Investigation: T.S., A.H.A., J.P.-M.; Writing - original draft: J.P.-M.; Writing - review & editing: T.S., A.H.A., A.L., A.B., J.P.-M.; Visualization: T.S.; Supervision: A.B., J.P.-M.; Project administration: A.B.; Funding acquisition: A.B.

Funding

This work was supported by the Max-Planck-Society (Max-Planck-Gesellschaft). Deposited in PMC for immediate release.

Supplementary information

Supplementary information available online at <http://dev.biologists.org/lookup/doi/10.1242/dev.169763.supplemental>

References

Ammer, G., Leonhardt, A., Bahl, A., Dickson, B. J. and Borst, A. (2015). Functional specialization of neural input elements to the *Drosophila* on motion detector. *Curr. Biol.* **25**, 2247-2253.

Apitz, H. and Salecker, I. (2015). A region-specific neurogenesis mode requires migratory progenitors in the *Drosophila* visual system. *Nat. Neurosci.* **18**, 46-55.

Apitz, H. and Salecker, I. (2018). Spatio-temporal relays control layer identity of direction-selective neuron subtypes in *Drosophila*. *Nat. Commun.* **9**, 2295.

Bahl, A., Ammer, G., Schilling, T. and Borst, A. (2013). Object tracking in motion-blind flies. *Nat. Neurosci.* **16**, 730-738.

Bahrampour, S., Gunnar, E., Jonsson, C., Ekman, H. and Thor, S. (2017). Neural lineage progression controlled by a temporal proliferation program. *Dev. Cell* **43**, 332-348.e334.

Boergens, K. M., Kapfer, C., Helmstaedter, M., Denk, W. and Borst, A. (2018). Full reconstruction of large lobula plate tangential cells in *Drosophila* from a 3D EM dataset. *PLoS ONE* **13**, e0207828.

Contreras, E. G., Palomino, T., Glavic, A., Brand, A. H., Sierralta, J. and Oliva, C. (2018). The transcription factor SoxD controls neuronal guidance in the *Drosophila* visual system. *Sci. Rep.* **8**, 13332.

Davis, F. P., Nern, A., Picard, S., Reiser, M. B., Rubin, G. M., Eddy, S. R. Henry, G. L. (2018). A genetic, genomic, and computational resource for exploring neural circuit function. *bioRxiv*.

Dietzl, G., Chen, D., Schnorrer, F., Su, K. C., Barinova, Y., Fellner, M., Gasser, B., Kinsey, K., Oppel, S., Scheiblauer, S. et al. (2007). A genome-wide transgenic RNAi library for conditional gene inactivation in *Drosophila*. *Nature* **448**, 151-156.

Dionne, H., Hibbard, K. L., Cavallaro, A., Kao, J. C. and Rubin, G. M. (2018). Genetic reagents for making split-GAL4 lines in *Drosophila*. *Genetics* **209**, 31-35.

Erclik, T., Li, X., Courgeon, M., Bertet, C., Chen, Z., Baumert, R., Ng, J., Koo, C., Arain, U., Behnia, R. et al. (2017). Integration of temporal and spatial patterning generates neural diversity. *Nature* **541**, 365-370.

Ferrero, E., Fischer, B. and Russell, S. (2014). SoxNeuro orchestrates central nervous system specification and differentiation in *Drosophila* and is only partially redundant with Dichaete. *Genome Biol.* **15**, R74.

Fischbach, K.-F. and Dittrich, A. P. M. (1989). The optic lobe of *Drosophila melanogaster*. I. A Golgi analysis of wild-type structure. *Cell Tissue Res.* **258**, 441-475.

Gao, S., Takemura, S.-Y., Ting, C.-Y., Huang, S., Lu, Z., Luan, H., Rister, J., Thum, A. S., Yang, M., Hong, S. T. et al. (2008). The neural substrate of spectral preference in *Drosophila*. *Neuron* **60**, 328-342.

Girard, F., Joly, W., Savare, J., Bonneaud, N., Ferraz, C. and Maschiat, F. (2006). Chromatin immunoprecipitation reveals a novel role for the *Drosophila* SoxNeuro transcription factor in axonal patterning. *Dev. Biol.* **299**, 530-542.

Haag, J., Arenz, A., Serbe, E., Gabbianni, F. and Borst, A. (2016). Complementary mechanisms create direction selectivity in the fly. *eLife* **5**, e17421.

Haag, J., Mishra, A. and Borst, A. (2017). A common directional tuning mechanism of *Drosophila* motion-sensing neurons in the ON and in the OFF pathway. *eLife* **6**, e29044.

Hasegawa, E., Kaido, M., Takayama, R. and Sato, M. (2013). Brain-specific homeobox is required for the specification of neuronal types in the *Drosophila* optic lobe. *Dev. Biol.* **377**, 90-99.

Hasegawa, E., Kitada, Y., Kaido, M., Takayama, R., Awasaki, T., Tabata, T. and Sato, M. (2011). Concentric zones, cell migration and neuronal circuits in the *Drosophila* visual center. *Development* **138**, 983-993.

Horbert, O. (2011). Regulation of terminal differentiation programs in the nervous system. *Annu. Rev. Cell Dev. Biol.* **27**, 681-696.

Horbert, O. (2016). Terminal selectors of neuronal identity. *Curr. Top. Dev. Biol.* **116**, 455-475.

Hofbauer, A. and Campos-Ortega, J. A. (1990). Proliferation pattern and early differentiation of the optic lobes in *Drosophila melanogaster*. *Roux's Arch. Dev. Biol.* **198**, 264-274.

Jarman, A. P., Grell, E. H., Ackerman, L., Jan, L. Y. and Jan, Y. N. (1994). Atonal is the proneural gene for *Drosophila* photoreceptors. *Nature* **369**, 398-400.

Joesch, M., Plett, J., Borst, A. and Reiff, D. F. (2008). Response properties of motion-sensitive visual interneurons in the lobula plate of *Drosophila melanogaster*. *Curr. Biol.* **18**, 368-374.

Joesch, M., Schnell, B., Raghav, S. V., Reiff, D. F. and Borst, A. (2010). ON and OFF pathways in *Drosophila* motion vision. *Nature* **468**, 300-304.

Kaya-Copur, A. and Schnorrer, F. (2016). A guide to genome-wide *in vivo* RNAi applications in *Drosophila*. *Methods Mol. Biol.* **1478**, 117-143.

Kitamoto, T. (2001). Conditional modification of behavior in *Drosophila* by targeted expression of a temperature-sensitive shibire allele in defined neurons. *J. Neurobiol.* **47**, 81-92.

Konstantinides, N., Kapuralin, K., Fadil, C., Barboza, L., Satija, R. and Desplan, C. (2018). Phenotypic convergence: distinct transcription factors regulate common terminal features. *Cell* **174**, 622-635.e13.

Kwan, K. Y., Lam, M. M., Krsnik, Z., Kawasawa, Y. I., Lefebvre, V. and Sestan, N. (2008). SOX5 postmitotically regulates migration, postmigratory differentiation, and projections of subplate and deep-layer neocortical neurons. *Proc. Natl. Acad. Sci. USA* **105**, 16021-16026.

Lai, T., Jabaoudi, D., Molyneaux, B. J., Azim, E., Arlotta, P., Menezes, J. R. and Macklis, J. D. (2008). SOX5 controls the sequential generation of distinct corticofugal neuron subtypes. *Neuron* **57**, 232-247.

Li, X., Erclik, T., Bertet, C., Chen, Z., Voutev, R., Venkatesh, S., Morante, J., Celik, A. and Desplan, C. (2013). Temporal patterning of *Drosophila* medulla neuroblasts controls neural fates. *Nature* **498**, 456-462.

Li, A., Hooli, B., Mullin, K., Tate, R. E., Bubnys, A., Kirchner, R., Chapman, B., Hofmann, O., Hide, W. and Tanzi, R. E. (2017). Silencing of the *Drosophila* ortholog of SOX5 leads to abnormal neuronal development and behavioral impairment. *Hum. Mol. Genet.* **26**, 1472-1482.

Locato, S. and Arlotta, P. (2015). Generating neuronal diversity in the mammalian cerebral cortex. *Annu. Rev. Cell Dev. Biol.* **31**, 699-720.

Maisak, M. S., Haag, J., Ammer, G., Serbe, E., Meier, M., Leonhardt, A., Schilling, T., Bahl, A., Rubin, G. M., Nern, A. et al. (2013). A directional tuning map of *Drosophila* elementary motion detectors. *Nature* **500**, 212-216.

Mauss, A. S., Meier, M., Serbe, E. and Borst, A. (2014). Optogenetic and pharmacologic dissection of feedforward inhibition in *Drosophila* motion vision. *J. Neurosci.* **34**, 2254-2263.

Mauss, A. S., Pankova, K., Arenz, A., Nern, A., Rubin, G. M. and Borst, A. (2015). Neural circuit to integrate opposing motions in the visual field. *Cell* **162**, 351-362.

Mora, N., Oliva, C., Fiers, M., Ejsmont, R., Soldano, A., Zhang, T. T., Yan, J., Claeys, A., De Geest, N. and Hassan, B. A. (2018). A temporal transcriptional switch governs stem cell division, neuronal numbers, and maintenance of differentiation. *Dev. Cell* **45**, 53-66.e55.

Nassif, C., Noveen, A. and Hartenstein, V. (2003). Early development of the *Drosophila* brain: III. The pattern of neuropile founder tracts during the larval period. *J. Comp. Neurol.* **455**, 417-434.

Nerier, N. and Desplan, C. (2014). Different ways to make neurons: parallel evolution in the SoxB family. *Genome Biol.* **15**, 116.

Nern, A., Pfeiffer, B. D., Svoboda, K. and Rubin, G. M. (2011). Multiple new site-specific recombinases for use in manipulating animal genomes. *Proc. Natl. Acad. Sci. USA* **108**, 14198-14203.

Nern, A., Pfeiffer, B. D. and Rubin, G. M. (2015). Optimized tools for multicolor stochastic labeling reveal diverse stereotyped cell arrangements in the fly visual system. *Proc. Natl. Acad. Sci. USA* **112**, E2967-E2976.

Ngo, K. T., Andrade, I. and Hartenstein, V. (2017). Spatio-temporal pattern of neuronal differentiation in the Drosophila visual system: a user's guide to the dynamic morphology of the developing optic lobe. *Dev. Biol.* **428**, 1-24.

Nose, A., Umeda, T. and Takeichi, M. (1997). Neuromuscular target recognition by a homophilic interaction of connectin cell adhesion molecules in Drosophila. *Development* **124**, 1433-1441.

Oliva, C., Choi, C. M., Nicolai, L. J., Mora, N., De Geest, N. and Hassan, B. A. (2014). Proper connectivity of Drosophila motion detector neurons requires Atonal function in progenitor cells. *Neural Dev.* **9**, 4.

Overton, P. M., Meadows, L. A., Urban, J. and Russell, S. (2002). Evidence for differential and redundant function of the Sox genes Dichaete and SoxN during CNS development in Drosophila. *Development* **129**, 4219-4228.

Pankova, K. and Borst, A. (2016). RNA-Seq transcriptome analysis of direction-selective T4/T5 neurons in Drosophila. *PLoS ONE* **11**, e0163986.

Peng, J., Santiago, I. J., Ahn, C., Gur, B., Tsui, C. K., Su, Z., Xu, C., Karakhanyan, A., Silies, M. and Pecot, M. Y. (2018). Drosophila Fezf coordinates laminar-specific connectivity through cell-intrinsic and cell-extrinsic mechanisms. *eLife* **7**, e33962.

Perkins, L. A., Holderbaum, L., Tao, R., Hu, Y., Sopko, R., McCall, K., Yang-Zhou, D., Flockhart, I., Binari, R., Shim, H. S. et al. (2015). The transgenic RNAi project at harvard medical school: resources and validation. *Genetics* **201**, 843-852.

Pfeiffer, B. D., Ngo, T. T., Hibbard, K. L., Murphy, C., Jenett, A., Truman, J. W. and Rubin, G. M. (2010). Refinement of tools for targeted gene expression in Drosophila. *Genetics* **186**, 735-755.

Phochanukul, N. and Russell, S. (2010). No backbone but lots of Sox: invertebrate Sox genes. *Int. J. Biochem. Cell Biol.* **42**, 453-464.

Pinto-Texeira, F., Koo, C., Rossi, A. M., Neric, N., Bertet, C., Li, X., Del-Valle-Rodriguez, A. and Desplan, C. (2018). Development of concurrent retinotopic maps in the fly motion detection circuit. *Cell* **173**, 485-498.e411.

Raghavan, S. and White, R. A. (1997). Connectin mediates adhesion in Drosophila. *Neuron* **18**, 873-880.

Savare, J., Bonneaud, N. and Girard, F. (2005). SUMO represses transcriptional activity of the Drosophila SoxNeuro and human Sox3 central nervous system-specific transcription factors. *Mol. Biol. Cell* **16**, 2660-2669.

Schilling, T. and Borst, A. (2015). Local motion detectors are required for the computation of expansion flow-fields. *Biol. Open* **4**, 1105-1108.

Schindelin, J., Arganda-Carreras, I., Frise, E., Kaynig, V., Longair, M., Pietzsch, T., Preibisch, S., Rueden, C., Saalfeld, S., Schmid, B. et al. (2012). Fiji: an open-source platform for biological-image analysis. *Nat. Methods* **9**, 676-682.

Schnell, B., Joesch, M., Forstner, F., Raghu, S. V., Otsuna, H., Ito, K., Borst, A. and Reiff, D. F. (2010). Processing of horizontal optic flow in three visual interneurons of the Drosophila brain. *J. Neurophysiol.* **103**, 1646-1657.

Scott, E. K., Raabe, T. and Luo, L. (2002). Structure of the vertical and horizontal system neurons of the lobula plate in Drosophila. *J. Comp. Neurol.* **454**, 470-481.

She, Z. Y. and Yang, W. X. (2015). SOX family transcription factors involved in diverse cellular events during development. *Eur. J. Cell Biol.* **94**, 547-563.

Shinomiya, K., Karuppudurai, T., Lin, T. Y., Lu, Z., Lee, C. H. and Meinertzhagen, I. A. (2014). Candidate neural substrates for off-edge motion detection in Drosophila. *Curr. Biol.* **24**, 1062-1070.

Shinomiya, K., Takemura, S. Y., Rivilin, P. K., Plaza, S. M., Scheffer, L. K. and Meinertzhagen, I. A. (2015). A common evolutionary origin for the ON- and OFF-edge motion detection pathways of the Drosophila visual system. *Front. Neural Circuits* **9**, 33.

Strother, J. A., Nern, A. and Reiser, M. B. (2014). Direct observation of ON and OFF pathways in the Drosophila visual system. *Curr. Biol.* **24**, 976-983.

Suzuki, T., Kaido, M., Takayama, R. and Sato, M. (2013). A temporal mechanism that produces neuronal diversity in the Drosophila visual center. *Dev. Biol.* **380**, 12-24.

Suzuki, T., Hasegawa, E., Nakai, Y., Kaido, M., Takayama, R. and Sato, M. (2016). Formation of neuronal circuits by interactions between neuronal populations derived from different origins in the Drosophila visual center. *Cell Reports* **15**, 499-509.

Takemura, S. Y., Nern, A., Chklovskii, D. B., Scheffer, L. K., Rubin, G. M. and Meinertzhagen, I. A. (2017). The comprehensive connectome of a neural substrate for 'ON' motion detection in Drosophila. *eLife* **6**, e24394.

Tirian, L. and Dickson, B. (2017). The VT GAL4, LexA, and split-GAL4 driver line collections for targeted expression in the Drosophila nervous system. *bioRxiv*.

Tuthill, J. C., Nern, A., Holtz, S. L., Rubin, G. M. and Reiser, M. B. (2013). Contributions of the 12 neuron classes in the fly lamina to motion vision. *Neuron* **79**, 128-140.

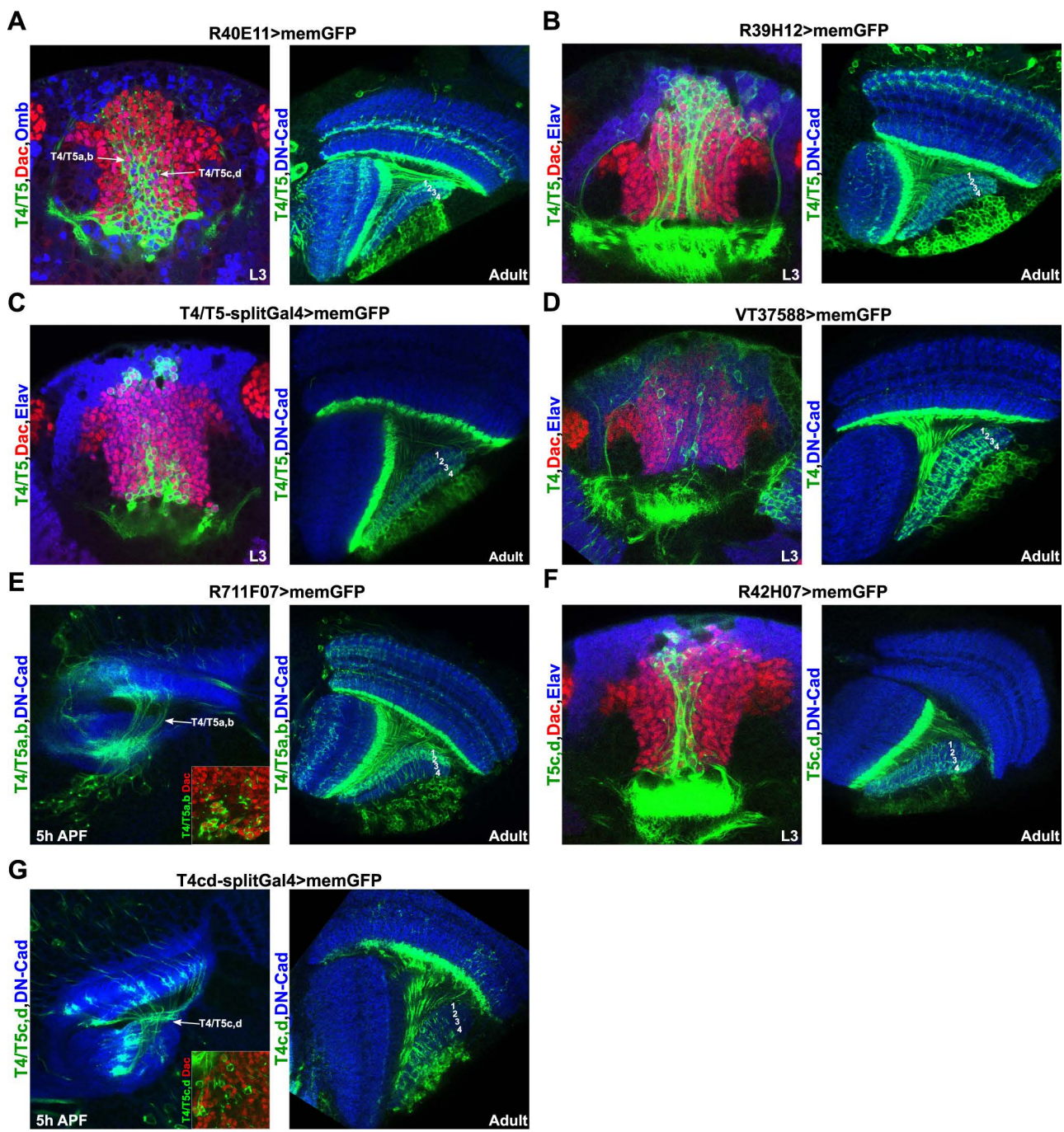


Figure S1. Characterization of enhancer-Gal4 driver lines used for *UAS-RNAi* transgene expression in T4/T5 neurons.

(A-G) Expression patterns of *R40E11-Gal4*, *R39H12-Gal4*, *T4/T5-splitGal4*, *VT37588-Gal4*, *R11F07-Gal4*, *R42H07-Gal4* and *T4_{c,d}-splitGal4* driver lines in late L3 larval or early pupal optic lobes (5 h APF), and in adult optic lobes. Arrows in A mark Dac⁺/Omb⁻ and Dac⁻/Omb⁺ somata, which correspond to T4/T5a,b and T4/T5c,d neurons, respectively. Inset in E shows that most T4/T5 somata labelled by the *R11F07-Gal4* at 5 h APF are Dac⁺. Inset in G shows that most T4/T5 somata labelled by the *T4_{c,d}-splitGal4* at 5 h APF are Dac⁻. Neuropils were labelled with anti-DN-Cad at pupal and adult stages.

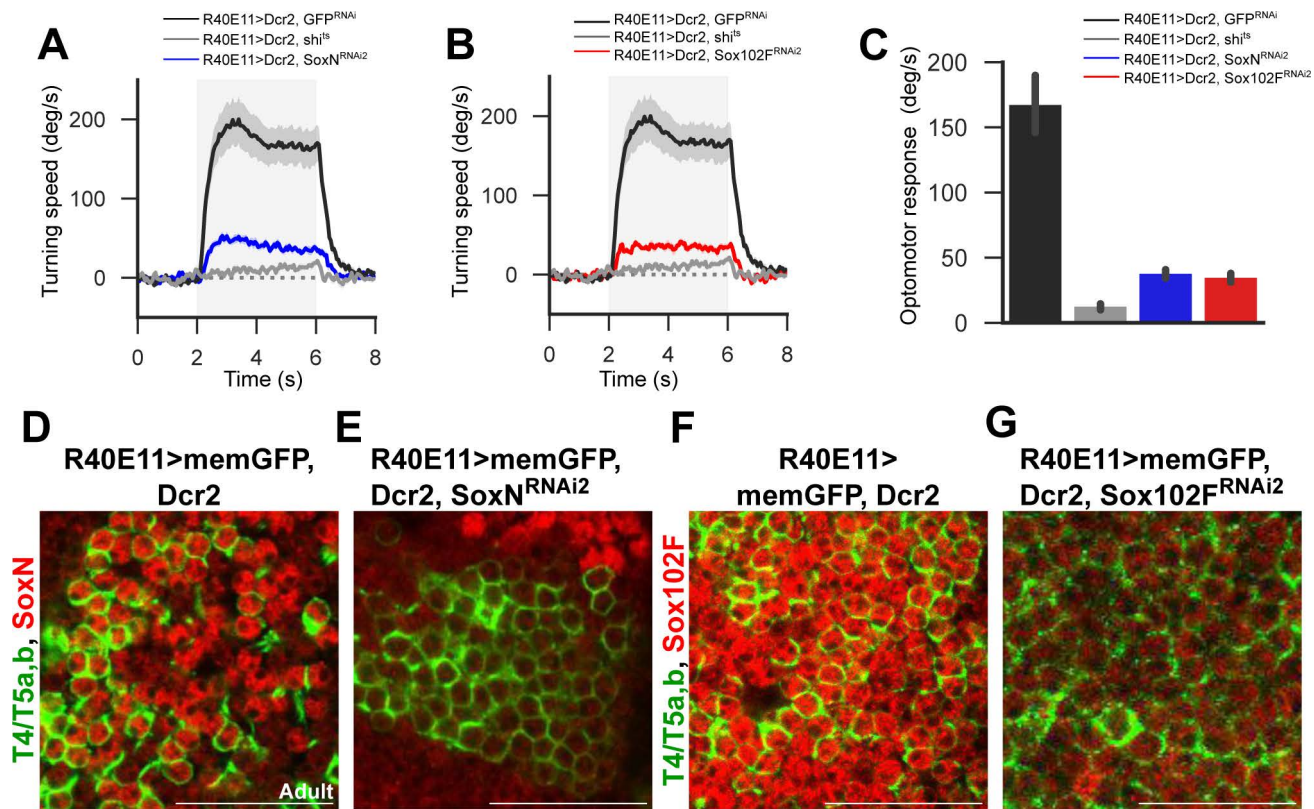


Figure S2. Use of additional *UAS-RNAi* transgenes supports that knockdown of *SoxN* or *Sox102F* in T4/T5 neurons impairs the optomotor response.

(A,B) Average turning speeds in response to rotation of a grating pattern (grey shaded areas) of flies expressing *GFP-RNAi* (negative control), *sh^{ts}* (positive control, T4/T5 block), *SoxN-RNAi2* or *Sox102F-RNAi2* in T4/T5 neurons (n = 10 flies per group).

(C) Average optomotor responses of flies expressing *GFP-RNAi*, *sh^{ts}*, *SoxN-RNAi2* or *Sox102F-RNAi2* in T4/T5 neurons (n = 10 flies per group).

(D-G) *SoxN* and *Sox102F* expression in adult optic lobes with wild-type T4/T5 neurons, and with T4/T5 neurons expressing *SoxN-RNAi2* or *Sox102F-RNAi2*.

Scale bars = 20 μ m.

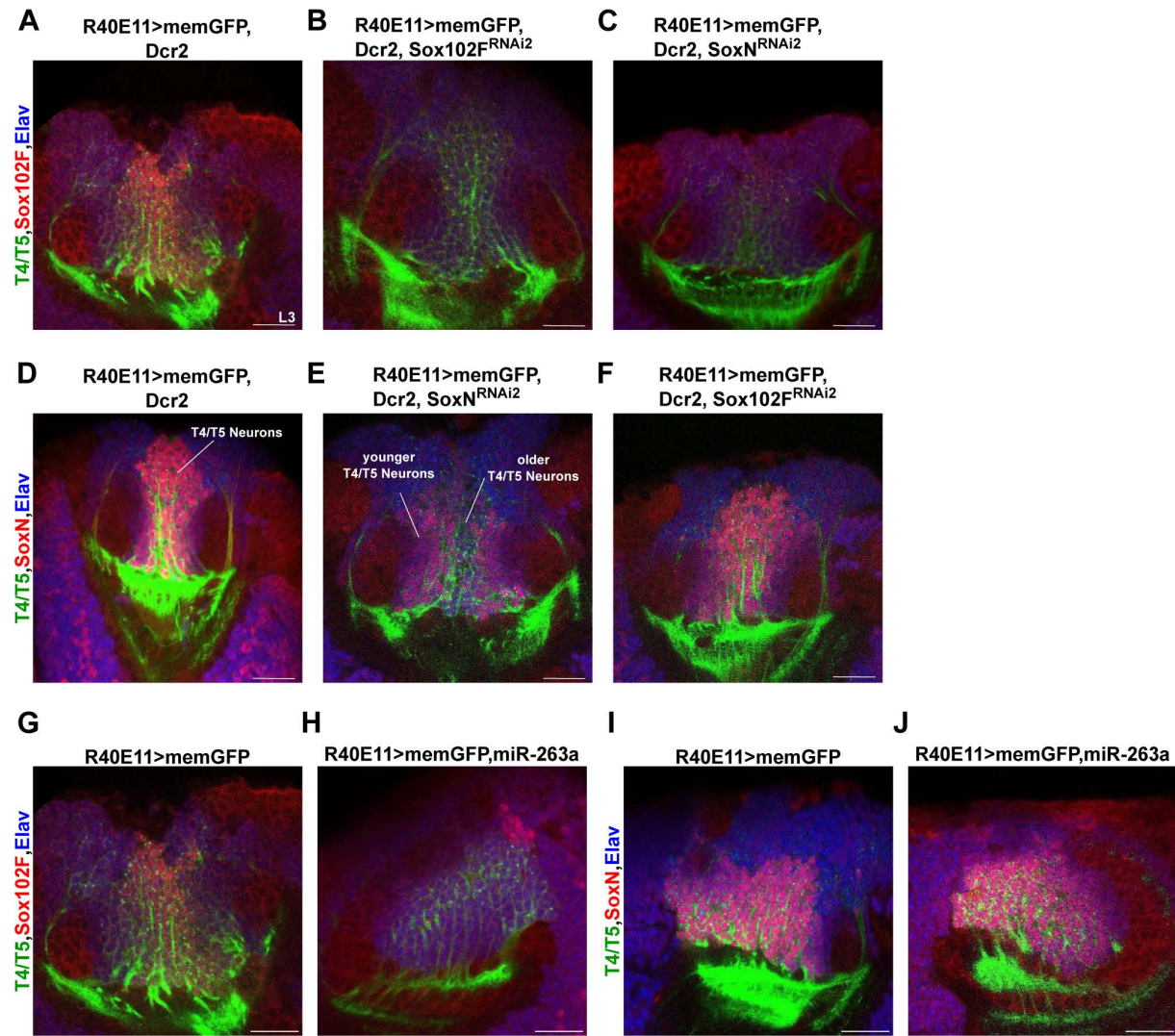


Figure S3. Use of additional *UAS-RNAi* transgenes and microRNA supports that *SoxN* is required for *Sox102F* expression while *Sox102F* is dispensable for *SoxN* expression in T4/T5 neurons.

(A-C) *Sox102F* expression in late L3 larval optic lobes with wild-type T4/T5 neurons, and with T4/T5 neurons expressing *Sox102F-RNAi2* or *SoxN-RNAi2*.

(D-F) *SoxN* expression in late L3 larval optic lobes with wild-type T4/T5 neurons and with T4/T5 neurons expressing *SoxN-RNAi2* or *Sox102F-RNAi2*.

(G-J) *Sox102F* and *SoxN* expression in late L3 larval optic lobes with wild-type T4/T5 neurons, and with T4/T5 neurons expressing *miR-263a*.

Scale bars = 20 μ m.

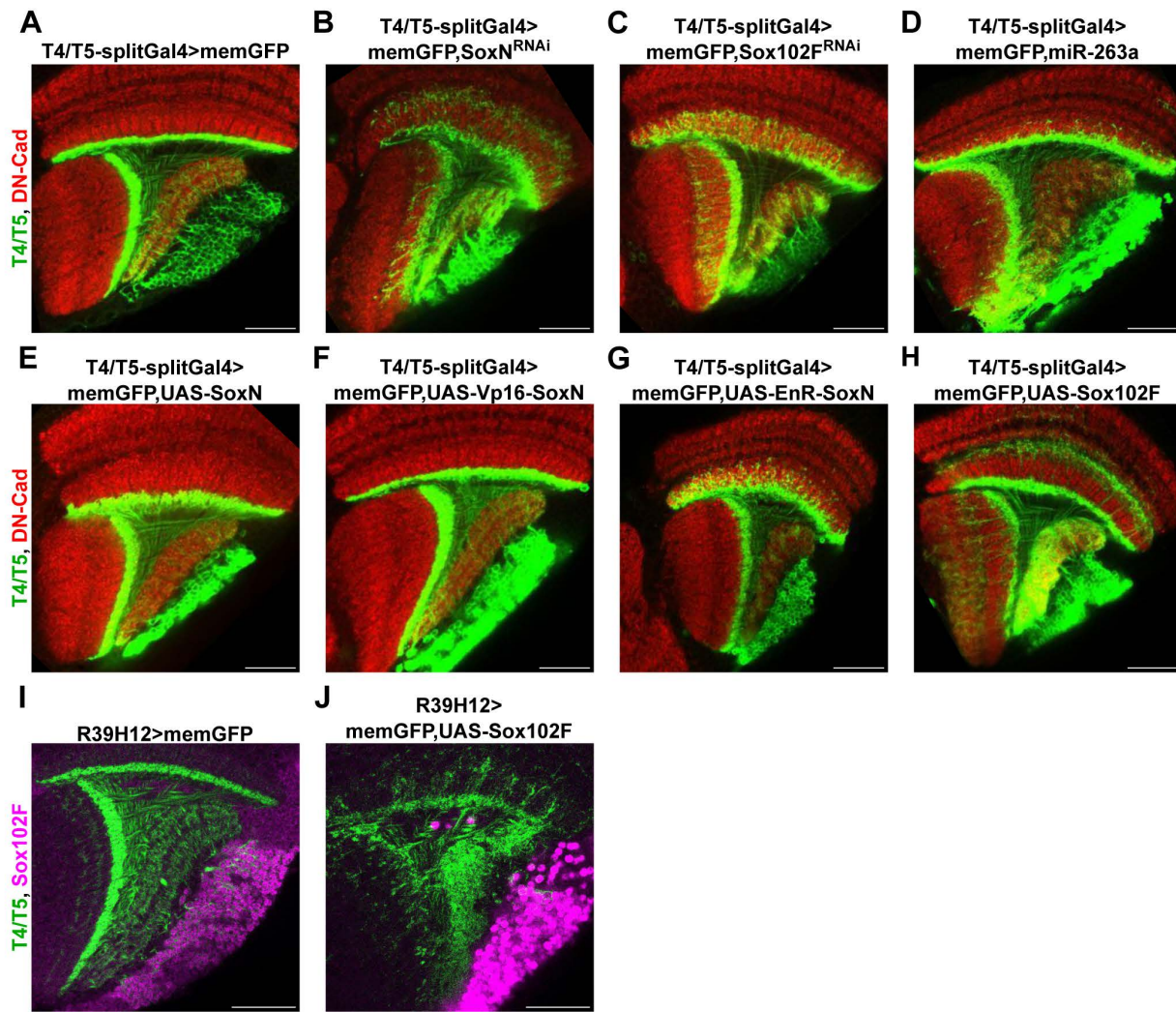


Figure S4. T4/T5 neuron morphology upon *SoxN* or *Sox102F* silencing, and upon *SoxN* or *Sox102F* overexpression with the *T4/T5-splitGal4* driver line.

(A-D) Adult optic lobes with wild-type T4/T5 neurons, and with T4/T5 neurons expressing *SoxN-RNAi*, *Sox102F-RNAi* or *miR-263a* by means of the *T4/T5-splitGal4* line.

(E-G) Adult optic lobes with T4/T5 neurons overexpressing three different versions of *SoxN* by using the *T4/T5-splitGal4* line: a wild-type version (*SoxN*), an obligatory activator version (*Vp16-SoxN*), or an obligatory repressor version (*EnR-SoxN*).

(H) Adult optic lobe with T4/T5 neurons overexpressing *Sox102F* by means of the *T4/T5-splitGal4* line.

(I-J) *Sox102F* expression in adult optic lobes with wild-type T4/T5 neurons, and with T4/T5 neurons overexpressing *Sox102F* by means of the *R39H12-Gal4* line.

Scale bars = 20 μ m.

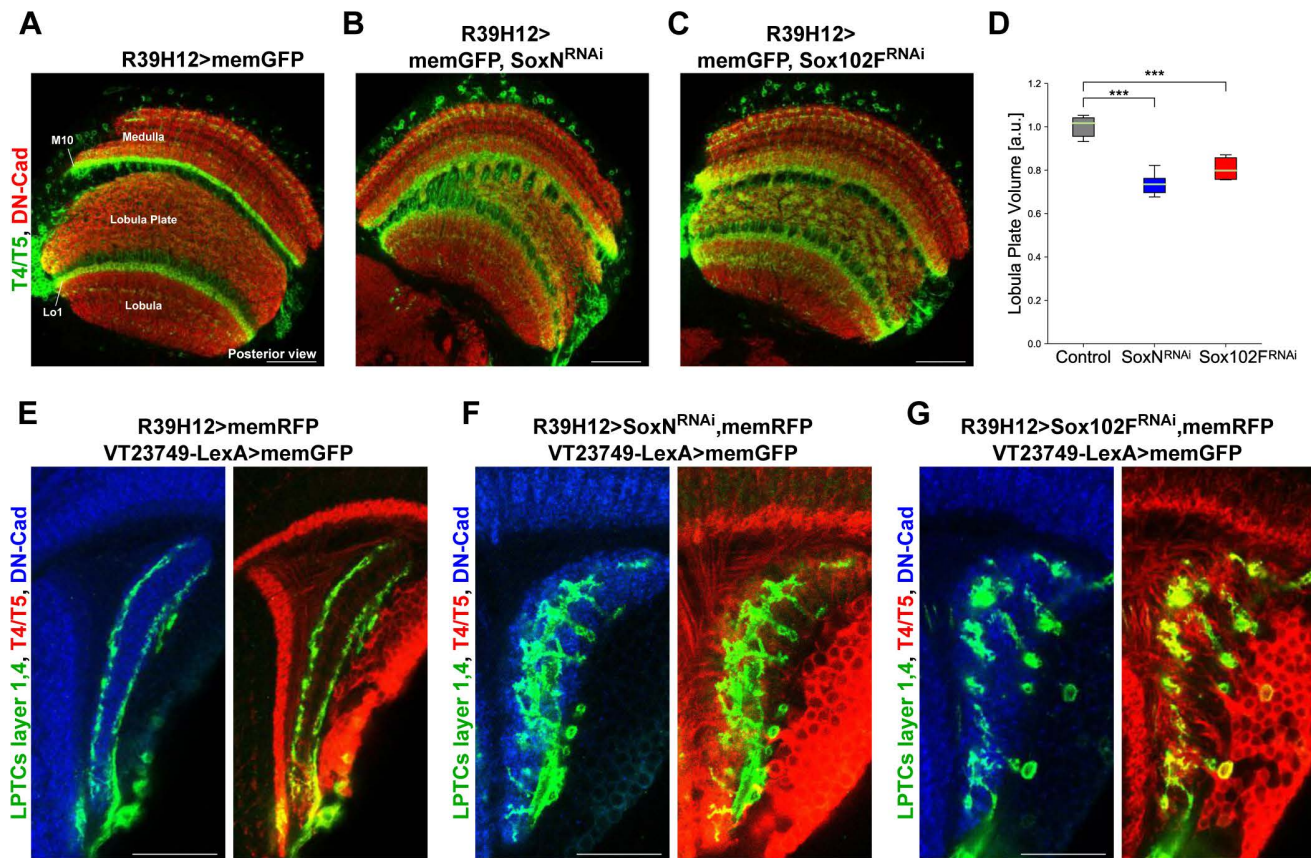


Figure S5. *SoxN* and *Sox102F* control dendritic development non-autonomously in LPTCs.

(A-C) Posterior views of adult optic lobes with wild-type T4/T5 neurons, and with T4/T5 neurons expressing *SoxN*-RNAi or *Sox102F*-RNAi.

(D) Average lobula plate volumes in adult flies with wild-type T4/T5 neurons (control), and with T4/T5 neurons expressing *SoxN*-RNAi or *Sox102F*-RNAi (n = 5 optic lobes per group). ***P<0.001.

(E-G) Dorsal view of lobula plates showing the dendrites of LPTCs in the presence of wild-type T4/T5 axons, and in the presence of T4/T5 axons expressing *SoxN*-RNAi or *Sox102F*-RNAi.

Scale bars: A-C = 40 μ m, E-G = 20 μ m.

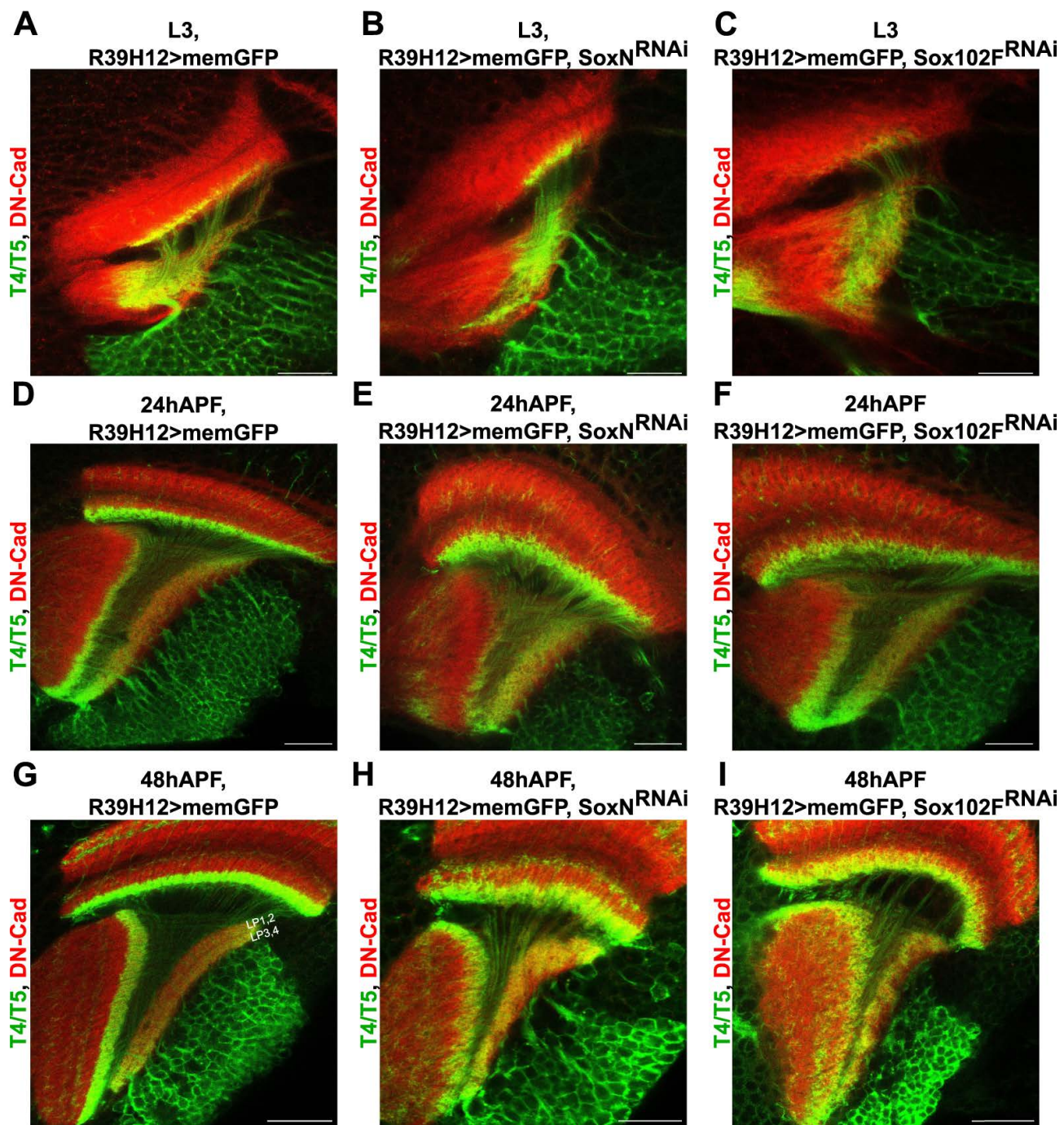


Figure S6. T4/T5 neuron morphology during development upon silencing *SoxN* and *Sox102F* with the *R39H12-Gal4* line.

(A-I) Dorsal views of optic lobes at late L3 larval stage, and at pupal stages 24 hours APF and 48 hours APF with wild-type T4/T5 neurons, and with T4/T5 neurons expressing *SoxN-RNAi* or *Sox102F-RNAi*.

Scale bars: A-C = 10 μ m, D-I = 20 μ m.

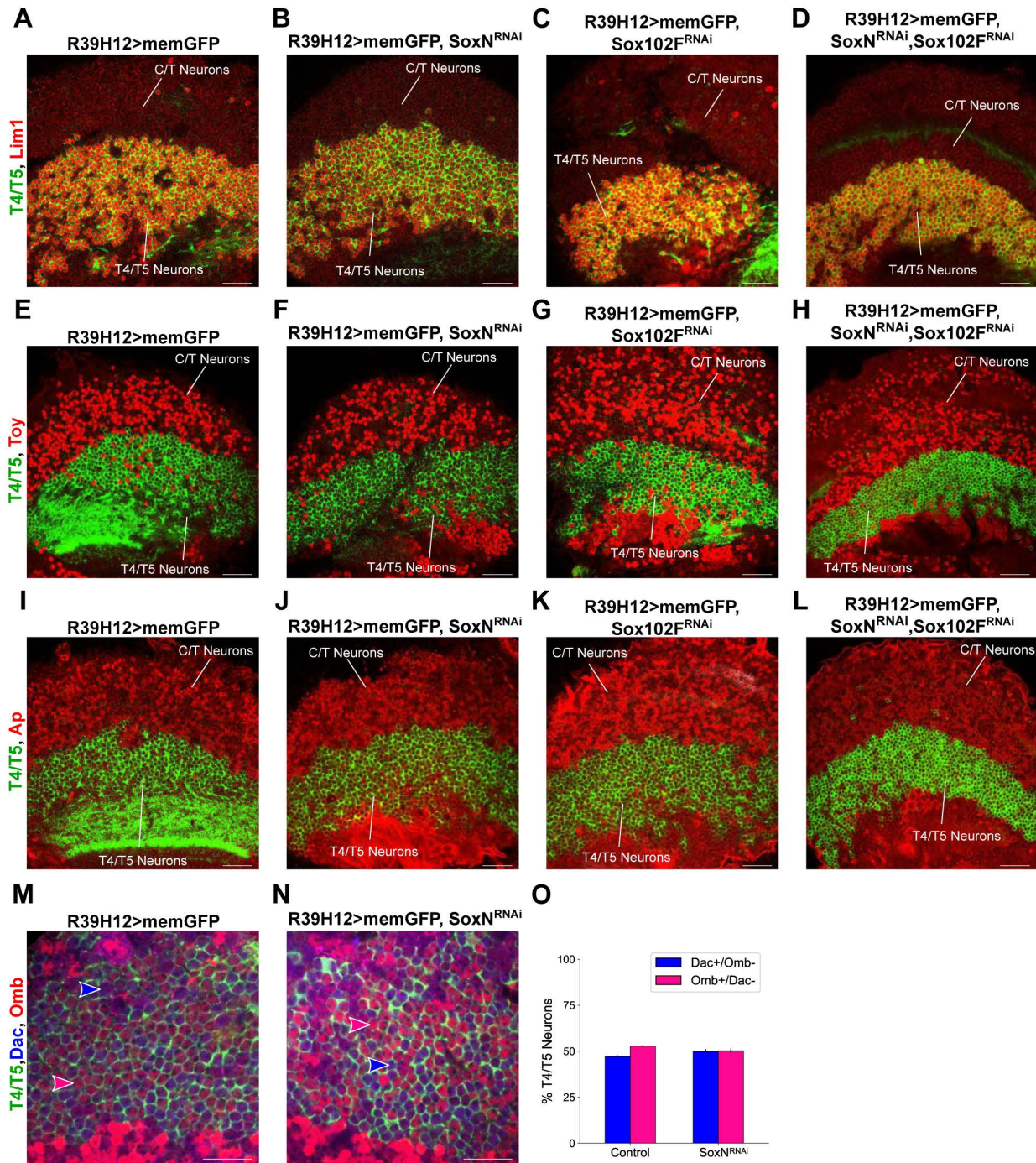


Figure S7. Lim1, Toy, Ap, Dac and Omb expression in optic lobes with wild-type T4/T5 neurons, and with T4/T5 neurons with *SoxN* and *Sox102F* silenced.

(A-L) Lim1, Toy and Ap expression in the region occupied by T4/T5 and C/T somata at adult stage. Wild-type T4/T5 somata, and somata from T4/T5 neurons expressing *SoxN-RNAi*, *Sox102F-RNAi*, or *SoxN-RNAi* and *Sox102F-RNAi* together were labelled with memGFP.

(M-O) Dac and Omb expression in adult, wild-type T4/T5 somata, and in adult, T4/T5 somata after knockdown of *SoxN*. Blue and magenta arrowheads indicate Dac^+/Omb^- and Dac^-/Omb^+ somata, respectively. The percentages of Dac^+/Omb^- (T4/T5_{a,b}) and Dac^-/Omb^+ (T4/T5_{c,d}) neurons in each condition are shown in O (n = 5 optic lobes per group, 150-200 somata examined per optic lobe).

Scale bars = 20 μ m.

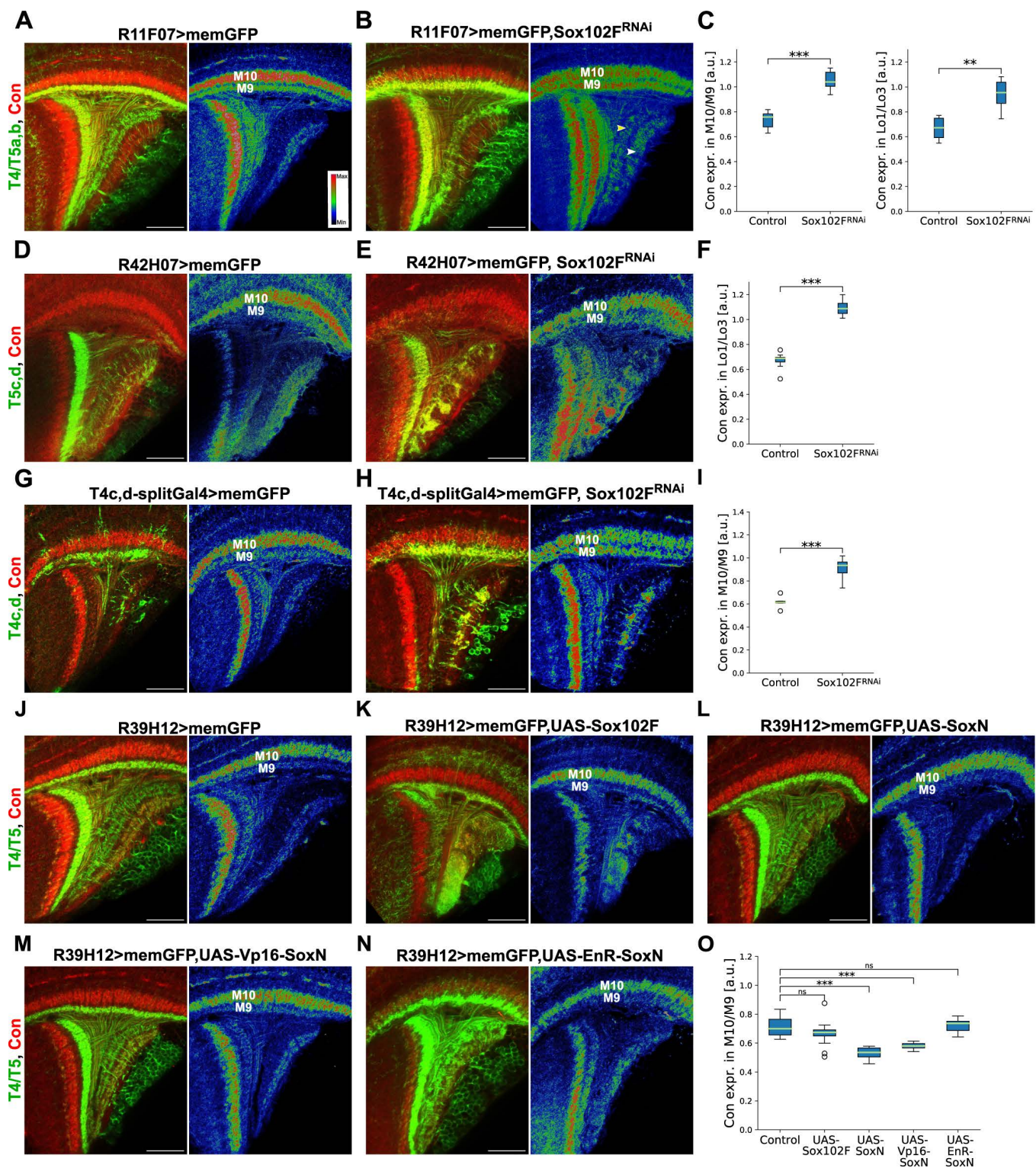


Figure S8. Connectin levels upon overexpression of SoxN or Sox102F in T4/T5 neurons, and upon silencing of SoxN or Sox102F in distinct T4/T5 neuron subtypes.

(A-C) Connectin expression in adult optic lobes with wild-type T4/T5a,b neurons, and with T4/T5a,b neurons expressing *Sox102F-RNAi*. Axons from T4/T5a,b neurons with *Sox102F* knockdown show similar Connectin levels (yellow arrowhead in B) than axons from wild-type T4/T5c,d neurons (white arrowhead in B). Ratios of Connectin signal in medulla layer M10 to Connectin signal in medulla layer M9, and ratios of Connectin signal in lobula layer Lo1 to Connectin signal in lobula layer Lo3 are shown in C (n = 8-13 optic lobes per group). The right panels show Connectin signals colour coded for intensity.

(D-F) Connectin expression in adult optic lobes with wild-type T5c,d neurons, and with T5c,d neurons expressing *Sox102F-RNAi*. Ratios of Connectin signal in lobula layer Lo1 to Connectin signal in lobula layer Lo3 are shown in F (n = 8-11 optic lobes per group).

(G-I) Connectin expression in adult optic lobes with wild-type T4c,d neurons, and with T4c,d neurons expressing *Sox102F-RNAi*. Ratios of Connectin signal in medulla layer M10 to Connectin signal in medulla layer M9 are shown in I (n = 6-8 optic lobes per group).

(J-O) Connectin expression in adult optic lobes with wild-type T4/T5 neurons, and with T4/T5 neurons overexpressing *Sox102F*, *SoxN* (wild-type version), *Vp16-SoxN* (obligatory activator version) or *EnR-SoxN* (obligatory repressor version). Ratios of Connectin signal in medulla layer M10 to Connectin signal in medulla layer M9 are shown in O (n = 7-14 optic lobes per group). ns, not significant ($P>0.05$); ** $P<0.01$; *** $P<0.001$.

Scale bars = 20 μ m.

Chapter 3

Discussion

Our understanding of the computation underlying direction selectivity of *Drosophila* optic lobe neurons has progressed quickly in recent years. Thanks to the more detailed connectomics data, the input neurons of the motion sensing T4 and T5 neurons are known as well as the localization and number of synapses on their dendrites (Takemura et al., 2017; Shinomiya et al., 2019). More sensitive and faster calcium detectors improved imaging methods, while the rapid rise in the quantity of GAL4 lines made even more specific neuron populations accessible (Pfeiffer et al., 2010; Tirian and Dickson, 2017). In addition, the increasing number of genetic methods enables different manipulations of *Drosophila* genes, proteins and neurons.

In the first publication included in this thesis, we could demonstrate that T4 and T5 are the first motion sensitive neurons in the visual pathway, with the four subtypes of T4 and T5 cells sensing rightward, leftward, upward and downward motion. In addition, we described T4 as the output of the ON pathway and T5 of the OFF pathway: while T4 cells respond to light increments, T5 cells are selective for light decrements. The second and third publications describe the behavioral effect of blocking T4 and T5 neurons. Without functional local motion sensing neurons, the flies are motion blind. These flies do no longer perform an optomotor response, but are still able to fixate a bar. In addition, T4 and T5 cells are important to detect expansion motion. Motion blind flies with blocked T4 and T5 output are unable to perform collision avoidance turns and landing responses, which are two behaviors dependent on looming detection. The last publication describes two transcription factors that are crucial for the proper development of T4 and T5 neuron morphology and function.

3.1 Direction Selectivity of T4 and T5 Neurons

While the functional properties of lobula plate tangential neurons of the horizontal and vertical system has been extensively studied, their input neurons T4 and T5 are almost too small for electrophysiological methods (but see Gruntman et al. (2018)). Anatomical studies in *Calliphora* described the connection between the bushy T4 cells and the lobula plate tangential cells (Strausfeld

and Lee, 1991). Blocking T4 and T5 cells with a specific GAL4 driver line confirmed their functional connection to lobula plate tangential cells (Schnell et al., 2012). The dendrites of T4 cells were described as spanning about eight columns, whereas their input neurons are unicolumnar (Strausfeld and Lee, 1991; Buschbeck and Strausfeld, 1997). Therefore, T4 cells were hypothesized to be the first direction sensitive neurons in the motion vision pathway (Douglass and Strausfeld, 2003). Their role was further examined by activity staining with the radioactive deoxyglucose technique: stimulation of fixed flies with a striped drum rotating only in one direction revealed a strong involvement of medulla layer 10 and lobula layer 1, the neuropil layers occupied by the T4 and T5 dendrites. The four lobula plate layers 1-4 were found to detect front-to-back, back-to-front, upwards and downwards motion, respectively (Buchner et al., 1984). Such an activity staining in mutant flies missing T4 and T5 cells further confirmed their role in motion detection. The lobula plate rudiment of these mutant flies showed no activity dependent staining, neither did the misguided lobula plate tangential cells (Bülthoff and Büchner, 1985). Therefore, the motion dependent activity staining of the lobula plate was suspected to visualize T4 and T5 cells.

A connection from the lamina monopolar cells L1 to T4 and from L2 to T5 was suggested (Bausenwein et al., 1992) after comparing the anatomy of the optic lobe neurons (Fischbach and Dittrich, 1989). Since L1 is an input cell to the ON and L2 to the OFF pathway (Joesch et al., 2010), a split of T4 and T5 neurons into ON and OFF sensitivity seemed likely. Electrophysiological recordings of T4 and T5 cells in a blow fly species, *Phaenicia sericata*, revealed that T4 cells depolarize in response to ON flicker, T5 in response to OFF flicker. Furthermore, T5 cells responded in a direction-selective way (Douglass and Strausfeld, 1996, 1995). However, these findings rest on recordings from a small number of cells with only two T5 and four T4 cells measured. In the first publication included in this thesis, we demonstrated that both T4 and T5 cells respond to visual motion in a direction-selective way by calcium imaging of T4/T5 activity. While T4 neurons detected moving ON edges, T5 cells detected moving OFF edges, with otherwise similar visual response properties.

What is the biophysical mechanism underlying the direction sensitive responses of T4 and T5 dendrites? The Hassenstein-Reichardt model (Hassenstein, 1951) uses enhancement of preferred direction by multiplication of two neighboring inputs, one of them temporally delayed. In comparison, the Barlow-Levick model (Barlow and Levick, 1965) suggests inhibition of the delayed signal to achieve direction selectivity, resulting in an inhibition of null direction. In the last years, several publications based on T4 or T5 activity concluded different mechanisms underlying their direction selectivity. Calcium imaging of sparsely labeled T4 and T5 cells indicated that the direction selectivity of T4 and T5 cells arises solely from preferred direction enhancement (Fisher et al., 2015). In contrast, another study imaging T5 cell activity reported two non linear mechanism: preferred direction enhancement and null direction suppression (Leong et al., 2016). A third study using whole cell patch clamp recordings of T4 activity found only evidence for null direction suppression (Gruntman et al., 2018). Sequential stimulation of single retina ommatidia with a telescope, while

imaging single axon units of T4c neurons in the lobula plate, suggested the involvement of both preferred direction enhancement and null direction suppression in motion detection (Haag et al., 2016). All T4 and T5 subtypes achieve direction selectivity by a combination of non linear preferred direction enhancement and null direction suppression (Haag et al., 2017). However, the biophysical mechanisms that give rise to these nonlinearities are likely to be different given the architectural and functional differences between T4 and T5 cells (see below).

The different conclusions about the origin of direction selectivity might stem from the varying stimulation conditions: Different stimulus size, timing and intensities could lead to a relative change in contribution of either preferred direction enhancement or null direction suppression.

3.1.1 Motion Detection in the T4 and T5 Dendrites

Electron microscopy studies completely reconstructing the T4 dendrites and all columnar neurons presynaptic to T4 depict an interesting anatomy: the dendrites of the four T4 subtypes are oriented along the axis of the neuron's null direction. The main input cells connect to distinct areas on the T4 dendrites. Mi1 and Tm3 connect to the middle part of the dendrite, whereas Mi4, C3 and CT1 build synapses on the base and Mi9 at the tips of the dendrite (Fig. 3.1 a) (Takemura et al., 2017; Shinomiya et al., 2019). The distribution of the inputs does not differ between the T4 subtypes, only the orientation of the dendrite. The neurotransmitters of the input cells are acetylcholine (Mi1 and Tm3), GABA (Mi4, C3 and CT1) and glutamate (Mi9), confirmed by antibody staining and RNA sequencing (Pankova and Borst, 2016; Takemura et al., 2017; Davis et al., 2018). In addition, T4 cells receive excitatory input from other T4 dendrites of the same subtypes (Shinomiya et al., 2019).

According to sequencing data of purified T4 cells, they express mRNA encoding for many different receptors (Pankova and Borst, 2016; Davis et al., 2018). The most highly expressed genes suggest that the GABAergic inputs activate a GABA-A receptor, which is a fast ionotropic receptor constituting a chloride channel (Fig. 3.1 b). Mi1 and Tm3 could depolarize T4 dendrites via nicotinic ACh receptors, while the most highly expressed glutamate receptor is another chloride channel, GluCl α . The glutamatergic input neuron, Mi9, is excited by OFF stimuli in contrast to the ON sensitive Mi1, Tm3 and Mi4 (Arenz et al., 2017). Therefore, an ON stimulation of a T4 dendrite would induce a release of Mi9 mediated inhibition. The input neurons differ in their temporal response properties: Mi1 and Tm3 act as fast band-pass filters whereas Mi9 and Mi4 are slow and more sustained (Arenz et al., 2017).

The input cells of T5 are distributed in a similar way. Tm1, Tm2 and Tm4 connect to the middle part of a T5 dendrite, CT1 to the base and Tm9 to the tips. As do T4 cells, T5 dendrites of the same subtypes connect to each other, likely enhancing the signal. In contrast to T4 dendrites, there is no glutamatergic input to T5. Tm1, Tm2, Tm4 as well as Tm9 are all cholinergic as they express *ChAT* and *VACHT*, only CT1 cells are GABAergic (Davis et al., 2018). While Tm9 could act as a low-pass filter, providing excitatory input at the dendritic tips, Tm1, Tm2 and

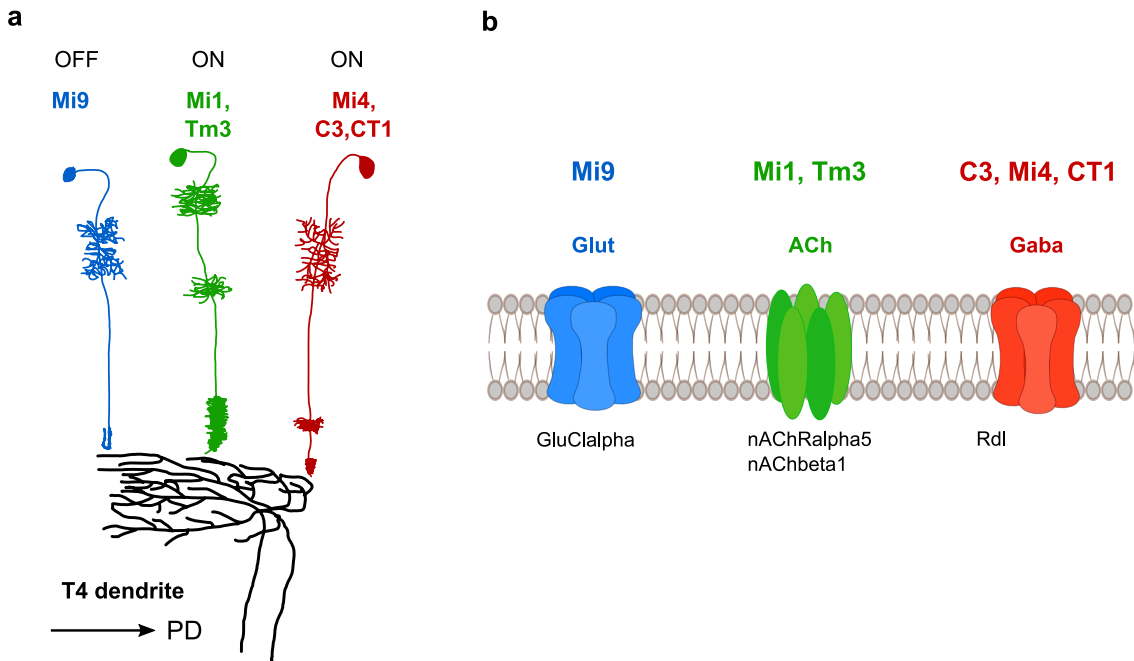


Figure 3.1: Inputs on the T4 Dendrite

a The main input cells to the T4 dendrites are Mi4, C3 and CT1 at the base of the dendrite, Mi1 and Tm3 in the middle area and Mi9 at the dendrite tips. b While Mi4, C3 and CT1 are GABAergic, Mi1 and Tm3 are cholinergic and Mi9 is glutamatergic. T4 cells highly express genes encoding GABA-A receptors, nicotinic ACh receptors and the glutamate receptor GluCl α (Pankova and Borst, 2016; Davis et al., 2018).

Tm4 respond like band-pass filters (comparable to Mi1 and Tm3) (Arenz et al., 2017). Since there is no sign inversion and Tm9 is OFF sensitive, the mechanism underlying preferred direction enhancement probably differs between T4 and T5. Tm9 is likely to provide slow, excitatory signals enhancing the fast signals provided by Tm1 and Tm2. In combination with, for example, voltage gated calcium channels, this could result in preferred direction enhancement.

A possible null direction suppression on T5 dendrites could only be mediated by the GABAergic CT1 neuron. So far, there is no functional data of CT1 published, leaving its temporal properties unknown. In contrast to the other, unicolumnar input neurons, CT1 is a multicolumnar amacrine cell with each columnar compartment being both pre- and postsynaptic (Shinomiya et al., 2019). Compared to T4, CT1 builds more synapses onto the dendrites of T5, possibly to maintain excitation/inhibition balance in the absence of other significant inhibitory inputs. CT1 receives input from Mi1, Mi9 and T4 in the medulla and from Tm1, Tm9 and T5 in the lobula. Other inhibitory neurons, namely TmY15, LT33 and Tm23, might provide a surround inhibition to T4 and T5.

The expression of receptor genes is very similar between T4 and T5 cells (Davis et al., 2018). The most highly expressed receptor genes in T5 cells encode a subunit of the nicotinic ACh receptor (a cation channel), a GABA-A receptor (a chloride channel) and the glutamate receptor GluCl α

(a chloride channel). Since the T5 dendrites do not receive glutamatergic input, the glutamate receptor might play a role in the axons or axon terminals.

T4 and T5 cells both express RNA encoding different ionotropic as well as metabotropic GABA, ACh and glutamate receptors (Pankova and Borst, 2016; Davis et al., 2018), however, data about the protein expression and localization is still missing. Specific antibody staining can prove receptor expression, without an available antibody, protein-trap lines using MiMIC or PBac insertions to induce a tagged endogenous protein can help to visualize a receptor (Venken et al., 2011; Quiñones-Coello et al., 2007). Due to the dense T4/T4 and T5/T5 network with many overlapping dendrites, localization of receptors could only be shown by labeling the receptor in sparse cells. For example, expression of a tagged receptor in a single cell could demonstrate, if the cell localizes the receptor exclusively to one dendritic compartment. Blocking receptors by application of an antagonist, while recording from a T4/T5 cell, might help to explore the functional role of the different receptors. Another possibility is to silence receptor genes by RNAi or by inducing a CRISPR knockout and subsequently perform calcium imaging or patch-clamp recordings from T4/T5 cells. Similarly, input neurons could be activated or silenced optogenetically while recording from T4/T5. Since blocking only one receptor might not prevent direction selectivity of T4/T5 cells, it might be necessary to record from single cells or stimulate single ommatidia, to measure preferred direction enhancement and null direction suppression.

3.1.2 Hassenstein-Reichardt/Barlow-Levick Detector

The compartmentalization of the T4 and T5 dendrites suggests, that the direction selectivity arises from at least three main input signals. A possible motion detection model using three input arms is the Hassenstein-Reichardt/Barlow-Levick (HR/BL) model, a combination of the Hassenstein-Reichardt and the Barlow-Levick model. The Barlow-Levick model achieves direction selectivity by a null direction inhibition mechanism: division of a fast signal by a delayed signal (Fig. 3.2 a). In contrast, the Hassenstein-Reichardt detector is based on preferred direction enhancement by multiplication of a fast with a temporally delayed signal (Fig. 3.2 b). The HR/BL detector uses two delayed input and combines both preferred direction enhancement and null direction suppression (Fig. 3.2 c). This results in a sharper directional tuning over a wider range of temporal frequencies (Arenz et al., 2017; Borst, 2018).

A cellular implementation of a motion detector for a T4 dendrite could be a three arm input model (Fig. 3.2 d). The preferred direction enhancement is provided by the combination of a delayed release from inhibition (Mi9 input) with a fast excitation (Mi1, Tm3 input). A delayed inhibition at the dendrite's base results in null direction inhibition. While Mi4 was demonstrated to have low-pass filter characteristics, functional data of CT1 and C3 are still missing. A model, in which a T4 dendrite carries out a multiplication of the sign-inverted low-pass input from the Mi9 and the input from Mi1, followed by a division by the Mi4 signal, demonstrated a strong directional tuning (Arenz et al., 2017). An inhibitory, slow OFF input could enhance an ON motion response

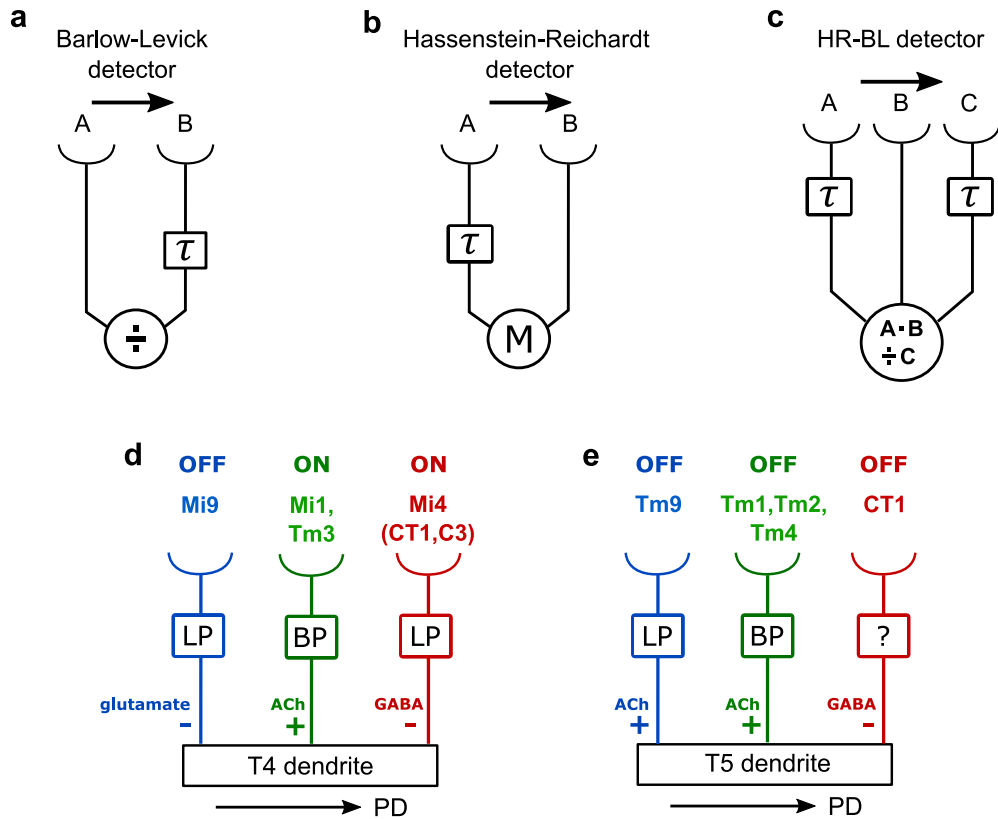


Figure 3.2: The HR/BL Detector: A Combination of Hassenstein-Reichardt and Barlow-Levick Detector. **a** The Barlow-Levick as well as the Hassenstein-Reichardt detector **b** each use two inputs, one of them temporally delayed. While the Barlow-Levick detector achieves direction selectivity by suppression of a null direction response, the Hassenstein-Reichardt detector performs an enhancement of the preferred direction by multiplying the delayed signal with the direct signal. **c** A combination of both, the HR/BL detector combines preferred direction enhancement with null direction suppression. Arrows point in the preferred direction. **d** The T4 dendrite: a combination of slow, sustained release from inhibition and fast excitation could provide preferred direction enhancement. Temporally delayed inhibition at the null direction side could result in null direction suppression. **e** The T5 dendrite: a multiplication like non-linear enhancement of the slow Tm9 signal with the fast Tm1, Tm2 and Tm4 signal, together with a null direction inhibition provided by CT1, could result in direction selectivity of T5 dendrites.

to the preferred direction: The release from inhibition would increase the input resistance (Borst, 2018), resulting in an enhanced response to the excitatory signal from Mi1 and Tm3. Even with a passive dendrite, this results in preferred direction enhancement (Borst, 2018). In addition, a low-pass filter inhibition at the dendritic base, provided by the GABAergic C3, Mi4 and CT1 cells, would result in a null direction suppression. The connections between T4 neurons of the same subtypes could further enhance the preferred direction signal, though the number of T4 to T4 synapses is low (Shinomiya et al., 2019). A nonlinear enhancement of preferred direction excitation

could also be biophysically implemented by voltage gated channels (Magee and Johnston, 2005).

A similar three arm detector, using a slow Tm9 and fast Tm1, Tm2 and Tm4 signal divided by a possibly delayed CT1 signal, is suggested for T5 dendrites (Shinomiya et al., 2019). A multiplication like nonlinearity between a delayed excitatory input (Tm9 signal) and fast excitatory inputs (Tm1, Tm2 and Tm4 signal) induces preferred direction enhancement. A shunting inhibition by a delayed input at the dendrites base induces null direction inhibition (Fig. 3.2 e). As for the temporal properties of the CT1 signal, a possible low-pass characteristic remains speculative.

3.1.3 Direction Selective Cells in the Mouse Retina

Another prominent model to study visual motion detection is the mouse retina. While the visual system in the mouse evolved independent from the visual system of flies, the composition of the circuit and the computation of the neurons are partly comparable (Borst and Helmstaedter, 2015). There are two types of direction-selective cells in the mouse retina, the starburst amacrine cells and the direction-selective retinal ganglion cells. The first direction-selective cells in the motion pathway of the retina are the starburst amacrine cells, their dendrites respond to outwards motion (relative to the soma) (Euler et al., 2002). The starburst amacrine cells have widely overlapping dendritic fields and connect to each other; their dendrites are both pre- and postsynaptic and release GABA as well as ACh as neurotransmitters.

Several mechanisms are currently discussed to generate direction selectivity in starburst amacrine cells. First, a spatial distribution of the excitatory and inhibitory inputs on their dendrites: Starburst amacrine cells receive excitatory input from bipolar cells and inhibitory input from other oppositely tuned starburst amacrine cells. The inhibitory, GABAergic synapses are located in the proximal third of their dendrite (Fig. 3.3 a) (Ding et al., 2016). Second, the excitatory bipolar input cells differ in their temporal properties and are distributed on the starburst amacrine dendrite in such a way, that the inputs connecting to the distal part of the dendrite are faster and more transient compared to the inputs connecting to the proximal part (Fig. 3.3 b) (Fransen and Borghuis, 2017). Hence, a sequential activation of the bipolar cells induces a preferred motion response of the starburst amacrine cell. Third, intrinsic properties of the dendrite can influence the direction selectivity. The proximal and distal localization of two different chloride transporters affects the influence of GABAergic inhibition in starburst amacrine cells (Gavrikov et al., 2006). Moreover, voltage gated calcium channels are suggested to induce nonlinear effects (Hausselt et al., 2007).

However, both the inhibitory and the excitatory network are sufficient to induce direction-selective output of starburst amacrine cells (Hanson et al., 2019). In addition, their direction selectivity is not dependent on GABAergic inhibition (Euler et al., 2002; Hanson et al., 2019). The different mechanisms might work together to ensure a strong directional sensitivity over a wide range of contrasts, luminance, and velocity of the visual input.

In a similar way, the direction selectivity of retinal ganglion cells arises from more than one mechanism. The direction-selective retinal ganglion cells are postsynaptic to bipolar cells and

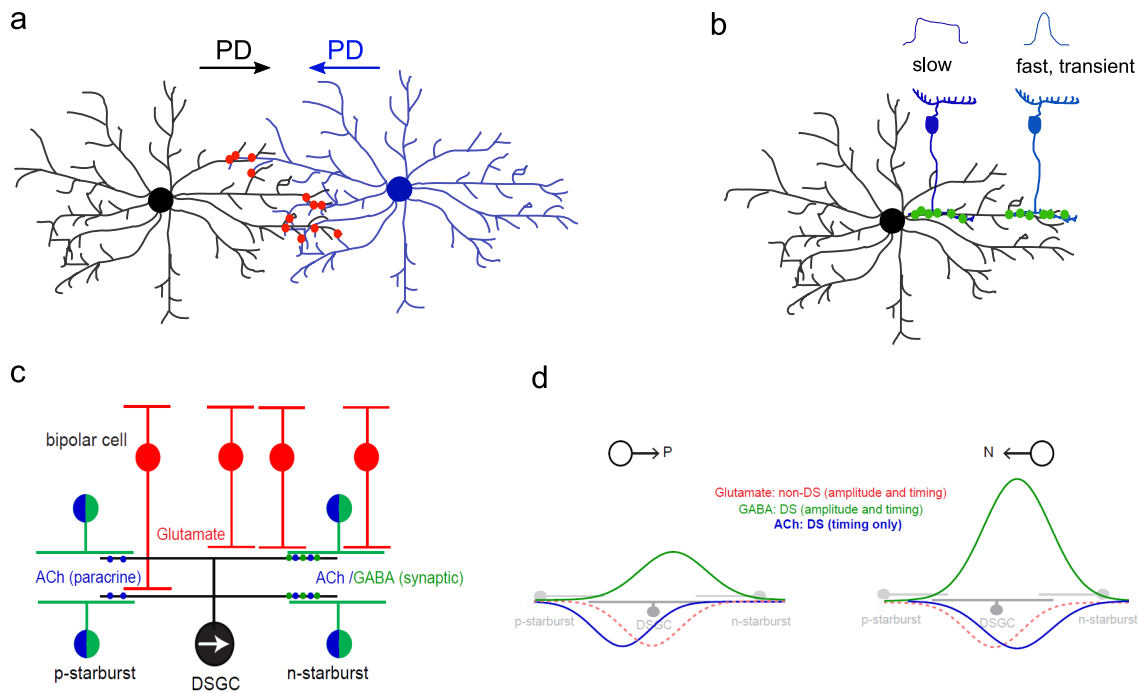


Figure 3.3: Direction Selectivity in the Mouse Retina

a Starburst amacrine dendrites tuned to the opposite direction connect to the distal part of the starburst amacrine dendrite, therefore providing null direction inhibition. **b** The excitatory input from bipolar cells is temporally different from the somatic to the distal area of the starburst amacrine dendrite, enhancing signal in the preferred direction. **c** The bipolar cells provide glutamatergic, non-directional input to the direction-selective retinal ganglion cell (DSGC). Starburst amacrine cells are GABAergic and cholinergic. While their excitatory synapses are located symmetrically on the dendrite, the GABAergic inhibition is located at the null direction side. **d** Temporal differences between inhibition and excitation could result in direction selectivity even without directional inhibition of the amacrine cells. **c** and **d** Images modified from Hanson et al. (2019).

starburst amacrine cells. The bipolar cells provide glutamatergic, excitatory input and the amacrine cells provide both inhibitory, GABAergic and excitatory, cholinergic input. The bipolar cells are not direction-selective, whereas the amacrine cells provide direction-selective input (Park et al., 2014). The input of the starburst amacrine cells provides a null direction inhibition through specific wiring: the cholinergic input from starburst amacrine cells is distributed symmetrically on the dendrite of the direction-selective retinal ganglion cell. In contrast, the direction-selective retinal ganglion cells receive inhibitory input from starburst amacrine cells with their soma at the null side of the receptive field of the retinal ganglion cell (Fig. 3.3 c) (Briggman et al., 2011). This wiring ensures a null direction inhibition. A recent paper suggested an additional mechanism to evoke direction-selectivity in retinal ganglion cells, since they still respond in a direction-selective way without directional inhibition from starburst amacrine cells. In addition to the null direction inhibition provided by starburst amacrine cells, differences in the onset latency between excitation

and inhibition induces direction selectivity (Fig. 3.3 d) (Hanson et al., 2019).

3.1.4 Comparison of DS Cells in the Mouse Retina and the Fly Optic Lobe

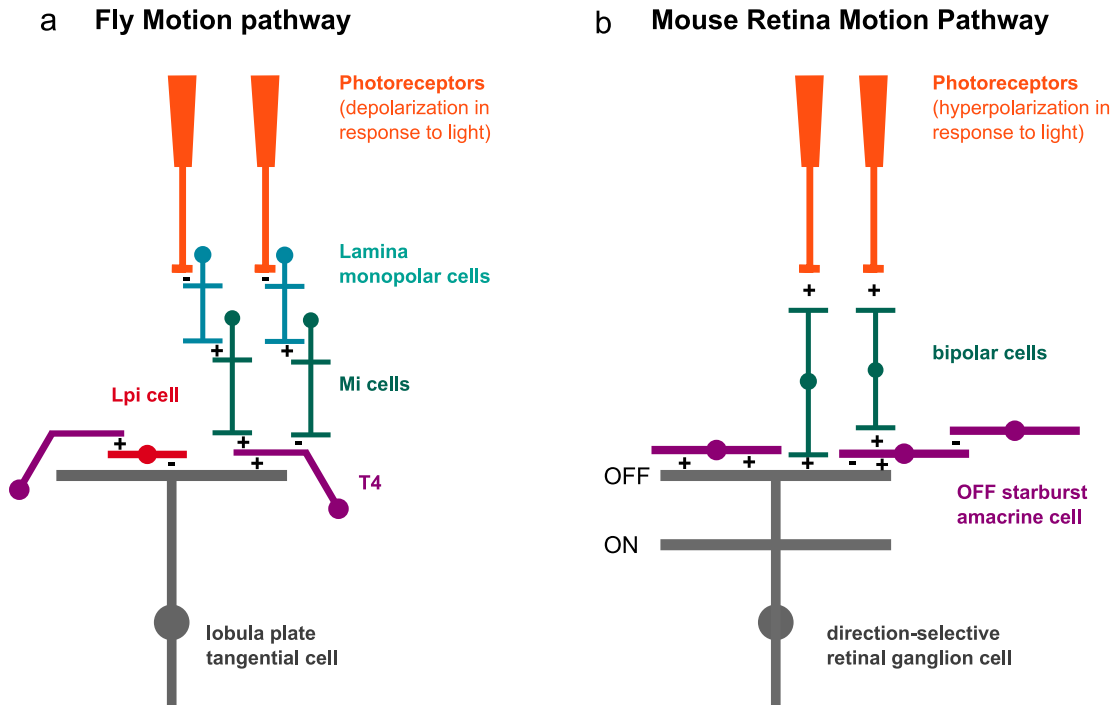


Figure 3.4: Comparison of the Fly and Mouse Motion Vision Pathway.

a Fly photoreceptors depolarize in response to light, but the lamina monopolar cells invert the signal. The medulla Mi and Tm cells are sensitive to either ON or OFF signals and differ in their temporal properties. Medulla cells with slower or faster temporal properties connect to different parts of the T4 or T5 dendrites, enabling their direction selectivity. T4 and T5 cells provide direction-selective, excitatory input to lobula plate tangential cells. In addition, T4 and T5 cells connect to lobula intrinsic cells, which provide null direction inhibition to lobula plate tangential cells. **a** In contrast to invertebrates, vertebrate photoreceptors hyperpolarize in response to light. The bipolar cells are subdivided in ON and OFF sensitive cells, similar to the medulla Mi and Tm cells of flies. The bipolar cells also differ in their temporal tuning properties, different subtypes connect to the more distal or proximal part of the starburst amacrine cell dendrites. Similar to T4 and T5 cells, the direction selectivity of starburst amacrine cells arises from both preferred direction enhancement and null direction suppression. They provide both inhibition and excitation to direction-selective retinal ganglion cells, with localized inhibitory synapses but more distributed excitatory synapses.

Comparing the fly optic lobe to the mouse retina, the photoreceptor input to the system differs substantially: while invertebrate photoreceptors depolarize in response to light, vertebrate photoreceptors hyperpolarize. However, the signal of the fly photoreceptors becomes inverted at the level of lamina monopolar cells via histamine gated chloride channels. Thus, on the level of

lamina monopolar cell output and the vertebrate photoreceptor output, the signals in the fly optic lobe and the vertebrate retina are OFF sensitive. Similar to the fly visual system, ON and OFF sensitive cells exist in the mouse retina (Stell et al., 1977); the bipolar cells as well as the starburst amacrine cells are either ON or OFF sensitive. The medulla Mi and Tm cells in the fly brain are comparable to the bipolar interneurons in the retina (Fig. 3.4). Both exist in ON and OFF sensitive subtypes and they are not direction-selective. The subtypes of bipolar cells but also Tm and Mi cells differ in their temporal response properties. Therefore, they enable preferred direction enhancement or null direction suppression in their postsynaptic neurons (Baden et al., 2013; Arenz et al., 2017).

The first direction-selective cells are the T4/T5 neurons in the fly optic lobe and the ON/OFF starburst amacrine cells in the mouse retina. The direction selectivity of T4 cells most likely originates from different mechanisms: release from inhibition together with fast excitation can enhance preferred direction response. In addition, slow inhibition at the dendritic base can inhibit responses to motion in the null direction. Starburst amacrine cells also combine null direction inhibition and preferred direction enhancement. The four different subtypes of T4 cells detect motion in the four cardinal directions and their dendrites are oriented towards the null direction of the cell. In the mouse retina, one amacrine cell with a symmetrical dendrite detects motion in all directions: the dendrite is sensitive to motion in the direction from proximal to distal (Euler et al., 2002).

Comparable to T4 dendrites, the starburst amacrine cells receive inhibition at their null direction onset side. However, starburst amacrine cells connect to each other with dendrites tuned to the opposite direction inhibiting the distal dendritic area (Lee and Zhou, 2006), while T4 cells receive non-directional inhibition. T4 cells of the same subtype connect to each other and likely enhance the response to motion in the preferred direction.

Starburst amacrine cells provide both excitation as well as a null direction inhibition to the direction-selective retinal ganglion dendrites. In contrast, T4/T5 cells are only cholinergic and excitatory, nevertheless they connect to bistratified, glutamatergic lobula plate intrinsic cells. These cells are postsynaptic to T4/T5 in one lobula plate layer and presynaptic to lobula plate tangential cells in the oppositely tuned layer (Mauss et al., 2015). Therefore, T4/T5 indirectly provide null direction inhibition to the lobula plate tangential cells, comparable to starburst amacrine cells.

3.2 Object Orientation

Information about local luminance changes could be used for different tasks: to find attractive objects and fly or walk towards them, to orient according to the position of a visual landmark or to detect the position of a potential predator and avoid it. While all these behaviors require motion vision, the detection of the position of objects is equally important.

Closed-loop fixation behavior of flies as well as their turning reaction to local motion can be explained by an asymmetric front-to-back than back-to-front motion response (Reichardt, 1973; Götz, 1975). However, such an asymmetric motion response fails to explain the strongly position dependent turning response of houseflies towards pure flicker stimuli (Pick, 1974). Several studies suggested that fly orientation towards local objects can be mediated without motion vision. Laser ablation of lobula plate tangential cells in houseflies reduced their optomotor response, but the flies could still orient towards single objects (Geiger and Nässel, 1981). Similar experiments were performed with the motion blind *Drosophila* mutant *omb* and the double mutant *rol sol*. These flies have difficulties following whole field motion, but react to landmark position (Bausenwein et al., 1986; Wolf and Heisenberg, 1986). This indicated, that a motion independent position system exists in the fly visual system, which is involved in object orientation behavior. Following this idea, Reichardt and Poggio (1976) described the turning response of *Drosophila* to a vertical bar moving around a fixed fly as the sum of a symmetrical motion response and a position dependent response.

We used a specific driver line to block the synaptic output of T4 and T5 cells by overexpression of shibire^{ts}. These flies were not able to perform an optomotor response, which confirmed that they are motion blind. Nevertheless, the T4/T5 blocked flies could fixate a vertical bar, albeit weaker than control flies. Presenting a rotating bar in an open-loop experiment demonstrated, that motion blind flies do respond to the position of the bar, but not to the direction of the bar motion. The motion blind flies reacted the same way to a flicker stimulus (a vertical bar appearing and disappearing) presented at different positions as control flies. To compare the flicker response with the response to local motion, we presented three stimuli with the same luminance change: a lateral bar moving locally in front-to-back direction, a lateral bar moving in back-to-front direction and a lateral appearing bar. While control flies reacted strongest to the front-to-back motion and weakest to the back-to-front motion, T4/T5 blocked flies did not distinguish between the three conditions. Therefore, flies are able to observe the position of luminance changes without functional T4/T5 cells, but not the direction of motion. We concluded, that the fixation behavior of flies is dependent on a motion-independent position system in combination with a symmetrical motion response. The position system induces strong reactions to local luminance changes at a lateral position.

Another study testing the dependence of flight fixation behavior on T4/T5 cells confirmed our results when using a low gain feedback in the closed-loop fixation, that means flight turns induce slow movements of the bar. However, the T4/T5 blocked flies were not able to fixate a bar under high feedback gain closed-loop conditions or with additional background motion (Fenk et

al., 2014). The bar fixation they found under low gain feedback conditions is very weak compared to the fixation we measured with walking flies. The lower fixation could arise from differences between walking and flight behavior. An alternative explanation would be an effect of the GAL4 driver line on the flight behavior. We found the T4/T5 driver line used by Fenk et al. (2014) to drive expression in motor neurons important for flight (data not published). Therefore, we used a more specific split-GAL line to block T4/T5 cells when measuring flight behavior (see the third manuscript included in this thesis). The impairments in flight could reduce the fixation ability of the flies and explain the weak flight fixation under all conditions.

In contrast to our results describing symmetric motion responses, Fenk et al. (2014) suggested the fixation behavior to rely on asymmetric motion responses of the horizontal system lobula plate tangential cells. A clarifying experiment could be to test fixation behavior while blocking the output of horizontal system lobula plate tangential cells. For example, expression of the light gated anion channel GtACR was shown to hyperpolarize these cells during illumination (Busch et al., 2018). However, depolarization as well as hyperpolarization of the horizontal system lobula plate tangential cells induced flies to walk slower (Busch et al., 2018), therefore blocking these cells directly might interfere with a fixation behavior.

A cellular implementation of a position system could be T4/T5-independent input to the lobula plate or a pathway from the medulla to the lobula. Lobula plate tangential cells do respond to local flicker without a T4/T5 input, but partly dependent on the medulla neurons Mi1 and Tm3 (Bahl et al., 2015). So far, no T4/T5 independent input to lobula plate tangential cells is described. Since many medulla cells project to the lobula and connect to lobula columnar cells, the cellular implementation of object recognition could be lobula columnar cells. For example, LC11 cells react specifically to small objects (Keleş and Frye, 2017; Wu et al., 2016). Such cells might receive information about local luminance changes directly from the medulla and additional motion information from the lobula plate. Therefore, lobula columnar cells might enable flies to react to local flicker without functional T4/T5 cells.

3.3 Looming Detection in *Drosophila*

Detection of expansion motion can elicit different behaviors in *Drosophila*. During flight the flies can respond with avoidance turns or a landing response, while walking flies react with an escape jump. The flight avoidance turns as well as landing responses were suggested to depend on Hassenstein-Reichardt type motion detectors (Borst and Bahde, 1986; Reiser and Dickinson, 2013). This indicates, that T4 and T5 cells are important for avoidance flight turns and landing behavior.

We characterized the avoidance turns of fixed flying *Drosophila* using different looming stimuli. The flies avoided dark and bright approaching objects at a lateral position, over a wide range of velocities. The avoidance behavior was not dependent on the overall luminance change, but on opposing motion in at least two directions. We found the output of T4 and T5 cells to be

essential for the avoidance turns of flying *Drosophila*. Moreover, flies with blocked T4 and T5 cells were unable to perform a landing response, elicited by a frontal looming stimulus. Therefore, we suspected that descending neurons involved in avoidance turns and landing behavior receive direct or indirect input from T4/T5.

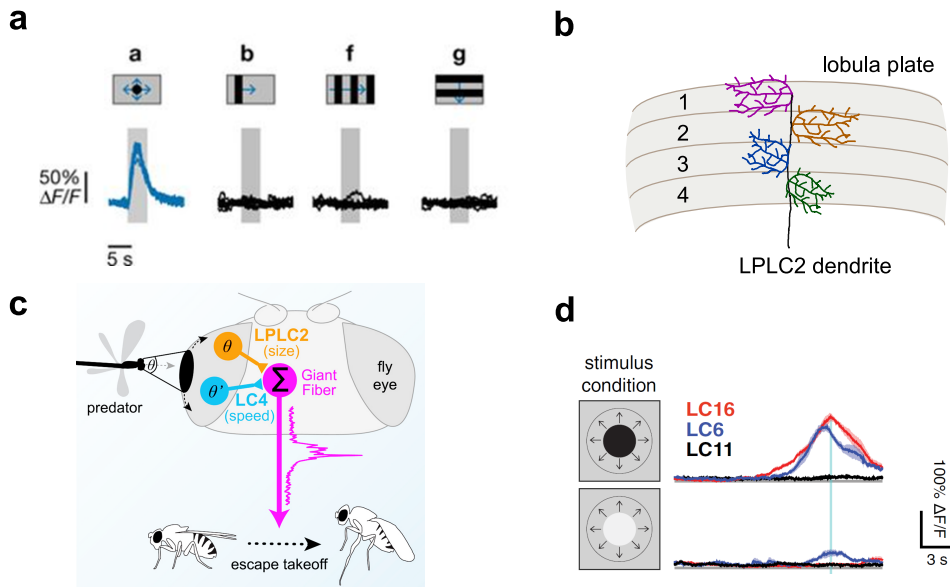


Figure 3.5: Looming Sensitive Neurons

a Calcium imaging of LPLC2 neurons reacting to looming but not to a moving bar or wide-field motion. Image modified from Klapoetke et al. (2017). b The dendritic arms of a LPLC2 neuron in the four lobula plate layers are oriented in four directions. c LC4 and LPLC2 are the main inputs to the giant fiber with LC4 encoding angular velocity and LPLC2 encoding angular size of a looming stimulus. Image modified from Ache et al. (2019). d Calcium imaging of LC16, LC6 and LC11 with a dark and a bright looming stimulus, LC6 and LC16 react strongly to dark looming. Image modified from Wu et al. (2016).

Looming sensitive neurons postsynaptic to T4/T5 cells were found in the *Drosophila* lobula plate, namely the lobula plate/lobula columnar, type II or LPLC2 cells. Optogenetic activation of LPLC2 cells induced escape jumps or backward walking (Wu et al., 2016). The LPLC2 neurons respond specifically to looming stimuli, but not to whole-field motion or moving objects (Fig. 3.5 a) (Klapoetke et al., 2017). These neurons react strongly to outward motion in at least two of the cardinal directions, i.e. upwards and downwards motion, but are inhibited by inward motion. The inhibition is provided by Lpi neurons (Klapoetke et al., 2017). The LPLC2 neurons collect input from the four lobula plate layers and the lobula layers Lo3 to Lo5. The dendrites in the lobula plate have a striking morphology: four dendritic arms reach into every lobula plate layer, with the dendritic arms pointing in four different directions (Fig. 3.5 b) (Klapoetke et al., 2017). Their axons project into the central brain, where LPLC2 neurons synapse on the giant fiber descending neuron (Fig. 3.5 c) (Klapoetke et al., 2017; Ache et al., 2019). The giant fiber

is important to elicit short-duration, undirected escape jumps (von Reyn et al., 2014). Silencing LPLC2 neurons impairs such fast escape jumps (von Reyn et al., 2017; Ache et al., 2019). The giant fiber receives information from two main input cell types, LPLC2 and LC4. The LPLC2 neurons provide excitatory information about the angular size of a looming stimulus to the giant fiber and LC4 provides information about the angular velocity (Ache et al., 2019).

Descending neurons important for avoidance turns and landing responses could receive their input from LPLC2, since no other neurons postsynaptic to T4/T5 and sensitive to looming stimuli are known so far. There is no knowledge about additional neurons postsynaptic to LPLC2 besides the giant fiber, which could mediate avoidance turns or landing responses. Schnell et al. (2017) described a descending neuron responsive to looming stimuli and important for fast, saccade like turns during flight. This neuron could be important for collision avoidance turns, but the input neurons providing looming sensitive information are not known yet. Descending neurons important for avoidance turns, landing behavior or slow escape jumps might receive information about expansion motion from both, T4/T5 dependent and independent neurons.

3.3.1 Looming Sensitive Cells in the Lobula

Optogenetic activation of different lobula columnar cells induced avoidance behavior: activation of LC6, LC15, and LC16 resulted in escape jumps or backward walking of the flies (Wu et al., 2016). Similar to the giant fiber input LPLC2, the lobula columnar cells LC6 and LC16 are looming sensitive (Fig. 3.5 d) (Wu et al., 2016). LC6 and LC16 dendrites overlap in the lobula layers 4 to 6, and their axon terminals project to the same region in the central brain (Wu et al., 2016; Panser et al., 2016). In contrast to the giant fiber and its input neurons, blocking LC6 neurons reduced the proportion of long-duration escape jumps after looming stimulation (Williamson et al., 2018). This suggests the LC6 plays a role in the detection of slow expansion motion. However, a descending neuron mediating short-duration, targeted escape jumps is not found yet. While LPLC2 receives input from the lobula plate and the lobula, the dendrites of the different lobula columnar cells are restricted to the lobula. LC4 and LC6 both detect looming stimuli (Wu et al., 2016; von Reyn et al., 2017), likely without a T4/T5 dependent input.

Next to LPLC2, there is another neuron that receives input from T4 and T5 cells, the lobula plate/lobula columnar, type I or LPLC1. Since optogenetic activation of these cells strongly induced jumps, they are likely involved in avoidance behavior. The location of their axon terminals suggest, that they could connect to the giant fiber (Panser et al., 2016).

Reconstruction of electron microscopy data (Zheng et al., 2018) will reveal the connectivity between lobula neurons and descending neurons in the central brain. In addition, calcium imaging of the different lobula columnar neurons and also LPLC1 will clarify which neurons detect expansion motion. Blocking such neurons or activating them with optogenetic tools while measuring flight behavior could help to identify neurons involved in avoidance turns and landing behavior. More than 100 descending neurons are described anatomically (Scott et al., 2018) in *Drosophila* and

driver lines for these neurons are available. With functional and anatomical data about lobula neurons and descending neurons in the central brain, the neuronal circuits underlying the different looming evoked behaviors will be solved.

3.3.2 Comparison to Looming Sensitive Neurons in other Arthropod Species

While it seems important for most animals to detect approaching objects, the induced behavior can differ substantially. An escape jump to avoid predators is only reasonable for an animal that is able to fly, while others might prefer not to move at all and rely on mimicry. Therefore, very different looming detecting neurons and subsequent descending neurons might have evolved for different arthropod species. While flies and locusts jump into the air, crabs escape walking and constantly adapt their direction and velocity during their escape (Oliva and Tomsic, 2012). While the looming detecting neurons of different arthropods differ in their anatomy and computations, there are some similarities: looming sensitive descending neurons receive input about angular velocity and angular size of the looming stimulus, resulting in a peak firing at the time before collision. Such a computation is performed by the lobula neuron LGMD of the locust, a lobula neuron in the crab *Neohelice*, and the giant fiber of *Drosophila* (Gabbiani et al., 1999; von Reyn et al., 2017; Oliva and Tomsic, 2014).

The input neurons of the locust LGMD neuron are supposed to detect information about local luminance change, not local motion (Jones and Gabbiani, 2010). A similar input is proposed for looming sensitive lobula neurons of the crab *Neohelice* (Oliva and Tomsic, 2014). In contrast, we found two different *Drosophila* behaviors elicited by looming stimuli to depend on the local motion sensing T4 and T5 cells. In addition, the looming sensitive LPLC2 cells postsynaptic to T4 and T5 cells were demonstrated to be a main input to the giant fiber (Ache et al., 2019). Other looming sensitive neurons in the lobula of *Drosophila*, like LC6 cells, likely detect looming stimuli through a different mechanism. Since the giant fiber receives input from lobula columnar cells and from the T4/T5 dependent LPLC2 neurons, one cell type providing angular velocity related input and the other angular size related, different looming computations might work in parallel to ensure an optimal avoidance reaction. A large cell spanning over the lobula like the LGMD does not exist in *Drosophila*. Nevertheless, looming detection based on different inputs, either sensing local motion or local luminance changes, might be conserved across arthropod species.

3.4 Differentiation of T4 and T5 Cells

The dendrites of T4 and T5 cells ramify in different neuropils; while the dendrites of the ON T4 cells are located in the medulla, the dendrites of the OFF sensitive T5 cells are located in the lobula. Both cell types have four subtypes, each one targets one layer in the lobula plate. There, the T4 and T5 subtypes connect to different lobula plate tangential cells, dependent on the lobula plate layer. Apart from these specializations, all T4 and T5 cells have some common morphological

properties. First, their dendrites and axon terminals are restricted to single neuropil layers. Second, their dendrites are oriented towards the neuron's null direction. Third, the synapses with their main input cells are distributed on three compartments on the T4 and T5 dendrites (Shinomiya et al., 2019). These common characteristics are thought to be crucial for their functional role as elementary motion detectors. How are the common characteristics established during development?

T4 and T5 cells arise from the same neuroblasts, which are defined by expression of Dachshund and Atonal (Apitz and Salecker, 2015, 2018). Both are essential for the differentiation of T4 and T5 cells (Oliva et al., 2014; Apitz and Salecker, 2018). We found two transcription factors, SoxN and Sox102F, to be highly expressed in all T4/T5 subtypes. The expression starts in the young, postmitotic neurons and is continued in the adult neurons, with SoxN activating the expression of Sox102F. We could further demonstrate, that the expression of SoxN and Sox102F depends on the neuroblast transcription factors Atonal and Dachshund with one of them being sufficient to induce SoxN and Sox102F expression. SoxN and Sox102F control the development of T4/T5 morphology and function. In late larval and young pupal brains with SoxN or Sox102F knockdown, we found correctly located T4/T5 cells in the developing medulla, lobula and lobula plate. We conclude that SoxN and Sox102F are not essential for the initial targeting of the neuropils by the young T4/T5 cells. The phenotypes appeared during later pupal development, when the layers of the neuropils are further defined and the neurons acquire their adult morphology (Ngo et al., 2017). Silencing SoxN or Sox102F resulted in severe overgrowth of the dendrites into the near medulla or lobula layers. The axon terminals of the affected T4/T5 cells aggregated to clusters and the division of the lobula plate into four layers was lost. Furthermore, we tested the functional effect of SoxN or Sox102F knockdown. Flies with SoxN or Sox102F silenced in T4/T5 cells were not able to perform an optomotor response anymore. The functional consequences of SoxN or Sox102F silencing could be due to incorrect connections with their pre- and postsynaptic partners or due to changes in the expression of function-related genes. Calcium imaging of T4/T5 dendrites with SoxN or Sox102F silenced could reveal, if the functional impairments already appear within the cells.

Silencing SoxN or Sox102F in all T4/T5 subtypes abolished the layer structure of the lobula plate and reduced the overall volume of the lobula plate. Other lobula plate neurons like lobula plate tangential cells were not able to develop their correct morphology. If SoxN or Sox102F were only silenced in a subset of T4/T5 cells, the unaffected cells grew normal and established the lobula plate layers. This suggests, that T4/T5 neurons are crucial for the establishment of the lobula plate layers and that the lobula plate tangential cells depend on the T4/T5 cells to establish the lobula plate neuropil. Since the lobula plate tangential cells develop from central brain neuroblasts, they might not grow in parallel to medulla neurons and other lobula plate neurons. Therefore, T4/T5 neurons are probably important to create the four layers of the lobula plate. The important role of Sox102F for T4 and T5 morphology and the establishment of the lobula plate was further confirmed by a recently published study (Contreras et al., 2018).

Other transcription factors might regulate the initial targeting of young T4/T5 neurons to their

neuropils, while SoxN and Sox102F control the differentiation of young neurons into the mature, functional T4/T5 neurons with oriented dendrites restricted to their medulla or lobula layer and axon terminals in one of the four lobula plate layers.

Future transcriptomics data of T4/T5 cells with SoxN or Sox102F knockout could reveal proteins important for the differentiation of T4/T5 neurons. Finding cell surface molecules important for the development of T4/T5 cell morphology would help to answer the following questions: How do T4 and T5 cells establish their similar morphology? What restricts the dendrites into one layer of the medulla or lobula? How do T4 and T5 cells establish the four layers of the lobula plate? Furthermore, the RNA expression data would reveal, if SoxN and Sox102F are only controlling genes important to establish the morphology of T4/T5 cells or also genes important for their function.

3.4.1 Possible Role of Sox102F in Defining Cell Identity

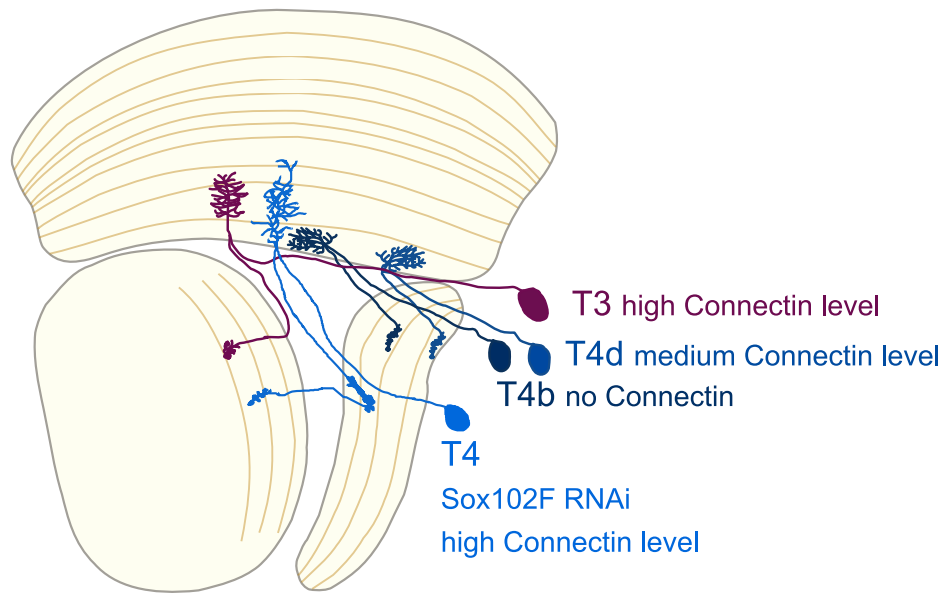


Figure 3.6: Comparison of Sox102F Knockdown T4 Cells with T3 Cells

Some T4 cells with silenced Sox102F resemble the morphology of T3 cells. In addition, the levels of Connectin reach high levels similar to those of T3 cells, while wild type T4 subtype a and b express no visible Connectin and T4 subtype c and d express a medium level of Connectin.

The C/T neurons (T2, T3, C2 and C3) originate from the same progenitors as T4 and T5 neurons. The dendrites of T3 cells are located in the medulla layer 9 and their axon terminals project to lobula layer 3 (Fig. 3.6). In contrast to T4 and T5 neurons, T3 cells are unicolumnar and their dendrites are not oriented. The neuroblasts producing T4 and T5 neurons are characterized by expression of Atonal and Dachshund. Cell clones mutant for either Atonal or Dachshund show overgrowth of the dendrites and were supposed to achieve T2/T3 like features (Oliva et al., 2014; Apitz and Salecker, 2018).

We found a dependence of SoxN and Sox102F expression on both Atonal and Dachshund in a redundant way. Silencing SoxN or Sox102F induced a similar overgrowth of the dendrites, but also a severe phenotype of the axon terminals. Silencing Sox102F in T4 cells induced some similarities with T3 cells: The dendrites strongly ramify in medulla layer 9, in addition to their normal medulla layer 10. By labeling single cells, we found about half of the axon terminals from T4 cells with Sox102F silenced to target an additional neuropil, the medulla or the lobula. Furthermore, their dendrites were not clearly multicolumnar anymore. Comparing Sox102F silenced T4 cells with T3 cells, the morphology of the cells is similar (Fig. 3.6). In addition, the Sox102F silenced T4 and T5 cells express high levels of Connectin. T3 cells express high levels of Connectin, while wild-type T4/T5 subtype c and d express a medium level of Connectin (Konstantinides et al., 2018). Using specific antibody staining of SoxN and Sox102F, we could show that they are not expressed in C/T cells. One role of Sox102F could be to control genes differentially expressed between T4/T5 cells and the related T2/T3 cells.

3.4.2 Sox Transcription Factors as Terminal Differentiation Factors in T4 and T5 Cells

Sox transcription factors are a group of highly conserved proteins characterized by their DNA binding domain, the SRY-related high mobility group box. Sox proteins act via cofactors, which are mostly other transcription factors (Kamachi and Kondoh, 2013). Eight different Sox proteins are known in *Drosophila*, they are homologous to the vertebrate Sox groups SoxB, Sox C, Sox D and Sox F (Crémazy et al., 2001). Sox2, the vertebrate homologous protein to SoxN, maintains the identity of neural progenitors by inhibiting neuronal differentiation (Graham et al., 2003). SoxN plays a similar role in the neuroectoderm of *Drosophila* embryos or larva. Together with the other *Drosophila* SoxB protein, Dichaete, SoxN is broadly expressed in neuroectoderm cells, partly overlapping with the expression of Dichaete (Crémazy et al., 2000). Mutant phenotypes indicate a redundant role of SoxN and Dichaete in the neuroectoderm (Overton et al., 2002). In the developing *Drosophila* optic lobe, SoxN is expressed in the OPC neuroectoderm and in neuroblasts, where it ensures the self-renewal of the neuroblasts (Suzuki et al., 2013). In addition to its role in neural progenitors, SoxN is also involved in the differentiation of some embryonic neurons, controlling the maturation of their morphology (Ferrero et al., 2014).

Consistent with this study reporting an uncommon role of SoxN in controlling neuronal morphology (Ferrero et al., 2014), we found that SoxN functions as a terminal differentiation factor in the development of T4/T5 neurons. This role is partly achieved by activating Sox102F. Nevertheless, we found differences in silencing SoxN (and therefore also Sox102F) or Sox102F alone. The vertebrate homologous protein to SoxN, Sox2, contains a transcriptional activation domain, but no repressor domain (Kamachi and Kondoh, 2013). However, Sox proteins act mainly through binding to cofactors. By overexpressing two SoxN versions, in which the regulating domain is replaced either by the strong transcriptional activator VP16 or the repressor domain of Engrailed,

we conclude that SoxN has a primarily activating role in T4/T5. While expression of VP16-SoxN had no effect, similar to overexpression of wild-type SoxN, the EnR-SoxN version induced a phenotype very similar to Sox102F knockdown. This suggested an activation of Sox102F expression by SoxN, which we could further confirm with Sox102F antibody staining in SoxN silenced cells. Since the phenotype of EnR-SoxN expression resembles more the Sox102F than SoxN knockdown, the EnR-SoxN protein can probably still perform some of the normal SoxN function.

Vertebrate SoxD proteins are involved in various processes of neural crest development and neuronal development, for example, cell fate decision and terminal differentiation (Lefebvre, 2010). Sox102F, the *Drosophila* version of SoxD, is expressed more specifically than SoxN in the developing embryo CNS (Adryan and Teichmann, 2010). Similar to SoxN, Sox102F was shown to regulate the Wingless pathway (Li et al., 2013). Silencing Sox102F in different types of neurons like sensory neurons or motor neurons, indicated a role of Sox102F in the establishment of adult morphology and function (Li et al., 2017a).

We found Sox102F to be important for the maturation of T4 and T5 cells, confirming a role of Sox102F in controlling the differentiation of adult neurons. The importance of Sox102F for the development of T4 and T5 was further verified by Contreras et al. (2018). Since silencing Sox102F strongly enhanced Connectin expression in all T4/T5, we propose a regulation of Connectin and other cell adhesion molecules by Sox102F. Overexpression of Sox102F in T4/T5 induced extreme overgrowth of the dendrites through the whole medulla or lobula. This further points towards a direct regulation of cell adhesion molecules and cell surface receptors by Sox102F. However, high Sox102F levels did not clearly suppress Connectin in T4/T5, which might be due to different effects in the T4/T5 subtypes. Possible are also a negative feedback regulation of Sox102F or Connectin on its own expression. The UAS-Sox102F line we created resulted in extremely high levels of Sox102F compared to the endogenous protein, which might have unexpected effects. Misexpressing Sox102F in photoreceptors or kenyon cells of the mushroom body severely affected their targeting and the cell morphology (Contreras et al., 2018), further indicating a role of Sox102F in neurite maturation and control of cell-cell contacts.

3.4.3 The T4 and T5 subtypes

While T4 and T5 cells share functional and morphological similarities, there are many genes differentially expressed between them (Davis et al., 2018). Such genes might primarily ensure the correct targeting of either the medulla or the lobula, but could also induce functional differences like the subtle distinctions in their temporal tuning properties (Leonhardt et al., 2016; Arenz et al., 2017). The vertical and horizontal motion subtypes of T4 and T5 cells also differ in their gene expression (Davis et al., 2018). The horizontal subtypes (T4/T5 a and b) express Dac, whereas the vertical subtypes (T4/T5 c and d) express Omb, Connectin and klingon (Apitz and Salecker, 2018; Davis et al., 2018). These differences arise early during T4/T5 development: the neuroblasts producing the vertical and horizontal subtypes derive from two different progenitor streams. The two progenitor

populations are distinguished in the neuroectoderm (Apitz and Salecker, 2018; Pinto-Teixeira et al., 2018).

We found both SoxN and Sox102F expressed in all T4 and T5 cells at the same level, as confirmed by transcriptomic data (Davis et al., 2018). Nevertheless, silencing Sox102F only in vertical or horizontal T4/T5 subtypes induced different phenotypes. Sox102F knockdown in T4 and T5 c,d resulted in bigger axonal clusters of the axon terminals. In contrast, we detected no differences between Sox102F knockdown in T4 or T5 cells. All T4/T5 subtypes express Sox102F at a high level, but additional transcription factors in the vertical versus horizontal subtypes might change expression of target genes. For example, Sox102F knockdown resulted in a strong increase of the cell adhesion molecule Connectin in all subtypes. Connectin is expressed at low levels in the horizontal subtypes T4/T5 a,b, but stronger in the vertical subtypes T4/T5 c,d. Sox102F might decrease the level of Connectin to a medium level and an additional transcription factor specific for T4/T5 a,b might further reduce Connectin levels. Therefore, conserved transcription factors like SoxN and Sox102F are expressed in all subtypes to ensure the common morphology, but their target genes can be further modified by specific factors in the T4/T5 subtypes.

Evolutionary Perspective on the T4/T5 Subtypes

The T4 and T5 cells, and also the monopolar lamina cells, are highly conserved throughout dipteran species (Buschbeck and Strausfeld, 1996, 1997). In contrast, higher order visual descending neurons like lobula plate tangential cells differ between fly species in their number and morphology (Buschbeck and Strausfeld, 1996). T4 and T5 cells are not only existent in diptera, similar cells were found in other insects. For example, T4 and T5 cells in the optic lobe of the moth *C. erythrocephala* have a comparable morphology as the dipteran T4 and T5 cells (Strausfeld, 1970). Even in hymenoptera, in which the lobula plate and the lobula form a lobula complex, T4 cells connect the medulla and the lobula complex of honeybees. Within their lobula complex, a bistratified amacrine cell resembles T5 cells (Strausfeld, 1970; Douglass and Strausfeld, 2001). Comparing the visual system of crabs to the one of flies even indicates, that a common ancestor of insects and crustaceans already processed vertical and horizontal motion, detected by T4/T5 ancestor cells: the small lobula plate of the crab *Neohelice granulata* is divided into four layers and medulla cells that resemble T4 neurons target the lobula plate. However, these cells project to two of the lobula plate layers, either layer 1 and 3 or layer 2 and 4 (Bengochea et al., 2018). While higher order neurons might differ even between closely related species, T4 and T5 cells are likely conserved due to their crucial function as elementary motion detectors.

It has been suggested that T4 and T5 cells originate from a common ancestor cell type, duplicating with the origin of the lobula neuropil (Shinomiya et al., 2015). Evidence for this is their close similarity in morphology and function, moreover, they develop from the same neuroblasts. The origin of T4 and T5 cells, as well as the horizontal and vertical subtypes, is evolutionary old since crustacea share a similar lobula plate structure and T4 like cells with insects. Nevertheless,

the differentiation of all T4 and T5 cells is controlled by the same neuroblast genes, *ataonal* and *dachshund*, and the same postmitotic transcription factors, SoxN and Sox102F. The essential function of T4 and T5 cells in detecting local motion is likely to be highly conserved. Therefore, ensuring the common morphology and function by expression of shared terminal differentiation factors in all T4 and T5 cells is likely. Transcriptomics data from T4/T5 single cell sequencing does not distinguish between the two vertical and the two horizontal subtypes, for example, between T4 a and T4 b (Konstantinides et al., 2018). Moreover, no proteins are described to be differentially expressed between them so far. This further indicates that the T4 and T5 subtypes are very closely related and genes important for their function are conserved in all subtypes.

Functional investigation of T4 or T5 like cells in other arthropod species could reveal, if the detection of the four cardinal direction of motion are conserved between different species. Furthermore, it could help to understand the origin of the motion computation. T4 and T5 dendrites differ in their input cells and likely their mechanism to enhance a response to the preferred direction. Studying T4 and T5 cells in different arthropod species could help to understand how the motion sensitivity of T4 and T5 cells evolved.

3.5 Outlook

During my time working on fly motion vision, I contributed to our growing understanding of direction-selective cells in the *Drosophila* visual system. Nevertheless, there are many questions unsolved regarding the T4 and T5 cells. After describing their function as local motion detectors and exploring their role in different visual behaviors, the biophysical mechanisms underlying the direction selectivity of T4 and T5 cells remain to be discovered. The detailed connectomic data about the input connections on T4 and T5 dendrites together with the T4 and T5 transcriptomics offer the prerequisites to study the molecular base of direction selectivity. The transcriptomics data reveals the neurotransmitters, neurotransmitter receptors, and other ion channels expressed on the level of RNA. Future work can confirm the expression on a protein level and describe the dendritic localization of different receptors. In addition, the role of voltage gated ion channels possibly located in the T4 or T5 dendrites can be investigated. So far, most functional studies on T4 and T5 cells were performed by imaging calcium levels. To learn more about the role of single ion channels, whole cell patch-clamp or voltage imaging would be more beneficial. Measuring the membrane potential while applying a receptor antagonist or with a knockout of the gene will help to understand the contribution of different ion channels to non-linear processes important for the direction selectivity.

When I started my thesis, no proteins were known involved in the differentiation of T4 and T5 cells. We could describe transcription factors controlling the common aspects of T4 and T5 cells. Comparing the anatomy of the adult cells, there are two important questions arising: First, how do the four subtypes grow their dendrites in four orientations? Detailed transcriptomic data

of the single subtypes will be necessary to approach the dendrite orientation. If surrounding cells provide an external cue to establish an anterior to posterior and ventral to dorsal axis, do the T4 and T5 subtypes express different receptors to detect such cues? Another possibility to grow dendrites oriented in four directions would be a purely intrinsic mechanism inducing a different orientation in each subtype. In this case, the transcriptomic data is even more important to find genes differentially expressed between the T4 and T5 subtypes. Furthermore, live imaging might help to understand the process of the oriented dendritic growth. The second question is how do the dendrites establish three different compartments connecting to different input cells? The development of dendrite compartments might be independent of differentially expressed genes. The mechanisms establishing a gradient within the dendrites might be conserved in all T4 and T5 subtypes. Therefore, genes known to be involved in cell polarization and expressed in all T4 and T5 subtypes could play a role in the dendrite compartmentalization. To test the importance of such genes, a readout of receptor localization or synapse distribution like single cell receptor labeling would be necessary. Knockout of candidate genes and live imaging of a tagged receptor could reveal mechanisms important for the distribution of input connections on T4 and T5 dendrites.

Despite the relative simplicity of the *Drosophila* brain, their motion vision pathway still offers many fundamental questions. It will help to understand the computation of neurons and the function of a neuronal circuit on the level of cell types, dendrites, proteins and genes.

Bibliography

(2001) Recurrent network interactions underlying flow-field selectivity of visual interneurons. *Journal of Neuroscience* 21(15):5685–5692.

Ache J. M., Polsky J., Alghailani S., Parekh R., Breads P., Peek M. Y., Bock D. D., von Reyn C. R., Card G. M. (2019) Neural Basis for Looming Size and Velocity Encoding in the Drosophila Giant Fiber Escape Pathway. *Current Biology* 29(6).

Adams M. D., Celtniker S. E., Holt R. A., Evans C. A., Gocayne J. D., Amanatides P. G., Scherer S. E., ..., Craig V. (2000) The genome sequence of *Drosophila melanogaster*. *Science* 287(5461):2185–2195.

Adryan B., Teichmann S. A. (2010) The developmental expression dynamics of *Drosophila melanogaster* transcription factors. *Genome Biology* 11(4):R40.

Agi E., Langen M., Altschuler S. J., Wu L. F., Zimmermann T., Hiesinger P. R. (2014) The evolution and development of neural superposition. *Journal of Neurogenetics* 28(3-4):216–232.

Ahnert-Hilger G., Weller U., Dauzenroth M.-E., Habermann E., Gratzl M. (1989) The tetanus toxin light chain inhibits exocytosis. *FEBS Letters* 242(2):245–248.

Aleksic J., Lazic R., Müller I., Russell S. R., Adryan B. (2009) Biases in *drosophila melanogaster* protein trap screens. *BMC Genomics* 10:249.

Antonny B., Burd C., Camilli P. D., Chen E., Daumke O., Faelber K., Ford M., Frolov V. A., Frost A., Hinshaw J. E., Kirchhausen T., Kozlov M. M., Lenz M., Low H. H., McMahon H., Merrifield C., Pollard T. D., Robinson P. J., Roux A., Schmid S. (2016) Membrane fission by dynamin: what we know and what we need to know. *The EMBO Journal* 35(21):2270–2284.

Apitz H., Salecker I. (2014) A challenge of numbers and diversity: neurogenesis in the *Drosophila* optic lobe. *Journal of Neurogenetics* 28(3-4):233–249.

Apitz H., Salecker I. (2015) A region-specific neurogenesis mode requires migratory progenitors in the *Drosophila* visual system. *Nature Neuroscience* 18(1):46–55.

Apitz H., Salecker I. (2018) Spatio-temporal relays control layer identity of direction-selective neuron subtypes in *Drosophila*. *Nature Communications* 9(1):2295.

Arenz A., Drews M. S., Richter F. G., Ammer G., Borst A. (2017) The temporal tuning of the *Drosophila* motion detectors is determined by the dynamics of their input elements. *Current Biology* 27(7):929–944.

Auerbach C. (1967) The chemical production of mutations. The effect of chemical mutagens on cells and their genetic material is discussed. *Science* 158(3805):1141–7.

Baden T., Berens P., Bethge M., Euler T. (2013) Spikes in mammalian bipolar cells support temporal layering of the inner retina. *Current Biology* 23(1):48–52.

Bahl A., Serbe E., Meier M., Ammer G., Borst A. (2015) neural mechanisms for *Drosophila* contrast vision. *Neuron* 88(6):1240–1252.

Baines R. A., Bate M. (1998) Electrophysiological development of central neurons in the *Drosophila* embryo. *Journal of Neuroscience* 18(12):4673–4683.

Baines R. A., Robinson S. G., Fujioka M., Jaynes J. B., Bate M. (1999) Postsynaptic expression of tetanus toxin light chain blocks synaptogenesis in *Drosophila*. *Current Biology* 9(21):1267–1270.

Ball W., Tronick E. (1971) Infant responses to impending collision: optical and real. *Science* 171(3973):818–20.

Barlow H. B., Levick W. R. (1965) The mechanism of directionally selective units in rabbit's retina. *Journal of Physiology* 178(3):477–504.

Barreto-Chang O. L., Dolmetsch R. E. (2009) Calcium imaging of cortical neurons using Fura-2 AM. *Journal of Visualized Experiments* 23:e1067.

Bartoletti R., Capozzoli B., Moore J., Moran J., Shrawder B., Vivekanand P. (2017) Short hairpin RNA is more effective than long hairpin RNA in eliciting pointed loss-of-function phenotypes in *Drosophila*. *Genesis* 55(7):e23036.

Bassett A. R., Tibbit C., Ponting C. P., Liu J.-L. (2013) Highly efficient targeted mutagenesis of *Drosophila* with the CRISPR/Cas9 system. *Cell Reports* 4(1):220–228.

Bausenwein B., Dittrich A. P. M., Fischbach K. F. (1992) The optic lobe of *Drosophila melanogaster*. *Cell & Tissue Research* 267(1):17–28.

Bausenwein B., Wolf R., Heisenberg M. (1986) Genetic dissection of optomotor behavior in *Drosophila melanogaster* studies on wild-type and the mutant *optomotor-blind*^{H31}. *Journal of Neurogenetics* 3(4):247.

Bellen H. J., Levis R. W., Liao G., He Y., Carlson J. W., Tsang G., Evans-Holm M., Hiesinger P. R., Schulze K. L., Rubin G. M., Hoskins R. A., Spradling A. C. (2004) The BDGP gene disruption project: single transposon insertions associated with 40 % of *Drosophila* genes. *Genetics* 167(2):761–81.

Bellen H. J., Tong C., Tsuda H. (2010) 100 years of *Drosophila* research and its impact on vertebrate neuroscience: a history lesson for the future. *Nature Reviews Neuroscience* 11(7):514–522.

Bender J. A., Dickinson M. H. (2006) Visual stimulation of saccades in magnetically tethered *Drosophila*. *Journal of Experimental Biology* 209(16):3170–3182.

Bengochea M., Berón de Astrada M., Tomsic D., Sztarker J. (2018) A crustacean lobula plate: Morphology, connections, and retinotopic organization. *Journal of Comparative Neurology* 526(1):109–119.

Bertet C., Li X., Erclik T., Cavey M., Wells B., Desplan C. (2014) Temporal patterning of neuroblasts controls Notch-mediated cell survival through regulation of Hid or Reaper. *Cell* 158(5):1173–1186.

Bertholf L. M. (1932) The extent of the spectrum for *Drosophila* and the distribution of stimulative efficiency in it. *Zeitschrift für vergleichende Physiologie* 18(1):32–64.

Bischof J., Maeda R. K., Hediger M., Karch F., Basler K. (2007) An optimized transgenesis system for *Drosophila* using germ-line-specific ϕ C31 integrases. *Proceedings of the National Academy of Sciences of the United States of America* 104(9):3312–7.

Bishop L. G., Keehn D. G., McCann G. D. (1968) Motion detection by interneurons of optic lobes and brain of the flies *Calliphora phaenicia* and *Musca domestica*. *Journal of Neurophysiology* 31(4):509–525.

Bishop L. G., Keehn D. G. (1966) Two types of neurones sensitive to motion in the optic lobe of the fly. *Nature* 212(5068):1374–1376.

Blondeau J. (1981) Electrically evoked course control in the fly *Calliphora erythrocephala*. *Journal of Experimental Biology* 92(1):143–153.

Blondeau J., Heisenberg M. (1982) The three-dimensional optomotor torque system of *Drosophila melanogaster*. *Journal of Comparative Physiology* 145(3):321–329.

Boergens K. M., Berning M., Bocklisch T., Bräunlein D., Drawitsch F., Frohnhofer J., Herold T., Otto P., Rzepka N., Werkmeister T., Werner D., Wiese G., Wissler H., Helmstaedter M. (2017) webKnossos: efficient online 3D data annotation for connectomics. *Nature Methods* 14(7):691–694.

Boergens K. M., Kapfer C., Helmstaedter M., Denk W., Borst A. (2018) Full reconstruction of large lobula plate tangential cells in *Drosophila* from a 3D EM dataset. *PLoS one* 13(11):e0207828.

Borst A. (1986) Time course of the houseflies' landing response. *Biological Cybernetics* 54(6):379–383.

Borst A., Bahde S. (1986) What kind of movement detector is triggering the landing response of the housefly? *Biological Cybernetics* 55(1):59–69.

Borst A. (2007) Correlation versus gradient type motion detectors: the pros and cons. *Philosophical Transactions of the Royal Society B: Biological Sciences* 362(1479):369–374.

Borst A. (2018) A biophysical mechanism for preferred direction enhancement in fly motion vision. *PLoS Computational Biology* 14(6):e1006240.

Borst A., Abarbanel H. D. (2007) Relating a calcium indicator signal to the unperturbed calcium concentration time-course. *Theoretical Biology and Medical Modelling* 4(1):7.

Borst A., Helmstaedter M. (2015) Common circuit design in fly and mammalian motion vision. *Nature Neuroscience* 18(8):1067–1076.

Braitenberg V. (1967) Patterns of projection in the visual system of the fly. I. Retina-lamina projections. *Experimental Brain Research* 3(3):271–298.

Braitenberg V., Braitenberg C. (1979) Geometry of orientation columns in the visual cortex. *Biological Cybernetics* 33(3):179–186.

Braitenberg V. (1966) Unsymmetrische Projektion der Retinulazellen auf die Lamina ganglionaris bei der Fliege *Musca domestica*. *Zeitschrift für Vergleichende Physiologie* 52(2):212–214.

Braitenberg V., Ferretti C. T. (1966) Landing reaction of *Musca domestica* induced by visual stimuli. *Die Naturwissenschaften* 53(6):155–155.

Brand A. H., Perrimon N. (1993) Targeted gene expression as a means of altering cell fates and generating dominant phenotypes. *Development* 118(2):401–15.

Brand A. H., Perrimon N. (1994) Raf acts downstream of the EGF receptor to determine dorsoventral polarity during *Drosophila* oogenesis. *Genes & Development* 8(5):629–39.

Briggman K. L., Helmstaedter M., Denk W. (2011) Wiring specificity in the direction-selectivity circuit of the retina. *Nature* 471(7337):183–188.

Broadie K., Prokop A., Bellen H. J., O'Kane C. J., Schulze K. L., Sweeney S. T. (1995) Syntaxin and synaptobrevin function downstream of vesicle docking in *Drosophila*. *Neuron* 15(3):663–673.

Brouns S. J. J., Jore M. M., Lundgren M., Westra E. R., Slijkhuis R. J. H., Snijders A. P. L., Dickman M. J., Makarova K. S., Koonin E. V., van der Oost J. (2008) Small CRISPR RNAs guide antiviral defense in prokaryotes. *Science* 321(5891):960–4.

Buchner E. (1976) Elementary movement detectors in an insect visual system. *Biological Cybernetics* 24(2):85–101.

Buchner E., Buchner S. (1980) Mapping stimulus-induced nervous activity in small brains by [3H]2-deoxy-D-glucose. *Cell & Tissue Research* 211(1):51–64.

Buchner E., Buchner S., Bülthoff I. (1984) Deoxyglucose mapping of nervous activity induced in *Drosophila* brain by visual movement. *Journal of Comparative Physiology A* 155(4):471–483.

Buchner E., Götz K. G., Straub C. (1978) Elementary detectors for vertical movement in the visual system of *Drosophila*. *Biological Cybernetics* 31(4):235–242.

Budick S. A., Reiser M. B., Dickinson M. H. (2007) The role of visual and mechanosensory cues in structuring forward flight in *Drosophila melanogaster*. *Journal of Experimental Biology* 210(23):4092–103.

Bülthoff H. (1982) *Drosophila* mutants disturbed in visual orientation. *Biological Cybernetics* 45(1):63–70.

Bülthoff I., Büchner E. (1985) Deoxyglucose mapping of nervous activity induced in *Drosophila* brain by visual movement. *Journal of Comparative Physiology A* 156(1):25–34.

Busch C., Borst A., Mauss A. S. (2018) Bi-directional Control of Walking Behavior by Horizontal Optic Flow Sensors. *Current Biology* 28(24):4037–4045.

Buschbeck E. K., Strausfeld N. J. (1997) The relevance of neural architecture to visual performance: phylogenetic conservation and variation in Dipteron visual systems. *Journal of Comparative Neurology* 383(3):282–304.

Buschbeck E. K., Strausfeld N. J. (1996) Visual motion-detection circuits in flies: small-field retinotopic elements responding to motion are evolutionarily conserved across Taxa. *Journal of Neuroscience* 16(15):4563–4578.

Bushby A. J., P'ng K. M. Y., Young R. D., Pinali C., Knupp C., Quantock A. J. (2011) Imaging three-dimensional tissue architectures by focused ion beam scanning electron microscopy. *Nature Protocols* 6(6):845–858.

Busto G. U., Guven-Ozkan T., Fulga T. A., Van Vactor D., Davis R. L. (2015) microRNAs that promote or inhibit memory formation in *Drosophila melanogaster*. *Genetics* 200(2):569–80.

C. Golgi (1873) Sulla sostanza grigia del cervello. *Gazetta Medica Italiana* 33:244–246.

Cajal S., Sanchez D. (1915) Contribución al conocimiento de los centros nerviosos de los insectos. Parte 1. Retina y centros ópticos. *Trab. Labor. Invest. biol. Univ. Madrid* 13:1–167.

Campos-Ortega J. A., Strausfeld N. J. (1972) The columnar organization of the second synaptic region of the visual system of *Musca domestica* L. *Zeitschrift für Zellforschung und Mikroskopische Anatomie* 124(4):561–585.

Cao G., Platasa J., Pieribone V. A., Raccuglia D., Kunst M., Nitabach M. N. (2013) Genetically targeted optical electrophysiology in intact neural circuits. *Cell* 154(4):904–913.

Card G., Dickinson M. H. (2008) Visually Mediated Motor Planning in the Escape Response of *Drosophila*. *Current Biology* 18(17):1300–1307.

Castle W. E., Carpenter F. W., Clark A. H., Mast S. O., Barrows W. M. (1906) The Effects of Inbreeding, Cross-Breeding, and Selection upon the Fertility and Variability of *Drosophila*. *Proceedings of the American Academy of Arts and Sciences* 41(33):731.

Chalfie M., Tu Y., Euskirchen G., Ward W. W., Prasher D. C. (1994) Green fluorescent protein as a marker for gene expression. *Science* 263(5148):802–5.

Chamberland S., Yang H. H., Pan M. M., Evans S. W., Guan S., Chavarha M., Yang Y., Salesse C., Wu H., Wu J. C., Clandinin T. R., Toth K., Lin M. Z., St-Pierre F. (2017) Fast two-photon imaging of subcellular voltage dynamics in neuronal tissue with genetically encoded indicators. *eLife* 6:e25690.

Chavez A., Scheiman J., Vora S., Pruitt B. W., Tuttle M., Iyer E., Lin S., Kiani S., Guzman C. D., Wiegand D. J., Ter-Ovanesyan D., Braff J. L., Davidsohn N., Housden B. E., Perrimon N., Weiss R., Aach J., Collins J. J., Church G. M. (2015) Highly efficient Cas9-mediated transcriptional programming. *Nature methods* 12(4):326–328.

Chen M. S., Obar R. A., Schroeder C. C., Austin T. W., Poodry C. A., Wadsworth S. C., Vallee R. B. (1991) Multiple forms of dynamin are encoded by *shibire*, a *Drosophila* gene involved in endocytosis. *Nature* 351(6327):583–586.

Chen Y.-W., Song S., Weng R., Verma P., Kugler J.-M., Buescher M., Rouam S., Cohen S. M. (2014a) Systematic Study of *Drosophila* MicroRNA Functions Using a Collection of Targeted Knockout Mutations. *Developmental Cell* 31(6):784–800.

Chen Y., Akin O., Nern A., Tsui C. Y. K., Pecot M. Y., Zipursky S. L. (2014b) Cell-type-specific labeling of synapses in vivo through synaptic tagging with recombination. *Neuron* 81(2):280–293.

Chiang A.-S., Lin C.-Y., Chuang C.-C., Chang H.-M., Hsieh C.-H., Yeh C.-W., Shih C.-T., ... (2011) Three-dimensional reconstruction of brain-wide wiring networks in *Drosophila* at single-cell resolution. *Current Biology* 21(1):1–11.

Chiappe M. E., Seelig J. D., Reiser M. B., Jayaraman V. (2010) Walking modulates speed sensitivity in *Drosophila* motion vision. *Current Biology* 20(16):1470–1475.

Chou W.-H., Hall K. J., Wilson D., Wideman C. L., Townson S. M., Chadwell L. V., Britt S. G. (1996) Identification of a novel *Drosophila* opsin reveals specific patterning of the R7 and R8 photoreceptor cells. *Neuron* 17(6):1101–1115.

Clark D., Bursztyn L., Horowitz M., Schnitzer M., Clandinin T. (2011) Defining the computational structure of the motion detector in *Drosophila*. *Neuron* 70(6):1165–1177.

Contreras E. G., Palominos T., Glavic Á., Brand A. H., Sierralta J., Oliva C. (2018) The transcription factor SoxD controls neuronal guidance in the *Drosophila* visual system. *Scientific Reports* 8(1):13332.

Cook K. R., Parks A. L., Jacobus L. M., Kaufman T. C., Matthews K. (2010) New research resources at the Bloomington *Drosophila* Stock Center. *Fly* 4(1):88–91.

Coombe P., Heisenberg M. (1986) The structural brain mutant vacuolar medulla of *Drosophila melanogaster* with specific behavioral defects and cell degeneration in the adult. *Journal of Neurogenetics* 3(3):135–158.

Crémazy F., Berta P., Girard F. (2000) Sox Neuro, a new *Drosophila* Sox gene expressed in the developing central nervous system. *Mechanisms of Development* 93(1-2):215–219.

Crémazy F., Berta P., Girard F. (2001) Genome-wide analysis of Sox genes in *Drosophila melanogaster*. *Mechanisms of Development* 109(2):371–375.

Croset V., Treiber C. D., Waddell S. (2018) Cellular diversity in the *Drosophila* midbrain revealed by single-cell transcriptomics. *eLife* 7:e34550.

Cruz T., Terufumi F., Varela N., Farhan M., Claridge-Chang A., Chiappe M. E. (2019) Motor context coordinates visually guided walking in *Drosophila*. *BioRxiv* p. 572792.

Davie K., Janssens J., Koldere D., De Waegeneer M., Pech U., Kreft Ł., Aibar S., Makhzami S., Christiaens V., Bravo González-Blas C., Poovathingal S., Hulselmans G., Spanier K. I., Moerman T., Vanspauwen B., Geurs S., Voet T., Lammertyn J., Thienpont B., Liu S., Konstantinides N., Fiers M., Verstreken P., Aerts S. (2018) A single-cell transcriptome atlas of the aging *Drosophila* brain. *Cell* 174(4):982–998.

Davis F. P., Nern A., Picard S., Reiser M. B., Rubin G. M., Eddy S. R., Henry G. L. (2018) A genetic, genomic, and computational resource for exploring neural circuit function. *Cell Press under review*.

de Talens A., Ferreti C. (1970) Landing reaction of *Musca domestica*: Dependence on dimensions and position of the stimulus. *Journal of Experimental Biology* 52(2):233–256.

Deal R. B., Henikoff S. (2011) The INTACT method for cell type–specific gene expression and chromatin profiling in *Arabidopsis thaliana*. *Nature Protocols* 6(1):56–68.

Delgado R., Delgado M. G., Bastin-Hélène L., Glavic A., O'Day P. M., Bacigalupo J. (2019) Light-Induced Opening of the TRP Channel in Isolated Membrane Patches Excised from Photosensitive Microvilli from *Drosophila* Photoreceptors. *Neuroscience* 396:66–72.

Deltcheva E., Chylinski K., Sharma C. M., Gonzales K., Chao Y., Pirzada Z. A., Eckert M. R., Vogel J., Charpentier E. (2011) CRISPR RNA maturation by trans-encoded small RNA and host factor RNase III. *Nature* 471(7340):602–607.

Denk W., Strickler J. H., Webb W. W. (1990) Two-photon laser scanning fluorescence microscopy. *Science* 248(4951):73–76.

Denk W., Horstmann H. (2004) Serial block-face scanning electron microscopy to reconstruct three-dimensional tissue nanostructure. *PLoS Biology* 2(11):e329.

Dietrich W. (1909) Die Facettenaugen der Dipteren. *PhD Diss.* .

Dietzl G., Chen D., Schnorrer F., Su K.-C., Barinova Y., Fellner M., Gasser B., Kinsey K., Oppel S., Scheiblauer S., Couto A., Marra V., Keleman K., Dickson B. J. (2007) A genome-wide transgenic RNAi library for conditional gene inactivation in *Drosophila*. *Nature* 448(7150):151–156.

Ding H., Smith R. G., Poleg-Polsky A., Diamond J. S., Briggman K. L. (2016) Species-specific wiring for direction selectivity in the mammalian retina. *Nature* 535(7610):105–110.

Dolan M.-J., Luan H., Shropshire W. C., Sutcliffe B., Cocanougher B., Scott R. L., Frechter S., Zlatic M., Jefferis G. S. X. E., White B. H. (2017) Facilitating neuron-specific genetic manipulations in *Drosophila melanogaster* using a split GAL4 repressor. *Genetics* 206(2):775–784.

Douglass J. K., Strausfeld N. J. (1995) Visual motion detection circuits in flies: peripheral motion computation by identified small-field retinotopic neurons. *Journal of Neuroscience* 15(8):5596–5611.

Douglass J. K., Strausfeld N. J. (1996) Visual motion-detection circuits in flies: parallel direction- and non-direction-sensitive pathways between the medulla and lobula plate. *Journal of Neuroscience* 16(15):4551–4562.

Douglass J. K., Strausfeld N. J. (2001) Pathways in dipteran insects for early visual motion processing In *Motion Vision*, pp. 68–82. Springer Berlin Heidelberg, Berlin, Heidelberg.

Douglass J. K., Strausfeld N. J. (2003) Anatomical organization of retinotopic motion-sensitive pathways in the optic lobes of flies. *Microscopy Research and Technique* 62(2):132–150.

Duistermars B. J., Care R. A., Frye M. A. (2012) Binocular interactions underlying the classic optomotor responses of flying flies. *Frontiers in Behavioral Neuroscience* 6:6.

Duistermars B. J., Chow D. M., Condro M., Frye M. A. (2007a) The spatial, temporal and contrast properties of expansion and rotation flight optomotor responses in *Drosophila*. *Journal of Experimental Biology* 210:3218–3227.

Duistermars B. J., Reiser M. B., Zhu Y., Frye M. A. (2007b) Dynamic properties of large-field and small-field optomotor flight responses in *Drosophila*. *Journal of Comparative Physiology A* 193(7):787–799.

Dvorak D. R., Bishop L. G., Eckert H. E. (1975a) Intracellular recording and staining of directionally selective motion detecting neurons in fly optic lobe. *Vision Research* 15(3):451–IN7.

Dvorak D. R., Bishop L. G., Eckert H. E. (1975b) On the identification of movement detectors in the fly optic lobe. *Journal of Comparative Physiology A* 100(1):5–23.

Ebert M. S., Neilson J. R., Sharp P. A. (2007) MicroRNA sponges: competitive inhibitors of small RNAs in mammalian cells. *Nature Methods* 4(9):721–726.

Egger B., Boone J. (2007) Regulation of spindle orientation and neural stem cell fate in the *Drosophila* optic lobe. *Neural Development* 2(1):1.

Egger B., Gold K. S., Brand A. H., Jimenez F., Brown S., Aguilera R. J., Nakano T., Honjo T., Mak T. W., Rossant J. (2010) Notch regulates the switch from symmetric to asymmetric neural stem cell division in the *Drosophila* optic lobe. *Development* 137(18):2981–2987.

Eichner H., Joesch M., Schnell B., Reiff D. F., Borst A. (2011) Internal structure of the fly elementary motion detector. *Neuron* 70(6):1155–1164.

Euler T., Detwiler P. B., Denk W. (2002) Directionally selective calcium signals in dendrites of starburst amacrine cells. *Nature* 418(6900):845–852.

Ewen-Campen B., Yang-Zhou D., Fernandes V. R., González D. P., Liu L.-P., Tao R., Ren X., Sun J., Hu Y., Zirin J., Mohr S. E., Ni J.-Q., Perrimon N. (2017) Optimized strategy for in vivo Cas9-activation in *Drosophila*. *Proceedings of the National Academy of Sciences of the United States of America* 114(35):9409–9414.

Farrow K., Haag J., Borst A. (2003) Input organization of multifunctional motion-sensitive neurons in the blowfly. *Journal of Neuroscience* 23(30):9805–9811.

Feinberg E. H., VanHoven M. K., Bendesky A., Wang G., Fetter R. D., Shen K., Bargmann C. I. (2008) GFP Reconstitution Across Synaptic Partners (GRASP) defines cell contacts and synapses in living nervous systems. *Neuron* 57(3):353–363.

Feng G., Mellor R. H., Bernstein M., Keller-Peck C., Nguyen Q. T., Wallace M., Nerbonne J. M., Lichtman J. W., Sanes J. R. (2000) Imaging neuronal subsets in transgenic mice expressing multiple spectral variants of GFP. *Neuron* 28(1):41–51.

Fenk L., Poehlmann A., Straw A. (2014) Asymmetric processing of visual motion for simultaneous object and background responses. *Current Biology* 24(24):2913–2919.

Fermi G., Richardt W. (1963) Optomotorische Reaktionen der Fliege *Musca Domestica*. *Kybernetik* 2(1):15–28.

Ferrero E., Fischer B., Russell S. (2014) SoxNeuro orchestrates central nervous system specification and differentiation in *Drosophila* and is only partially redundant with Dichaete. *Genome Biology* 15(5):R74.

Fire A., Xu S., Montgomery M. K., Kostas S. A., Driver S. E., Mello C. C. (1998) Potent and specific genetic interference by double-stranded RNA in *Caenorhabditis elegans*. *Nature* 391(6669):806–811.

Fischbach K. F. (1981) Habituation and sensitization of the landing response of *Drosophila melanogaster*. *Naturwissenschaften* 68(6):332–332.

Fischbach K.-F., Barleben F., Boschert U., Dittrich A. P. M., Gschwander B., Houbé B., Jäger R., Kaltenbach E., Ramos R. G. P., Schlosser G. (1989) Developmental studies on the optic lobe of *Drosophila melanogaster* using structural brain mutants In *Neurobiology of Sensory Systems*, pp. 171–194. Springer US, Boston, MA.

Fischbach K.-F., Dittrich A. (1989) The optic lobe of *Drosophila melanogaster*. I. A Golgi analysis of wild-type structure. *Cell and Tissue Research* 258(3):441–475.

Fischer J. A., Giniger E., Maniatis T., Ptashne M. (1988) GAL4 activates transcription in *Drosophila*. *Nature* 332(6167):853–856.

Fisher Y. E., Silies M., Clandinin T. R. (2015) Orientation selectivity sharpens motion detection in *Drosophila*. *Neuron* 88(2):390–402.

Fisher Y. E., Yang H. H., Isaacman-Beck J., Xie M., Gohl D. M., Clandinin T. R. (2017) FlpStop, a tool for conditional gene control in *Drosophila*. *eLife* 6:e22279.

Fite K. V. (1968) Two types of optomotor response in the domestic pigeon. *Journal of Comparative and Physiological Psychology* 66(2):308–314.

Förstemann K., Horwich M. D., Wee L., Tomari Y., Zamore P. D. (2007) *Drosophila* microRNAs are sorted into functionally distinct argonaute complexes after production by dicer-1. *Cell* 130(2):287–297.

Fosque B. F., Sun Y., Dana H., Yang C.-T., Ohyama T., Tadross M. R., Patel R., Zlatic M., Kim D. S., Ahrens M. B., Jayaraman V., Looger L. L., Schreiter E. R. (2015) Neural circuits. Labeling of active neural circuits in vivo with designed calcium integrators. *Science* 347(6223):755–60.

Fotowat H., Fayyazuddin A., Bellen H. J., Gabbiani F. (2009) A novel neuronal pathway for visually guided escape in *Drosophila melanogaster*. *Journal of Neurophysiology* 102(2):875–885.

Franconville R., Beron C., Jayaraman V. (2018) Building a functional connectome of the *Drosophila* central complex. *eLife* 7:e37017.

Fransen J. W., Borghuis B. G. (2017) Temporally diverse excitation generates direction-selective responses in ON- and OFF-Type retinal starburst amacrine cells. *Cell Reports* 18(6):1356–1365.

Fry S. N., Sayaman R., Dickinson M. H. (2003) The aerodynamics of free-flight maneuvers in *Drosophila*. *Science* 300(5618):495–498.

Fujiwara T., Cruz T. L., Bohnslav J. P., Chiappe M. E. (2017) A faithful internal representation of walking movements in the *Drosophila* visual system. *Nature Neuroscience* 20(1):72–81.

Gabbiani F., Krapp H. G., Laurent G. (1999) Computation of object approach by a wide-field, motion-sensitive neuron. *Journal of Neuroscience* 19(3):1122–41.

Gabbiani F., Cohen I., Laurent G. (2005) Time-dependent activation of feed-forward inhibition in a looming-sensitive neuron. *Journal of Neurophysiology* 94(3):2150–2161.

Gabbiani F., Krapp H. G., Koch C., Laurent G. (2002) Multiplicative computation in a visual neuron sensitive to looming. *Nature* 420(6913):320–324.

Garneau J. E., Dupuis M.-È., Villion M., Romero D. A., Barrangou R., Boyaval P., Fremaux C., Horvath P., Magadán A. H., Moineau S. (2010) The CRISPR/Cas bacterial immune system cleaves bacteriophage and plasmid DNA. *Nature* 468(7320):67–71.

Gasiunas G., Barrangou R., Horvath P., Siksnys V. (2012) Cas9-crRNA ribonucleoprotein complex mediates specific DNA cleavage for adaptive immunity in bacteria. *Proceedings of the National Academy of Sciences of the United States of America* 109(39):E2579–E2586.

Gauck V., Borst A. (1999) Spatial response properties of contralateral inhibited lobula plate tangential cells in the fly visual system. *Journal of Comparative Neurology* 406(1):51–71.

Gavrikov K. E., Nilson J. E., Dmitriev A. V., Zucker C. L., Mangel S. C. (2006) Dendritic compartmentalization of chloride cotransporters underlies directional responses of starburst amacrine cells in retina. *Proceedings of the National Academy of Sciences of the United States of America* 103(49):18793–18798.

Geiger G. (1981) Is there a motion-independent position computation of an object in the visual system of the housefly? *Biological Cybernetics* 40(1):71–75.

Geiger G., Nässel D. R. (1981) Visual orientation behaviour of flies after selective laser beam ablation of interneurones. *Nature* 293(5831):398–399.

Geiger G., Nässel D. R. (1982) Visual processing of moving single objects and wide-field patterns in flies: behavioural analysis after laser-surgical removal of interneurons. *Biological Cybernetics* 44(2):141–149.

Gengs C., Leung H.-T., Skingsley D. R., Iovchev M. I., Yin Z., Semenov E. P., Burg M. G., Hardie R. C., Pak W. L. (2002) The target of Drosophila photoreceptor synaptic transmission is a histamine-gated chloride channel encoded by ort (hclA). *Journal of Biological Chemistry* 277(44):42113–42120.

Ghosh S., Tibbit C., Liu J.-L. (2016) Effective knockdown of Drosophila long non-coding RNAs by CRISPR interference. *Nucleic Acids Research* 44(9):e84.

Gilbert L. A., Larson M. H., Morsut L., Liu Z., Brar G. A., Torres S. E., Stern-Ginossar N., Brandman O., Whitehead E. H., Doudna J. A., Lim W. A., Weissman J. S., Qi L. S. (2013) CRISPR-Mediated Modular RNA-Guided Regulation of Transcription in Eukaryotes. *Cell* 154(2):442–451.

Giraldo Y. M., Leitch K. J., Ros I. G., Warren T. L., Weir P. T., Dickinson M. H. (2018) Sun navigation requires compass neurons in Drosophila. *Current Biology* 28(17):2845–2852.

Götz K. G. (1970) Fractionation of Drosophila populations according to optomotor traits. *Journal of Experimental Biology* 52(2):419–36.

Götz K. G. (1987) Course-control, metabolism and wing interference during ultralong tethered flight in *Drosophila melanogaster*. *Journal of Experimental Biology* 128(1):35–46.

Götz K. G. (1964) Optomotorische Untersuchung des visuellen Systems einiger Augenmutanten der Fruchtfliege *Drosophila*. *Kybernetik* 2(2):77–92.

Götz K. G. (1968) Flight control in *Drosophila* by visual perception of motion. *Kybernetik* 4(6):199–208.

Götz K. G. (1975) The optomotor equilibrium of the *Drosophila* navigation system. *Journal of Comparative Physiology* 99(3):187–210.

Götz K. G., Wenking H. (1973) Visual control of locomotion in the walking fruitfly *Drosophila*. *Journal of Comparative Physiology* 85(3):235–266.

Govorunova E. G., Sineshchekov O. A., Janz R., Liu X., Spudich J. L. (2015) Natural light-gated anion channels: A family of microbial rhodopsins for advanced optogenetics. *Science* 349(6248):647–650.

Graham V., Khudyakov J., Ellis P., Pevny L. (2003) SOX2 functions to maintain neural progenitor identity. *Neuron* 39(5):749–765.

Grigliatti T. A., Hall L., Rosenbluth R., Suzuki D. T. (1973) Temperature-sensitive mutations in *Drosophila melanogaster*. *MGG Molecular & General Genetics* 120(2):107–114.

Groschner L. N., Chan Wah Hak L., Bogacz R., DasGupta S., Miesenböck G. (2018) Dendritic integration of sensory evidence in perceptual decision-making. *Cell* 173(4):894–905.e13.

Groth A. C., Fish M., Nusse R., Calos M. P. (2004) Construction of transgenic *Drosophila* by using the site-specific integrase from phage ϕ C31. *Genetics* 166(4):1775–1782.

Gruntman E., Romani S., Reiser M. B. (2018) Simple integration of fast excitation and offset, delayed inhibition computes directional selectivity in *Drosophila*. *Nature Neuroscience* 21(2):250–257.

Grynkiewicz G., Poenie M., Tsien R. (1985) A new generation of Ca^{2+} indicators with greatly improved fluorescence properties. *Journal of Biological Chemistry* 260(6):34440–3450.

Haag J., Arenz A., Serbe E., Gabbiani F., Borst A. (2016) Complementary mechanisms create direction selectivity in the fly. *eLife* 5:e17421.

Haag J., Borst A. (1997) Encoding of visual motion information and reliability in spiking and graded potential neurons. *Journal of Neuroscience* 17(12):4809–4819.

Haag J., Borst A. (2004) Neural mechanism underlying complex receptive field properties of motion-sensitive interneurons. *Nature Neuroscience* 7(6):628–634.

Haag J., Borst A. (2005) Dye-coupling visualizes networks of large-field motion-sensitive neurons in the fly. *Journal of Comparative Physiology A* 191(5):445–454.

Haag J., Mishra A., Borst A. (2017) A common directional tuning mechanism of *Drosophila* motion-sensing neurons in the ON and in the OFF pathway. *eLife* 6:e29044.

Hadley P. B. (1906) The relation of optical stimuli to rheotaxis in the American lobster, *Homarus americanus*. *American Journal of Physiology-Legacy Content* 17(4):326–343.

Haikala V., Joesch M., Borst A., Mauss A. S. (2013) Optogenetic control of fly optomotor responses. *Journal of Neuroscience* 33(34):13927–13934.

Hammond S. M., Boettcher S., Caudy A. A., Kobayashi R., Hannon G. J. (2001) Argonaute2, a link between genetic and biochemical analyses of RNAi. *Science* 293(5532):1146–50.

Hanson L., Sethuramanujam S., Jain V., Awatramani G. (2019) Retinal direction selectivity in the absence of asymmetric starburst amacrine cell responses. *eLife* 8:e42392.

Hardie R., Laughlin S., Osorio D. (1989) Early visual processing in the compound eye: physiology and pharmacology of the retina-lamina projection in the fly In *Neurobiology of Sensory Systems*, pp. 23–42. Springer US, Boston, MA.

Hardie R. C. (2001) Phototransduction in *Drosophila melanogaster*. *Journal of Experimental Biology* 204(20):3403–3409.

Hardie R. C., Franz K. (2012) Photomechanical responses in *Drosophila* photoreceptors. *Science* 338(6104):260–263.

Hardie R. C., Juusola M. (2015) Phototransduction in *Drosophila*. *Current Opinion in Neurobiology* 34:37–45.

Harzer H., Berger C., Conder R., Schmauss G., Knoblich J. A. (2013) FACS purification of *Drosophila* larval neuroblasts for next-generation sequencing. *Nature Protocols* 8(6):1088–1099.

Hassenstein B., Reichardt W. (1956) Systemtheoretische Analyse der Zeit-, Reihenfolgen- und Vorzeichenauswertung bei der Bewegungsperzeption des Rüsselkäfers *Chlorophanus*. *Zeitschrift für Naturforschung B* 11(9-10):513–524.

Hassenstein B. (1951) Ommatidienraster und afferente Bewegungsintegration. *Zeitschrift für vergleichende Physiologie* 33(4):301–326.

Hassenstein B. (1957) Über die Wahrnehmung der Bewegung von Figuren und unregelmässigen Hell-Ligkeitsmustern. *Zeitschrift für Vergleichende Physiologie* 40(6):556–592.

Hassenstein B. (1961) Wie sehen Insekten Bewegungen? *Naturwissenschaften* 48(7):207–214.

Hausen K., Wehrhahn C. (1990) Neural circuits mediating visual flight control in flies. II. Separation of two control systems by microsurgical brain lesions. *Journal of Neuroscience* 10(1):351–360.

Hausen K. (1982) Motion sensitive interneurons in the optomotor system of the fly. *Biological Cybernetics* 45(2):143–156.

Hausen, K. Wehrhahn, C. B. (1983) Microsurgical lesion of horizontal cells changes optomotor yaw responses in the blowfly *Calliphora erythrocephala*. *Proceedings of the Royal Society of London. Series B. Biological Sciences* 219(1215):211–216.

Hausselt S. E., Euler T., Detwiler P. B., Denk W. (2007) A dendrite-autonomous mechanism for direction selectivity in retinal starburst amacrine cells. *PLoS Biology* 5(7):e185.

Heim N., Griesbeck O. (2004) Genetically encoded indicators of cellular calcium dynamics based on troponin C and green fluorescent protein. *Journal of Biological Chemistry* 279(14):14280–14286.

Heimburger L., Poggio T., Reichardt W. (1976) A special class of nonlinear interactions in the visual system of the fly. *Biological Cybernetics* 21(2):103–105.

Heisenberg M., Wolf R. (1979) On the fine structure of yaw torque in visual flight orientation of *Drosophila melanogaster*. *Journal of Comparative Physiology A* 130(2):113–130.

Heisenberg M., Wonneberger R., Wolf R. (1978) Optomotor-blind H31-a *Drosophila* mutant of the lobula plate giant neurons. *Journal of Comparative Physiology* 124(4):287–296.

Heisenberg M., Buchner E. (1977) The role of retinula cell types in visual behavior of *Drosophila melanogaster*. *Journal of Comparative Physiology* 117(2):127–162.

Helassa N., Podor B., Fine A., Török K. (2016a) Design and mechanistic insight into ultrafast calcium indicators for monitoring intracellular calcium dynamics. *Scientific Reports* 6:38276.

Helassa N., Podor B., Fine A., Török K. (2016b) Development of Fast-Response GCaMP6 Calcium Sensors for Monitoring Neuronal Action Potential. *Biophysical Journal* 110(3):372a.

Helmchen F., Denk W. (2005) Deep tissue two-photon microscopy. *Nature Methods* 2(12):932–940.

Hengstenberg R. (1982) Common visual response properties of giant vertical cells in the lobula plate of the blowfly *Calliphora*. *Journal of Comparative Physiology A: Neuroethology, Sensory, Neural, and Behavioral Physiology* 149(2):179–193.

Hengstenberg R., Hausen K., Hengstenberg B. (1982) The number and structure of giant vertical cells (VS) in the lobula plate of the blowfly *Calliphora erythrocephala*. *Comparative Physiology A: Neuroethology, Sensory, Neural, and Behavioral Physiology* 149(2):163–177.

Hengstenberg R. (1988) Mechanosensory control of compensatory head roll during flight in the blowfly *Calliphora erythrocephala* Meig. *Journal of Comparative Physiology A* 163(2):151–165.

Herskowitz I. (1987) Functional inactivation of genes by dominant negative mutations. *Nature* 329(6136):219–222.

Hillman P., Hochstein S., Minke B. (1983) Transduction in invertebrate photoreceptors: role of pigment bistability. *Physiological reviews* 63(2):668–772.

Hofbauer A., Campos-Ortega J. A. (1990) Proliferation pattern and early differentiation of the optic lobes in *Drosophila melanogaster*. *Roux's archives of developmental biology* 198(5):264–274.

Holmqvist M., Srinivasan M. (1991) A visually evoked escape response of the housefly. *Journal of Comparative Physiology A* 169(4):451–459.

Hopp E., Borst A., Haag J. (2014) Subcellular mapping of dendritic activity in optic flow processing neurons. *Journal of Comparative Physiology A* 200(5):359–370.

Horn E., Wehner R. (1975) The mechanism of visual pattern fixation in the walking fly, *Drosophila melanogaster*. *Journal of Comparative Physiology* 101(1):39–56.

Hoskins R. A., Carlson J. W., Wan K. H., Park S., Mendez I., Galle S. E., Booth B. W., ..., Celniker S. (2015) The Release 6 reference sequence of the *Drosophila melanogaster* genome. *Genome Research* 25(3):445–458.

Hu Y., Comjean A., Roesel C., Vinayagam A., Flockhart I., Zirin J., Perkins L., Perrimon N., Mohr S. E. (2017) FlyRNAi.org - the database of the *Drosophila* RNAi screening center and transgenic RNAi project: 2017 update. *Nucleic Acids Research* p. gkw977.

Hu Y., Sopko R., Foos M., Kelley C., Flockhart I., Ammeux N., Wang X., Perkins L., Perrimon N., Mohr S. E. (2013) FlyPrimerBank: an online database for *Drosophila melanogaster* gene expression analysis and knockdown evaluation of RNAi reagents. *G3: Genes, Genomes, Genetics* 3(9):1607–1616.

Huang J., Liu C.-H., Hughes S. A., Postma M., Schwiening C. J., Hardie R. C. (2010) Activation of TRP channels by protons and phosphoinositide depletion in *Drosophila* photoreceptors. *Current Biology* 20(3):189–197.

Huang Y., Wang Y., Zeng B., Liu Z., Xu X., Meng Q., Huang Y., Yang G., Vasseur L., Gurr G. M., You M. (2017) Functional characterization of Pol III U6 promoters for gene knockdown and knockout in *Plutella xylostella*. *Insect Biochemistry and Molecular Biology* 89:71–78.

Ikeda K., Kaplan W. D. (1970) Patterned neural activity of a mutant *Drosophila melanogaster*. *Proceedings of the National Academy of Sciences of the United States of America* 66(3):765–772.

Ish-Horowicz D., Pinchin S. M. (1987) Pattern abnormalities induced by ectopic expression of the *Drosophila* gene hairy are associated with repression of *ftz* transcription. *Cell* 51(3):405–415.

Ishino Y., Shinagawa H., Makino K., Amemura M., Nakata A. (1987) Nucleotide sequence of the *iap* gene, responsible for alkaline phosphatase isozyme conversion in *Escherichia coli*, and identification of the gene product. *Journal of Bacteriology* 169(12):5429–5433.

Jansen R., van Embden J. D. A., Gaastra W., Schouls L. M. (2002) Identification of genes that are associated with DNA repeats in prokaryotes. *Molecular Microbiology* 43(6):1565–1575.

Jenett A., Rubin G. M., Ngo T.-T., Shepherd D., Murphy C., Dionne H., Pfeiffer B. D., ..., Zugates C. T. (2012) A GAL4-Driver Line Resource for *Drosophila* Neurobiology. *Cell Reports* 2(4):991–1001.

Jia Y., Xu R.-G., Ren X., Ewen-Campen B., Rajakumar R., Zirin J., Yang-Zhou D., ..., Jian-Quan N. (2018) Next-generation CRISPR/Cas9 transcriptional activation in *Drosophila* using flySAM. *Proceedings of the National Academy of Sciences of the United States of America* 115(18):4719–4724.

Jiang F., Ye X., Liu X., Fincher L., McKearin D., Liu Q. (2005) Dicer-1 and R3D1-L catalyze microRNA maturation in *Drosophila*. *Genes & Development* 19(14):1674–1679.

Jin L., Han Z., Platasa J., Woolerton J., Cohen L., Pieribone V. (2012) Single action potentials and subthreshold electrical events imaged in neurons with a fluorescent protein voltage probe. *Neuron* 75(5):779–785.

Jinek M., Chylinski K., Fonfara I., Hauer M., Doudna J. A., Charpentier E. (2012) A programmable dual-RNA-guided DNA endonuclease in adaptive bacterial immunity. *Science* 337(6096):816–821.

Joesch M., Plett J., Borst A., Reiff D. F. (2008) Response properties of motion-sensitive visual interneurons in the lobula plate of *Drosophila melanogaster*. *Current Biology* 18(5):368–374.

Joesch M., Schnell B., Raghu S. V., Reiff D. F., Borst A. (2010) ON and OFF pathways in *Drosophila* motion vision. *Nature* 468(7321):300–304.

Joesch M., Weber F., Eichner H., Borst A. (2013) Functional specialization of parallel motion detection circuits in the fly. *Journal of Neuroscience* 33(3):902–905.

Johannsen O. A. (1924) Eye structure in normal and eye-mutant *Drosophila*s. *Journal of Morphology* 39(2):337–349.

Jones P. W., Gabbiani F. (2010) Synchronized neural input shapes stimulus selectivity in a collision-detecting neuron. *Current Biology* 20(22):2052–2057.

Jung S. N., Borst A., Haag J. (2011) Flight activity alters velocity tuning of fly motion-sensitive neurons. *Journal of Neuroscience* 31(25):9231–9237.

Kalmus H. (1943) The optomotor responses of some eye mutants of *Drosophila*. *Journal of Genetics* 45(2):206–213.

Kamachi Y., Kondoh H. (2013) Sox proteins: regulators of cell fate specification and differentiation. *Development* 140(20):4129–4144.

Karmeier K., Tabor R., Egelhaaf M., Krapp H. (2001) Early visual experience and the receptive-field organization of optic flow processing interneurons in the fly motion pathway. *Visual Neuroscience* 18(1):1–8.

Karuppudurai T., Lin T.-Y., Ting C.-Y., Pursley R., Melnattur K., Diao F., White B., Macpherson L., Gallio M., Pohida T., Lee C.-H. (2014) A hard-wired glutamatergic circuit pools and relays UV signals to mediate spectral preference in *Drosophila*. *Neuron* 81(3):603–615.

Kazama H. (2015) Systems neuroscience in *Drosophila*: Conceptual and technical advantages. *Neuroscience* 296:3–14.

Keene A. C., Waddell S. (2007) *Drosophila* olfactory memory: single genes to complex neural circuits. *Nature Reviews Neuroscience* 8(5):341–354.

Keleş M. F., Frye M. A. (2017) Object-detecting neurons in *Drosophila*. *Current Biology* 27(5):680–687.

Kim A. J., Fenk L. M., Lyu C., Maimon G. (2017) Quantitative predictions orchestrate visual signaling in *Drosophila*. *Cell* 168(1-2):280–294.

Kim A. J., Fitzgerald J. K., Maimon G. (2015) Cellular evidence for efference copy in *Drosophila* visuomotor processing. *Nature Neuroscience* 18(9):1247–1255.

Kim K., Vinayagam A., Perrimon N. (2014) A rapid genome-wide microRNA screen identifies miR-14 as a modulator of Hedgehog signaling. *Cell Reports* 7(6):2066–2077.

King D. G., Wyman R. J. (1980) Anatomy of the giant fibre pathway in *Drosophila*. I. Three thoracic components of the pathway. *Journal of Neurocytology* 9(6):753–770.

King R. B., Douglass J. K., Phillips J. B., Baube C. L. (1993) Scotopic spectral sensitivity of the optomotor response in the green treefrog *Hyla cinerea*. *Journal of Experimental Zoology* 267(1):40–46.

Kirschfeld K. (1967) The projection of the optical environment on the screen of the rhabdomere in the compound eye of the *Musca*. *Experimental Brain Research* 3(3):248–270.

Kirschfeld K., Franceschini N., Minke B. (1977) Evidence for a sensitising pigment in fly photoreceptors. *Nature* 269(5627):386–390.

Kitamoto T. (2001) Conditional modification of behavior in *Drosophila* by targeted expression of a temperature-sensitive *shibire* allele in defined neurons. *Journal of Neurobiology* 47(2):81–92.

Klapoetke N. C., Murata Y., Kim S. S., Pulver S. R., Birdsey-Benson A., Cho Y. K., Morimoto T. K., ..., Boyden E. S. (2014) Independent optical excitation of distinct neural populations. *Nature Methods* 11(3):338–346.

Klapoetke N. C., Nern A., Peek M. Y., Rogers E. M., Breads P., Rubin G. M., Reiser M. B., Card G. M. (2017) Ultra-selective looming detection from radial motion opponency. *Nature* 551(7679):237–241.

Klein A. M., Mazutis L., Akartuna I., Tallapragada N., Veres A., Li V., Peshkin L., Weitz D. A., Kirschner M. W. (2015) Droplet barcoding for single-cell transcriptomics applied to embryonic stem cells. *Cell* 161(5):1187–1201.

Klemenz R., Weber U., Gehring W. J. (1987) The white gene as a marker in a new P-element vector for gene transfer in *Drosophila*. *Nucleic Acids Research* 15(10):3947–3959.

Knott G., Marchman H., Wall D., Lich B. (2003) Dendritic development of *Drosophila* high order visual system neurons is independent of sensory experience. *BMC Neuroscience* 4(1):14.

Knott G., Marchman H., Wall D., Lich B. (2008) Serial section scanning electron microscopy of adult brain tissue using focused ion beam milling. *Journal of Neuroscience* 28(12):2959–2964.

Konermann S., Brigham M. D., Trevino A. E., Joung J., Abudayyeh O. O., Barcena C., Hsu P. D., Habib N., Gootenberg J. S., Nishimasu H., Nureki O., Zhang F. (2015) Genome-scale transcriptional activation by an engineered CRISPR-Cas9 complex. *Nature* 517(7536):583–588.

Konstantinides N., Kapuralin K., Fadil C., Barboza L., Satija R., Desplan C. (2018) Phenotypic convergence: distinct transcription factors regulate common terminal features. *Cell* 174(3):622–635.

Kosaka T., Ikeda K. (1983) Reversible blockage of membrane retrieval and endocytosis in the garland cell of the temperature-sensitive mutant of *Drosophila melanogaster*, *shibirets1*. *The Journal of Cell Biology* 97(2):499–507.

Krapp H. G., Hengstenberg B., Hengstenberg R. (1998) Dendritic structure and receptive-field organization of optic flow processing interneurons in the fly. *Journal of Neurophysiology* 79(4):1902–1917.

Krapp H. G., Hengstenberg R. (1996) Estimation of self-motion by optic flow processing in single visual interneurons. *Nature* 384(6608):463–466.

Kraus M. E., Lis J. T. (1994) The concentration of B52, an essential splicing factor and regulator of splice site choice in vitro, is critical for *Drosophila* development. *Molecular and Cellular Biology* 14(8):5360–5370.

Lai E. C. (2002) Micro RNAs are complementary to 3' UTR sequence motifs that mediate negative post-transcriptional regulation. *Nature genetics* 30(4):363–364.

Lai S.-L., Lee T. (2006) Genetic mosaic with dual binary transcriptional systems in *Drosophila*. *Nature Neuroscience* 9(5):703–709.

Larderet I., Fritsch P. M., Gendre N., Larisa Neagu-Maier G., Fetter R. D., Schneider-Mizell C. M., Truman J. W., Zlatic M., Cardona A., Sprecher S. G. (2017) Organization of the *Drosophila* larval visual circuit. *eLife* 6:e28387.

Lee R. C., Feinbaum R. L., Ambros V. (1993) The *C. elegans* heterochronic gene lin-4 encodes small RNAs with antisense complementarity to lin-14. *Cell* 75(5):843–854.

Lee S., Zhou Z. J. (2006) The synaptic mechanism of direction selectivity in distal processes of starburst amacrine cells. *Neuron* 51(6):787–799.

Lee T., Luo L. (1999) Mosaic analysis with a repressible cell marker for studies of gene function in neuronal morphogenesis. *Neuron* 22(3):451–461.

Lee T., Luo L. (2001) Mosaic analysis with a repressible cell marker (MARCM) for *Drosophila* neural development. *Trends in Neurosciences* 24(5):251–254.

Lee Y., Ahn C., Han J., Choi H., Kim J., Yim J., Lee J., Provost P., Rådmark O., Kim S., Kim V. N. (2003) The nuclear RNase III Drosha initiates microRNA processing. *Nature* 425(6956):415–419.

Lee Y. S., Nakahara K., Pham J. W., Kim K., He Z., Sontheimer E. J., Carthew R. W. (2004) Distinct roles for *Drosophila* Dicer-1 and Dicer-2 in the siRNA/miRNA silencing pathways. *Cell* 117(1):69–81.

Lefebvre V. (2010) The SoxD transcription factors - Sox5, Sox6, and Sox13 - are key cell fate modulators. *The International Journal of Biochemistry & Cell Biology* 42(3):429–432.

Leong J. C. S., Esch J. J., Poole B., Ganguli S., Clandinin T. R. (2016) Direction selectivity in *Drosophila* emerges from preferred-direction enhancement and null-direction suppression. *Journal of Neuroscience* 36(31):8078–8092.

Leonhardt A., Ammer G., Meier M., Serbe E., Bahl A., Borst A. (2016) Asymmetry of *Drosophila* ON and OFF motion detectors enhances real-world velocity estimation. *Nature Neuroscience* 19(5):706–715.

Levine J., Tracey D. (1973) Structure and function of the giant motorneuron of *Drosophila melanogaster*. *Journal of Comparative Physiology A: Neuroethology, Sensory, Neural, and Behavioral Physiology* 87(3):213–235.

Li A., Ahsen O. O., Liu J. J., Du C., McKee M. L., Yang Y., Wasco W., Newton-Cheh C. H., O'Donnell C. J., Fujimoto J. G., Zhou C., Tanzi R. E. (2013) Silencing of the *Drosophila* ortholog of SOX5 in heart leads to cardiac dysfunction as detected by optical coherence tomography. *Human Molecular Genetics* 22(18):3798–3806.

Li A., Hooli B., Mullin K., Tate R. E., Bubnys A., Kirchner R., Chapman B., Hofmann O., Hide W., Tanzi R. E. (2017a) Silencing of the *Drosophila* ortholog of SOX5 leads to abnormal neuronal development and behavioral impairment. *Human Molecular Genetics* 26(8):1472–1482.

Li H., Horns F., Wu B., Xie Q., Li J., Li T., Luginbuhl D. J., Quake S. R., Luo L. (2017b) Classifying *Drosophila* olfactory projection neuron subtypes by single-cell RNA sequencing. *Cell* 171(5):1206–1220.

Li X., Erclik T., Bertet C., Chen Z., Voutev R., Venkatesh S., Morante J., Celik A., Desplan C. (2013) Temporal patterning of *Drosophila* medulla neuroblasts controls neural fates. *Nature* 498(7455):456–462.

Lima S. Q., Miesenböck G. (2005) Remote control of behavior through genetically targeted photostimulation of neurons. *Cell* 121(1):141–152.

Lin S., Ewen-Campen B., Ni X., Housden B. E., Perrimon N. .

Lin T.-Y., Luo J., Shinomiya K., Ting C.-Y., Lu Z., Meinertzhagen I. A., Lee C.-H. (2016) Mapping chromatic pathways in the *Drosophila* visual system. *Journal of Comparative Neurology* 524(2):213–227.

Liu G., Seiler H., Wen A., Zars T., Ito K., Wolf R., Heisenberg M., Liu L. (2006a) Distinct memory traces for two visual features in the *Drosophila* brain. *Nature* 439(7076):551–556.

Liu X., Jiang F., Kalidas S., Smith D., Liu Q. (2006b) Dicer-2 and R2D2 coordinately bind siRNA to promote assembly of the siRISC complexes. *RNA* 12(8):1514–20.

Lovick J. K., Ngo K. T., Omoto J. J., Wong D. C., Nguyen J. D., Hartenstein V. (2013) Postembryonic lineages of the *Drosophila* brain: I. Development of the lineage-associated fiber tracts. *Developmental Biology* 384(2):228–257.

Luan H., Peabody N. C., Vinson C. R., White B. H. (2006) Refined spatial manipulation of neuronal function by combinatorial restriction of transgene expression. *Neuron* 52(3):425–436.

Luo L., Liao Y. J., Jan L. Y., Jan Y. N. (1994) Distinct morphogenetic functions of similar small GT-Pases: *Drosophila* Drac1 is involved in axonal outgrowth and myoblast fusion. *Genes & Development* 8(15):1787–1802.

Lutz F. E., Richtmyer F. K. (1922) The reaction of *Drosophila* to ultraviolet. *Science* 55(1428):519.

Lutz F. E. (1907) The Merits of the Fruit Fly. *School Science and Mathematics* 7(8):672–673.

Lyon E. P. (1904) On Rheotropism I. - Rheotropism in Fishes. *American Journal of Physiology* 12(2):149–161.

Ma Y., Creanga A., Lum L., Beachy P. A. (2006) Prevalence of off-target effects in *Drosophila* RNA interference screens. *Nature* 443(7109):359–363.

Macosko E. Z., Basu A., Satija R., Nemesh J., Shekhar K., Goldman M., Tirosh I., Bialas A. R., ..., McCarroll S. A. (2015) Highly parallel genome-wide expression profiling of individual cells using nanoliter droplets. *Cell* 161(5):1202–1214.

Macpherson L. J., Zaharieva E. E., Kearney P. J., Alpert M. H., Lin T.-Y., Turan Z., Lee C.-H., Gallio M. (2015) Dynamic labelling of neural connections in multiple colours by trans-synaptic fluorescence complementation. *Nature Communications* 6:10024.

Magee J. C., Johnston D. (2005) Plasticity of dendritic function. *Current Opinion in Neurobiology* 15(3):334–342.

Maimon G., Straw A. D., Dickinson M. H. (2008) A simple vision-based algorithm for decision making in flying *Drosophila*. *Current Biology* 18(6):464–470.

Maimon G., Straw A. D., Dickinson M. H. (2010) Active flight increases the gain of visual motion processing in *Drosophila*. *Nature Neuroscience* 13(3):393–399.

Mali P., Esvelt K. M., Church G. M. (2013) Cas9 as a versatile tool for engineering biology. *Nature Methods* 10(10):957–963.

Mank M., Reiff D. F., Heim N., Friedrich M. W., Borst A., Griesbeck O. (2006) A FRET-based calcium biosensor with fast signal kinetics and high fluorescence change. *Biophysical Journal* 90(5):1790–1796.

Mastebroek H., Zaagman W., Lenting B. (1980) Movement detection: Performance of a wide-field element in the visual system of the blowfly. *Vision Research* 20(6):467–474.

Masuyama K., Zhang Y., Rao Y., Wang J. W. (2012) Mapping neural circuits with activity-dependent nuclear import of a transcription factor. *Journal of Neurogenetics* 26(1):89–102.

Mauss A. S., Busch C., Borst A. (2017) Optogenetic neuronal silencing in *Drosophila* during visual processing. *Scientific Reports* 7(1):13823.

Mauss A. S., Pankova K., Arenz A., Nern A., Rubin G. M., Borst A. (2015) Neural circuit to integrate opposing motions in the visual field. *Cell* 162(2):351–362.

McCann G. D., Dill J. C. (1969) Fundamental properties of intensity, form, and motion perception in the visual nervous systems of *Calliphora phaenicia* and *Musca domestica*. *Journal of General Physiology* 53(4):385–413.

McEwen R. S. (1918) The reactions to light and to gravity in *Drosophila* and its mutants. *Journal of Experimental Zoology* 25(1):49–106.

McGuire S. E., Le P. T., Osborn A. J., Matsumoto K., Davis R. L. (2003) Spatiotemporal rescue of memory dysfunction in *Drosophila*. *Science* 302(5651):1765–1768.

Meinertzhagen I., Hanson T. (1993) The development of *Drosophila melanogaster*. *The development of the optic lobe* pp. 1363–1491.

Meister G., Landthaler M., Dorsett Y., Tuschl T. (2004) Sequence-specific inhibition of microRNA- and siRNA-induced RNA silencing. *RNA* 10(3):544–550.

Melnattur K. V., Pursley R., Lin T.-Y., Ting C.-Y., Smith P. D., Pohida T., Lee C.-H. (2014) Multiple redundant medulla projection neurons mediate color vision in *Drosophila*. *Journal of Neurogenetics* 28(3–4):374–388.

Menne D., Spatz H. C. (1977) Colour vision in *Drosophila melanogaster*. *Journal of Comparative Physiology A* 114(3):301–312.

Misquitta L., Paterson B. M. (1999) Targeted disruption of gene function in *Drosophila* by RNA interference (RNA-i): a role for nautilus in embryonic somatic muscle formation. *Proceedings of the National Academy of Sciences of the United States of America* 96(4):1451–1456.

Miyawaki A., Llopis J., Heim R., McCaffery J. M., Adams J. A., Ikura M., Tsien R. Y. (1997) Fluorescent indicators for Ca²⁺ based on green fluorescent proteins and calmodulin. *Nature* 388(6645):882–887.

Miyoshi K., Tsukumo H., Nagami T., Siomi H., Siomi M. C. (2005) Slicer function of *Drosophila* Argonautes and its involvement in RISC formation. *Genes & Development* 19(23):2837–2848.

Mora N., Oliva C., Fiers M., Ejsmont R., Soldano A., Zhang T.-T., Yan J., Claeys A., De Geest N., Hassan B. A. (2018) A temporal transcriptional switch governs stem cell division, neuronal numbers, and maintenance of differentiation. *Developmental Cell* 45(1):53–66.

Morgan T. H., Cattell E. (1912) Data for the study of sex-linked inheritance in *Drosophila*. *Journal of Experimental Zoology* 13(1):79–101.

Mosca T. J., Luo L. (2014) Synaptic organization of the *Drosophila* antennal lobe and its regulation by the Teneurins. *eLife* 3:e03726.

Mronz M., Lehmann F.-O. (2008) The free-flight response of *Drosophila* to motion of the visual environment. *Journal of Experimental Biology* 211(13):2026–2045.

Muijres F. T., Elzinga M. J., Melis J. M., Dickinson M. H. (2014) Flies evade looming targets by executing rapid visually directed banked turns. *Science* 344(6180):172–177.

Muller H. J. (1927) Artificial transmutation of the gene. *Science* 66(1699):84–87.

Nagarkar-Jaiswal S., Lee P.-T., Campbell M. E., Chen K., Anguiano-Zarate S., Cantu Gutierrez M., Busby T., Lin W.-W., ..., Duncan D. (2015) A library of MiMICs allows tagging of genes and reversible, spatial and temporal knockdown of proteins in *Drosophila*. *eLIFE* 4:e05338.

Nagel G., Szellas T., Huhn W., Kateriya S., Adeishvili N., Berthold P., Ollig D., Hegemann P., Bamberg E. (2003) Channelrhodopsin-2, a directly light-gated cation-selective membrane channel. *Proceedings of the National Academy of Sciences of the United States of America* 100(24):13940–13945.

Nakai J., Ohkura M., Imoto K. (2001) A high signal-to-noise Ca²⁺ probe composed of a single green fluorescent protein. *Nature Biotechnology* 19(2):137–141.

Nakanishi K. (2016) Anatomy of RISC: how do small RNAs and chaperones activate Argonaute proteins? *Wiley Interdisciplinary Reviews* 7(5):637–660.

Nern A., Pfeiffer B. D., Rubin G. M. (2015) Optimized tools for multicolor stochastic labeling reveal diverse stereotyped cell arrangements in the fly visual system. *Proceedings of the National Academy of Sciences of the United States of America* 112(22):E2967–E2976.

Neuser K., Triphan T., Mronz M., Poeck B., Strauss R. (2008) Analysis of a spatial orientation memory in *Drosophila*. *Nature* 453(7199):1244–1247.

Ngo K. T., Andrade I., Hartenstein V. (2017) Spatio-temporal pattern of neuronal differentiation in the *Drosophila* visual system: A user's guide to the dynamic morphology of the developing optic lobe. *Developmental Biology* 428(1):1–24.

Nüsslein-Volhard C., Wieschaus E. (1980) Mutations affecting segment number and polarity in *Drosophila*. *Nature* 287:795–801.

Ofstad T. A., Zuker C. S., Reiser M. B. (2011) Visual place learning in *Drosophila melanogaster*. *Nature* 474(7350):204–207.

Ogueta M., Hardie R. C., Stanewsky R. (2018) Non-canonical phototransduction mediates synchronization of the *Drosophila melanogaster* circadian clock and retinal light responses. *Current Biology* 28(11):1725–1735.

Oliva C., Choi C.-M., Nicolai L. J. J., Mora N., De Geest N., Hassan B. A. (2014) Proper connectivity of *Drosophila* motion detector neurons requires Atonal function in progenitor cells. *Neural Development* 9(1):4.

Oliva D., Tomsic D. (2012) Visuo-motor transformations involved in the escape response to looming stimuli in the crab *Neohelice* (=Chasmagnathus) granulata. *Journal of Experimental Biology* 215(19):3488–3500.

Oliva D., Tomsic D. (2014) Computation of object approach by a system of visual motion-sensitive neurons in the crab *Neohelice*. *Journal of Neurophysiology* 112(6):1477–1490.

Olsen S. R., Wilson R. I. (2008) Cracking neural circuits in a tiny brain: new approaches for understanding the neural circuitry of *Drosophila*. *Trends in Neurosciences* 31(10):512–520.

Omoto J. J., Keleş M. F., Nguyen B.-C. M., Bolanos C., Lovick J. K., Frye M. A., Hartenstein V. (2017) Visual input to the *Drosophila* central complex by developmentally and functionally distinct neuronal populations. *Current Biology* 27(8):1098–1110.

Omoto J. J., Nguyen B.-C. M., Kandimalla P., Lovick J. K., Donlea J. M., Hartenstein V. (2018) Neuronal constituents and putative interactions within the *Drosophila* ellipsoid body neuropil. *Frontiers in neural circuits* 12:103.

Overton P. M., Meadows L. A., Urban J., Russell S. (2002) Evidence for differential and redundant function of the Sox genes *Dichaete* and *SoxN* during CNS development in *Drosophila*. *Development* 129(18):4219–4228.

Pan Y., Zhou Y., Guo C., Gong H., Gong Z., Liu L. (2009) Differential roles of the fan-shaped body and the ellipsoid body in *Drosophila* visual pattern memory. *Learning & Memory* 16(5):289–295.

Pankova K., Borst A. (2016) RNA-Seq transcriptome analysis of direction-selective T4/T5 neurons in *Drosophila*. *PloS one* 11(9):e0163986.

Panser K., Tirian L., Schulze F., Villalba S., Jefferis G., Bühler K., Straw A. (2016) Automatic segmentation of *Drosophila* neural compartments using GAL4 expression data reveals novel visual pathways. *Current Biology* 26(15):1943–1954.

Pantazis A., Segaran A., Liu C.-H., Nikolaev A., Rister J., Thum A. S., Roeder T., Semenov E., Juusola M., Hardie R. C. (2008) Distinct roles for two histamine receptors (hClA and hClB) at the *Drosophila* photoreceptor synapse. *Journal of Neuroscience* 28(29):7250–7259.

Papatsenko D., Sheng G., Desplan C. (1997) A new rhodopsin in R8 photoreceptors of *Drosophila*: evidence for coordinate expression with Rh3 in R7 cells. *Development* 124(9):1665–1673.

Paradis S., Sweeney S. T., Davis G. W. (2001) Homeostatic control of presynaptic release is triggered by postsynaptic membrane depolarization. *Neuron* 30(3):737–749.

Park S. J. H., Kim I.-J., Looger L. L., Demb J. B., Borghuis B. G. (2014) Excitatory synaptic inputs to mouse on-off direction-selective retinal ganglion cells lack direction tuning. *Journal of Neuroscience* 34(11):3976–3981.

Parkhurst S. M., Ish-Horowicz D. (1991) Mis-regulating segmentation gene expression in *Drosophila*. *Development* 111(4):1121–1135.

Pfeiffer B. D., Jenett A., Hammonds A. S., Ngo T.-T. B., Misra S., Murphy C., Scully A., ..., Rubin G. M. (2008) Tools for neuroanatomy and neurogenetics in *Drosophila*. *Proceedings of the National Academy of Sciences of the United States of America* 105(28):9715–9720.

Pfeiffer B. D., Ngo T.-T. B., Hibbard K. L., Murphy C., Jenett A., Truman J. W., Rubin G. M. (2010) Refinement of tools for targeted gene expression in *Drosophila*. *Genetics* 186(2):735–755.

Pflugfelder G. O., Heisenberg M. (1995) Optomotor-blind of *Drosophila melanogaster*: a neurogenetic approach to optic lobe development and optomotor behaviour. *Comparative Biochemistry and Physiology Part A: Physiology* 110(3):185–202.

Pham J. W., Pellino J. L., Lee Y. S., Carthew R. W., Sontheimer E. J. (2004) A Dicer-2-dependent 80s complex cleaves targeted mRNAs during RNAi in *Drosophila*. *Cell* 117(1):83–94.

Picao-Osorio J., Lago-Baldaia I., Patraquim P., Alonso C. R. (2017) Pervasive behavioral effects of microRNA regulation in *Drosophila*. *Genetics* 206(3):1535–1548.

Pick B. (1974) Visual flicker induces orientation behaviour in the fly *Musca*. *Zeitschrift für Naturforschung C* 29(5-6):310–312.

Pickard G. E., Sollars P. J. (2011) Intrinsically photosensitive retinal ganglion cells. In *Reviews of Physiology, Biochemistry and Pharmacology*, Vol. 162, pp. 59–90. Springer, Berlin, Heidelberg.

Pierantoni R. (1976) A look into the cock-pit of the fly. *Cell and Tissue Research* 171(1):101–122.

Pinto-Teixeira F., Koo C., Rossi A. M., Nericc N., Bertet C., Li X., Del-Valle-Rodriguez A., Desplan C. (2018) Development of concurrent retinotopic maps in the fly motion detection circuit. *Cell* 173(2):485–498.

Pollack I., Hofbauer A. (1991) Histamine-like immunoreactivity in the visual system and brain of *Drosophila melanogaster*. *Cell and Tissue Research* 266(2):391–398.

Poodry C. A., Edgar L. (1979) Reversible alteration in the neuromuscular junctions of *Drosophila melanogaster* bearing a temperature-sensitive mutation, shibire. *The Journal of Cell Biology* 81(3):520–527.

Port F., Chen H.-M., Lee T., Bullock S. L. (2014) Optimized CRISPR/Cas tools for efficient germline and somatic genome engineering in *Drosophila*. *Proceedings of the National Academy of Sciences of the United States of America* 111(29):E2967–E2976.

Ptashne M. (1988) How eukaryotic transcriptional activators work. *Nature* 335(6192):683–689.

Pulver S. R., Pashkovski S. L., Hornstein N. J., Garrity P. A., Griffith L. C. (2009) Temporal dynamics of neuronal activation by Channelrhodopsin-2 and TRPA1 determine behavioral output in *Drosophila* larvae. *Journal of Neurophysiology* 101(6):3075–3088.

Quiñones-Coello A. T., Petrella L. N., Ayers K., Melillo A., Mazzalupo S., Hudson A. M., Wang S., Castiblanco C., Buszczak M., Hoskins R. A., Cooley L. (2007) Exploring strategies for protein trapping in *Drosophila*. *Genetics* 175(3):1089–1104.

Radl E. (1903) *Untersuchungen über den Phototropismus der Tiere* W. Engelmann.

Raghu S. V., Joesch M., Borst A., Reiff D. F. (2007) Synaptic organization of lobula plate tangential cells in *Drosophila*: γ -Aminobutyric acid receptors and chemical release sites. *Journal of Comparative Neurology* 502(4):598–610.

Reichardt W. (1973) Musterinduzierte Flugorientierung. *Naturwissenschaften* 60(3):122–138.

Reichardt W., Poggio T. (1976) Visual control of orientation behaviour in the fly: Part I. A quantitative analysis. *Quarterly Reviews of Biophysics* 9(3):311–375.

Reichardt W., Wenking H. (1969) Optical detection and fixation of objects by fixed flying flies. *Die Naturwissenschaften* 56(8):424–424.

Reiff D. F., Ihring A., Guerrero G., Isacoff E. Y., Joesch M., Nakai J., Borst A. (2005) In vivo performance of genetically encoded indicators of neural activity in flies. *Journal of Neuroscience* 25(19):4766–4778.

Reiser M. B., Dickinson M. H. (2008) A modular display system for insect behavioral neuroscience. *Journal of Neuroscience Methods* 167(2):127–139.

Reiser M. B., Dickinson M. H. (2010) *Drosophila* fly straight by fixating objects in the face of expanding optic flow. *Journal of Experimental Biology* 213(10):1771–1781.

Reiser M. B., Dickinson M. H. (2013) Visual motion speed determines a behavioral switch from forward flight to expansion avoidance in *Drosophila*. *Journal of Experimental Biology* 216(4):719–732.

Ren X., Sun J., Housden B. E., Hu Y., Roesel C., Lin S., Liu L.-P., Yang Z., Mao D., Sun L., Wu Q., Ji J.-Y., Xi J., Mohr S. E., Xu J., Perrimon N., Ni J.-Q. (2013) Optimized gene editing technology for *Drosophila melanogaster* using germ line-specific Cas9. *Proceedings of the National Academy of Sciences of the United States of America* 110(47):19012–19017.

Ribeiro I. M., Drews M., Bahl A., Machacek C., Borst A., Dickson B. J. (2018) Visual projection neurons mediating directed courtship in *Drosophila*. *Cell* 174(3):607–621.

Richards M. H., Furrow E. Y. (1925) The eye and optic tract in normal and "eyeless" *Drosophila*. *The Biological Bulletin* 48(4):243–258.

Robertson R., Johnson A. (1993) Collision avoidance of flying locusts: steering torques and behaviour. *Journal of Experimental Biology* 183(1):35–60.

Robie A. A., Straw A. D., Dickinson M. H. (2010) Object preference by walking fruit flies, *Drosophila melanogaster*, is mediated by vision and graviperception. *Journal of Experimental Biology* 213(14):2494–2506.

Rørth P. (1998) Gal4 in the *Drosophila* female germline. *Mechanisms of Development* 78(1-2):113–118.

Rosenzweig M., Brennan K. M., Tayler T. D., Phelps P. O., Patapoutian A., Garrity P. A. (2005) The *Drosophila* ortholog of vertebrate TRPA1 regulates thermotaxis. *Genes & Development* 19(4):419–424.

Rubin G. M., Spradling A. C. (1983) Vectors for P element-mediated gene transfer in *Drosophila*. *Nucleic Acids Research* 11(18):6341–6351.

Sakmann B., Neher E. (1984) Patch clamp techniques for studying ionic channels in excitable membranes. *Annual Review of Physiology* 46(1):455–472.

Salcedo E., Huber A., Henrich S., Chadwell L. V., Chou W. H., Paulsen R., Britt S. G. (1999) Blue- and green-absorbing visual pigments of *Drosophila*: ectopic expression and physiological characterization of the R8 photoreceptor cell-specific Rh5 and Rh6 rhodopsins. *Journal of Neuroscience* 19(24):10716–10726.

Santer R. D., Yamawaki Y., Rind F. C., Simmons P. J. (2008) Preparing for escape: an examination of the role of the DCMD neuron in locust escape jumps. *Journal of Comparative Physiology A* 194(1):69–77.

Sato K., Yamawaki Y. (2014) Role of a looming-sensitive neuron in triggering the defense behavior of the praying mantis *Tenodera aridifolia*. *Journal of Neurophysiology* 112(3):671–682.

Schlieper C. (1927) Farbensinn der Tiere und optomotorische Reaktionen. *Zeitschrift für Vergleichende Physiologie* 6(3):453–472.

Schnaitmann C., Garbers C., Wachtler T., Tanimoto H. (2013) Color discrimination with broadband photoreceptors. *Current Biology* 23(23):2375–2382.

Schnaitmann C., Haikala V., Abraham E., Oberhauser V., Thestrup T., Griesbeck O., Reiff D. F. (2018) Color processing in the early visual system of *Drosophila*. *Cell* 172(1-2):318–330.

Schnaitmann C., Vogt K., Triphan T., Tanimoto H. (2010) Appetitive and aversive visual learning in freely moving *Drosophila*. *Frontiers in Behavioral Neuroscience* 4:10.

Schneider-Mizell C. M., Gerhard S., Longair M., Kazimiers T., Li F., Zwart M. F., Champion M. F. M., Fetter R. D., Saalfeld S., Cardona A. (2016) Quantitative neuroanatomy for connectomics in *Drosophila*. *eLife* 5:e12059.

Schnell B., Joesch M., Forstner F., Raghu S. V., Otsuna H., Ito K., Borst A., Reiff D. F. (2010) Processing of horizontal optic flow in three visual interneurons of the *Drosophila* brain. *Journal of Neurophysiology* 103(3):1646–1657.

Schnell B., Raghu S. V., Nern A., Borst A. (2012) Columnar cells necessary for motion responses of wide-field visual interneurons in *Drosophila*. *Journal of Comparative Physiology A* 198(5):389–395.

Schnell B., Ros I. G., Dickinson M. H. (2017) A descending neuron correlated with the rapid steering maneuvers of flying *Drosophila*. *Current Biology* 27(8):1200–1205.

Schnell B., Weir P. T., Roth E., Fairhall A. L., Dickinson M. H. (2014) Cellular mechanisms for integral feedback in visually guided behavior. *Proceedings of the National Academy of Sciences of the United States of America* 111(15):5700–5705.

Schneuwly S., Klemenz R., Gehring W. J. (1987) Redesigning the body plan of *Drosophila* by ectopic expression of the homoeotic gene *Antennapedia*. *Nature* 325(6107):816–818.

Schroll C., Riemensperger T., Bucher D., Ehmer J., Völler T., Erbguth K., Gerber B., Hendel T., Nagel G., Buchner E., Fiala A. (2006) Light-induced activation of distinct modulatory neurons triggers appetitive or aversive learning in *Drosophila* larvae. *Current Biology* 16(17):1741–1747.

Scott E. K., Raabe T., Luo L. (2002) Structure of the vertical and horizontal system neurons of the lobula plate in *Drosophila*. *Journal of Comparative Neurology* 454(4):470–481.

Scott K., Namiki S., Dickinson M. H., Wong A. M., Korff W., Card G. M. (2018) The functional organization of descending sensory-motor pathways in *Drosophila*. *eLife* p. e34272.

Sebo Z. L., Lee H. B., Peng Y., Guo Y. (2014) A simplified and efficient germline-specific CRISPR/Cas9 system for *Drosophila* genomic engineering. *Fly* 8(1):52–57.

Seelig J. D., Chiappe M. E., Lott G. K., Dutta A., Osborne J. E., Reiser M. B., Jayaraman V. (2010) Two-photon calcium imaging from head-fixed *Drosophila* during optomotor walking behavior. *Nature Methods* 7(7):535–540.

Seelig J. D., Jayaraman V. (2013) Feature detection and orientation tuning in the *Drosophila* central complex. *Nature* 503(7475):262–266.

Seelig J. D., Jayaraman V. (2015) Neural dynamics for landmark orientation and angular path integration. *Nature* 521(7551):186–191.

Sen R., Wu M., Branson K., Robie A., Rubin G. M., Dickson B. J. (2017) Moonwalker descending neurons mediate visually evoked retreat in *Drosophila*. *Current Biology* 27(5):766–771.

Shaner N. C., Campbell R. E., Steinbach P. A., Giepmans B. N. G., Palmer A. E., Tsien R. Y. (2004) Improved monomeric red, orange and yellow fluorescent proteins derived from *Discosoma* sp. red fluorescent protein. *Nature Biotechnology* 22(12):1567–1572.

Shaw S. R., Fröhlich A., Meinertzhagen I. A. (1989) Direct connections between the R7/8 and R1/6 photoreceptor subsystems in the dipteran visual system. *Cell and Tissue Research* 257(2):295–302.

Sherman A., Camhi J., Ito K., Strausfeld N. J. (2004) Summation of visual and mechanosensory feedback in *Drosophila* flight control. *Journal of Experimental Biology* 207(1):133–142.

Shinomiya K., Huang G., Lu Z., Parag T., Xu S., Aniceto R., Ansari N., ..., Meinertzhagen I. A. (2019) Comparisons between the ON-and OFF-edge motion pathways in the *Drosophila* brain. *eLife* 8:e40025.

Shinomiya K., Takemura S.-y., Rivlin P. K., Plaza S. M., Scheffer L. K., Meinertzhagen I. A. (2015) A common evolutionary origin for the ON- and OFF-edge motion detection pathways of the *Drosophila* visual system. *Frontiers in Neural Circuits* 9:33.

Shiozaki H. M., Kazama H. (2017) Parallel encoding of recent visual experience and self-motion during navigation in *Drosophila*. *Nature Neuroscience* 20(10):1395–1403.

Simmons P. J., Rind F. C., Santer R. D. (2010) Escapes with and without preparation: The neuroethology of visual startle in locusts. *Journal of Insect Physiology* 56(8):876–883.

Spradling A., Rubin G. (1982) Transposition of cloned P elements into *Drosophila* germ line chromosomes. *Science* 218(4570):341–347.

St-Pierre F., Marshall J. D., Yang Y., Gong Y., Schnitzer M. J., Lin M. Z. (2014) High-fidelity optical reporting of neuronal electrical activity with an ultrafast fluorescent voltage sensor. *Nature neuroscience* 17(6):884–889.

Staehling-Hampton K., Hoffmann F. M. (1994) Ectopic *decapentaplegic* in the *Drosophila* midgut alters the expression of five homeotic genes, *dpp*, and *wingless*, causing specific morphological defects. *Developmental Biology* 164(2):502–512.

Stell W., Ishida A., Lightfoot D. (1977) Structural basis for on-and off-center responses in retinal bipolar cells. *Science* 198(4323):1269–1271.

Stevens N. M. (1905) A study of the germ cells of *Aphis rosæ* and *Aphis œnotheræ*. *Journal of Experimental Zoology* 2(3):313–333.

Stevens N. M. (1908) A study of the germ cells of certain diptera, with reference to the heterochromosomes and the phenomena of synapsis. *Journal of Experimental Zoology* 5(3):359–374.

Strausfeld N. J. (1971) The organization of the insect visual system (Light microscopy). *Zeitschrift für Zellforschung und Mikroskopische Anatomie* 121(3):377–441.

Strausfeld N. J., Bassemir U. K. (1983) Cobalt-coupled neurons of a giant fibre system in Diptera. *Journal of Neurocytology* 12(6):971–991.

Strausfeld N. J. (1970) Golgi studies on insects Part II. The optic lobes of Diptera. *Philosophical Transactions of the Royal Society of London. B, Biological Sciences* 258(820):135–223.

Strausfeld N. J., Braitenberg V. (1970) The compound eye of the fly (*Musca domestica*): connections between the cartridges of the lamina ganglionaris. *Zeitschrift für vergleichende Physiologie* 70(2):95–104.

Strausfeld N. J., Lee J.-K. (1991) Neuronal basis for parallel visual processing in the fly. *Visual Neuroscience* 7(1-2):13–33.

Strausfeld N., Bassemir U., Singh R., Bacon J. (1984) Organizational principles of outputs from Dipteran brains. *Journal of Insect Physiology* 30(1):73–93.

Strausfeld N., Bassemir U. (1985) Lobula plate and ocellar interneurons converge onto a cluster of descending neurons leading to neck and leg motor neuropil in *Calliphora erythrocephala*. *Cell and Tissue Research* 240(3):617–640.

Strauss R., Pichler J. (1998) Persistence of orientation toward a temporarily invisible landmark in *Drosophila melanogaster*. *Journal of Comparative Physiology A* 182(4):411–423.

Strauss R., Schuster S., Götz K. G. (1997) Processing of artificial visual feedback in the walking fruit fly *Drosophila melanogaster*. *Journal of Experimental Biology* 200(9):1281–1296.

Struhl G. (1985) Near-reciprocal phenotypes caused by inactivation or indiscriminate expression of the *Drosophila* segmentation gene *ftz*. *Nature* 318(6047):677–680.

Sun Y., Nern A., Franconville R., Dana H., Schreiter E. R., Looger L. L., Svoboda K., Kim D. S., Her mundstad A. M., Jayaraman V. (2017) Neural signatures of dynamic stimulus selection in *Drosophila*. *Nature Neuroscience* 20(8):1104–1113.

Suster M. L., Seugnet L., Bate M., Sokolowski M. B. (2004) Refining GAL4-driven transgene expression in *Drosophila* with a GAL80 enhancer-trap. *Genesis* 39(4):240–245.

Sutton E. (1943) Bar Eye in *Drosophila Melanogaster*: A Cytological Analysis of Some Mutations and Reverse Mutations. *Genetics* 28(2):97–107.

Suver M., Mamiya A., Dickinson M. (2012) Octopamine neurons mediate flight-induced modulation of visual processing in *Drosophila*. *Current Biology* 22(24):2294–2302.

Suver M., Dickinson M. (2016) Sensory integration by descending interneurons in the flying fruit fly. *Integrative and Comparative Biology* 56(S1):E216.

Suzuki T., Hasegawa E., Nakai Y., Kaido M., Takayama R., Sato M. (2016) Formation of neuronal circuits by interactions between neuronal populations derived from different origins in the *Drosophila* visual center. *Cell Reports* 15(3):499–509.

Suzuki T., Kaido M., Takayama R., Sato M. (2013) A temporal mechanism that produces neuronal diversity in the *Drosophila* visual center. *Developmental Biology* 380(1):12–24.

Sweeney S. T., Broadie K., Keane J., Niemann H., O’Kane C. J. (1995) Targeted expression of tetanus toxin light chain in *Drosophila* specifically eliminates synaptic transmission and causes behavioral defects. *Neuron* 14(2):341–351.

Szüts D., Bienz M. (2000) LexA chimeras reveal the function of *Drosophila* Fos as a context-dependent transcriptional activator. *Proceedings of the National Academy of Sciences of the United States of America* 97(10):5351–5356.

Taddei-Ferretti C., de Talens A. F. P. (1973) Landing reaction of *Musca domestica*, IV: A. Monocular and binocular vision; B. Relationships between landing and optomotor reactions. *Zeitschrift für Naturforschung C* 28(9-10):579–592.

Takemura S.-Y., Aso Y., Hige T., Wong A., Lu Z., Xu S., Rivlin P. K., ..., Scheffer L. K. (2017) A connectome of a learning and memory center in the adult *Drosophila* brain. *eLife* 6:e26975.

Takemura S.-Y., Bharioke A., Lu Z., Nern A., Vitaladevuni S., Rivlin P. K., Katz W. T., ..., Chklovskii D. B. (2013) A visual motion detection circuit suggested by *Drosophila* connectomics. *Nature* 500(7461):175–181.

Takemura S.-Y., Nern A., Chklovskii D. B., Scheffer L. K., Rubin G. M., Meinertzhagen I. A. (2017) The comprehensive connectome of a neural substrate for ‘ON’ motion detection in *Drosophila*. *eLife* 6:e24394.

Tammero L. F., Dickinson M. H. (2002a) Collision-avoidance and landing responses are mediated by separate pathways in the fruit fly, *Drosophila melanogaster*. *Journal of Experimental Biology* 205(18):2785–2789.

Tammero L. F., Dickinson M. H. (2002b) The influence of visual landscape on the free flight behavior of the fruit fly *Drosophila melanogaster*. *Journal of Experimental Biology* 205(3):327–343.

Tammero L. F., Frye M. A., Dickinson M. H. (2004) Spatial organization of visuomotor reflexes in *Drosophila*. *Journal of Experimental Biology* 207(1):113–122.

Tanouye M. A., Wyman R. J. (1980) Motor outputs of giant nerve fiber in *Drosophila*. *Journal of Neurophysiology* 44(2):405–421.

Thomas J. B., Wyman R. J. (1984) Mutations altering synaptic connectivity between identified neurons in *Drosophila*. *Journal of Neuroscience* 4(2):530–538.

Thummel C. S., Boulet A. M., Lipshitz H. D. (1988) Vectors for *Drosophila* P-element-mediated transformation and tissue culture transfection. *Gene* 74(2):445–456.

Tirian L., Dickson B. (2017) The VT GAL4, LexA, and split-GAL4 driver line collections for targeted expression in the *Drosophila* nervous system. *BioRxiv* p. 198648.

Tsutsumi A., Kawamata T., Izumi N., Seitz H., Tomari Y. (2011) Recognition of the pre-miRNA structure by *Drosophila* Dicer-1. *Nature Structural & Molecular Biology* 18(10):1153–1158.

Turner G. C., Bazhenov M., Laurent G. (2008) Olfactory representations by *Drosophila* mushroom body neurons. *Journal of Neurophysiology* 99(2):734–746.

Turner-Evans D., Wegener S., Rouault H., Franconville R., Wolff T., Seelig J. D., Druckmann S., Jayaraman V. (2017) Angular velocity integration in a fly heading circuit. *eLife* 6:e23496.

Venken K. J. T., Schulze K. L., Haelterman N. A., Pan H., He Y., Evans-Holm M., Carlson J. W., Levis R. W., Spradling A. C., Hoskins R. A., Bellen H. J. (2011) MiMIC: a highly versatile transposon insertion resource for engineering *Drosophila melanogaster* genes. *Nature Methods* 8(9):737–743.

von Reyn C. R., Breads P., Peek M. Y., Zheng G. Z., Williamson W. R., Yee A. L., Leonardo A., Card G. M. (2014) A spike-timing mechanism for action selection. *Nature Neuroscience* 17(7):962–970.

von Reyn C. R., Nern A., Williamson W. R., Breads P., Wu M., Namiki S., Card G. M. (2017) Feature integration drives probabilistic behavior in the *Drosophila* escape response. *Neuron* 94(6):1190–1204.

Voolstra O., Rhodes-Mordov E., Katz B., Bartels J.-P., Oberegelsbacher C., Schotthöfer S. K., Yasin B., Tzadok H., Huber A., Minke B. (2017) The Phosphorylation State of the *Drosophila* TRP Channel Modulates the Frequency Response to Oscillating Light In Vivo. *Journal of Neuroscience* 37(15):4213–4224.

Wang H., Dewell R. B., Zhu Y., Gabbiani F. (2018) Feedforward inhibition conveys time-varying stimulus information in a collision detection circuit. *Current Biology* 28(10):1509–1521.e3.

Wang J. W., Wong A. M., Flores J., Vosshall L. B., Axel R. (2003) Two-photon calcium imaging reveals an odor-evoked map of activity in the fly brain. *Cell* 112(2):271–282.

Wang X., Wang T., Jiao Y., von Lintig J., Montell C. (2010) Requirement for an enzymatic visual cycle in *Drosophila*. *Current Biology* 20(2):93–102.

Wardill T. J., List O., Li X., Dongre S., McCulloch M., Ting C.-Y., O’Kane C. J., Tang S., Lee C.-H., Hardie R. C., Juusola M. (2012) Multiple spectral inputs improve motion discrimination in the *Drosophila* visual system. *Science* 336(6083):925–931.

Weir P. T., Dickinson M. H. (2012) Flying *Drosophila* orient to sky polarization. *Current Biology* 22(1):21–27.

Weir P. T., Dickinson M. H. (2015) Functional divisions for visual processing in the central brain of flying *Drosophila*. *Proceedings of the National Academy of Sciences of the United States of America* 112(40):E5523–E5532.

Wernet M. F., Mazzoni E. O., Çelik A., Duncan D. M., Duncan I., Desplan C. (2006) Stochastic spineless expression creates the retinal mosaic for colour vision. *Nature* 440(7081):174–180.

Wernet M. F., Velez M. M., Clark D. A., Baumann-Klausener F., Brown J. R., Klovstad M., Labhart T., Clandinin T. R. (2012) Genetic dissection reveals two separate retinal substrates for polarization vision in *Drosophila*. *Current Biology* 22(1):12–20.

Wertz A., Borst A., Haag J. (2008) Nonlinear integration of binocular optic flow by DNOVS2, a descending neuron of the fly. *Journal of Neuroscience* 28(12):3131–3140.

White J. G., Southgate E., Thomson J. N., Brenner S. (1986) The structure of the nervous system of the nematode *Caenorhabditis elegans*. *Philosophical Transactions of the Royal Society B: Biological Sciences* 314(1165):1–340.

White K. (1982) Neural development in an imaginal disc mutant of *Drosophila melanogaster*. *Developmental Genetics* 3(2):143–154.

Williamson W. R., Peek M. Y., Breads P., Coop B., Card G. M. (2018) Tools for rapid high-resolution behavioral phenotyping of automatically isolated *Drosophila*. *Cell Reports* 25(6):1636–1649.

Wilson R. I., Turner G. C., Laurent G. (2004) Transformation of olfactory representations in the *Drosophila* antennal lobe. *Science* 303(5656):366–370.

Wolf R., Heisenberg M. (1986) Visual orientation in motion-blind flies is an operant behaviour. *Nature* 323(6084):154–156.

Wolff T., Rubin G. M. (2018) Neuroarchitecture of the *Drosophila* central complex: A catalog of nodulus and asymmetrical body neurons and a revision of the protocerebral bridge catalog. *The Journal of Comparative Neurology* 526(16):2585–2611.

Wolken J., Capenos J., Turano A. (1957) Photoreceptor structures. III. *Drosophila melanogaster*. *The Journal of Biophysical and Biochemical Cytology* 3(3):441–448.

Wong D. C., Lovick J. K., Ngo K. T., Borisuthirattana W., Omoto J. J., Hartenstein V. (2013) Postembryonic lineages of the *Drosophila* brain: II. Identification of lineage projection patterns based on MARCM clones. *Developmental Biology* 384(2):258–289.

Wu C. F., Wong F. (1977) Frequency characteristics in the visual system of *Drosophila*: genetic dissection of electroretinogram components. *The Journal of General Physiology* 69(6):705–724.

Wu L.-Q., Niu Y.-Q., Yang J., Wang S.-R. (2005) Tectal neurons signal impending collision of looming objects in the pigeon. *European Journal of Neuroscience* 22(9):2325–2331.

Wu M., Nern A., Williamson W., Morimoto M., Reiser M. B., Card G. M., Rubin G. M. (2016) Visual projection neurons in the *Drosophila* lobula link feature detection to distinct behavioral programs. *eLIFE* 5:e21022.

Xue Z., Wu M., Wen K., Ren M., Long L., Zhang X., Gao G. (2014) CRISPR/Cas9 mediates efficient conditional mutagenesis in *Drosophila*. *G3: Genes, Genomes, Genetics* 4(11):2167–2173.

Yamaguchi S., Desplan C., Heisenberg M. (2010) Contribution of photoreceptor subtypes to spectral wavelength preference in *Drosophila*. *Proceedings of the National Academy of Sciences of the United States of America* 107(12):5634–5639.

Yamaguchi S., Wolf R., Desplan C., Heisenberg M. (2008) Motion vision is independent of color in *Drosophila*. *Proceedings of the National Academy of Sciences of the United States of America* 105(12):4910–4915.

Yang H. H., St-Pierre F., Sun X., Ding X., Lin M. Z., Clandinin T. R. (2016) Subcellular Imaging of Voltage and Calcium Signals Reveals Neural Processing in vivo. *Cell* 166(1):245–257.

Yasugi T., Umetsu D., Murakami S., Sato M., Tabata T. (2008) *Drosophila* optic lobe neuroblasts triggered by a wave of proneural gene expression that is negatively regulated by JAK/STAT. *Development* 135(8):1471–1480.

Yeom K.-H., Lee Y., Han J., Suh M. R., Kim V. N. (2006) Characterization of DGCR8/Pasha, the essential cofactor for Drosha in primary miRNA processing. *Nucleic Acids Research* 34(16):4622–4629.

Yilmaz M., Meister M. (2013) Rapid innate defensive responses of mice to looming visual stimuli. *Current Biology* 23(20):2011–2015.

Yuste R. (2008) Circuit neuroscience: the road ahead. *Frontiers in Neuroscience* 2:17.

Yuste R., Denk W. (1995) Dendritic spines as basic functional units of neuronal integration. *Nature* 375(6533):682–684.

Zeleny C. (1922) The effect of selection for eye facet number in the white bar-eye race of *Drosophila melanogaster*. *Genetics* 7(1):1–115.

Zemelman B. V., Lee G. A., Ng M., Miesenböck G. (2002) Selective photostimulation of genetically chARGed neurons. *Neuron* 33(1):15–22.

Zhang F., Wang L.-P., Brauner M., Liewald J. F., Kay K., Watzke N., Wood P. G., Bamberg E., Nagel G., Gottschalk A., Deisseroth K. (2007) Multimodal fast optical interrogation of neural circuitry. *Nature* 446(7136):633–639.

Zhang G., Gurtu V., Kain S. R. (1996) An enhanced green fluorescent protein allows sensitive detection of gene transfer in mammalian cells. *Biochemical and Biophysical Research Communications* 227(3):707–711.

Zhang W., Ge W., Wang Z. (2007) A toolbox for light control of *Drosophila* behaviors through Channelrhodopsin 2-mediated photoactivation of targeted neurons. *European Journal of Neuroscience* 26(9):2405–2416.

Zheng Z., Lauritzen J. S., Perlman E., Robinson C. G., Nichols M., Milkie D., Torrens O., Price J., Fisher C. B., Sharifi N., Calle-Schuler S. A., Kmecova L., Ali I. J., Karsh B., Trautman E. T., Bogovic J. A., Hanslovsky P., Jefferis G. S., Kazhdan M., Khairy K., Saalfeld S., Fetter R. D., Bock D. D. (2018) A complete electron microscopy volume of the brain of adult *Drosophila melanogaster*. *Cell* 174(3):730–743.

Zhou L., Schnitzler A., Agapite J., Schwartz L. M., Steller H., Nambu J. R. (1997) Cooperative functions of the reaper and head involution defective genes in the programmed cell death of *Drosophila* central nervous system midline cells. *Proceedings of the National Academy of Sciences of the United States of America* 94(10):5131–5136.

Zhu Y., Nern A., Zipursky S. L., Frye M. A. (2009) Peripheral visual circuits functionally segregate motion and phototaxis behaviors in the fly. *Current Biology* 19(7):613–619.

Zhu Y., Dewell R. B., Wang H., Gabbiani F. (2018) Pre-synaptic muscarinic excitation enhances the discrimination of looming stimuli in a collision-detection neuron. *Cell Reports* 23(8):2365–2378.

Danksagung

Zunächst möchte ich Axel Borst dafür danken, mir eine Doktorarbeit am MPI ermöglicht zu haben. Danke für die Freiheiten, die ich während dieser Zeit hatte, die es Jesús und mir ermöglichte unseren Ideen nachzugehen. Besonders danken möchte ich für die Unterstützung während der Schwangerschaft und der Mutterschutz/Babyzeit. Danke für Begeisterung für die Wissenschaft und für alle unseren kleinen Fortschritte.

Während meiner Doktorarbeit haben mich viele Kollegen auf unterschiedliche Art und Weise unterstützt. Ich möchte Jesús danken, der mit mir ein neues Projekt begonnen hat. Danke dafür, dass du mein Interesse an der Dendriten-Morphologie und ihrer Entwicklung geweckt hast. Während langer, emotionaler Diskussionen hatten wir viel gelernt und ein sehr schönes Paper veröffentlicht. Danke natürlich an das ganze Development Team, Niko and Aicha, für die gute Arbeit und alles was noch kommen wird. Vielen Dank besonders an Aicha, die beste Hiwi Studentin die ich mir hätte wünschen können, inzwischen die beste Teamkollegin und auch eine gute Freundin.

Danke an das ganze Labor für die gute Stimmung, die gute Mitarbeit und auch das Feiern miteinander. Speziell danke ich den Mädels im Labor für die gegenseitige Unterstützung und die schönen Abende miteinander. Besonderen Dank an Sandra, für viele Gespräche über Wissenschaft und alles andere. Danke an Alexander für die aufbauende Gespräche in schwierigen Situationen. Vielen Dank an alle, die meine Thesis oder Teile davon gelesen und korrigiert hatten, insbesondere Ines und Lukas.

Am wichtigsten in allem ist meine Familie, danke an meinen Mann Andreas und natürlich an meinen Sohn Mats, der mich daran erinnert was wichtig ist. Danke im Nachhinein an meine Oma für die Unterstützung während dem Studium. Auch danke ich meine grossartigen Geschwister, die immer für mich da sind.

Curriculum Vitae

Tabea Rebecca Schilling

Juni 2012 - August 2019

Ludwig Maximilian University of Munich

PhD student

Max Plack Institute of Neurobiology

Dep. Circuits - Computation – Models

‘Functional and Developmental Characterization of Local Motion Sensing Neurons in the Fly Visual System’

(Prof. Alexander Borst)

Oct. 2009 – Jan. 2012

University of Regensburg

Dep. Developmental Biology

Biological Science M.Sc.

‘*A Drosophila melanogaster model of ALS Effects of -Dynactin-1^{G59S} overexpression*’

(Prof. Stefan Schneuwly)

Oct. 2006 – August 2009

University of Konstanz

Biological Science B.Sc.

Dep. Molecular Toxicology

‘*Einfluss der humanen PARP-1 DNA-Bindedomäne auf die Aktivität der PARP-1 und PARP-2 in MEFs nach DNA Schädigung*’

(Prof. Alexander Bürkle)

Sept. 2004 – July 2006

Gymnasium Kloster Wald

general qualification for university entrance

Addition Skills

Programming: Python

Graphics design: Inkscape, ImageJ, Gimp

Language: English (fluent in spoken & written)